

Synchronous machine identification by a simple step-response test

Citation for published version (APA):

Vleeshouwers, J. M. (1998). *Synchronous machine identification by a simple step-response test*. [Phd Thesis 1 (Research TU/e / Graduation TU/e), Electrical Engineering]. Technische Universiteit Eindhoven.
<https://doi.org/10.6100/IR511971>

DOI:

[10.6100/IR511971](https://doi.org/10.6100/IR511971)

Document status and date:

Published: 01/01/1998

Document Version:

Publisher's PDF, also known as Version of Record (includes final page, issue and volume numbers)

Please check the document version of this publication:

- A submitted manuscript is the version of the article upon submission and before peer-review. There can be important differences between the submitted version and the official published version of record. People interested in the research are advised to contact the author for the final version of the publication, or visit the DOI to the publisher's website.
- The final author version and the galley proof are versions of the publication after peer review.
- The final published version features the final layout of the paper including the volume, issue and page numbers.

[Link to publication](#)

General rights

Copyright and moral rights for the publications made accessible in the public portal are retained by the authors and/or other copyright owners and it is a condition of accessing publications that users recognise and abide by the legal requirements associated with these rights.

- Users may download and print one copy of any publication from the public portal for the purpose of private study or research.
- You may not further distribute the material or use it for any profit-making activity or commercial gain
- You may freely distribute the URL identifying the publication in the public portal.

If the publication is distributed under the terms of Article 25fa of the Dutch Copyright Act, indicated by the "Taverne" license above, please follow below link for the End User Agreement:

www.tue.nl/taverne

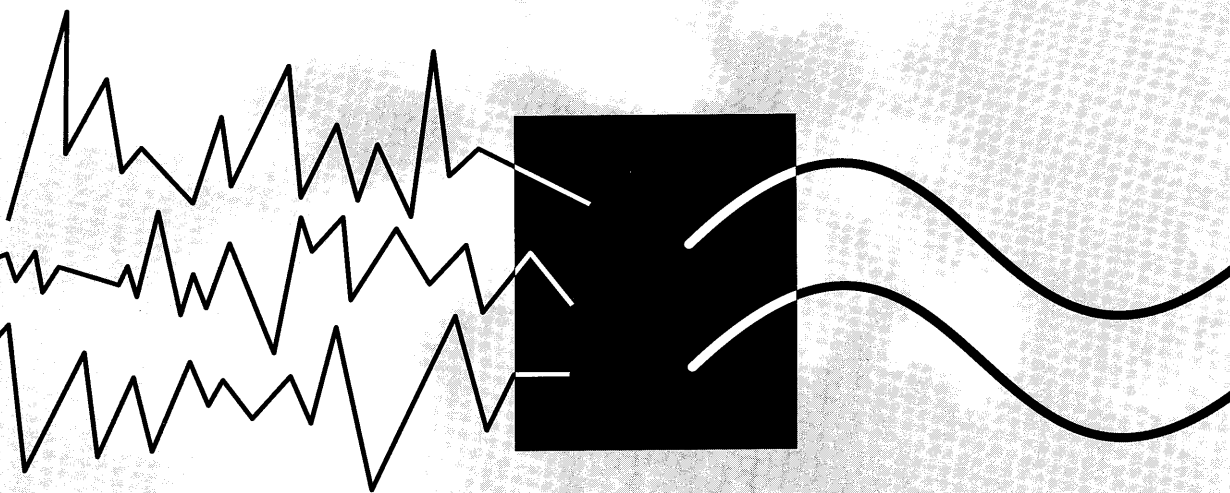
Take down policy

If you believe that this document breaches copyright please contact us at:

openaccess@tue.nl

providing details and we will investigate your claim.

Jan Vleeshouwers



***Synchronous machine
identification
by a simple
step-response test***

SYNCHRONOUS MACHINE IDENTIFICATION BY A SIMPLE STEP-RESPONSE TEST

PROEFSCHRIFT

ter verkrijging van de graad van doctor aan de
Technische Universiteit Eindhoven,
op gezag van de Rector Magnificus, prof. dr. M. Rem,
voor een commissie aangewezen door
het College van Promoties
in het openbaar te verdedigen op
maandag 8 juni 1998 om 16.00 uur

door

JOANNES MARIA VLEESHOUWERS

geboren te Schaesberg

Dit proefschrift is goedgekeurd door de promotoren:

prof. dr. ir. A.J.A. Vandenput
prof. dr. ir. P.P.J. van den Bosch

Copromotor:

dr. ir. M.J. Hoeijmakers

CIP-DATA LIBRARY TECHNISCHE UNIVERSITEIT EINDHOVEN

Vleeshouwers, Joannes M.

Synchronous machine identification by a simple step-response test / by Joannes M. Vleeshouwers. - Eindhoven : Technische Universiteit Eindhoven, 1998.

Proefschrift. - ISBN 90-386-0460-2

NUGI 832

Trefw. : elektrische machines ; parameterschatting / synchrone machines / parameteridentificatie.

Subject headings: synchronous machines / identification / parameter estimation / step response

COLOFON

Drukwerk:

Ponsen & Looijen bv, Wageningen

Vormgeving en lay out:

Nathalie van Iersel, Eindhoven



*"... aiming at simplicity and lucidity
is a moral duty
of all intellectuals ..."*

Karl Popper
Scientific Knowledge
1972







VOORWOORD

't Heeft er tijdens mijn studie Elektrotechniek altijd om gespannen in welk vakgebied ik mijn specialisatie zou zoeken: energietechniek of meten en regelen. Uiteindelijk gaf Wim de Zeeuw de doorslag: door zijn fascinatie voor vermogens-elektronika bracht hij me in aanraking met windenergie, en Martin Hoeijmakers beklonk de zaak door me een ideaal afstudeerproject aan te bieden op het grensvlak van beide vakgebieden. Ik maakte kennis met hoe je parameters van motoren en generatoren bepaalt, (ofwel: hoe je machines identificeert), en was daar ook na mijn afstuderen een aantal jaren in diverse projecten steeds diepgaander mee bezig. Wat me eerst een grensvlak toescheen, zou ik nu eerder karakteriseren als een grensrivier, en aan beide oevers wordt gewerkt aan bruggen. Beide zijden van de rivier werken tegenwoordig op de TU Eindhoven samen in één vakgroep, "Meet- en besturingssystemen". Dat geeft goede hoop voor het verbinden van beide oevers, maar de taal- en cultuurverschillen aan weerszijden zijn onmiskenbaar. Hoewel de noodzaak van de identificatie van elektrische machines als een paal boven water staat, bespeur ik toch vaak een aarzeling bij machine-specialisten om zich op dit gebied te begeven. Kant-en-klare oplossingen gepresenteerd door identificatie-specialisten gaan echter vaak voorbij aan het speciale karakter van elektrische machines en aan de cultuur van dat vakgebied, en vinden zo slechts langzaam ingang.

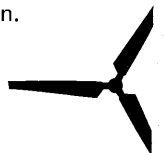
Dit proefschrift kunt u beschouwen als een brug van het vakgebied van de elektrische machines (motoren, generatoren) naar het vakgebied van de identificatie (parameterbepaling). Een brug met zijn beperkingen en onvolkomenheden, zeker, maar desondanks toch een brug. Zonder de steun en hulp van velen was het nooit zover gekomen. Enkelen van hen wil ik speciaal bedanken.

Allereerst mijn promotoren Martin Hoeijmakers, André Vandenput en Paul van den Bosch: voor hun kritiek, geduld, en voor de getoonde moeite met mij onbekende kennisgebieden te ontdekken.

Voor hun hulp op het gebied van de identificatie dank ik met name Ad van de Boom, Ad Damen, en Yucai Zhu. Hun suggesties en ook hun scepsis waren van grote waarde.

Een essentieel onderdeel van het werk achter dit proefschrift zijn de diverse metingen. Daarvoor ben ik dank verschuldigd aan de technici van E-laag: Marijn Uyt De Willigen, Toon Mariën, Henk van de Braken, Jan Sanders, Wim Thirion en Johan van Doorn. Ik klopte nooit tevergeefs bij hen aan. En bij Joke Verhoef kon ik altijd terecht voor secretariële ondersteuning.

Ook het faculteitsburo, waar ik tijdens het werk aan dit proefschrift een halve aanstelling had als studie-adviseur, dank ik voor het geduld en de flexibiliteit. Het was lang niet altijd eenvoudig om de promotie te combineren met werk en gezin.



Tenslotte wil ik bedanken voor de persoonlijke steun van gezin, vrienden en familie. Met name voor Thijske en de kinderen was het promotiewerk een last in een toch al woelige periode van ons leven. Desondanks ontbrak het niet aan steun en begrip. Teun en Anne zullen blij zijn dat ze eindelijk weer op de computer spelletjes mogen doen.

JV





CONTENTS

1	Introduction	
1.1	The synchronous machine with rectifier	9
1.2	Identifying the synchronous machine	11
1.3	Thesis overview	12
2	Synchronous machine identification	
2.1	Synchronous machine modelling aims	15
2.2	Modelling the synchronous machine	16
2.3	The identification experiment	18
2.4	Parameter estimation	27
2.5	Evalidation of the identification results	29
3	A model of the synchronous machine with rectifier	
3.1	A model of the synchronous machine	31
3.2	A model of the three-phase diode-bridge rectifier	34
3.3	Coupling the models of machine and rectifier	35
3.4	A model of the synchronous machine with rectifier	41
4	The modified step-response test	
4.1	The standstill test concept	45
4.2	The modified step-response test	50
4.3	The protocol of the modified step-response test	58
5	Completing the identification	
5.1	Estimating a single transfer function	59
5.2	The transfer function to be estimated	67
6	Theoretical analysis of the excitation source and of temperature influences	
6.1	Aims of this chapter	71
6.2	The choice of the excitation source	71
6.3	The effect of winding resistance changes	76
7	Evaluation of the modified step-response test by measurements	
7.1	Aims of this chapter	79
7.2	Standard machine data and steady-state tests	80
7.3	Modified step-response test	82
7.4	Reference test: the DC-decay test	88
7.5	Reference test: the standstill frequency-response test	90
7.6	Measured dynamic behaviour of the synchronous machine with rectifier	94
7.7	Simulated dynamic behaviour of the synchronous machine with rectifier	99

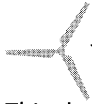


8 Conclusions	105
Summary	109
Samenvatting	111
References	115
List of symbols	119

Appendices

A1 The relation between bandwidth and noise content of a step signal	125
A2 Handling stator resistance changes due to heating and cooling	131
A3 Handling excitation-winding resistance changes due to heating and cooling	135
A4 Figures of chapter	139





1.1 The synchronous machine with rectifier

This thesis originates from a rather simple question concerning the use of a synchronous machine (generator) in combination with a rectifier. For a number of decades, this combination has been put to work successfully in traction and in other essentially *fixed-speed* situations. Will it also function in a *variable-speed* environment, for example in wind turbines? Expecting an affirmative answer, the synchronous machine with rectifier became a topic of research in a number of projects which have been carried out in the Group Electromechanics and Power Electronics, which is part of the Department of Electrical Engineering at the Eindhoven University of Technology.

Figure 1.1 shows a way of applying the synchronous machine with rectifier for variable-speed energy conversion. The machine is driven by a turbine through a gear-box, and the rectifier is connected to the grid via a smoothing coil and an inverter. In this way, the frequencies of generator and grid are independent, and electrical energy may be generated for a range of rotor speeds. Compared to fixed-speed systems, this has the advantage of using the energy in the wind more efficiently (especially at low wind speeds), and of reducing the mechanical forces in the system. The idea has been adopted by (for example) the NEWECS 45 wind turbine, by the experimental wind farm in Sexbierum, Friesland (figure 1.2), and more recently by wind turbines produced by Enercon and Lagerwey.

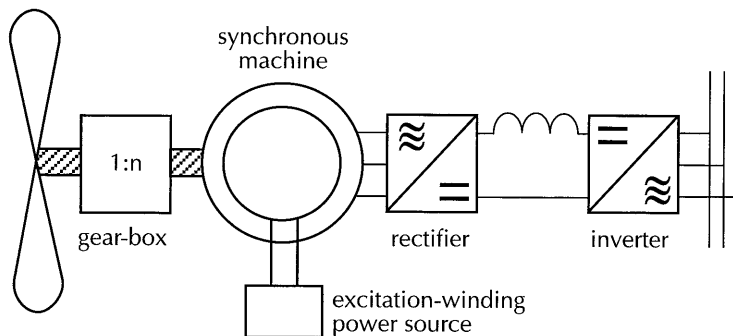


Figure 1.1
Wind-energy conversion system with a synchronous machine (SM) and a rectifier





Figure 1.2
The wind farm at Sexbierum, Friesland (foto: SEP)

Most of the research attention was focused on the model of the machine with diode-bridge rectifier. The earlier projects in the late seventies, which were aimed at *designing* the system, used a steady-state model in which all losses were neglected. The model behaved reasonably well for small (30 kVA) machines [Bon82]. Further research into the special and allegedly harmful losses which originate from loading the machine with a rectifier, showed that these losses do not have to cause problems [Hoe84a].

Instability

Although the results of these earlier projects were promising, problems were encountered during laboratory experiments in 1982: the system appeared to exhibit spontaneous oscillations with a frequency in the order of 1 Hz (see also [Aui80]). These oscillations could be suppressed by using a current source instead of a voltage source to supply the excitation winding, but this solution is not practical for large machines. It was suggested that the instability could also be avoided by applying a machine without damper windings. The idea has been investigated [Hoe84b], but this did not lead to a better understanding of the instability phenomenon nor to other ways of suppressing the oscillations.

Again, the attention was directed at modelling the machine with a diode-bridge rectifier, but now the main interest turned to *large-signal dynamic models*. With such a model we expected to be able to simulate the oscillations, to increase the knowledge of their nature, and to test solutions for suppression of the oscillations prior to carrying out experiments. A second incentive for deriving a dynamic model came from a parallel research project at the Delft University of Technology. This project aimed at deriving a dynamic model of a complete wind turbine (i.e. including mechanical parts and tower), in which the system of figure 1.1 would convert the mechanical energy into electrical energy [Bon90]. From our perspective, we were particularly interested in the interaction of the machine with rectifier and the mechanical system of the turbine, which has resonance frequencies in the same area (1 - 10 Hz) as observed in the machine with rectifier.



A simple model

A research project was set up to construct a model of the synchronous machine with a controllable rectifier (which is only slightly more complex than a diode-bridge rectifier), which could be used for fast (real-time) simulation and control. The model should be simple enough to both clarify the reasons for instability and be a functional part of the integral model of a wind turbine. The strategy which was followed, was to focus on the fundamental harmonic component of the AC-currents in the circuit, and to neglect all ripples on the DC-current. The resulting simple, large-signal dynamic model has been described in detail [Hoe88, Hoe89a, Hoe90]. Control of the delay angle of the controllable rectifier appeared to be an effective measure to keep the system stable.

To gain practical usefulness, the model has been enhanced in two ways: a model of a brushless exciter has been added [Vle92b], and a very simple saturation model has been incorporated [Hoe89b].



1.2 Identifying the synchronous machine

From 1986 onwards, the topic of determining the synchronous-machine model parameters, or, more generally, of identifying the machine, has been an aspect of the research projects concerning the synchronous machine with rectifier. For most machines in which we were interested (ranging from approximately 10 kVA to 1 MVA), a rough estimate of parameter values could be based on manufacturer data or on (scarcely available) additional measurements. As the projects evolved, the need for more accurate parameter values became increasingly urgent. To fulfil this need, it was decided to look for an appropriate identification technique.

Identification is the process of creating a model of a given system, on the basis of measurements, and to achieve specific goals. It consists of a number of successive steps:

- the choice of a set or class of possible models;
- the choice of the identification experiment (test signal, set-up);
- the choice of a specific model from the model-set, using measured data from the system under test (which includes the determination of the parameter values);
- validation of the results.

An appropriate identification technique would have to accommodate a number of criteria. Below, these criteria are formulated in relation to the given identification steps.

With respect to the necessary measurements, the main requirement was that the technique should be *simple*, because of the need to carry out measurements even if the machine had been installed in a wind turbine. In such case our access to the machine would be limited to short periods of repair or maintenance, with the machine at standstill. This resulted in the following preferences with respect to the necessary measurements and measurement set-up.

- 1 The measurements should have a low power consumption (and therefore low voltage measurements are preferred).
- 2 The measurement equipment should be compact.
- 3 Terminal measurements should be sufficient.
- 4 Measurements should be possible while the machine is at standstill.
- 5 The measurement time should be limited.



Initially, the identification technique to be adopted was not expected to include choices with respect to the synchronous-machine model structure and order. The machine model was considered given and only the parameter values remained to be determined. Over time, also the *model order* was left to be determined by the identification technique.

With respect to the resulting machine model, the identification technique should meet the following requirements.

- 1 It should allow identification of the dynamic behaviour of a synchronous machine of about 100 kVA.
- 2 The identification procedure should allow stressing the identification of the synchronous-machine model characteristics which are responsible for the instable behaviour observed in the system of the machine with rectifier. This is a rather abstract criterion, but if the Park-transformation is used to model the synchronous machine (see chapter 2 and 3), the criterion may be implemented as straightforward weighting factors on the frequency response of the Park-transformed machine model, in a frequency band around 1 Hz.
- 3 It should allow determination of the subtransient inductance values of the machine. Subtransient values are associated with relatively high frequencies, in the order of 100 Hz - 1 kHz, which is the frequency band in which the switching phenomena of the rectifier take place.

With these demands in mind, a technique to identify the synchronous machine may be selected. In a number of cases, compromises are necessary, e.g. since the final two criteria are difficult to match simultaneously.

The description of the chosen technique and its validation are the central topics of this thesis.



1.3 Thesis overview

A synchronous-machine identification technique

The goal of this thesis is to describe and validate a simple technique to identify the synchronous machine. In chapter 2, '*Synchronous-machine identification*', the main decisions with respect to the choice of an identification technique are discussed, taking into consideration the available literature on this subject. The main conclusion of this chapter is that the standstill step-response test is an acceptable compromise between the conflicting criteria formulated in section 1.2. The next three chapters (3 - 5) describe the chosen identification procedure. Chapter 3, '*A model of the synchronous machine with rectifier*', describes the model of the synchronous machine with rectifier, referred to before as the 'simple model', which is slightly adapted to accommodate the identification.

The identification experiment is described in chapter 4, '*The modified step-response test*' (MSR test). The MSR test has an extremely simple measurement set-up, simpler than other step-response tests described in the literature, and apart from enabling identification of the synchronous machine in the required frequency range, it also allows acquisition of measurement data which may be used to determine a value for the subtransient self-inductance (the inductance which is effective during the commutation in the rectifier).

Chapter 5 '*Completing the identification*' describes how the measured data are used to obtain values of the model order and parameters.



Evaluation of the Modified Step-Response Test

In chapter 6 and in chapter 7 the MSR test is evaluated. A theoretical analysis is given in chapter 6, *'Theoretical analysis of the excitation source and of temperature influences'*, with emphasis on:

- the choice of the excitation voltage source;
- analysis of temperature effects.

In chapter 7, *'Evaluation of the modified step-response test by measurements'*, the MSR test is evaluated empirically. Two synchronous machines with rated power of about 30 kVA are submitted to the modified step-response test and to two standard tests (the DC-decay test and the Standstill Frequency-Response test). The models identified by the MSR test and the two standard tests are used to simulate the dynamic behaviour of the synchronous machine with rectifier. The same dynamic behaviour is also measured (using a real measurement set-up), and differences are compared.

Chapters 6 and 7 show that the MSR test performs as might be expected from a step-response test: a bandwidth of approximately 2 decades, a close similarity to identification results obtained from the DC-decay test, and better results than those obtained from the Standstill Frequency-Response test at equal excitation levels.

For the system of synchronous machine with rectifier, the differences between the three simulations and the measurement concentrate at the steady-state. Dynamic differences are small, and evenly spread over the three applied identification techniques. The conclusion from the experimental evaluation is, that no single test performs best.

Essentially, the evaluation leads to the conclusion that the choice of the synchronous-machine identification technique is not very crucial for the simulation results (at least for this specific configuration with a rectifier), and that the choice will have to be based on other criteria, like practical usefulness. At this criterion, the MSR test clearly performs better than both standard tests considered.





2 SYNCHRONOUS-MACHINE IDENTIFICATION

In this chapter the choice of a synchronous-machine identification technique is discussed, using the successive steps of the identification process as a guideline, and taking into consideration the literature on this subject. By the end of this chapter, there will be an outline of an identification technique which satisfies our criteria.

2.1 Synchronous-machine modelling aims

Identification is generally defined as the process of creating a model of a given system, on the basis of measurements, and to achieve specific goals. It consists of a number of successive steps (see e.g. [Lju87, Bos94]):

- the choice of a set or class of possible models;
- the choice of the identification experiment (test signal, set-up);
- the choice of a specific model from the model-set, using measurement data from the system under test (which includes the determination of parameter values);
- the validation of the results.

As already mentioned in chapter 1, a model of the synchronous machine was needed

- to simulate (real-time) and control the system of the synchronous machine with a controllable rectifier;
- to clarify the reasons and circumstances for the instability (with a frequency in the order of 1 Hz) which is sometimes observed when the synchronous machine is connected to a rectifier;
- as a functional part of the integral model of a wind turbine.

As a consequence, the model should satisfy the following criteria:

- M1: the model describes the synchronous-machine system dynamically;
- M2: the model description is based on input and output relationships;
- M3: the model is valid within a wide range of operating conditions;
- M4: the model has low complexity.

The first step in the identification process is to choose a model-set to describe the machine, given these criteria. Most decisions with respect to this step have already been made prior to the study of this thesis, see [Hoe88, Hoe89a, Hoe89b, Hoe90, Vle92b], but since the design of the (rest of the) identification process depends on these modelling decisions, they will be discussed in the next section.



2.2 Modelling the synchronous machine

The first step in the identification process is the *choice of a model-set*. In the literature on synchronous machines this is usually referred to as 'modelling' or 'deriving a model', but the term 'model-set' is preferred as long as the modelling result is a description with unknown parameters. A *model-set* potentially describes a range of systems. The term *model* refers to the situation where the parameters are known: a model actually describes a single real system (see figure 2.1). Several modelling decisions have been made in the research projects which preceded this thesis (see references at the end of section 2.1).

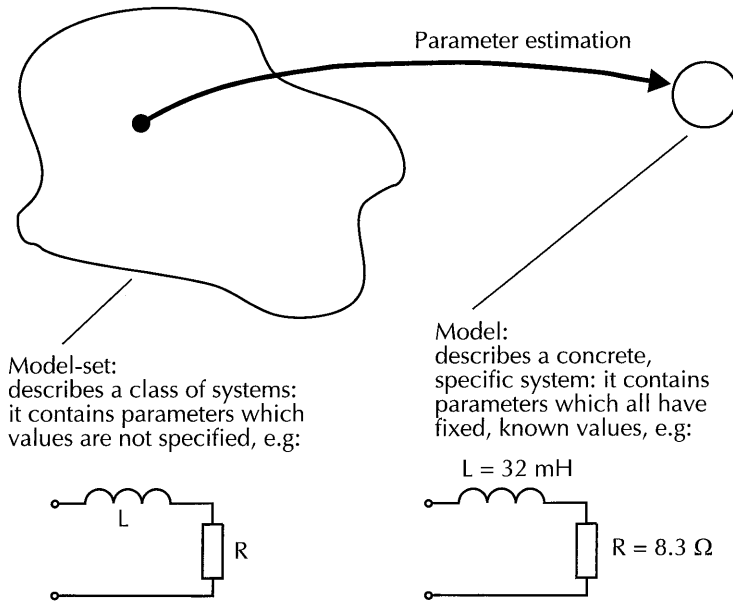


Figure 2.1
Model and model-set

The input-output black-box approach

Although the tools for creating input-output models of the synchronous machine (Ohm's law, the induction laws of Faraday and the Kirchhoff network theorems) were known in the middle of the 19th century, i.e. long before the first synchronous machines were applied in the generation of electrical energy [Nei91], there was no successful mathematical input-output description of the machine until Park presented his *two-axis theory* around 1930 [Par29, Par33].

The essential aspect of Park's theory is that it separates the *rotation of the machine* from its *electrical behaviour*. Park's theory describes the machine by (see figure 2.2):

- two so-called *axis models* (a *direct-axis* model and a *quadrature-axis* model);
- a transformation matrix for the stator quantities, called after Park.

(For the conditions under which the Park-transformation may be applied, see section 3.1).

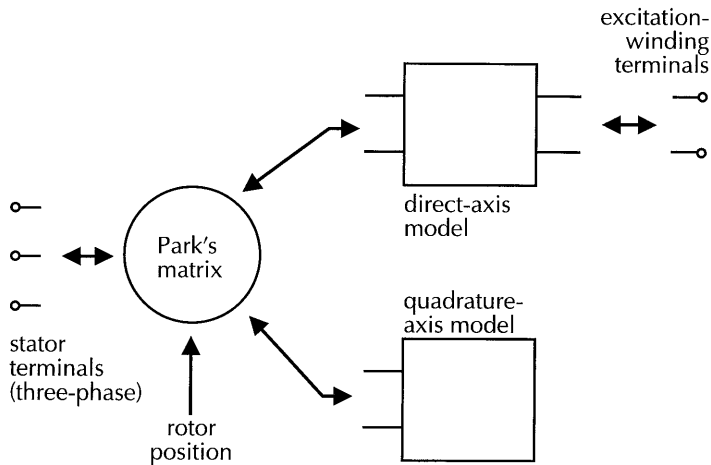


Figure 2.2
Park's two-axis theory for the synchronous machine

The axis models are *independent of rotor position*, and they are *baseband models*, i.e. the frequency band of the axis-model input and output signals is centred around 0 Hz. The rotor position appears only in the Park matrix, which modulates the stator quantities of the axis models, giving the actual stator quantities a frequency content which centres around the rotor angular frequency.

Since Park's matrix does not contain any parameters, Park's theory allows the machine to be modelled completely by two models which are independent of rotor position (if necessary even linear). This is the crucial aspect which is responsible for the fact that the theory is still widely used. This thesis is no exception. More details of the Park-transformation are given in chapter 3, where the model of the machine with rectifier is described.

Axis models

Park's axis models are constructs without a physical counterpart. But several aspects of the axis models are quite easily given a physical interpretation, causing the *electrical network* to become a popular form to describe the axis models. Published network models consist of resistances and coupled inductances, and the network structure is usually chosen such that it reflects the main flux paths of the machine. Individual network elements represent the losses in the machine, the excitation winding and the damper windings. Some of the circuit elements (usually the so-called *synchronous inductances*) may be non-linear, to account for saturation (see e.g. [ELS92]).

Although the ability of the network model for physical interpretation is an aid in understanding the system, a network model has also the disadvantage that a given model order and terminal behaviour may be realised by many different networks. To reduce the variability, the network topology is chosen fixed, which creates two problems concerning identification:

- The network may be such that its elements may not be identifiable from terminal measurements, e.g. because of their number, or because of structural interdependency. This situation may be hard to detect, and even harder to avoid.
- With a fixed topology, a network has a *fixed order*. If the network serves as a model-set, this complicates order tests.



For some specific network models, the order can be easily changed by adding or removing 'damper windings', see e.g. [Hoe90], or the Appendix of [IEE87]. For other models, such as the one adopted in [Hoe88], this is not the case.

Model choices

In the research projects preceding this thesis [Hoe88, Hoe89a, Hoe89b, Hoe90, Vle92b], electrical networks were adopted to describe Park's axis models, since the choice complied with all the criteria formulated in section 2.1. To reduce complexity, both axis models were chosen to be linear.

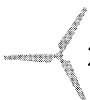
The range of operating conditions for which the model should be valid, should coincide with common operating conditions of a machine in a wind-energy system: powers from 0 up to rated power, and speeds from 0.7 to 1.1 times rated speed. Since the generator of the AC-DC-AC system of figure 1.1 decelerates when the wind velocity decreases, low speeds and low powers occur simultaneously. Because the voltage of the DC-circuit is more or less fixed, a DC-current can only be generated by increasing the excitation-winding current, which drives the machine into saturation. Therefore, saturation will affect the validity of the model at low speeds and low powers.

Dynamically, a range from 0.1 to 10 Hz is desired for signals pertaining to Park's axis models: the machines of our interest (100 kVA) have no time-constants above 10 s (which corresponds to 0.1 Hz), and 10 Hz is well above the frequency of the observed oscillations (around 1 Hz).

Since the most important source of non-linearity, saturation, only plays a role at relatively unimportant operating conditions, choosing linear axis models is not as unrealistic as may seem.

Furthermore, the model is considered a starting point. The performance of the identified linear axis models is used to decide whether the model and/or the demanded range of operating conditions needs to be changed. The systems which have been identified so far, have been a reason to change the model order, but not to give up the linearity or to decrease the range of valid operating conditions.

Due to the network-model disadvantages mentioned above, this thesis uses an alternative linear description of the axis models: the transfer functions which relate the model inputs and outputs, see section 2.4. This choice allows a more straightforward identification procedure, including order tests, at the expense of lacking much of the ability for physical interpretation.



2.3 The identification experiment

Once the synchronous-machine model-set has been established, an identification experiment must be chosen or designed. The experiment must produce sufficient information about the system under test, so that values may be determined for the parameters which appear in the model-set.

As already stated in chapter 1, the identification experiment needed to be as simple as possible. The criteria are as follows:

- X1: The measurements should have a low power consumption (and therefore low voltage measurements are preferred).
- X2: The measurement equipment should be compact.
- X3: Terminal measurements should be sufficient.
- X4: Measurements should be possible while the machine is at standstill.
- X5: The measurement time should be limited.

Identification experiments and tests

In the literature on synchronous-machine identification, the phrase 'identification experiment' is rarely used. Instead, 'tests' are described. Although a test is not completely equivalent to an identification experiment (especially in older literature, it means both the identification experiment and the subsequent data-processing), in this thesis no clear distinction between both will be made.

Searching the literature

An obvious place to search for usable identification experiments, is the literature which concerns our specific application of the synchronous machine (i.e. with a three-phase bridge rectifier). About every second publication in this field describes simulations of the system, and therefore needs a synchronous-machine model including parameter values (for an overview see [Owe93]). However, information with respect to *how* parameter values are obtained, is usually absent. In some studies, references are given to the source of the parameters [Abo88, Ser88, ElH89, Kin89, Hoe88], but these should be treated with some reluctance: in e.g. [Abo88] the parameter values are taken from another paper which in its turn does not clarify their source. In [Wil95], a finite-element model of the synchronous machine is used, but the source of the information needed to obtain this model, remains undescribed. Summarising, the literature on the synchronous machine with rectifier is of no aid in our search for an identification experiment.

The literature which covers the identification of synchronous machines in general, has more to offer. The most prominently described identification experiment is the *sudden three-phase short-circuit test* (SSC). In the decades before the 2nd world war, the utilities' prime interest was to predict and eventually control short-circuit currents, which caused the SSC test to become popular [Wri31] and even standardised. In the past decades, attention has shifted to accurate stability analysis, safeguarding and control of increasingly complex power networks, but still the SSC test is often proposed and used for synchronous-machine identification.

The sudden three-phase short-circuit test

In the SSC test, the phase-current responses are measured after a sudden three-phase short-circuit (see figure 2.3), with the machine initially running at rated speed without load. The test has several disadvantages, and many publications propose to enhance the standardised SSC test procedure:

- From the standard test procedure only a direct-axis model may be identified. Additional procedures are proposed to enable full identification of the machine, i.e. including a quadrature-axis model, from the SSC-test data [Kam90, Bis93, Kam94a].
- In practice some requirements for the test are difficult to realise (especially constant speed and constant excitation-winding voltage during the test). Suggestions are given for dealing with these difficulties [Kam90, Kam91].
- The standardised data-processing is essentially carried out by hand. This is considered subjective, incomplete and inaccurate. Better ways of processing the measurement data are proposed, mainly by using estimators [DeM81, Bed88, Alv89, Jin90, Kam91, Erl94, Kam94a, Kam94b].
- The theory behind the SSC test involves a number of simplifying assumptions. Some of these may be avoided [Sha74, Sha77, Alv89, Kam90].



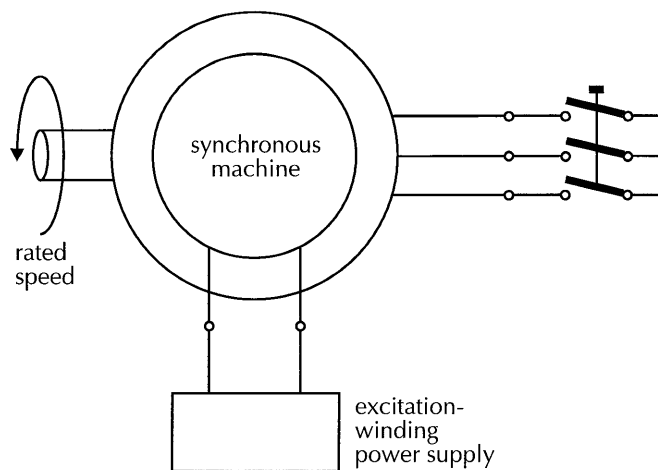


Figure 2.3
The sudden three-phase short-circuit test

Despite its disadvantages, the test continues to be a benchmark, and most publications on synchronous-machine identification refer to it. For our case, the SSC test is not suitable, since the test requires a running machine.

Standstill tests

Due to the disadvantages of the SSC test, some authors propose to replace it by alternative tests which are conducted with the machine at standstill. Standstill tests are very attractive from a practical viewpoint, since driving the machine is often a serious complication of the measurement set-up, if it is at all possible.

As for the SSC test, the starting point for standstill tests is Park's two-axis theory. From this theory it follows, that for some specific rotor positions the behaviour of the machine is described by just one of the two axis models. This means that information may be gathered about the whole machine by two successive measurements which have the rotor fixed at two of these positions (for more details, see chapter 4).

The two essential criteria for applicability of a standstill test are, that the stator windings are distributed sinusoidally (required for Park's theory to be applicable), and that the stator iron has good magnetic qualities (low hysteresis, low loss). The second criterion ensures that the flux distribution during the test is representative of the distribution in a rotating machine (for critical remarks, see [Kam92, ElS93, Bac95]).

Standstill tests are described in a general sense by [Dan86, Rit86, Kam91, Kam92, Bey94], and some criticism may be found in [DeM83, Dan86, Jac87]. Several kinds of excitation signals have been reported:

- step excitation [Rit86, Cal86];
- ramp excitation [Iri86];
- sinusoidal excitation (SSFR) [Wat73, IEE87];
- random excitation [Bol76, Bol82, Tou94].

The *standstill frequency-response (SSFR) test* using sinusoidal excitations, has been standardised [IEE87, IEC85], and described in comparison to other tests in [Sau91, Key92b]. The IEC-standard 34-4 [IEC85] also includes two step-excitation standstill tests: the DC-decay test and the sudden-DC test. Significant progress has been

reported for the sinusoidal excitation, e.g. by using a multisine excitation [Kam92, Bey94]. Research on the random excitation, e.g. using pseudo-random binary noise sequences, has continued within the specific field of on-line testing (see *Other tests*).

In most standstill-test descriptions, the stator windings are used to excite the machine. In this configuration, the resistance of the stator windings contributes considerably to the system response. Since the resistance is sensitive to temperature changes, and since this phenomenon is usually unmodelled, stator winding temperature changes may be a source of identification errors. The standards suggest cooling the winding, but in the literature precautions are rarely mentioned. Measures seem to be necessary only for long measurements, e.g. for the SSFR test at low frequencies.

Three regularly used standstill tests will be discussed in more detail below.

The standstill frequency-response (SSFR) test

The standstill frequency-response test (SSFR) is based on the fact that a linear system is fully characterised by its response to a range of sinusoidal input signals. The experimental set-up is sketched in figure 2.4.

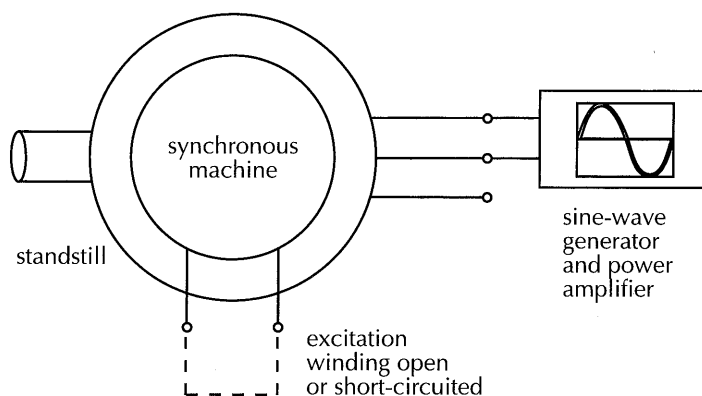


Figure 2.4
The standstill frequency-response test

Characteristic aspects of the test in its standardised form are the long overall duration of the test, due to the fact that for a common machine the measurement needs to be repeated for quite a number of frequencies, and the requirement of large signal amplitudes (see below, under *Hysteresis and saturation*). To alleviate the burden of measurement length, modern test set-ups are largely automated (see e.g. the discussion in [Bey94]), or the sinusoidal signals are replaced by broad-band signals, e.g. multisines (a sum of a large number of sine waves) or random signals (see references above).

A major complication of the SSFR test in its standardised form is the effort needed to keep the stator winding temperature constant. High-frequency measurements are difficult because of the inductive character of the machine: to obtain a constant current amplitude at all frequencies, the necessary voltages may become very high.



The DC-decay test and the sudden-DC test

The DC-decay test and the sudden-DC test apply a step excitation to the system under test. In the DC-decay test the step excitation is generated by short-circuiting two stator phase windings, in which a DC-current is flowing. In the sudden-DC test, the step excitation is generated by switching a current-source-like device onto two stator phase terminals (see figure 2.5).

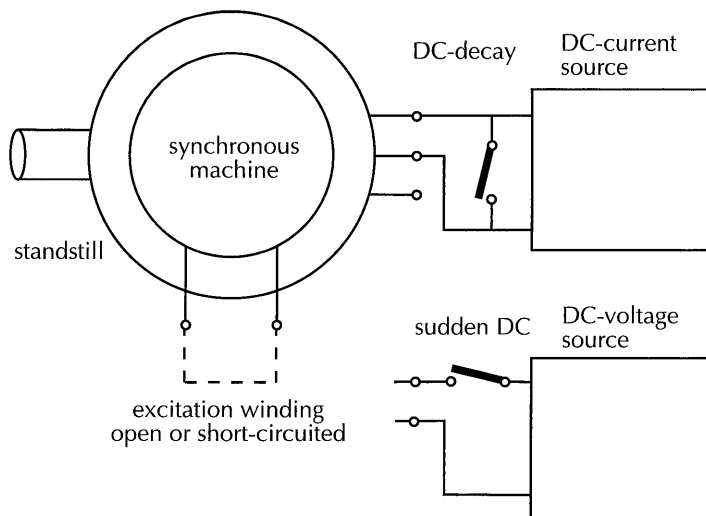


Figure 2.5
The DC-decay test and the sudden-DC test

Ideally, the obtained data lead to the same transfer functions as the SSFR test, but due to the step spectrum, the presence of noise and of non-linearities, the transfer functions obtained from the DC-decay test and the sudden-DC test are inferior. On the other hand, the main disadvantages of the SSFR test are absent: the measurement is short (in the order of seconds), and much smaller measurement signal levels may be used, provided the machine is brought into a fixed magnetic state before the measurement (see below, under *Hysteresis and saturation*). Due to the short measurement length and the small signal amplitude the temperature effect on the stator resistance can be kept low.

The main practical problem of the DC-decay test is the *preliminary magnetisation*: the machine must be brought in a fixed magnetic state prior to the actual test, by a large current. The necessary power source (not drawn in figure 2.5) must be sufficiently large to saturate the machine, and it must also be a *controlled* source since the current transition from saturation level back to measurement level must be achieved carefully (without undershoot).

The sudden-DC test also requires preliminary magnetising and demagnetising, but a controlled source is not necessary. Thus, the practical problem of the DC-decay test is avoided by the sudden-DC test.

Another practical problem is the choice of switch: it should close without bouncing. If a thyristor is used instead of a switch, the residual voltage across the thyristor is not negligible and must be accounted for in the data-processing to follow. Neither description in [IEC85] accounts for this effect. In fact, they assume that the step response is ideal.

Other tests

All synchronous-machine identification experiments discussed so far have in common that the machine under test has to be taken out of regular operation. This may not be practical or possible. *On-line tests* have been described which collect test data while the machine remains operational [Lan83, Fai90, Hua94, Ma_94, Wan95]. The tests aim at continually identifying the machine under different operating conditions, usually by assuming linearity around a fixed operating point. For our research, this technique might be applicable in the future, but for now it is too unpractical.

In still another class of papers, the need for tests is largely eliminated by proposing *finite-element techniques* to calculate synchronous-machine parameters from design data (geometry, materials used) [Min83, Jac87, Non94]. Since design data are hardly supplied by the machine manufacturer, the finite-element technique does not qualify for our research.

Choosing an identification experiment

From a theoretical viewpoint, the results of the published identification techniques are impressive, although much experimental verification is still lacking. There is no standard technique which may be adopted right away, but there is a large choice of *possible* techniques.

Criterion X4 (page 18) restricts the choice to standstill tests. Standstill tests primarily differ on the kind of excitation applied. There are two important aspects on which these excitations ought to be compared:

- the ability of the excitation signal to *persistently excite* the system under test;
- the behaviour of the excitation signal in the presence of *hysteresis and saturation*.

Persistent excitation

A persistently exciting signal has signal energy at every frequency which is of interest for the identified system. Figure 2.6 shows (idealised) spectra of the excitations mentioned earlier. With respect to persistent excitation, the step excitation and ramp excitation perform considerably worse in the high-frequency region than the other two, which usually is a reason to be careful in using them (see e.g. [Rak80]). The best choices are the random excitation and the sinusoidal excitation at various frequencies.

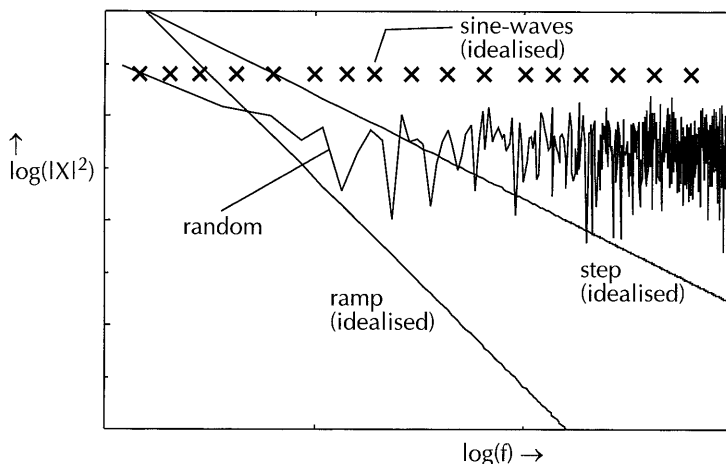


Figure 2.6
Spectra of standstill excitations

Hysteresis and saturation

Hysteresis and saturation are non-linear phenomena which may be modelled (see e.g. [Mel88, May91]), but usually they are not. Hysteresis manifests itself in a machine when (part of) its magnetic circuit is excited on a flux level far below the design level. Saturation, on the other hand, is observed when the magnetic circuit is excited near or above the design level. Often the cost of modelling these phenomena (added complexity) outweighs the benefit of a better model. When they remain unmodelled, as is the case in this thesis, they may have an adverse effect on the quality of the identification measurements, which must be considered in the experiment design.

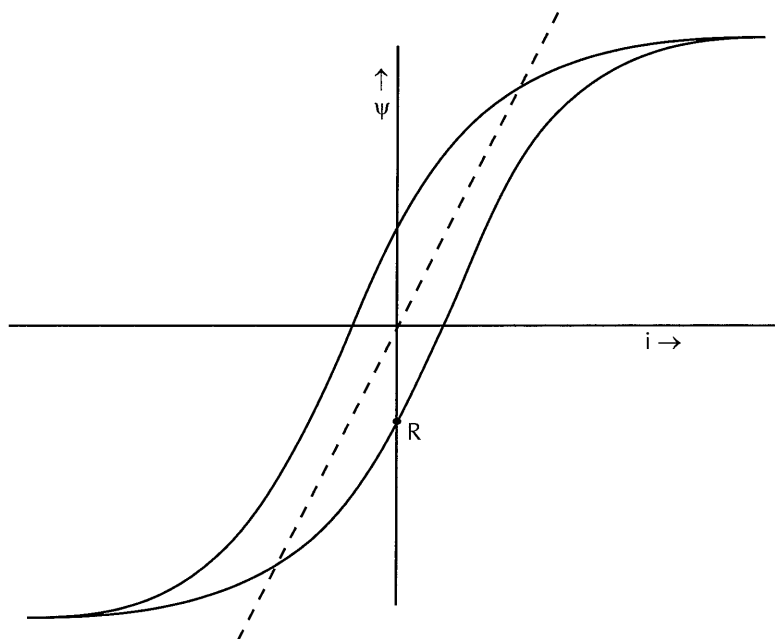


Figure 2.7a
Hysteresis loop with approximate slope

To analyse the interaction of hysteresis, saturation and the excitation signal, consider the following identification experiment: one of the stator windings of the machine is excited while the machine is at standstill. The excited system (in fact equivalent to a smoothing coil) is identified using a very simple linear model-set: a series circuit of a resistance and a self-inductance. The self-inductance is the so-called *synchronous inductance*, a parameter of prime importance for the steady-state behaviour of the machine. In most machine models, this inductance is explicitly present. (The synchronous inductance depends on the rotor position, but this is not essential for the discussion here.)

The model-set implies a linear relationship between the current i through the stator winding and the flux linkage ψ : $\psi = Li$, where L is the self-inductance which must be determined. A value of L is determined by fitting a straight line to the measured current and flux data, the slope of which gives L .

Due to hysteresis and saturation, the relationship between i and ψ is non-linear: it is characterised by a hysteresis loop such as shown in figure 2.7a by the solid line. (The width of the loop is exaggerated, for actual loops see figure 7.2.) The loop gives the maximum and minimum value of the flux ψ as a function of the current i . The

actual value of ψ depends on the history of i , so the identification experiment results in a flux-current trajectory somewhere within the hysteresis loop. The identified value L is the *approximate slope* of this trajectory, and therefore varies depending on:

- the initial magnetic state (the remanent flux);
- the values of the current i during the measurement.

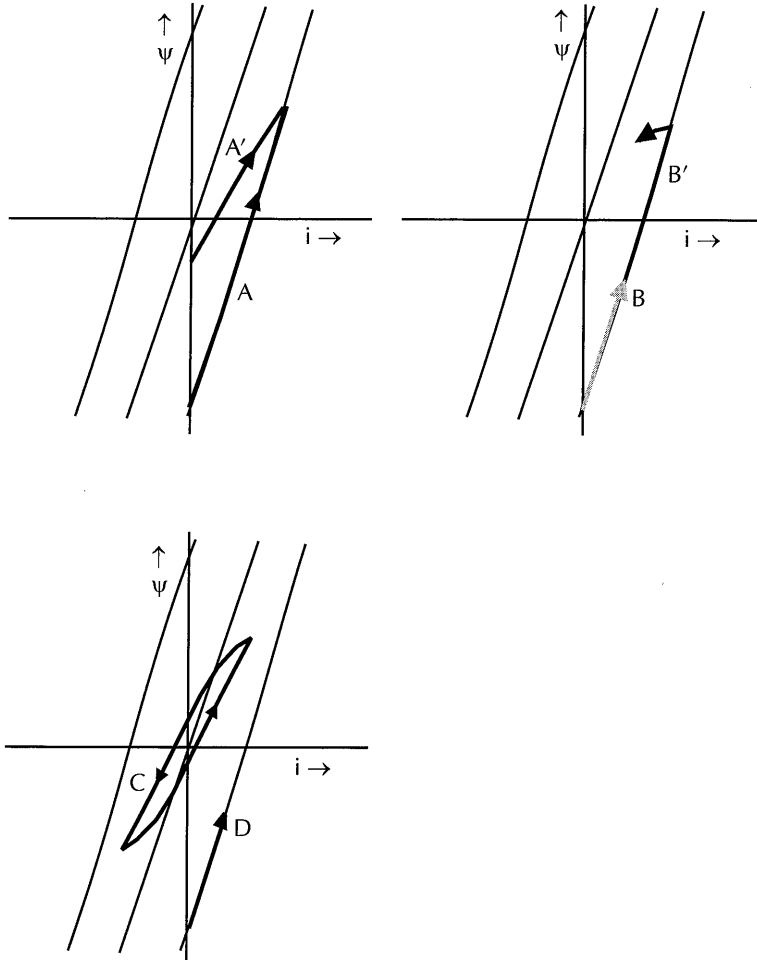


Figure 2.7b
Hysteresis loop trajectories of several standstill excitations

In figure 2.7b some examples have been sketched. Trajectories A and A' result from starting a measurement at a different initial magnetic state. Trajectory A starts at a lower remanent flux than trajectory A', and has a larger slope. Trajectories B and B' show the effect of measurement currents with the same start and end value, one of which (B') exhibits overshoot. The approximate slope of trajectory B' is larger than that of B.

Particularly interesting are the stationary trajectory of a small sinusoidal current (C), and the trajectory of a small current step, with the initial magnetic state on the hysteresis loop (D). Trajectory C is a so-called *minor loop*, which is symmetric with respect to the origin, but which has a smaller overall slope than the full loop



(without the saturated tips). Although trajectory D travels only a small part of the full loop, its slope coincides with the full loop slope. For actual machines, the difference may be as much as 20%.

Random signals also tend to travel minor loops, so random signal excitations lead to similar results as sinusoidal signals. The only way to force a better correspondence with the slope of the full loop, is to use large signal amplitudes.

The consequences of these differences for the identified model depends on what is demanded of the model. If the identified model should enable the calculation of the steady-state, or of large-signal dynamic behaviour, then the slope of the full loop is the best value for L. This value may be obtained in two ways:

- by a *small positive uni-directional signal* (step, ramp) with preliminary magnetisation of the magnetic circuit, so that the initial magnetic state is fixed on the low boundary of the hysteresis loop (location R in figure 2.7a, see e.g. the description of the DC-decay test, in [IEC85]);
- by a *large bi-directional signal* (sinusoidal, noise); data obtained from *small bi-directional signals* (5% of rated value) may be 'corrected' on an ad hoc basis, see [Dan86, IEE87].

If the identified model should enable the calculation of small-signal dynamic behaviour at given operating conditions, these conditions determine which slope is the best value for L. In this case small bi-directional signals which travel minor hysteresis loops, may give good results. However, they do not fulfil our model criterion M3 (section 2.1).

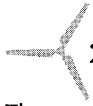
For additional discussion on this topic, see e.g. [Min86].

The step-response test

From the discussion above it may be concluded that with respect to the excitation signal, the demand of persistent excitation conflicts with the demand of practicality (i.e. the demand of a small excitation signal generated simply).

For our situation, simplicity of the identification experiment was an important criterion (see section 2.3). As a compromise between persistent excitation and ease of implementation, the *standstill step-response test* was chosen. The small uni-directional step excitation is generated very easily, and although its performance with respect to persistency is not the best possible, experiments have shown that a two decade bandwidth is possible, which is sufficient (see end of section 2.2). The preliminary magnetisation requires a current much larger than the response current, but the way in which it is generated is not critical. For the machines we tested (appr. 30 kVA), a 12V battery and a switch were quite sufficient to generate the current.

In the literature, standstill step-response test procedures have been described which try to approximate an *ideal* step (i.e. zero before the step moment, and a constant non-zero value after): [Cra82, Rit86] and [IEC85] (the DC-decay test and the sudden-DC test). It is much simpler, however, not to demand an ideal step, but generate a roughly step-like excitation signal. This, finally, is the identification experiment we adopted. It has been published previously in [Hoe89a, Hoe90, Vle90, Vle92a] under the name *Modified Step-Response (MSR)* test. Simplified step-response tests have also been proposed by Boje e.a. [Boj90] and by Keyani e.a. [Key94, Tum95]. With respect to asynchronous machines, a simplified step-response test has been described in [Ruf92, Moo94]. The Modified Step-Response test is described in detail in chapter 4. Topics related to the identification experiment, such as the specific choice of the step-excitation source and preventing aliasing, are discussed in chapter 6.



2.4 Parameter estimation

The next step in the identification process is the choice of a specific model from the model-set, using the measurement data. Two aspects of this step are:

- the choice of the appropriate model order;
- the calculation of the values of the model parameters

Both aspects centre around the *estimator*, a (usually complex) numerical tool which calculates parameter values given a model-set and a set of measurement data.

Since the literature does not offer a specific strategy with respect to parameter estimation using step-response data, we shall try to describe one in this thesis which is as straightforward as possible, and which uses standard techniques and commonly available software.

The estimator

The *estimator* calculates parameter values given a model-set and a set of measurement data. Usually the estimator takes the form of an optimisation: it determines parameter values $\underline{\theta}_{\min}$ which minimise a specific function E of the parameters $\underline{\theta}$, the measured input data \underline{X} and the output data \underline{Y} . Mathematically this may be formulated as:

$$\underline{\theta}_{\min} = \arg \min_{\underline{\theta}} (E(\underline{\theta}, \underline{X}, \underline{Y})) \quad (2.1)$$

Since there is always some uncertainty in the calculated values $\underline{\theta}_{\min}$ due to the presence of noise, measurement errors or modelling errors, the calculated values are *estimates* of the (theoretical) true model parameters, which explains the word 'estimator'.

In the literature on synchronous-machine identification, no final statement about choosing an estimator may be found [Key89, Key92a, Key92b, Kam92]. Our main criterion for the estimator is (see chapter 1):

- E1: the estimator should allow stressing model accuracy in the frequency band around 1 Hz.

For this reason, a frequency-domain estimator is preferred. A frequency-domain estimator also allows easy monitoring of possibly adverse effects of the uneven distribution of the step-signal energy over the frequency axis (see figure 2.6).

Data preprocessing

To be able to apply a frequency-domain estimator, time-domain data must be transformed into the frequency domain. The Discrete Fourier Transform (in the form of the FFT-algorithm) is chosen as transformation tool. The exact implementation is described in section 5.1.

Frequency-domain estimator

The estimator finds values of the model parameters. As motivated in section 2.1 (and chapter 3), the models used in this thesis are transfer functions. These transfer functions are parametrised as a polynomial fraction:

$$H(\underline{\theta}, s) = \frac{B(\underline{\theta}, s)}{A(\underline{\theta}, s)} = \frac{b_m s^m + b_{m-1} s^{m-1} + \dots + b_1 s + b_0}{a_n s^n + a_{n-1} s^{n-1} + \dots + a_1 s + 1} \quad (2.2a)$$

and the parameters $\underline{\theta}$ are therefore the coefficients of the numerator and denominator polynomials $A(\underline{\theta}, s)$ and $B(\underline{\theta}, s)$:

$$\underline{\theta} = (b_m, b_{m-1}, \dots, b_0, a_n, a_{n-1}, \dots, a_1) \quad (2.2b)$$



The initial estimator choice was a straightforward least-squares (LS) estimator which fitted a transfer function parametrised as in (2.2), to the frequency-domain input and output data. If the input and output samples at angular frequency ω_k are denoted by X_k and Y_k , where $k \in \{1..N\}$ with N the number of samples, and the transfer function is denoted by $H(\underline{\theta}, j\omega)$, where $\underline{\theta}$ are the parameters of the transfer function (e.g. the coefficients of its numerator and denominator polynomials), then the estimator minimised the loss E defined by:

$$E = \sum_{k=1}^N e_k e_k^* \quad (2.3)$$

where $*$ denotes conjugation and where the residuals e_k are given by:

$$e_k = \frac{Y_k}{X_k} - H(\underline{\theta}, j\omega_k) \quad (2.4)$$

Since (2.4) is not linear in the parameters $\underline{\theta}$, an iterative minimisation algorithm must be used to minimise E with respect to the parameters. The minimal value of the loss E may be interpreted as a measure of the overall fit of the estimated model to the measured data. Initial parameter values for the iteration were obtained from a second, non-iterative estimator [Lev59].

Although the estimator is attractive because of its low complexity, it does not work properly in conjunction with DFT-transformed step-response signals. Since the DFT results in frequency samples which are linearly spaced along the frequency axis, and since the step-response signal to noise ratio is approximately inversely proportional to frequency, there is a relative abundance of high-frequency samples with a large noise content. This results in poor transferfunction fits, even at low frequencies where the step signals have sufficient energy.

Accounting for the step-signal spectrum

In a general sense, solutions to this problem may be obtained by introducing *weighting factors*, i.e. by replacing (2.4) with:

$$e_k = w_k \left(\frac{Y_k}{X_k} - H(\underline{\theta}, j\omega_k) \right) \quad (2.5a)$$

where w_k are weighting factors chosen in some predetermined way.

There are several options. To account for the fact that the step-response signal to noise ratio is approximately inversely proportional to frequency, the following weighting factors may be applied, which give more weight to measurements with a lower frequency (and, at least expected, a larger signal to noise ratio):

$$w_k = \frac{1}{\omega_k} \quad (2.5b)$$

Alternatively, weighting factors can be chosen which reflect the actual noise in X_k and Y_k , if these values are known. The maximum likelihood (ML) estimator described in [Pin90] implements this choice. Instead of (2.5a) it has:

$$e_k = w_k (B_k(\underline{\theta}, j\omega_k) X_k - A_k(\underline{\theta}, j\omega_k) Y_k) \quad (2.6a)$$

with weighting factors

$$w_k = \frac{1}{\sqrt{\sigma_{Y_k}^2 |A_k(\underline{\theta}, j\omega_k)|^2 + \sigma_{X_k}^2 |B_k(\underline{\theta}, j\omega_k)|^2 - \text{Re}(\text{cov}(X_k, Y_k) A_k^*(\underline{\theta}, j\omega_k) B_k(\underline{\theta}, j\omega_k))}} \quad (2.6b)$$

The estimator is considered a good choice compared to other frequency-domain estimators [Pin94], and is implemented as the *elis*-estimator in the Matlab Frequency-Domain Identification Toolbox [Kol94].

By applying the *elis* ML-estimator, or by applying estimator (2.3)/(2.5), the problem of the LS estimator (2.3)/(2.4) with the step-signal spectrum is largely solved, but still the high-frequency region of the transfer function receives some extra emphasis. Experiments with MSR test data show that often one may simply disregard samples above a certain frequency to neutralise this emphasis. The exact location of this boundary depends on the specifics of the measurement and the system under test. The topic is analysed in more detail in section 7.7 (page 99).

Choice of the estimator

Although there are several frequency-domain estimators available from the literature, the discussion above shows that the actual choice was between just two: the LS-estimator of equation (2.3)/(2.5), and the *elis* ML-estimator. With appropriate decimation of the high-frequency samples, both estimators gave satisfactory results. Since the *elis*-estimator is available within Matlab, this estimator was chosen.

Order tests

In most identification schemes, the model order of a model-set is not fixed, but left to be determined on the basis of the identification experiment data. An appropriate model order is determined by an *order test*. A straightforward implementation of an order test is to estimate the values of the model parameters for several values of the model order, and compare the results with respect to some characteristic aspects. We have used the loss E , equation (2.3), and the location and the variance of the poles and zeros of the estimated model (for more details see sections 7.3 - 7.5).

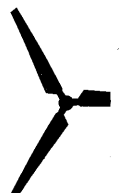


2.5 Evaluation of the identification results

The last step in the identification process is the validation or evaluation of the identification results. The results of the identification procedure are analysed, either with or without the use of auxiliary measurements.

Evaluation in the literature

In the literature, identified synchronous-machine models are mostly evaluated without using auxiliary measurements. In a couple of papers which survey modern identification procedures for use with synchronous machines (e.g. [Key92a]), *parameter errors* are presented. A procedure is followed as outlined in figure 2.8. No actual measurements are carried out; the resulting parameter errors are often well below 1%, which should be interpreted as the error added by the identification procedure.



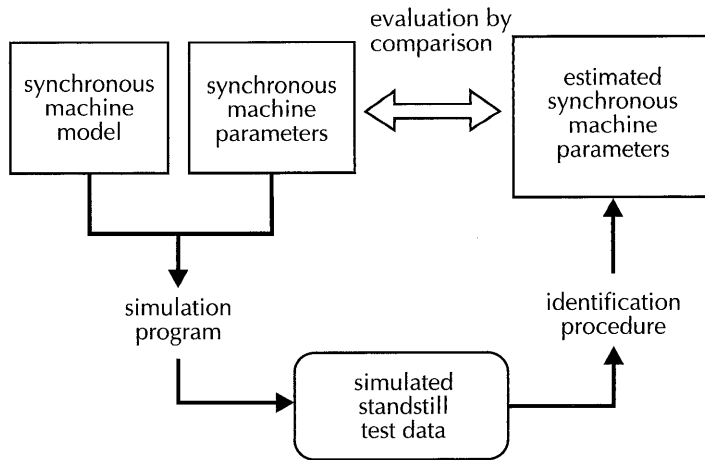


Figure 2.8
Identification evaluation based on simulated test data

For the validation of actual identification results, the concept of parameter errors is meaningless, since the reference values (the 'true' parameters) are unknown. Residual analysis, as suggested generally by identification textbooks, is not found in the literature on synchronous-machine identification.

Auxiliary evaluation measurements

Identification results may also be evaluated using auxiliary measurements, but in the literature on synchronous-machine identification this is very uncommon. Cross-checking the identification result with a second measured response, as suggested by identification textbooks, is rarely done. An evaluation using several distinct identification techniques is found in [Erl94]. This study shows, for a number of common steady-state machine parameters, differences of at least 10% when varying the identification procedure.

Evaluation of the identified models in this thesis

Considering the literature on identification in general and on synchronous-machine identification in particular, in this thesis the identification results are evaluated with and without the use of auxiliary measurements.

The following two checks do not require additional measurements:

- How is the fit between the estimated transfer function and the measured frequency-domain data (checked by inspection) ?
- What are the characteristics of the residuals (e.g. whiteness) ?

These checks may serve as a minimal validation, and do not depend on the context within which the MSR test is applied. Therefore, they are considered part of the MSR test identification procedure.

In chapter 7, where the MSR test is evaluated as a whole, the validation of the identification results will be given more attention, also using auxiliary measurements.

A MODEL OF THE SYNCHRONOUS MACHINE WITH RECTIFIER

In this chapter a model of the synchronous machine with diode-bridge rectifier is presented and discussed. First the individual models are described separately, and then both models are combined using the concept of the internal machine.

3.1 A model of the synchronous machine

The choice of the model of the synchronous machine, with which the combination of machine and rectifier is analysed, is a topic which has already been dealt with some time before the research of this thesis started. The model is described in [Hoe88, Hoe89a, Hoe90], and the model has been enhanced by adding saturation [Hoe89b] and a model of the exciter [Vle92b].

In this section a model of a salient-pole synchronous machine will be presented similar to the model derived in [Hoe90], i.e. without modelling saturation and exciter. However, unlike [Hoe90], the number of damper circuits on the rotor will be free. The model is given for an arbitrary number of pole-pairs; figure 3.1 depicts the special case with only one pole-pair. The machine has the usual three stator windings, each 120 (electrical) degrees apart. The stator windings are star connected, without external connection. The rotor has only one accessible circuit, the *field* or *excitation* winding, and an indefinite number of additional, inaccessible circuits which represent the damping effect of the machine. The inaccessible circuits are not sketched in figure 3.1.

The magnetic circuit of the rotor is symmetrical with respect to two mutually perpendicular axes (the *direct* and the *quadrature* axis), see figure 3.1, and the magnetic circuit of the machine is supposed to be *linear*. This means that saturation and hysteresis are neglected.

Saturation may be modelled by adding non-linear elements to an existing model with a linear magnetic circuit (see e.g. [Hoe89b]). But if the machine is used in a wind-energy system, the urge to model saturation is relatively small (see section 2.2). Hysteresis is a phenomenon which may be observed, but modelling this effect is not expected to pay off (it is very complicated, see e.g. [May91]).

For the rotor, it is supposed that the excitation winding has its field axis on the direct axis, and is symmetric with respect to this axis. For the stator, it is also supposed that:

- the stator inner side is circular cylindrical and smooth, the effects of slots are neglected;
- the stator windings are distributed sinusoidally along the stator circumference;
- the stator leakage flux is independent of the rotor position.

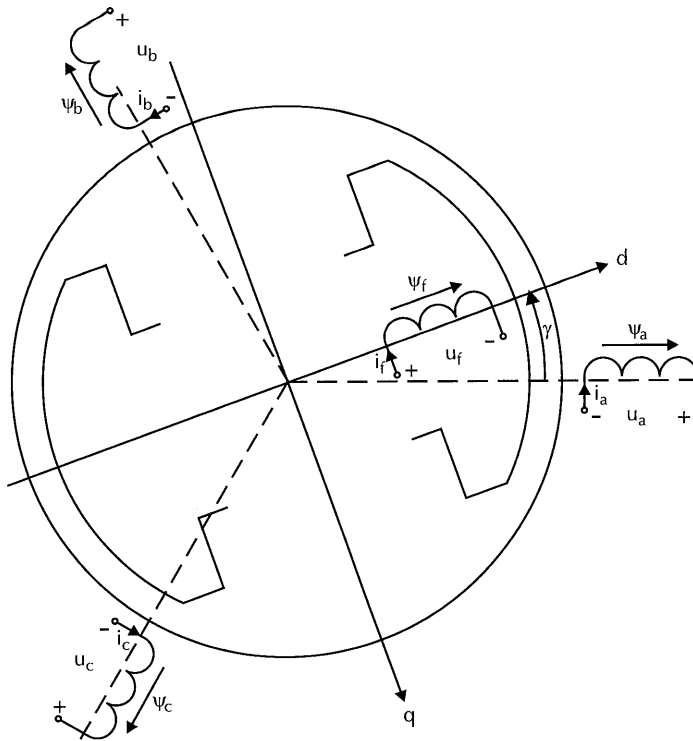


Figure 3.1
Schematic diagram of a salient-pole synchronous machine

The above assumptions are commonly used in textbooks (e.g. [Con51]) to derive the model which is given below. For a derivation refer to [Hoe90] or to the textbooks.

The voltage equations of the synchronous machine

The voltage equations of the machine are conveniently expressed in terms of Park-transformed quantities. The Park-transformation is a transformation which depends on the rotor position γ and the number of pole-pairs p . In its normalised form it is power-invariant, and its transformation matrix \mathbf{P} is orthonormal (its inverse equals its transpose):

$$\mathbf{P} = \sqrt{\frac{2}{3}} \begin{pmatrix} \cos(p\gamma) & \cos(p\gamma - \frac{2}{3}\pi) & \cos(p\gamma - \frac{4}{3}\pi) \\ \sin(p\gamma) & \sin(p\gamma - \frac{2}{3}\pi) & \sin(p\gamma - \frac{4}{3}\pi) \\ \frac{1}{2}\sqrt{2} & \frac{1}{2}\sqrt{2} & \frac{1}{2}\sqrt{2} \end{pmatrix} \quad (3.1)$$

The actual stator phase voltages u_a , u_b and u_c are transformed into u_d , u_q and u_0 (and back) by:

$$\begin{pmatrix} u_d \\ u_q \\ u_0 \end{pmatrix} = \mathbf{P} \begin{pmatrix} u_a \\ u_b \\ u_c \end{pmatrix}, \quad \begin{pmatrix} u_a \\ u_b \\ u_c \end{pmatrix} = \mathbf{P}^T \begin{pmatrix} u_d \\ u_q \\ u_0 \end{pmatrix} \quad (3.2)$$

For the phase currents and phase fluxes the same relations hold. The index 'd' refers to the direct axis, the index 'q' to the quadrature axis. Due to the open star-connection, the homopolar quantity (with index 0) will be equal to zero, and may therefore be disregarded.

Using the generator convention for the stator circuits, the voltage equations of the machine may be expressed in Park-transformed quantities:

$$\begin{aligned}
 -u_d &= R_a i_d + \frac{d\psi_d}{dt} + p \frac{d\gamma}{dt} \psi_q \\
 u_f &= R_f i_f + \frac{d\psi_f}{dt} \\
 -u_q &= R_a i_q + \frac{d\psi_q}{dt} - p \frac{d\gamma}{dt} \psi_d
 \end{aligned} \tag{3.3}$$

R_a is the stator resistance of one phase, R_f is the excitation-winding resistance and γ is the rotor position as defined in figure 3.1. The equations resemble closely the voltage equations of a set of coupled windings, except for two *rotational* terms which depend on the rotor speed $d\gamma/dt$.

The flux-current relationships

Equations (3.1) - (3.3) are still an incomplete description of the synchronous machine, since the fluxes ψ_d , ψ_q and ψ_f depend on the currents i_d , i_q and i_f . Under the assumptions made earlier, the direct-axis quantities ψ_d , ψ_f , i_d , and i_f are independent of the quadrature-axis quantities ψ_q and i_q .

Since the magnetic circuit of the machine is supposed to be linear, the direct-axis quantities ψ_d , ψ_f , i_d , and i_f constitute a linear 2-port with equations:

$$\begin{aligned}
 \Psi_d &= L_{do}(s)I_d + L_{dfo}(s)I_f \\
 \Psi_f &= L_{fdo}(s)I_d + L_{fo}(s)I_f
 \end{aligned} \tag{3.4a}$$

where capitals indicate Laplace-transformed quantities, and where transfer functions $L_{do}(s)$, $L_{dfo}(s)$, $L_{fdo}(s)$, and $L_{fo}(s)$ have been introduced, which functions depend on the design of the machine. The transfer functions $L_{fdo}(s)$ and $L_{dfo}(s)$ are equal, since linear 2-ports without internal sources are reciprocal. For more details, see chapter 4, equation (4.9).

Similarly, the quadrature-axis quantities ψ_q and i_q constitute a linear 1-port. If again the current is considered as input, the general equation of this 1-port is:

$$\Psi_q = L_q(s)I_q \tag{3.4b}$$

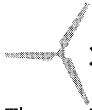
where again capitals indicate Laplace-transformed quantities, and where a transfer function $L_q(s)$ has been introduced, which function depends on the design of the machine.

Transfer functions and identification

Within the context of the synchronous machine, the transfer functions introduced in (3.4) are usually called *operational inductances*. They resemble coefficients of inductance, since they all relate a current to a flux, but they are generally *frequency dependent*, because they include the effect of the inaccessible rotor circuits. In this thesis, however, the more general term 'transfer function' will be used.

The transfer functions of (3.4) are rarely used in this general form. Usually they are parametrised, e.g. by electrical networks (see section 2.2, or [Hoe90, IEC87, Can89] and many others). In this thesis the transfer functions are parametrised in a more general way, by polynomial fractions according to equation (2.2).





3.2 A model of the three-phase diode-bridge rectifier

The rectifier model which is used in this thesis, is a standard model and described in detail in [Hoe90]. It models a three-phase diode-bridge rectifier, which is fed by a three-phase symmetrical voltage source with series commutation self-inductances L_c . The rectified voltage and current are u_g and i_g (see figure 3.2).

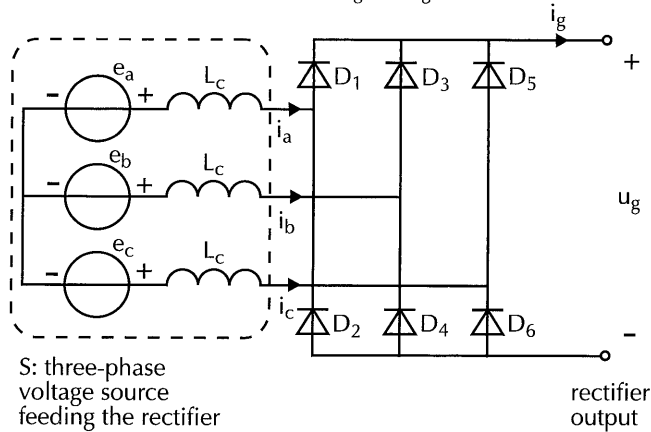


Figure 3.2

Schematic diagram of a three-phase bridge rectifier with AC-voltage source

It incorporates the effect of *simple* commutation (i.e. no more than 3 diodes are conducting at the same time). In the derivation the effect of the ripple on the rectified current i_g is neglected. This implies that the model is only valid for inductive loads, e.g. loads which include a smoothing coil to reduce the ripple on i_g . The diodes are assumed to be ideal switches. The AC-source voltages are sinusoidal, and given by:

$$\begin{aligned} e_a &= \hat{e} \cos(\omega t + \varepsilon) \\ e_b &= \hat{e} \cos(\omega t - \frac{2}{3}\pi + \varepsilon) \\ e_c &= \hat{e} \cos(\omega t - \frac{4}{3}\pi + \varepsilon) \end{aligned} \quad (3.5)$$

The angle ε introduced in (3.5) has no significance for the rectifier model equations, but is necessary when coupling the rectifier model to the synchronous-machine model. The DC-circuit obeys a first-order differential equation:

$$\frac{3}{\pi} \sqrt{3} \hat{e} = 2L_c \frac{di_g}{dt} + \frac{3}{\pi} \omega L_c i_g + \tilde{u}_g \quad (3.6)$$

with the rectified current i_g as state variable, and with inputs \hat{e} (the AC-voltage amplitude) and \tilde{u}_g (the rectified voltage averaged over 1/6 of a period). The equation may be interpreted as representing the circuit depicted in figure 3.3. The additional 'resistance' $\frac{3}{\pi} \omega L_c$ is due to the commutation.

Using (3.5) and the assumption that i_g is constant during the commutation, the following expression for the commutation angle μ (angle of overlap) may be derived:

$$\mu = \arccos \left(1 - \frac{2\omega L_c i_g}{\sqrt{3} \hat{e}} \right) \quad (3.7)$$



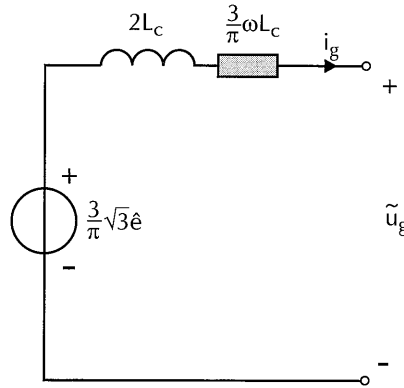


Figure 3.3
DC-circuit representation of a three-phase bridge rectifier

Apart from a fundamental component, the phase currents i_a , i_b and i_c contain harmonics at $6n \pm 1$ times the fundamental frequency ($n = 1, 2, \dots$). Only the fundamental component of the a-phase AC-current i_a , denoted by i_{a1} , will be considered as model output. The fundamental component i_{a1} relates to the input \hat{e} and via (3.7) to the state i_g by:

$$i_{a1} = \frac{3\hat{e}}{2\pi\omega L_c} \left(\sin^2(\mu) \cos(\omega t + \varepsilon) + (\mu - \sin(\mu) \cos(\mu)) \sin(\omega t + \varepsilon) \right) \quad (3.8)$$

Although the model has been derived with constant voltages and currents, the model is also expected to be valid if they vary slowly, i.e. if the spectra of these quantities are low-pass with respect to the commutation phenomena (≈ 300 Hz). The only parameter of the rectifier model is commutation self-inductance L_c . In the next section (page 40) and at the end of section 4.2 the identification of L_c will be described



3.3 Coupling the models of machine and rectifier

In this section, a possible way of coupling the models of synchronous machine and rectifier is discussed. The essence of this way is that the machine model is moulded into the voltage source S of figure 3.2, a three-phase symmetrical voltage source with series self-inductances.

After rewriting the machine model equations of section 3.1 for constant rotor speed, the machine model and the three-phase voltage source S are compared, and conditions are formulated under which the voltage source S may be replaced by the machine model. (The assumption of constant rotor speed is not essential, see [Hoe96], but simplifies the analysis.) Next, a way of obtaining a proper value of the commutation self-inductance L_c is discussed. Finally, the resulting model equations are transformed into a state-space form.

Machine equations with constant rotor speed

If the rotor angular speed $d\gamma/dt$ is constant and equal to ω_m , with ω_m the constant mechanical angular speed of the machine, then equations (3.3) may be transformed into the frequency domain:



$$\begin{aligned}
-U_d &= R_a I_d + s\Psi_d + p\omega_m \Psi_q \\
U_f &= R_f I_f + s\Psi_f \\
-U_q &= R_a I_q + s\Psi_q - p\omega_m \Psi_d
\end{aligned} \tag{3.9}$$

Using (3.4) and the equality of $L_{fdo}(s)$ and $L_{dfo}(s)$, (3.9) becomes:

$$\begin{aligned}
-U_d &= \{R_a + sL_{do}(s)\} I_d + sL_{fdo}(s) I_f + p\omega_m L_q(s) I_q \\
U_f &= sL_{fdo}(s) I_d + \{R_f + sL_{fo}(s)\} I_f \\
-U_q &= \{R_a + sL_q(s)\} I_q - p\omega_m \{L_{do}(s) I_d + L_{fdo}(s) I_f\}
\end{aligned} \tag{3.10}$$

These equations relate the machine voltages and currents (in the frequency domain), while the machine is at constant speed. In (3.10) the excitation-winding current I_f is an input. More common, however, is to assume that the excitation winding is fed by a voltage source. The second equation of (3.10) may be used to exchange the roles of I_f and U_f . The resulting model equations are:

$$\begin{aligned}
-U_d &= \{R_a + sL_d(s)\} I_d - sG_{fd}(s) U_f + p\omega_m L_q(s) I_q \\
I_f &= sG_{fd}(s) I_d + \frac{U_f}{R_f + sL_{fo}(s)} \\
-U_q &= \{R_a + sL_q(s)\} I_q - p\omega_m \{L_d(s) I_d - G_{fd}(s) U_f\}
\end{aligned} \tag{3.11}$$

where two new transfer functions are introduced: the direct-axis synchronous inductance $L_d(s)$ and the direct-axis gain $G_{fd}(s)$. These relate to the transfer functions of (3.10) by:

$$L_d(s) = L_{do}(s) - \frac{sL_{fdo}^2(s)}{R_f + sL_{fo}(s)} \tag{3.12a}$$

$$L_{do}(s) = L_d(s) + sG_{fd}^2(s) \{R_f + sL_{fo}(s)\} \tag{3.12b}$$

$$G_{fd}(s) = -\frac{L_{fdo}(s)}{R_f + sL_{fo}(s)} \tag{3.12c}$$

$$L_{fdo}(s) = -G_{fd}(s) \{R_f + sL_{fo}(s)\} \tag{3.12d}$$

In the remaining part of this thesis, the transfer functions of (3.10) and (3.11) will be referenced often. To facilitate this, the following definitions are introduced:

$$\frac{1}{R_a + sL_d(s)} = \left. \frac{I_d}{-U_d} \right|_{U_f=0} \triangleq Y_d(s) \triangleq Z_d^{-1}(s) \tag{3.13a}$$

$$\frac{1}{R_a + sL_{do}(s)} = \left. \frac{I_d}{-U_d} \right|_{I_f=0} \triangleq Y_{do}(s) \tag{3.13b}$$

$$\frac{1}{R_a + sL_q(s)} = \frac{I_q}{-U_q} \hat{=} Y_q(s) \hat{=} Z_q^{-1}(s) \quad (3.13c)$$

$$\frac{1}{R_f + sL_{fo}(s)} = \frac{I_f}{U_f} \Big|_{i_d = 0} \hat{=} Y_{fo}(s) \quad (3.13d)$$

$$\frac{1}{sL_{fdo}(s)} = \frac{I_d}{U_f} \Big|_{i_f = 0} \hat{=} Y_{fdo}(s) \quad (3.13e)$$

Combination of (3.12d) and (3.13d) gives:

$$Y_{fo}(s) = -\frac{sG_{fd}(s)}{sL_{fdo}(s)} = -sG_{fd}(s)Y_{fdo}(s) \quad (3.14)$$

Comparing the three-phase symmetrical voltage source to the synchronous-machine model

For the comparison of the machine model (3.11) with the three-phase symmetrical voltage source with series self-inductances (source S in figure 3.2), the Park-transformation of the voltage equations of source S is determined. These equations are:

$$\begin{aligned} u_a &= -L_c \frac{di_a}{dt} + e_a \\ u_b &= -L_c \frac{di_b}{dt} + e_b \\ u_c &= -L_c \frac{di_c}{dt} + e_c \end{aligned} \quad (3.15)$$

with e_a , e_b , and e_c given by (3.5).

Using the Park-transformation (3.1) and (3.2) with

$$\gamma = \omega_m t + \gamma_0 \quad (3.16)$$

and

$$\omega = p\omega_m \quad (3.17)$$

to transform the voltages u_a , u_b , u_c , e_a , e_b and e_c , and the currents i_a , i_b and i_c , equation (3.15) becomes:

$$\begin{aligned} u_d &= -L_c \frac{di_d}{dt} - p\omega_m L_c i_q + e_d \\ u_q &= -L_c \frac{di_q}{dt} + p\omega_m L_c i_d + e_q \end{aligned} \quad (3.18)$$



with e_d and e_q constant voltages as given by:

$$e_d = \sqrt{\frac{3}{2}} \hat{e} \cos(\varepsilon - p\gamma_0) \quad (3.19)$$

$$e_q = -\sqrt{\frac{3}{2}} \hat{e} \sin(\varepsilon - p\gamma_0)$$

with ε the angle which appears in (3.5). The result of the transformation is sketched in figure 3.4a (left-hand side of the figure).

In the Park-transformed equations (3.18), the self-inductance terms $L_c di_d/dt$ and $L_c di_q/dt$ are accompanied by controlled voltage sources ($p\omega_m L_c i_q$ and $p\omega_m L_c i_d$). The same self-inductance and controlled voltage sources are now extracted from the respective synchronous-machine axis models (figure 3.4b, right-hand side of the figure). By this extraction, two submodels are created, which are called the *internal direct-axis model* and the *internal quadrature-axis model*. The voltage equations of figure 3.4b are identical to equations (3.18), although now e_d and e_q are not constant voltages. The equations for the internal axis models follow from (3.11) and (3.18). Equation (3.18) may be given in the frequency domain as:

$$U_d = -sL_c I_d + E_d - p\omega_m L_c I_q \quad (3.20)$$

$$U_q = -sL_c I_q + E_q + p\omega_m L_c I_d$$

By substitution of (3.20) into (3.11), we obtain:

$$-E_d = \{R_a + s(L_d(s) - L_c)\} I_d - sG_{fd}(s) U_f + p\omega_m (L_q(s) - L_c) I_q$$

$$I_f = sG_{fd}(s) I_d + \frac{U_f}{R_f + sL_{f0}(s)} \quad (3.21)$$

$$-E_q = \{R_a + s(L_q(s) - L_c)\} I_q - p\omega_m \{(L_d(s) - L_c) I_d - G_{fd}(s) U_f\}$$

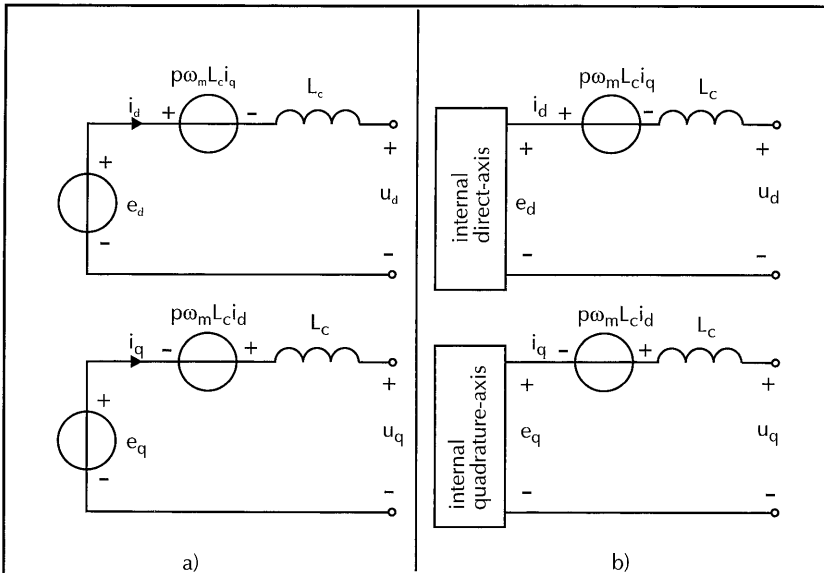


Figure 3.4
Comparison of three-phase symmetrical voltage source (a) to machine axis models (b)

Equation (3.21) gives expressions for the voltages E_d and E_q (in the frequency domain). The internal-machine model equations just slightly differ from the original model equations (3.11). Instead of the $L_d(s)$ and $L_q(s)$ the internal machine has:

$$L_{di}(s) = L_d(s) - L_c \quad (3.22a)$$

$$L_{qi}(s) = L_q(s) - L_c \quad (3.22b)$$

and related impedances:

$$Z_{di}(s) = Z_d(s) - sL_c \quad (3.23a)$$

$$Z_{qi}(s) = Z_q(s) - sL_c \quad (3.23b)$$

Otherwise, the equations are identical. By defining internal fluxes Ψ_{di} and Ψ_{qi} according to:

$$\Psi_{di} = (L_d(s) - L_c) I_d - G_{fd}(s) U_f \quad (3.24)$$

$$\Psi_{qi} = (L_q(s) - L_c) I_q$$

and by using (3.22) and (3.23), the machine model equations (3.21) may be subdivided into two equation sets, each of which contains transfer functions of just one axis:

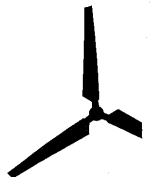
$$\begin{aligned} -E_d &= Z_{di}(s) I_d - sG_{fd}(s) U_f + p\omega_m \Psi_{qi} \\ I_f &= s G_{fd}(s) I_d + Y_{fo}(s) U_f \end{aligned} \quad (3.25a)$$

$$\Psi_{di} = L_{di}(s) I_d - G_{fd}(s) U_f$$

$$\begin{aligned} -E_q &= Z_{qi}(s) I_q - p\omega_m \Psi_{di} \\ \Psi_{qi} &= L_{qi}(s) I_q \end{aligned} \quad (3.25b)$$

We may now compare the model of the three-phase voltages source S (figure 3.4a and equation (3.20)) to the synchronous-machine model (figure 3.4b and equation (3.25)). The main difference is, that where the three-phase source has *constant voltage sources* e_d and e_q , the machine has *controlled voltage sources*, namely the internal-machine axis models, the equations of which are given in (3.25). The requirement for the coupling of the rectifier model and the synchronous machine is therefore that the internal-machine voltages E_d and E_q are constants, which is obviously not the case.

However, considering the assumption made at the end of section 3.2 (that slow variations are allowed), it may be asked if there are conditions under which E_d and E_q only vary slowly. Variations in E_d and E_q are caused by the external excitation-winding voltage U_f and by the stator currents I_d and I_q . The spectra of I_d and I_q are as wide as the spectra of the model inputs U_f and U_g , since all higher harmonics in the phase currents are neglected. Only the fundamental component is included in the model, which transforms into slowly varying currents I_d and I_q . Therefore, the internal stator voltages E_d and E_q vary slowly if U_f and U_g vary slowly, i.e. their frequency content is limited to a small frequency band around 0 Hz.



A sufficient condition for coupling the synchronous-machine model to the rectifier model is therefore that the model inputs U_f and \tilde{U}_g are low-pass with respect to the commutation phenomena (≈ 300 Hz).

The choice of the commutation self-inductance L_c

A value for L_c is commonly calculated by [Büh77, Hoe84a, Hoe90]:

$$L_c = \frac{L_d'' + L_q''}{2} \quad (3.26)$$

where L_d'' and L_q'' are the subtransient inductances of the respective axis models. In principle, L_d'' and L_q'' are quantities which are only defined if $L_d(s)$ and $L_q(s)$ are given by their poles and zeros. Suppose that $L_d(s)$ is given by:

$$L_d(s) = L_d(0) \frac{\prod_{i=1}^n (1 + \tau_d^{(i)} s)}{\prod_{i=1}^n (1 + \tau_{do}^{(i)} s)} \quad (3.27)$$

where $\tau_d^{(1)} = \tau_d'$, $\tau_{do}^{(1)} = \tau_{do}'$, $\tau_d^{(2)} = \tau_d''$, etc., and n an integer. Now L_d'' is defined by:

$$L_d'' = \lim_{\omega \rightarrow \infty} L_d(j\omega) \Big|_{n=2} = L_d(0) \frac{\tau_d^{(1)} \tau_d^{(2)}}{\tau_{do}^{(1)} \tau_{do}^{(2)}} \quad (3.28)$$

The definition is only valid for 2nd order models of $L_d(s)$ ($n = 2$). For higher order models an approximate value of L_d'' may be given if an ω can be found which satisfies:

$$\begin{cases} \omega \tau_d^{(i)} \gg 1, & \omega \tau_{do}^{(i)} \gg 1, & i = 1, 2 \\ \omega \tau_d^{(i)} \ll 1, & \omega \tau_{do}^{(i)} \ll 1, & i > 2 \end{cases} \quad (3.29)$$

If ω satisfies (3.29), then $L_d(j\omega)$ approximately equals the right-hand side expression of (3.28), and may therefore be interpreted as the subtransient self-inductance L_d'' . For L_q'' and $L_q(s)$ similar equations may be given.

If $L_d(s)$ and $L_q(s)$ are not given by their poles and zeros, (3.26) may still be applied, but L_d'' and L_q'' must be interpreted as high-frequency values of $L_d(s)$ and $L_q(s)$, where 'high' is several times the frequency associated with the commutation phenomena (300 Hz in a six-pulse rectifier bridge fed by a 50 Hz source).

Determination of $L_d(s)$ and $L_q(s)$ at these high frequencies is not possible by the Modified Step-Response test. Its bandwidth, as used in this thesis, is limited to about 50 Hz. (Of course, models may be fitted to the test results, and they may be extrapolated for the high-frequency region, but there is obviously no guarantee that this will lead to a proper value of L_d'' and L_q'' .)

The subtransient self-inductances are therefore determined by a separate step-response test, using a high sample rate (see section 4.2). Equation (3.26) is then used to calculate a value for the commutation self-inductance L_c .

The internal-machine model

In the rectifier model the voltage \hat{e} plays a central role, while the actual voltages at the terminals of the three-phase source are irrelevant. Therefore, the model of the *internal* machine is essential for simulation of the machine with rectifier, not the model derived in section 3.1. The internal-machine equations are given by (3.25). Table 3.1 summarises the inputs and outputs of the internal-machine model, and the transfer functions in (3.25) which are to be identified from measurement data.

direct axis		outputs:		
		I_d	U_f	$p\omega_m\Psi_{qi}$
inputs:	$-E_d$	$Z_{di}(s)$	$-sG_{fd}(s)$	1
	I_f	$sG_{fd}(s)$	$Y_{fo}(s)$	0
	Ψ_{di}	$L_{di}(s)$	$-G_{fd}(s)$	0

quadrature axis		outputs:	
		I_d	$p\omega_m\Psi_{di}$
inputs:	$-E_q$	$Z_{qi}(s)$	-1
	Ψ_{qi}	$L_{qi}(s)$	0

Table 3.1
Internal-machine inputs and outputs, and transfer functions (the coefficients of model equations (3.25)).

As motivated in section 2.2, each transfer function is parametrised as a *polynomial fraction* according to equation (2.2).

3.4 A model of the synchronous machine with rectifier

Finally, the link from the internal machine to the rectifier model must be made. Using the Park-transformation (3.1) and (3.2), the phase voltage e_a and current i_a may be expressed as a function of direct-axis and quadrature-axis quantities:

$$e_a = \sqrt{\frac{2}{3}}(e_d \cos(p\gamma) + e_q \sin(p\gamma)) \quad (3.30)$$

$$i_a = \sqrt{\frac{2}{3}}(i_d \cos(p\gamma) + i_q \sin(p\gamma))$$

Using (3.16), comparison with e_a from (3.5) and i_{a1} (3.8) gives (3.17), and also:

$$\begin{aligned} \sqrt{\frac{2}{3}} e_d &= \hat{e} \cos(\varepsilon - p\gamma_0) \\ \sqrt{\frac{2}{3}} e_q &= -\hat{e} \sin(\varepsilon - p\gamma_0) \end{aligned} \quad (3.31a)$$



$$\sqrt{\frac{2}{3}} i_d = \frac{3\hat{e}}{2\pi\omega L_c} \left(\sin^2(\mu) \cos(\varepsilon - p\gamma_0) + (\mu - \sin(\mu) \cos(\mu)) \sin(\varepsilon - p\gamma_0) \right)$$

$$\sqrt{\frac{2}{3}} i_q = \frac{3\hat{e}}{2\pi\omega L_c} \left(-\sin^2(\mu) \sin(\varepsilon - p\gamma_0) + (\mu - \sin(\mu) \cos(\mu)) \cos(\varepsilon - p\gamma_0) \right)$$

(3.31b)

$$\hat{e} = \sqrt{\frac{2}{3}} \sqrt{e_d^2 + e_q^2}$$

(3.31c)

The angle γ_0 is the rotor position at $t = 0$. For the simulation it may be chosen arbitrarily. The commutation self-inductance is calculated from (3.26). The model of the machine with rectifier now consists of the internal-machine equations (3.25) and of the equations (3.6), (3.7) and (3.31). Figure 3.5 gives a block-diagram of the complete model. (If the fundamental component of the phase current i_a, i_{a1} , is considered an output, rectifier equation (3.8) must also be included.)

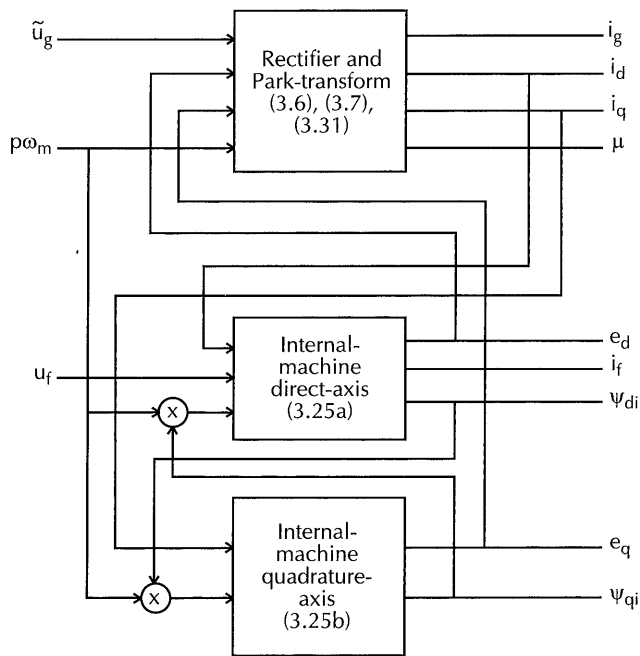
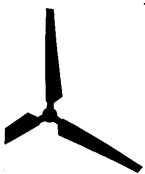


Figure 3.5
Block-diagram of the model of the synchronous machine with diode-bridge rectifier

Simulating the synchronous machine with rectifier

If the commutation self-inductance L_c is calculated from (3.26), and if the transfer functions of table 3.1 are given as a polynomial fraction (or by poles and zeros), then the model can be simulated easily (since standard algorithms may be applied to turn (3.25) into state-space models).

The only restriction is that all transfer functions must be *proper*: the denominator polynomial orders must be greater than or equal to the corresponding numerator



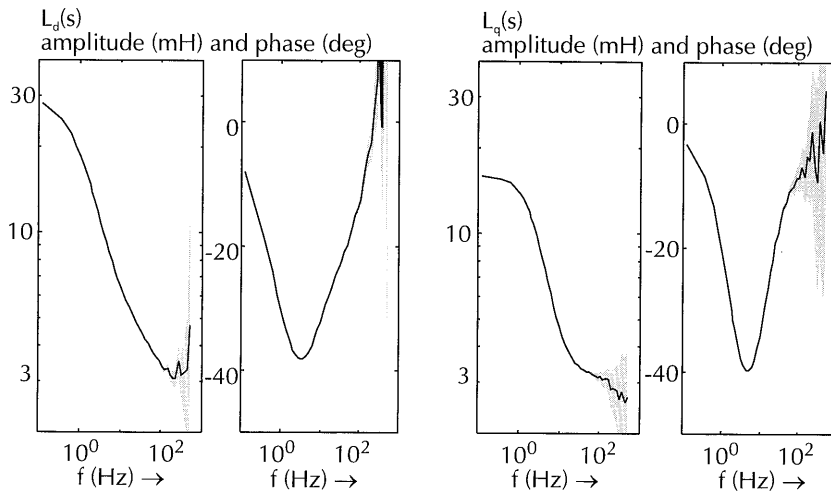
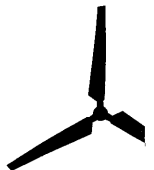


Figure 3.6
Typical Bode-diagrams of $L_d(2\pi jf)$ or $L_q(2\pi jf)$

polynomial orders. This restriction with respect to numerator and denominator orders is a complication for $Z_{di}(s)$ and $Z_{qi}(s)$ (defined in 3.23, appearing in (3.25)). In general, it is unlikely that $L_d(s)-L_c$ and $L_q(s)-L_c$ will both tend to zero for high frequencies. To illustrate this, figure 3.6 shows the Bode-diagrams of a typical $L_d(s)$ and $L_q(s)$, calculated from step-response time-domain data, where the shaded areas represent the uncertainty in the curves. There is no one value of L_c which will cause both $L_d(s)-L_c$ and $L_q(s)-L_c$ to tend to zero for high frequencies. If $L_d(s)-L_c$ and $L_q(s)-L_c$ are modelled by a polynomial fraction, the numerator order will equal the denominator order. The resulting $Z_{di}(s)$ and $Z_{qi}(s)$ will therefore not be proper. The problem may be evaded as follows: since the transfer functions of the internal-machine model are only aimed at low-frequency use, $L_d(s)$ and $L_q(s)$ are modified in such a way, that both $L_d(s)-L_c$ and $L_q(s)-L_c$ tend to zero for high frequencies. This results in proper transfer functions $Z_{di}(s)$ and $Z_{qi}(s)$, which is a prerequisite for creating state-space models.

Now, the synchronous machine with rectifier may be simulated, but there is one more aspect which needs care: the model incorporates an algebraic loop. The quantities i_d and i_q are directly (i.e. without intervening states) related to e_d and e_q a) through the internal-machine equations (3.25), and b) through the rectifier, equations (3.7), (3.8) and (3.31). This algebraic loop is non-linear, and attempts at solving it analytically have failed. Furthermore, the loop exhibits a one-way character: the rectifier equations allow i_d and i_q to be calculated from e_d and e_q , but for the reverse direction we did not find analytical expressions. The implication of this is that the internal-machine models must necessarily have the currents as inputs.

Previously, when the system was simulated using ACSL, a subroutine was constructed to solve the loop iteratively. The simulations of this thesis are carried out in Matlab/Simulink, which detects and solves algebraic loops automatically. In both cases however, the iterative solution of non-linear algebraic equations at every time step significantly slows down the simulation. Some speed may be gained by inserting delays in the loop.





4 THE MODIFIED STEP-RESPONSE TEST

In chapter 2 the standstill step-response concept was adopted for use in our research of the synchronous machine with rectifier. Using the model described in chapter 3, the concept of the test will be discussed in this chapter: first the standstill aspect, and then the step-response aspect.

4.1 The standstill test concept

The choice for a standstill test has been motivated in section 2.3. All standstill tests are variations on the same concept. Consider the synchronous-machine model equations (3.10) and (3.11), which are equivalent, and assume that the rotor angular speed ω_m equals 0. Now (3.10), using (3.13), simplifies to:

$$\begin{aligned}
 -U_d &= Y_{do}^{-1}(s) I_d + Y_{fdo}^{-1}(s) I_f \\
 U_f &= Y_{fdo}^{-1}(s) I_d + Y_{fo}^{-1}(s) I_f \\
 -U_q &= Y_q^{-1}(s) I_q
 \end{aligned}
 \tag{4.1}$$

In (4.1) transfer functions have been chosen which tend to zero for high frequencies. The currents I_q , I_d and I_f are inputs, and the voltages U_q , U_d and U_f are outputs (see figure 4.1a). As in chapter 3, capitals indicate Laplace-transformed quantities, and the admittances are possibly frequency-dependent.

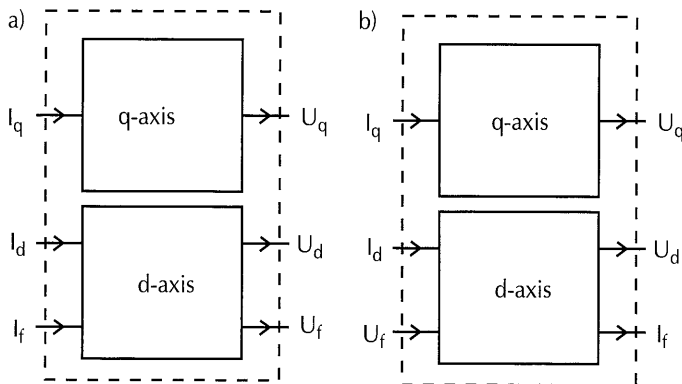
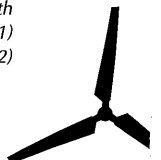


Figure 4.1
 Inputs and outputs of the synchronous-machine model equations with
 a) I_f as input, eq. (4.1)
 b) I_f as output, eq. (4.2)



The model equations (3.11), which have U_f as input instead of I_f (see figure 4.1b), and contain different transfer functions, similarly simplify to:

$$\begin{aligned} -U_d &= Y_d^{-1}(s) I_d - s G_{fd}(s) U_f \\ I_f &= s G_{fd}(s) I_d + Y_{fo}(s) U_f \\ -U_q &= Y_q^{-1}(s) I_q \end{aligned} \quad (4.2)$$

From (4.1) or (4.2) it follows that at standstill, there is no interaction between the direct axis and the quadrature axis. Furthermore, as will be shown below, it follows from the Park-transformation (3.1) and (3.2), that it is possible to either excite the direct axis or excite the quadrature axis by choosing an appropriate rotor position (see figure 4.2).

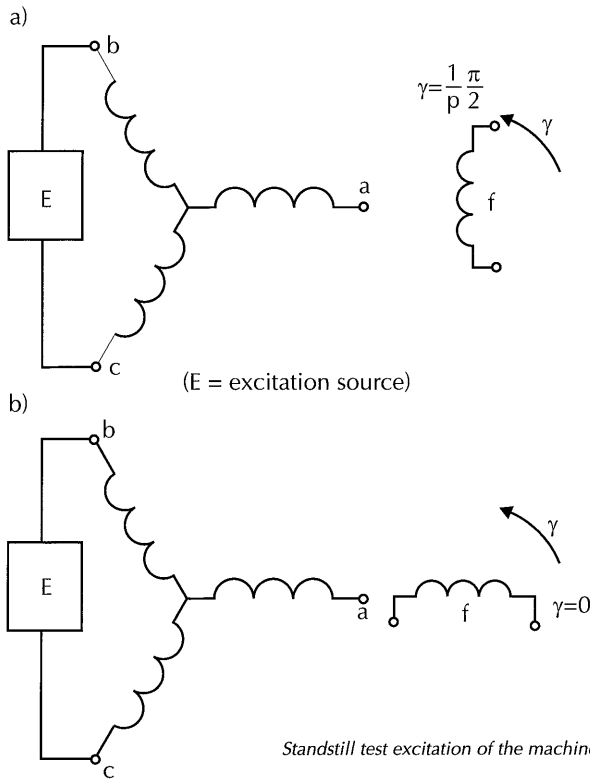


Figure 4.2
Standstill test excitation of the machine, at two rotor positions
a) direct-axis excitation
b) quadrature-axis excitation

If the stator b-c-terminals are excited while the a-terminal remains open, and if the excitation-winding axis is parallel to the a-phase winding ($\gamma = 0$), then it follows from (3.1) and (3.2) that:

$$\begin{aligned} u_q &= \frac{1}{2} \sqrt{2} (u_c - u_b) & u_d &= 0 \\ i_q &= \sqrt{2} i_c & i_d &= 0 \end{aligned} \quad (4.3)$$



For $\gamma = 0$, we therefore excite the quadrature axis of the machine. If the excitation-winding axis is perpendicular to the a-phase winding axis ($\gamma = \pi/2p$), it follows that:

$$\begin{aligned} u_q &= 0 & u_d &= -\frac{1}{2}\sqrt{2}(u_c - u_b) \\ i_q &= 0 & i_d &= -\sqrt{2}i_c \end{aligned} \quad (4.4)$$

For $\gamma = \pi/2p$, we therefore excite the direct axis.

Summarising, we may conclude that at standstill there is no interaction between the direct axis and the quadrature axis, and both axes may be excited separately from the machine terminals, depending on the rotor position. Using this conclusion, the identification processes for both axes may be carried out separately. Below, these two processes are outlined, answering the question which measurements are necessary and sufficient, but without going into detail about the actual processing steps.

Quadrature-axis identification

In the synchronous-machine model equations (3.11) (or (3.10)), the transfer function $Y_q^{-1}(s) = Z_q(s) = R_a + sL_q(s)$ is a full description of the quadrature axis of the machine. From (4.1) it follows, that:

$$Y_q(s) = \frac{i_q}{-U_q} \quad (4.5)$$

For the identification of $Y_q(s)$, and therefore for the identification of the quadrature axis, knowledge of the quadrature-axis voltage u_q and current i_q is necessary and sufficient. Equation (4.3) states how these quantities may be measured. The standstill test quadrature-axis measurement will be denoted by a capital 'Q'.

Direct-axis identification

The identification of the direct axis is more complex because it is a 2-port, and several suggestions may be found in the literature for how to excite the direct-axis system. IEEE-standard 115a [IEE87] proposes two separate measurements, which both excite the stator port, one with open and one with short-circuited excitation winding (see figure 4.3). This proposition is also made in [Jin90, Kam94b], and observations from two-port theory show that this is sufficient.

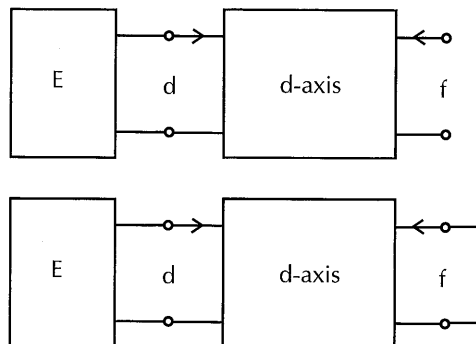
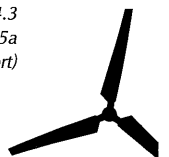


Figure 4.3
Direct-axis identification measurement configuration according to IEEE-standard 115a
(E = excitation source, d = stator port, f = excitation-winding port)



Using the IEEE-standard approach, the direct-axis identification is hindered by a practical problem. This problem is related to the fact that the excitation winding of a synchronous machine is commonly fed by a so-called exciter. An exciter (see figure 4.4) consists of a rectifier which is mounted on the main machine mechanical shaft, and of a small, inverted synchronous machine which feeds this rectifier. Inverted means that the three phase windings of the machine rotate, while the excitation winding is fixed to the stator housing.

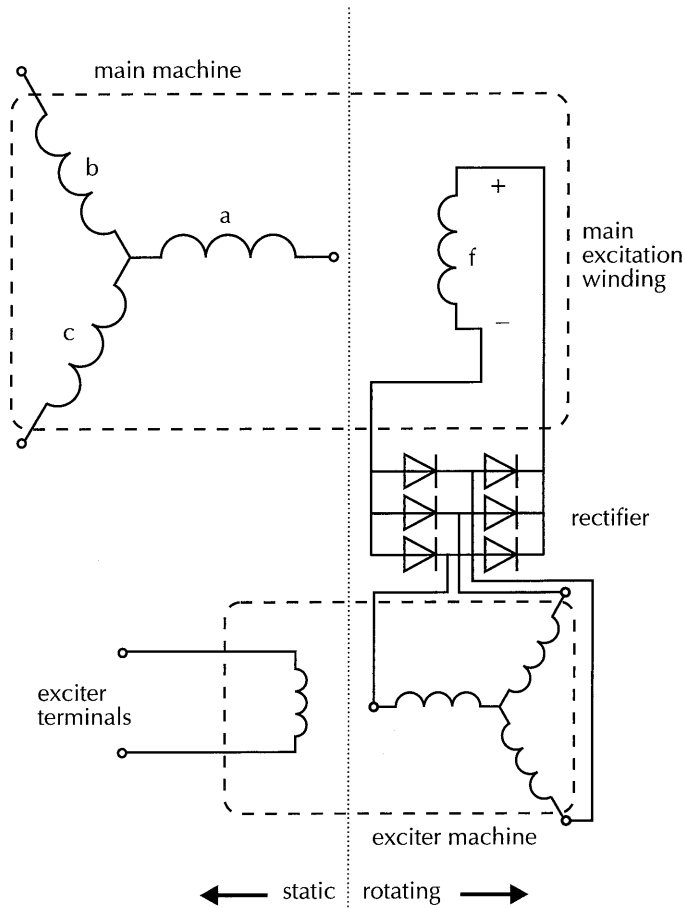


Figure 4.4
Synchronous machine equipped with an exciter

To withstand the forces which are exerted on the rotor, the exciter rectifier and its connections to the excitation winding of the main machine are built compactly and tightly. The excitation-winding port is therefore difficult to access, and in most cases it cannot be disconnected from the exciter rectifier without damaging the machine. If the exciter rectifier may not be disconnected, the possibilities to use the excitation-winding port for measurements are restricted, and depend on the configuration of the diodes of the rectifier. If a diode-bridge rectifier is encountered (as sketched in figure 4.4), MSR-test measurements are valid as long as the rectifier diodes block, i.e. as long as the polarity of the induced voltage in the excitation winding is as indicated in the figure. Since in the MSR test the induced voltage is uni-polar, it is



possible to measure excitation-winding response voltages, after having enforced the right polarity. Under the same condition, excitation-winding response currents can be measured, after short-circuiting the winding terminals with a shunt.

A second practical problem of the direct-axis identification is that the measurement with open excitation winding may result in very high induced voltages. If necessary, the induced voltage may be limited by using an excitation-winding shunt resistor, which must be high enough to approximate an open excitation winding, but low enough to prevent the high induced voltages.

Taking these complications into consideration, the modified step-response test follows the suggestion of IEEE-standard 115a [IEE87], and therefore consists of two measurements for the identification of the direct axis:

- 1) a measurement with $\gamma = \pi/2p$, with excitation of the stator port, while the excitation winding is short-circuited;
- 2) a measurement with $\gamma = \pi/2p$, with excitation of the stator port, while the excitation winding is left open.

In the sequel, these measurements will be denoted by 'D' and 'DO' respectively.

The 'D'-measurement has a short-circuited excitation winding, and therefore $u_f = 0$. By setting U_f to 0 in (4.2), it follows that:

$$Y_d(s) = \left. \frac{I_d}{-U_d} \right|_{u_f = 0} \quad (4.6a)$$

$$sG_{fd}(s) = \left. \frac{I_f}{I_d} \right|_{u_f = 0} \quad (4.6b)$$

Therefore, for the identification of the transfer functions $Y_d(s)$ and $sG_{fd}(s)$ of the direct-axis model (4.2), knowledge of the direct-axis voltage u_d , current i_d , and current i_f are necessary and sufficient. Equation (4.4) states how the Park-transformed quantities may be measured.

The 2nd measurement (the 'DO'-measurement) has an open excitation winding, and therefore $i_f = 0$. By setting I_f to 0 in (4.1), it follows that:

$$Y_{do}(s) = \left. \frac{I_d}{-U_d} \right|_{i_f = 0} \quad (4.7a)$$

$$Y_{fdo}(s) = \left. \frac{I_d}{U_f} \right|_{i_f = 0} \quad (4.7b)$$

Therefore, for the identification of the transfer functions $Y_{do}(s)$ and $Y_{fdo}(s)$ of the direct-axis model, knowledge of the direct-axis voltage u_d , current i_d , and voltage u_f are necessary and sufficient. Equation (4.4) states how the Park-transformed quantities may be measured.



Having identified $Y_d(s)$, $sG_{fd}(s)$, $Y_{do}(s)$ and $Y_{fdo}(s)$, the direct-axis identification is not complete yet: $Y_{fo}(s)$ still needs to be identified (see equations (4.1) and (4.2)). From equation (3.14), (4.6b) and (4.7b) it follows that:

$$Y_{fo}(s) = -\frac{I_f}{I_d} \Big|_{u_f=0} \quad \frac{I_d}{U_f} \Big|_{i_f=0} \quad (4.8)$$

so the combined direct-axis measurements contain sufficient information to identify the direct axis. If the direct-axis model of the machine is described by the transfer functions in (4.2), $Y_d(s)$, $sG_{fd}(s)$, and $Y_{fo}(s)$, the same conclusion is drawn.

Equations (4.6) - (4.8) show that the direct-axis measurements theoretically contain sufficient information to identify the direct axis. But there is an excess of information: for the identification of the direct-axis transfer functions of (4.1) ($Y_{do}(s)$, $Y_{fdo}(s)$, and $Y_{fo}(s)$), all data of the 'DO'-measurement are used, but of the 'D'-measurement only i_f and i_d . The information contained in the stator voltage u_d of the 'D'-measurement is not used in the identification. Similarly, for the identification of the direct-axis transfer functions of (4.2), the information contained in the stator voltage u_d of the 'DO'-measurement is not used.

The unused measurement data may be applied to check the direct-axis *reciprocity assumption* made in section 3.1. From (3.12) and (3.13), which equations assume reciprocity, it may be derived that the direct-axis transfer functions given in (4.6) and (4.7) obey

$$\frac{s G_{fd}(s)}{Y_{fdo}(s)(Y_d^{-1}(s) - Y_{do}^{-1}(s))} = 1 \quad (4.9)$$

For the derivation of equation (4.9), the assumption of reciprocity is essential. To check criterion (4.9), all measured direct-axis data are needed, including the quantity which is not needed for the identification. This may be shown by substitution of (4.6) and (4.7) into (4.9):

$$\frac{\frac{I_f}{I_d} \Big|_{u_f=0}}{\frac{I_d}{U_f} \Big|_{i_f=0} \left(-\frac{U_d}{I_d} \Big|_{u_f=0} + \frac{U_d}{I_d} \Big|_{i_f=0} \right)} = 1 \quad (4.10)$$

In (4.10) all measured direct-axis data are present, including the quantity which is not needed for the identification.

4.2 The modified step-response test

Although far from ideal from an identification point of view, the step-response experiment has been chosen to identify the synchronous machine (see section



2.3). In the literature it is attempted to *approximate an ideal step* as closely as possible [Rit86, Cal86], but for the information content of the measured data, this is not an essential aspect: other excitation signals which only resemble a step, may even perform better.

Considering this, a very simple measurement set-up may be used (see figure 4.5), which we have published previously in [Hoe89a, Hoe90, Vle90, Vle92a] under the name Modified Step-Response (MSR) test. A step-like excitation is generated by switching on a low-power DC-voltage source (e.g. a battery) which is connected to two stator terminals of the machine. For the switching, a thyristor (T) is applied.

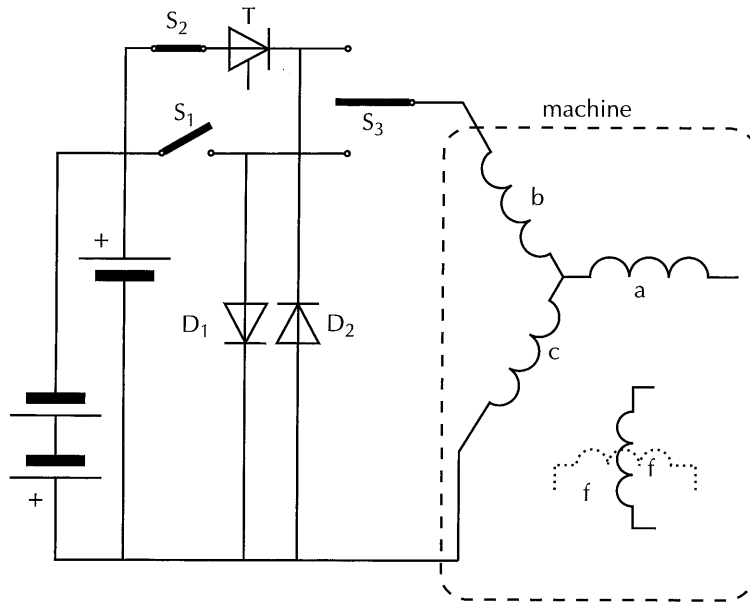


Figure 4.5
Measurement set-up of the modified step-response test

The use of a thyristor (T) instead of a common mechanical switch eliminates the problem of bouncing. The resistance of the thyristor in the conduction state is irrelevant, since responses as well as the excitation are measured. As in the DC-decay test, preliminary magnetisation of the circuit is necessary to arrive at reproducible results, but unlike the DC-decay test it is sufficient that the magnetisation-current source can just be switched on and off (by switch S_1). The only demand is that it is able to supply an approximately rated current. Therefore, a battery (or set of batteries) may be used. Precautions may be necessary to prevent high induced voltages when switching off the magnetisation current. For this reason free-wheeling diodes are included in the set-up (diodes D_1 and D_2 in figure 4.5). Switch S_3 is used to switch from the magnetisation circuit to the actual step-response circuit, while the system is at rest.

For the machines we tested (appr. 30 kVA), a 4 V battery could be applied for the actual step-response measurement. For the magnetisation a 12 V battery was necessary. Switch S_2 switches off the measurement current.

Figure 4.6 shows a recorded excitation voltage and response current (4096 samples at a sample period of 1 ms), and their spectra, compared to the spectrum of an ideal step. The step-character of the measured signals is evident: most of the signal



energy is concentrated at the lower part of the frequency band. The effective bandwidth of the signal is limited by the noise level of the measurement (see also Appendix A1), but is still larger than the bandwidth necessary to identify the system (indicated by the shaded area in figure 4.6, 0.1 Hz - 10 Hz, see section 2.2). The quality of the measured signals shown in figure 4.6 is better than if the system were excited by an ideal voltage step, but worse than if an ideal current step were used. For a further analysis see section 6.2. The remainder of this section is dedicated to some practical aspects of the test.

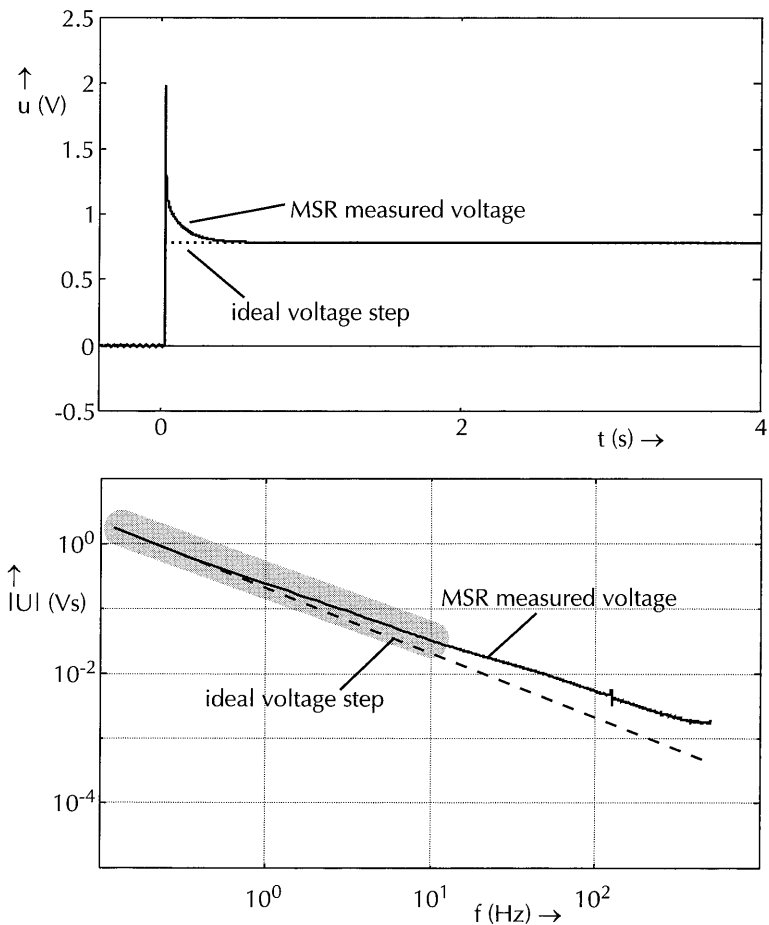


Figure 4.6a
The voltage signal of the modified step-response test



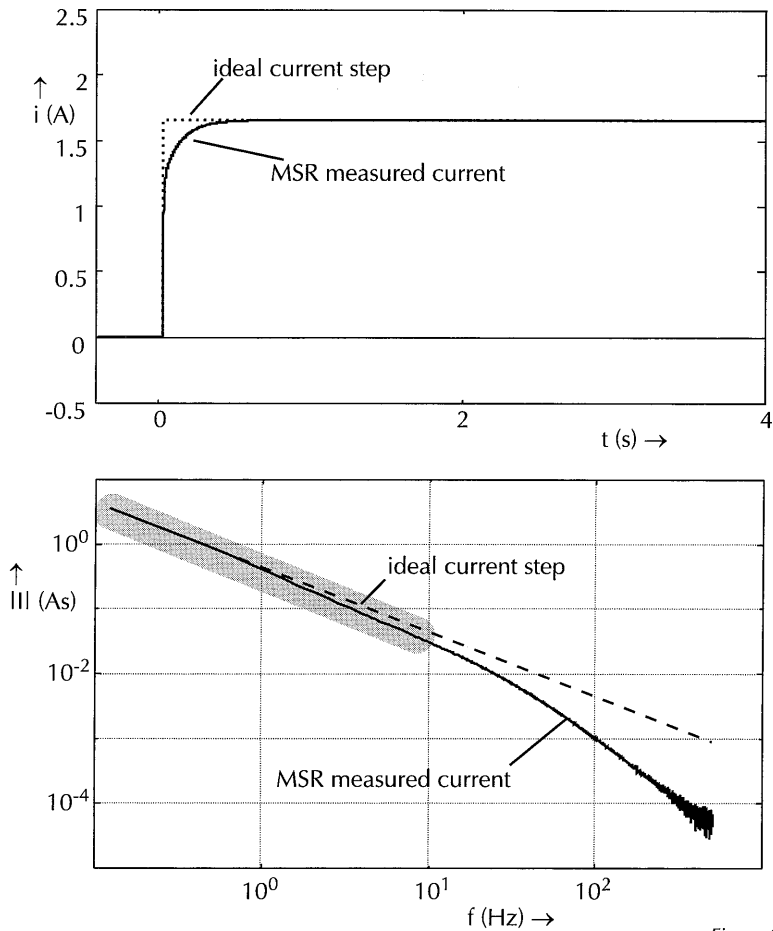


Figure 4.6b
The current signal of the modified step-response test

Practical considerations

The test conditions for the modified step-response test are similar to those for other standstill tests (compare, for example, the description of the SSFR test [IEC85]). The machine must be shut down and electrically isolated. A facility to position and subsequently fix the rotor must be present. The excitation winding is either short-circuited by a shunt or left open.

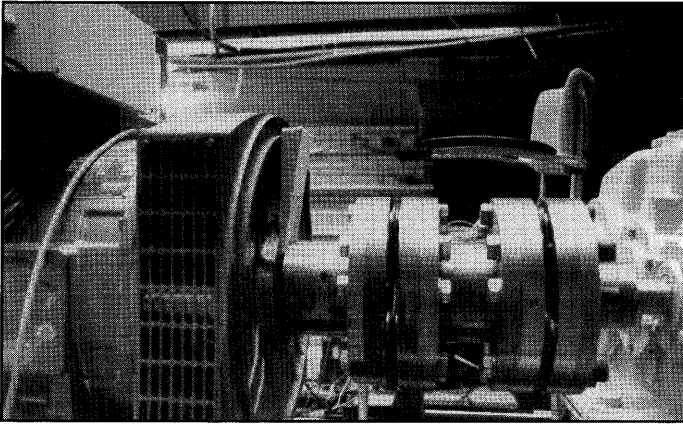
The rotor must be positioned in a direct-axis or a quadrature-axis position with respect to the two stator windings which are included in the stator circuit. The correct rotor position for the *quadrature-axis measurement* may be found by applying a 50 Hz voltage to terminals b and c (see figure 4.2b), and turning the rotor until the induced voltage in the excitation winding is minimal. Similarly, the correct rotor position for the *direct-axis measurement*, might be found by maximising the induced voltage in the excitation winding, but this cannot be done accurately. It is more accurate to find the correct rotor position indirectly, i.e. by applying the 50 Hz voltage to terminals a and the star-connection (see figure 4.2a), and to minimise the induced voltage. After having detected the appropriate rotor position, the rotor is fixed.

Figure 4.7 shows details of a MSR-test measurement set-up.

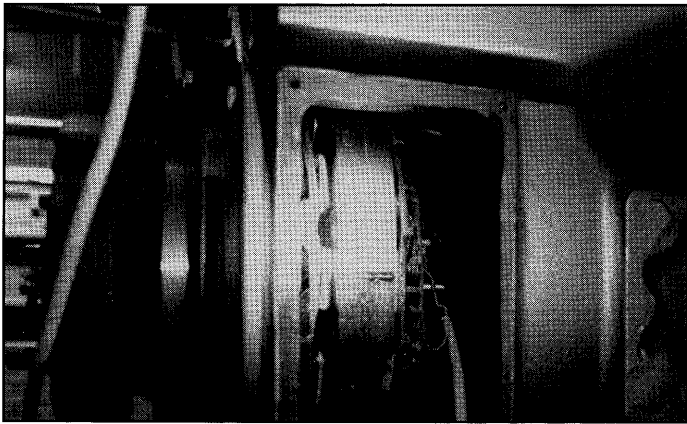




4.7a

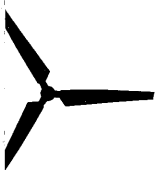


4.7b



4.7c

Figure 4.7
Details of a MSR-test measurement set-up
a) Batteries to generate the excitation and the preliminary magnetisation currents.
b) Fixing the rotor (by a wooden peg).
c) Accessing the excitation-winding terminals.



Hysteresis and armature resistance

As has been discussed in section 2.3, special attention should be given to the hysteresis of the magnetic circuit: the magnetic situation prior to the measurement must be fixed. This is achieved by driving the circuit into saturation with a large current. The saturating current and the measurement current flow in opposite directions (see figure 4.8).

For every standstill test, the standards warn against stator-winding temperature increase, which may have an adverse effect on the identification. The dissipation of power during the test may cause the winding temperature to vary during the measurement. Especially the saturating current may result in an increase in winding temperature. After the current is switched off, the winding temperature again decreases to ambient temperature.

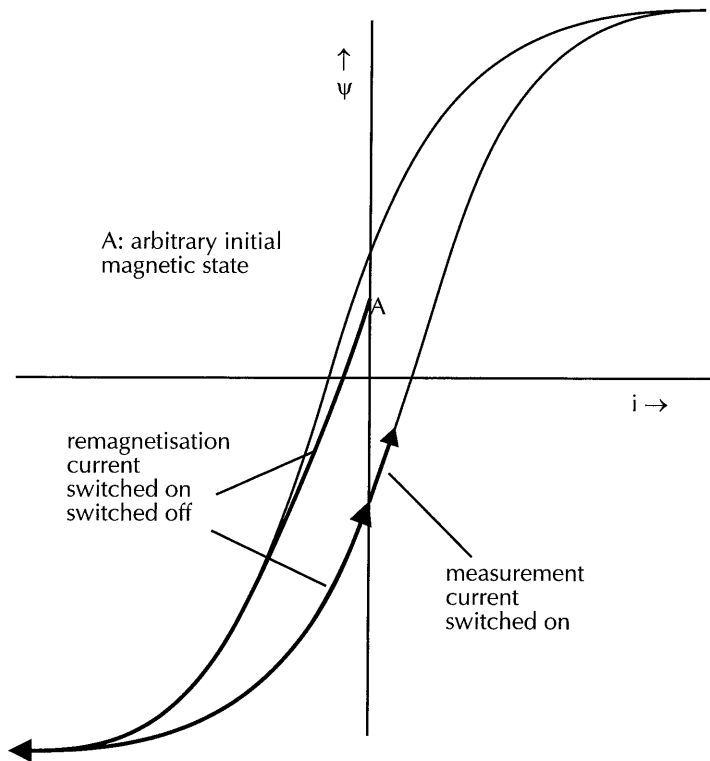
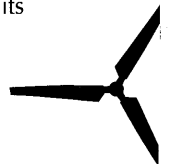


Figure 4.8
The preliminary magnetisation current and the measurement current

The stator winding resistance changes during a MSR test are in the order of 1%, which have been measured in two ways:

- By a long DC-measurement: the measurement current is supplied to the winding for e.g. 0.5 to 1 hour, and the long-term resistance change is determined; the resistance change during the MSR test is found by taking the initial slope of an exponential curve which is fitted to the measured resistance values [Dir92];
- By short DC-measurements *after* an individual MSR test; after the measurement data have been acquired, the current is not switched off, but after a short pause (in the order of 5 times the measurement length), the winding voltage and the winding current are measured again, and the winding resistance as well as its rate of change are determined.



The consequences of winding resistance variations for the identification of the machine are analysed in more detail in section 6.3. The conclusion of this analysis is that the currents used (5% - 10% of rated armature current) lead to temperature changes which may be neglected.

Ambient temperature

Repeated measurements may result in different winding resistance values, which may be caused by measurement errors, but may also be due to differences in the temperature of the machine at the moment of the test. To have a clue of their origin, the machine temperature is monitored. Since the machine, when tested, will usually have been at rest for some time, the machine temperature will equal the ambient temperature and the temperature of the machine housing, which may be measured by a regular thermometer.

Measurement settings

For the modified step-response test the following settings must be determined:

- the signal level;
- the level of the saturating current;
- the length of the measurement and the sample rate.

The *response current level* is chosen as suggested in the IEC-description of the sudden-DC test: 5 % of the rated stator current. Using this value and the value of the stator resistance, the excitation voltage may be determined. The internal resistance of the applied power source may have a significant effect on the signal levels. The response level is best determined by just carefully carrying out the test. The *level of the saturating stator current* which is applied before the measurement, is in the order of the rated current of the machine. An auxiliary power source (e.g. a set of batteries) may be necessary to supply this current. It does not have to be controllable (compare the description of the DC-decay test, section 2.3).

The *lower bound of the desired bandwidth* is somewhat lower than the frequency associated with the largest time-constant τ_{\max} of the machine. For the machines we have analysed (appr. 30 kVA), this associated frequency is about 0.5 Hz. As a rule of thumb, to achieve this lower bound, the measurement length must be in the order of this time-constant. Simulated MSR experiments show that the best choice for the measurement length is:

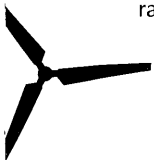
$$T = 2\tau_{\max} \cdots 5\tau_{\max} \quad (4.11)$$

If the manufacturer does not provide this value, an initial test must be carried out to determine an appropriate measurement length.

The *upper bound of the desired bandwidth* is approximately 10 Hz (see section 2.2), which means that a sample rate of 50 Hz would be sufficient. The upper bandwidth limit must be reached with a negligible amount of aliasing, by applying appropriate anti-aliasing filters. Considering the step-signal spectrum, which is inversely proportional to frequency, it may be asked whether anti-aliasing are strictly necessary. In section 6.2 this idea will be analysed in more detail. The conclusion from that section is that aliasing may also be avoided by choosing the sample rate high enough.

The high-frequency self-inductance

To determine an approximate value for the subtransient self-inductances L_d'' and L_q'' which are necessary to determine the value of the commutation self-inductance L_c , eq. (3.26), the step-response test is also carried out with a relatively high sample rate (10 - 100 μ s).



If the high-frequency behaviour of a 1-port is inductive, with inductance L_{HF} and resistance R_{HF} , and the port is excited by a step, then the response of the port shortly after the step moment may be described by:

$$u \equiv R_{HF}i + L_{HF} \frac{di}{dt} \quad (4.12)$$

From (4.12) follows:

$$L_{HF} \equiv \frac{u - R_{HF}i}{\frac{di}{dt}} \quad (4.13)$$

From the quantities appearing in (4.13) the terminal voltage u and the current i are measured. Since the current is still small just after the moment of the step, the term $R_{HF}i$ is small. The resistance R_{HF} may either be taken equal to 0, or to the DC-value of the circuit resistance. The derivative di/dt may now be calculated by a numerical approximation formula.

Figure 4.9 shows an example of the calculation of the high-frequency self-inductance. The ragged solid line marked 'A' gives L_{HF} calculated using (4.13). The dotted line 'B' is a straight line approximation of curve 'A'. Apparently, the inductance L_{HF} is not constant, but there is a definite limit value for t approaching 0.

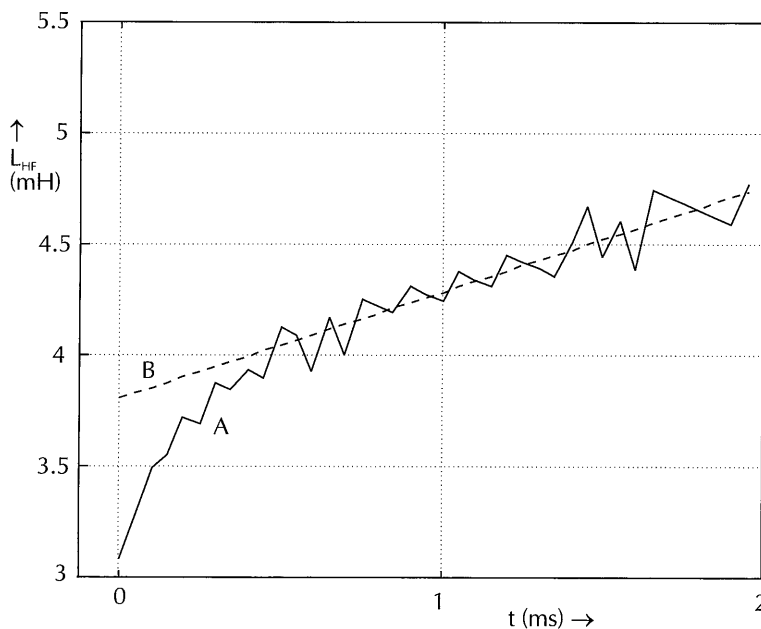


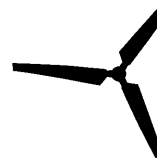
Figure 4.9

Calculation of the high-frequency stator self-inductance of a machine axis from step-response data

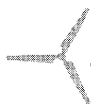
A: di/dt approximated by $(i_{k+1} - i_k)/T_s$, where i_k is the k -th sample and T_s the sample period

B: linear interpolation of A

Nevertheless, a choice of a value for L_{HF} remains to some extent arbitrary: within the time interval of a common commutation time, about 0.2 ms, L_{HF} may be chosen between 3.1 and 3.7 mH.



For one of the tested machines, high-frequency stator self-inductance data are available [Hoe84a]. There is a reasonable correspondence with the value obtained from the fast step-response test by (4.13).



4.3 The protocol of the modified step-response test

The protocol of the modified step-response test consists of two parts, an explorative part to prepare the test, and an executive part for the actual test.

Protocol (explorative part)

1. Gather name plate data (rated current).
2. Create access to the excitation-winding terminals.
3. Measure winding resistances.
4. Estimate the capacity and the voltage of the necessary batteries.
5. Build the measurement set-up.
6. Carry out initial step-response tests to determine
 - a. appropriate sample period and number of samples;
 - b. appropriate signal levels and shunt values.
7. If temperature effects are expected to be relevant: apply the chosen excitation currents to the stator winding for a long time (in the order of an hour), while recording the winding voltage and current.

Protocol (executive part)

1. Record ambient and machine housing temperature.
2. Quadrature-axis measurement (measurement 'Q').
 - a. Position the rotor for the quadrature-axis measurement, and fix the rotor.
 - b. Adjust switch S_3 (figure 4.5) for preliminary magnetisation.
 - c. Switch the magnetisation current on, wait for the transient to decay, and switch the current off (switch S_1 , figure 4.5).
 - d. Adjust switch S_3 for the actual step-response measurement.
 - e. Arm the data-acquisition equipment.
 - f. Trigger thyristor T (the stator voltage and current signals are now being recorded).
 - g. Switch off the current after the data acquisition has been completed.
 - h. Repeat 2.b to 2.g with a high sample rate.
3. Direct-axis measurement with open excitation winding (measurement 'DO').
 - a. Position the rotor for the direct-axis measurements, and fix the rotor.
 - b. Open the excitation-winding terminals.
 - c. Repeat 2.b to 2.h. At step f. the stator voltage, the stator current and the voltage induced in the excitation winding are recorded.
4. Direct-axis measurement with short-circuited excitation winding (measurement 'D').
 - a. Short-circuit the excitation winding (with a shunt).
 - b. Repeat 2.b to 2.h. At step f. the stator voltage, the stator current and the current induced in the excitation winding are recorded.
5. Record ambient and machine housing temperature.

If necessary, the step-response test may be carried out at different current levels.



5 COMPLETING THE IDENTIFICATION

After measurement data have been acquired, the data must be processed in order to identify the synchronous machine. i.e. to estimate the parameters of the transfer functions of the internal-machine model of chapter 3. In sections 2.4 and 2.5 the most important choices with respect to these topics have been made. In this chapter the procedure is described in more detail.

5.1 Estimating a single transfer function

After the identification measurements have been carried out, the identification process proceeds with the estimation and its validation (see section 2.1). Using the data acquired by the modified step-response test (chapter 4), the two internal-machine axis models described by equations (3.25a&b), the parametrisation (2.2) of the transfer functions of the model, the model order and the model parameters are estimated, as outlined in section 2.4.

Basically, the estimation procedure for a single transfer function is as follows:

- determine which pair of signals forms the excitation and the response of the transfer function;
- preprocess these two signals (in particular: remove offset);
- transform the signals into the frequency domain;
- determine an appropriate value of the order of the transfer function;
- estimate the parameters of the transfer function;
- validate the result.

Determining the excitation and response signal pair

The essential transfer functions to be identified, those of the internal machine, have been listed in table 3.1. Figure 5.1 shows how these transfer functions relate to the MSR measurement data, and also shows the relations with other transfer functions used in chapters 3 and 4. Three sets of transfer functions may be distinguished:

- the *basic set* of transfer functions, which directly follow from the MSR measurement data (equations (4.5), (4.6) and (4.7));
- an *extended set* of transfer functions used for data analysis, which includes most of the basic set quantities, but also some more commonly used inductances, and a derived quantity, $Y_{f_0}(s)$ (equations (3.13) and (3.14));
- the *internal-machine set*, the set of internal-machine transfer functions which finally have to be identified (equations (3.13), (3.22) and (3.23)).

Where relevant, figure 5.1 gives the pertinent equations. Four internal-machine transfer functions also need a value of the commutation inductance L_C , which

must be supplied externally. It is calculated from (3.26) using the subtransient self-inductances L_d'' and L_q'' , which are identified by a separate step-response measurement as described in section 4.2, page 56.

For the transfer functions of the basic set, the excitation and response signal pairs are easily pointed out. However, for some transfer functions of the extended set and the internal-machine set, it is not immediately obvious which signals are the excitation and response signal pair. Analysis of this problem requires some details of the estimation procedure, and is therefore postponed to section 5.2.

In this section the transfer function $Y_d(s)$ will be used as an example. From figure 5.1

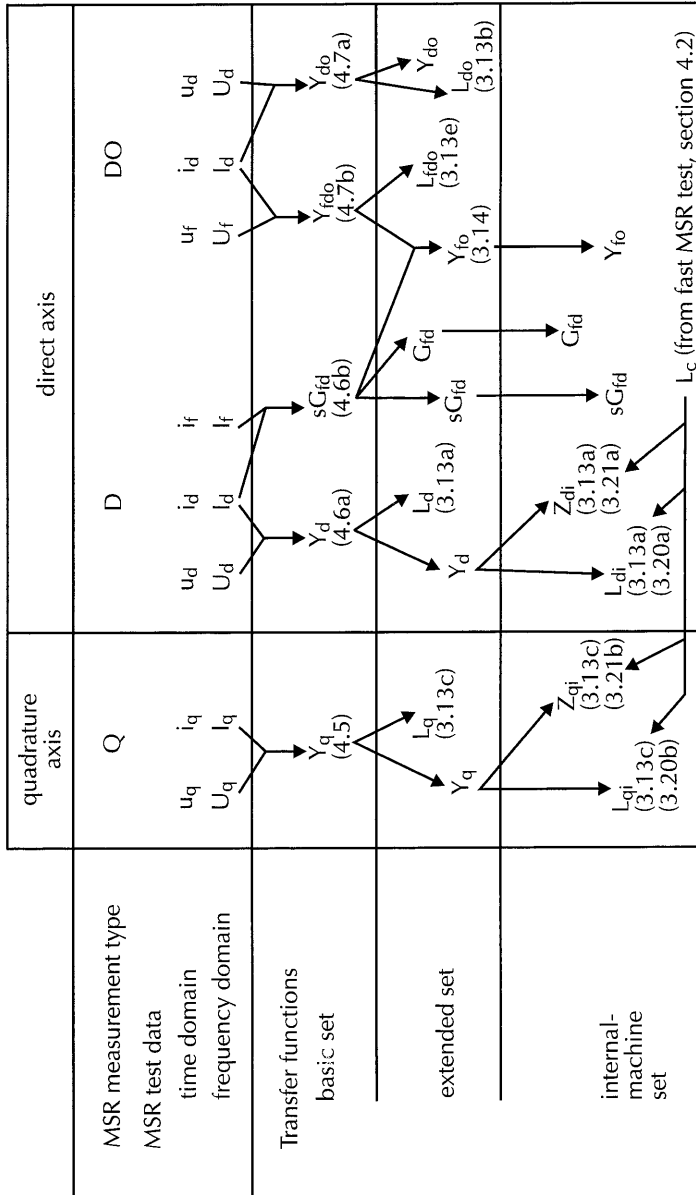


Figure 5.1 Relationships between several sets of transfer functions and the MSR-test data

follows, that the excitation and response signal pair for this transfer function is u_d and i_d , from the 'D'-measurement.

Preprocessing the data

The necessary *preprocessing* of the time-domain data is limited, since the MSR test results in relatively clean signals (see figure 5.2, for the example data). They may contain a slight offset, but there is no need for trend removal, for elimination of spikes, or for estimation of time delays. The noise content of the signals is low: a signal-noise ratio of 70 dB may be obtained without any specific measures. The quantisation noise is kept low by using 14-bit A-D-convertors (full scale signal-noise ratio: 84 dB).

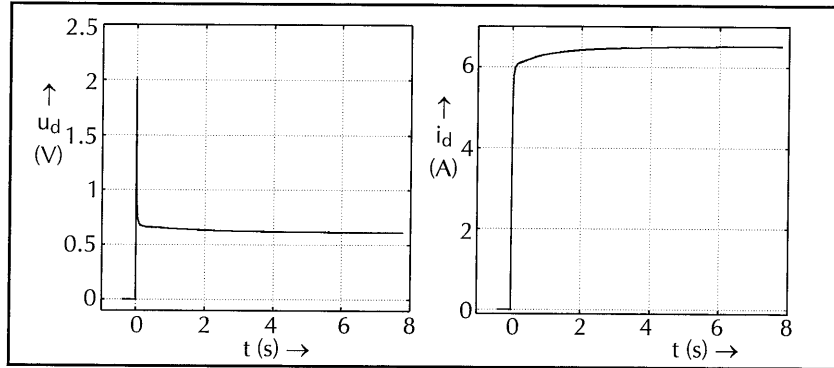


Figure 5.2
Time-domain MSR signals for transfer function $Y_d(s)$ (excitation u_d , response i_d , from the 'D'-measurement)

Offsets are removed using pre-step data samples. Since the system is not excited and at rest, the mean value of the measured signals should be zero. Non-zero mean values are corrected by subtracting them from the time-domain data. After removing offsets, equations (4.3) and (4.4) are applied to calculate the transformed direct-axis and quadrature-axis signals.

In section 6.3 the effect of possible armature winding temperature changes during the measurement are analysed. It appears that for the measurements we have carried out, the temperature increase of the stator winding during the measurement may be neglected. If the temperature changes would not be negligible, some extra preprocessing would be necessary, which is described in Appendix A2. The remaining four steps of the estimation procedure are described in the remainder of this section.

Transforming step-response data into the frequency domain

After preprocessing the measured signals, the time-domain data must be transformed into the frequency domain. Since the measured quantities are step signals (see figure 5.2), a straightforward frequency transformation using the discrete Fourier transform (DFT) is not correct, and another technique should be applied to transform the signals into the frequency domain, as shown below (see figure 5.3).

Suppose the step signal $x(t)$ is recorded from $t = 0$ to $t = T$. If transformed directly, the calculated spectrum is actually the spectrum of a 'block' signal $x'(t)$:

$$x'(t) = \begin{cases} x(t) & t \in [0, T] \\ 0 & \text{otherwise} \end{cases} \quad (5.1)$$



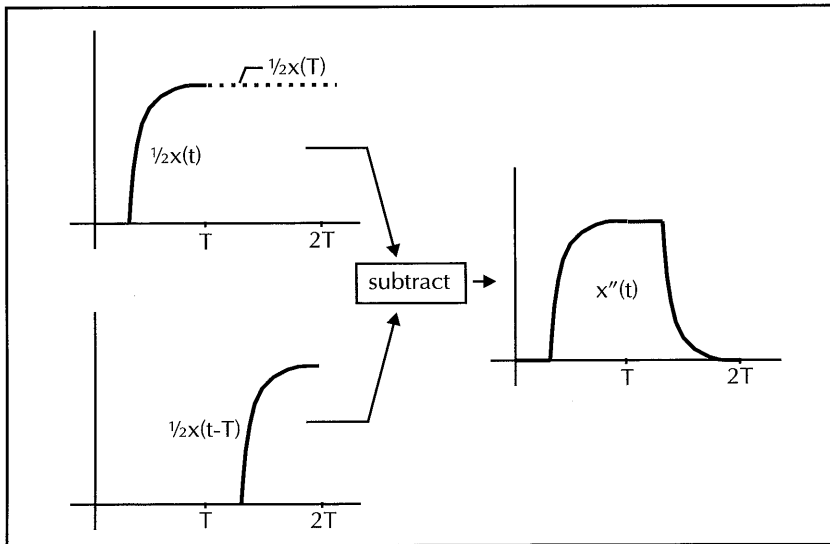


Figure 5.3
The construction of a time-limited signal from a recorded step

which is not the signal we want to transform. An elegant way of determining the step-signal transform is by constructing $x''(t)$ as follows:

$$x''(t) = \begin{cases} \frac{1}{2}x(t) & t \in [0, T] \\ \frac{1}{2}x(T) - \frac{1}{2}x(t-T) & t \in (T, 2T] \\ 0 & \text{otherwise} \end{cases} \quad (5.2)$$

The signal $x''(t)$ has the nice property of being equal to zero outside the interval $(0, 2T)$, and may therefore be transformed using the DFT without having to neglect any part of the signal outside this interval. The transform $X''(\omega)$ relates to the transform of the original signal by:

$$X''(\omega) = \frac{1}{2} \left(1 - e^{-j\omega T} \right) X(\omega) \quad (5.3)$$

The DFT computes values for the transform $X''(\omega)$ at $\omega_k = 2\pi k/2T$, with $k = 0..N-1$, and N the number of samples in $x''(t)$. Therefore (5.3) simplifies to:

$$X''(\omega_k) = \begin{cases} X(\omega_k) & \text{odd } k \\ 0 & \text{even } k \neq 0 \end{cases} \quad (5.4)$$

Using (5.2) and (5.4), the DFT may be used for an indirect calculation of the frequency transform of the step signal $x(t)$.

A possible problem of the use of this time-transpose technique is, that the calculation is sensitive to errors in $x(T)$, and to deviations of $x(0)$ from 0. Due to the low noise level of the MSR-test signals and by ensuring a sufficiently long measurement time, errors can be kept low in practice.

Figure 5.4 shows the frequency transforms of the signals of figure 5.2, calculated as described above. The phase angle shown is the phase of I_d with respect to U_d .

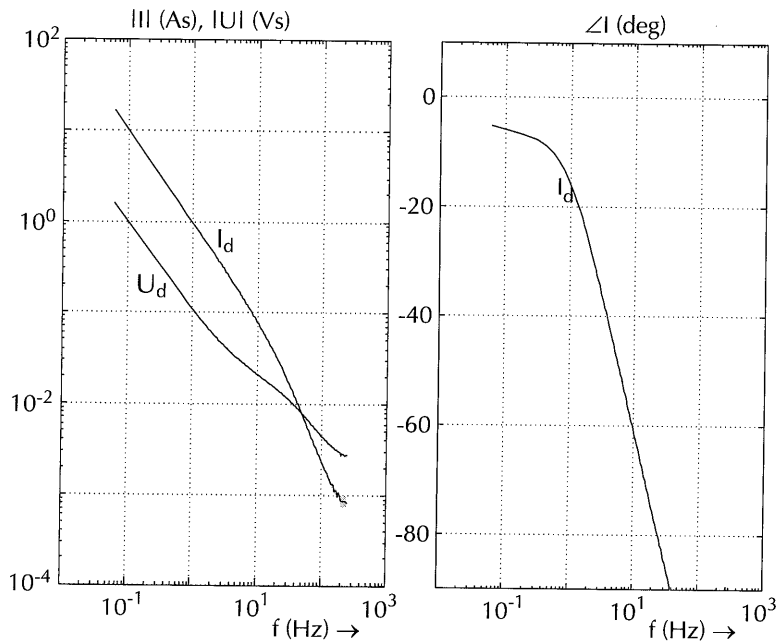


Figure 5.4
Frequency transforms of the MSR signals of figure 5.2

Order tests and parameter estimation

Given a transfer function of figure 5.1, its parametrisation (equation (2.2)), and the appropriate frequency-domain data, order tests may be carried out and the parameters of the transfer function may be estimated and validated. The main tool to do this, the *estimator*, has been chosen in section 2.4, equations (2.1), (2.2), (2.3), and (2.7): the *elis* maximum likelihood estimator implemented in the Matlab Frequency-Domain Identification Toolbox [Kol94]. In this section some details are given.

Estimator input data

The estimator requires frequency-domain excitation and response data, i.e. a set of samples X_k and Y_k at different frequencies f_k , where $k = 1..N$ and N the number of samples. But the estimator also requires the variance and covariance values of these frequency-domain data: $\langle e5_x1 \rangle$.

For the MSR test it is assumed that the noise in each time-domain sample has equal variance (and zero mean), so that a single time-domain variance value may be derived for each measured signal, using the standard mean and variance formulas on the N_p pre-step samples of each time-domain signal (represented here by x_k):

$$\bar{x} = \frac{1}{N_p} \sum_{k=1}^{N_p} x_k \quad (5.5)$$

$$\sigma_x^2 = \frac{1}{N_p - 1} \sum_{k=1}^{N_p} (x_k - \bar{x})^2 \quad (5.6)$$



From the time-domain variance, the variance of the real and imaginary part of the frequency-domain samples is given by:

$$\sigma_{\text{Re}(X)}^2 = \sigma_{\text{Im}(X)}^2 = \frac{1}{2} N T_s^2 \sigma_x^2 \quad (5.7)$$

Equation (5.6) may be derived in a way similar to equation (A1.15) in Appendix A1, on the assumption that the time-domain noise samples are mutually independent.

Estimator results

The estimation results in:

- estimated parameter values, i.e. a value of $\underline{\theta}$, the coefficients of the transfer function given in (2.2);
- a coefficient-covariance-matrix which contains the variances of the estimated parameter values on its diagonal, and mutual covariances at other locations in the matrix;
- the loss E of equation (2.3);
- the residuals e_k , $k = 1..N$, equation (2.6).

The coefficient-covariance-matrix contains information about the variance (uncertainty) of the estimated parameter values, given the variance in the data supplied to the estimator. Off-diagonal values give information about the correlation between the variances of each pair of estimates.

Order tests

Order tests determine appropriate model orders (i.e. values for m and n in (2.2)) on the basis of the measured data. A straightforward order test is to apply the estimator to given measurement data for several values of the numerator and denominator polynomial orders, and analyse the estimation result.

The general trend of an order test is that the higher the model order, the lower the minimal loss $\min(E)$ and the more uncertain the estimated parameters. Usually, the set of tested model orders may be divided into two regions. A region with low model orders gives estimates with small standard deviations, and a high rate of change of $\min(E)$, and a region with high model orders gives estimates with large standard deviations and/or with improbable locations, and a low rate of change of $\min(E)$. The order at which both regions meet, is a logical choice to adopt as model order.

Figure 5.5 shows both aspects of the order test combined into one graph, for the example transfer function. First of all, the *location and standard deviation of the estimated poles and zeros* are given as a function of the model order. The model order is given on the x-axis, in the format 'm/n', where m and n are the polynomial orders of (2.2). On the y-axis the (absolute value of the real part of the) estimated poles and zeros is shown: poles are indicated by a cross ('x'), zeros by a circle ('o'). The standard deviation of the poles and zeros is indicated by a shaded rectangle ($\pm 3\sigma$). With increasing model order, the estimated standard deviations usually increases, and some of the poles and zeros may move out of the frequency band of the graph, or may even become unstable. The unstable or unshown poles and/or zeros for a given model order are indicated by the annotations '+0/1 x0/0' and '+1/1 x0/0'.

For order 3/3 it means that one pole is not shown ('+0/1'), for order 3/4 one zero and one pole are not shown ('+1/1'). In both cases there are no unstable poles or zeros ('x0/0').

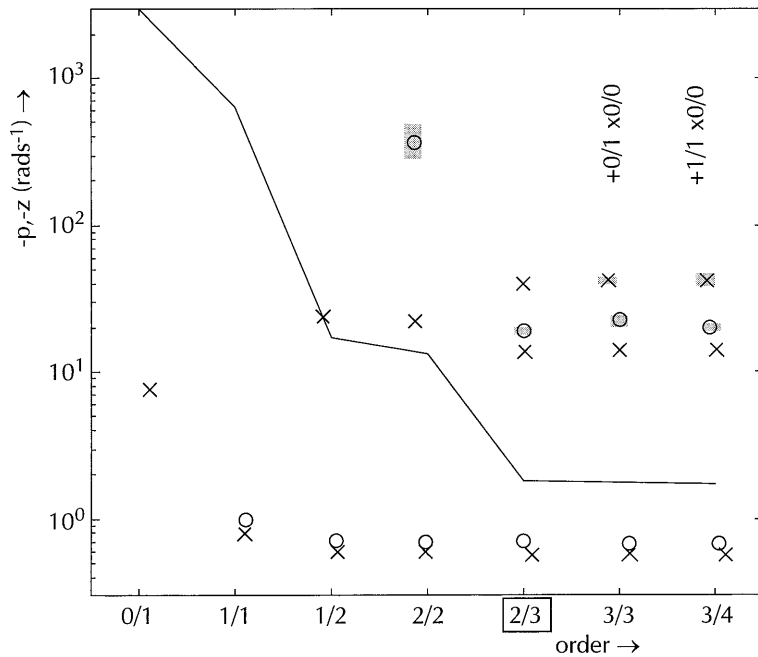


Figure 5.5
Order-test results for the transfer function $Y_d(s)$, using the frequency transforms of figure 5.4

The second order-test aspect shown in the graph, is the logarithm of the minimal value of the loss E , as defined in (2.3), as a function of the model order. It is displayed as a solid line which crosses the graph diagonally from the upper left corner to the lower right corner. It has no y-axis scaling associated to it, since not its actual value is relevant, but its shape. With increasing model order, the identified model fits better to the measurement data, and $\min(E)$ decreases. As already mentioned (page 64), there usually is a more or less distinct order below which $\min(E)$ decreases rapidly, but above which $\min(E)$ only decreases slowly, and it is this order which is looked for in an order test. Since this order is found without using actual values of $\min(E)$ or $\log(\min(E))$, an associated y-axis scale is not necessary. In figure 5.5, combining both order test aspects leads to a model order of $m=2$ and $n=3$.

Validation

To validate the estimation result:

- the poles and zeros of the estimated transfer function are calculated and checked on stability and location;
- the fit between estimated and measured transfer function is inspected;
- the spectrum of the residuals is checked on flatness;
- the distribution of the residuals is inspected.

For the example transfer function, the poles and zeros are shown in the order test graph (figure 5.5): for the chosen model order, none of the poles are unstable, and none of the poles and zeros lie very far outside of the frequency range of the samples used for the estimation (60 mHz - 30 Hz). Figure 5.6 shows the measured transfer function I_d/U_d , the estimated one $Y_d(s)$, and their relative difference.

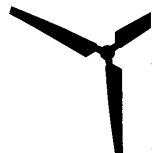


Figure 5.7 shows the spectrum and the distribution of the residuals. The residual spectrum is relatively flat, considering that the amplitude range of the frequency-domain data I_d and U_d is 3 to 4 decades (see figure 5.4), and the distribution of the residuals resembles a normal distribution. Both observations indicate that there is not much reason to reject the identified model. The auto- and cross-correlation functions, which are often used for analysis of time-domain residuals, are not known to be used for frequency-domain residuals.

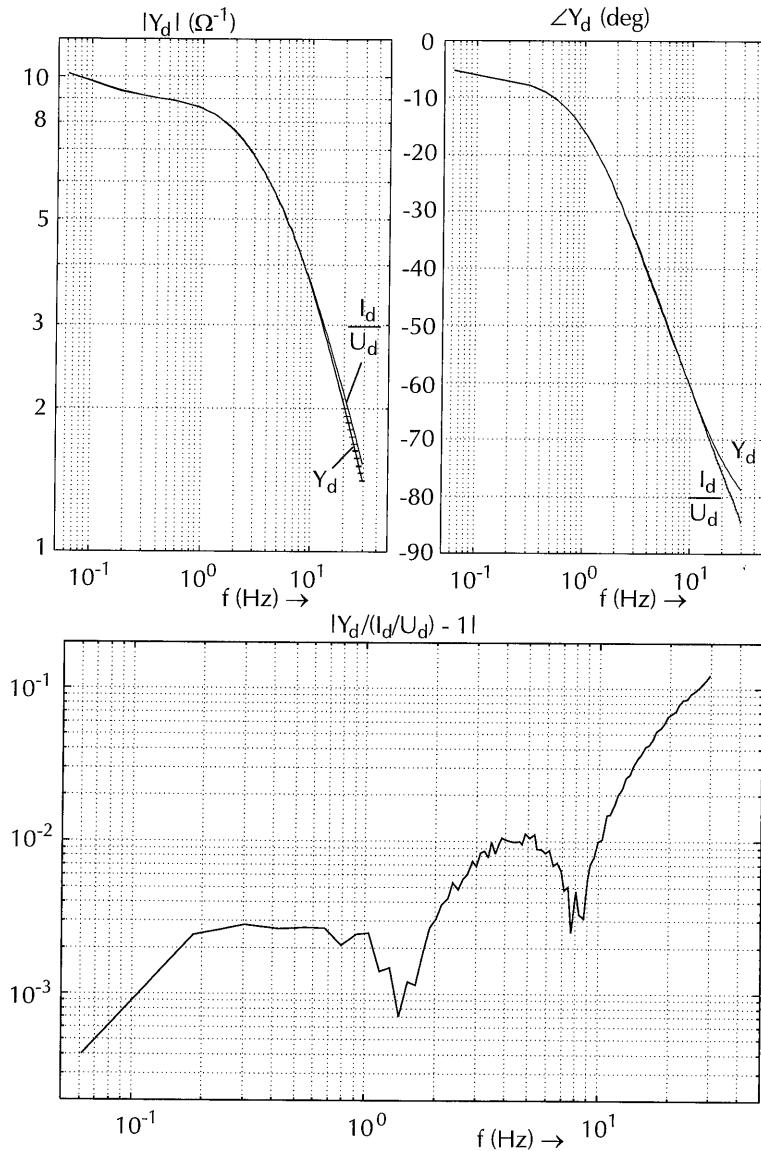


Figure 5.6
Estimated transfer function $Y_d(s)$, the quotient of the frequency-domain data I_d/U_d , and their relative difference $|Y_d/(I_d/U_d) - 1|$

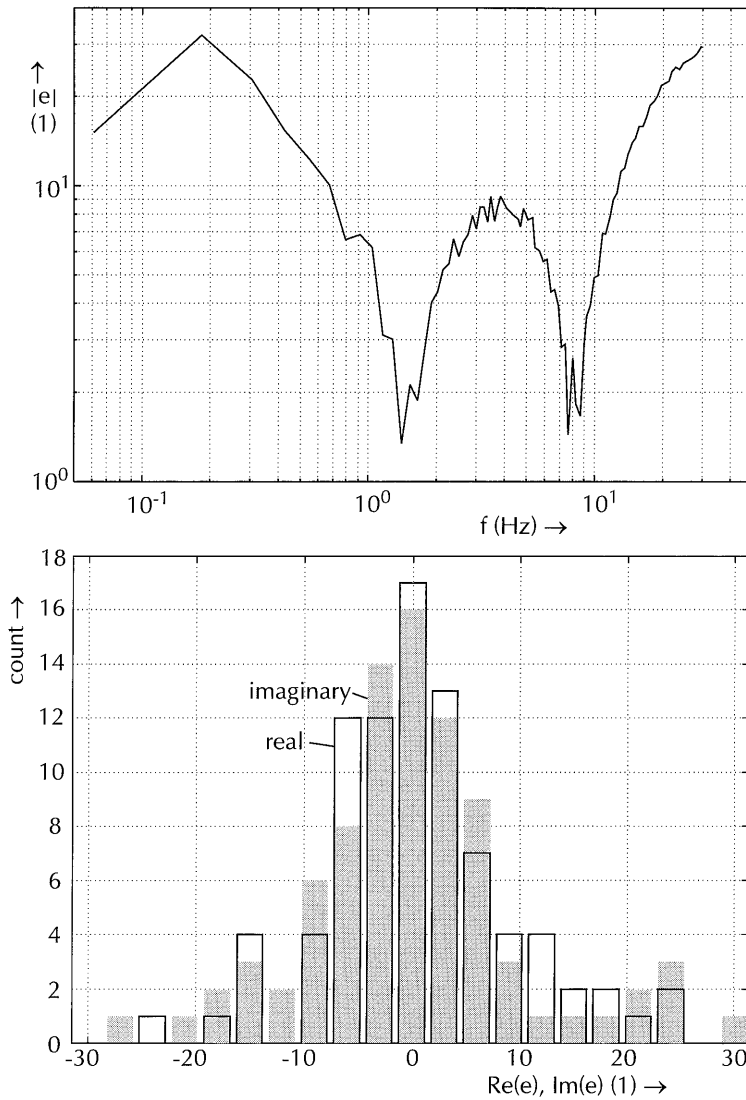


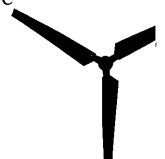
Figure 5.7
Spectrum and distribution of the residuals e



5.2 The transfer functions to be estimated

Having discussed the basic estimation procedure, we may again consider the problem of determining the excitation and response signal pair for a given transfer function.

For the transfer functions of the basic set ($Y_q(s)$, $Y_d(s)$, $sG_{fd}(s)$, $Y_{do}(s)$ and $Y_{fdo}(s)$), see figure 5.1) there is no problem: equations (4.5) - (4.7) define which measured signals of which experiment must be used to identify each of the transfer functions. The identification of some of the transfer functions in the other two sets is less straightforward since the input-output data which define the transfer functions, are



not readily available. The following transfer functions are involved: $L_q(s)$, $L_d(s)$, $G_{fd}(s)$, $Y_{fo}(s)$, $L_{fdo}(s)$, $L_{do}(s)$, $Z_{qi}(s)$, $L_{qi}(s)$, $Z_{di}(s)$, and $L_{dj}(s)$. Taking $L_{qi}(s)$ as an example, figure 5.8 shows that there are two ways to identify this transfer function. Following the left path, first an order test and an estimation are carried out on measured data, which gives parameters of $Y_q(s)$, and subsequently equations (3.13c) and (3.22b) are used to calculate the parameters of $L_{qi}(s)$. In the right path, both steps are reversed. For the other transfer functions mentioned above similar alternatives may be described.

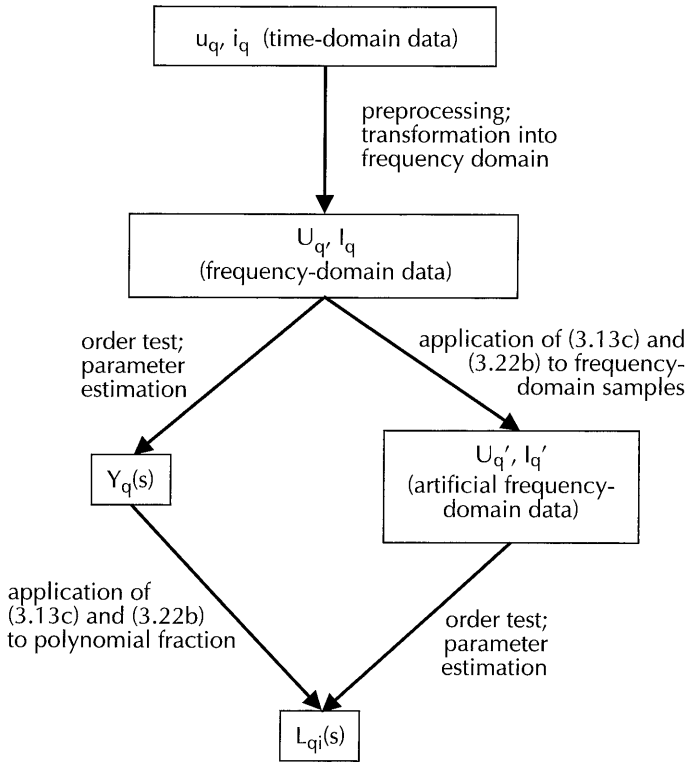


Figure 5.8
Parameter estimation procedure for transfer function $L_{qi}(s)$: two options

Polynomial or sample calculations?

Using the *left path* approach, only a basic set transfer function is actually estimated. Other quantities are derived by substitution of polynomial fractions into the appropriate equations (given in figure 5.1). These polynomial calculations have the advantage of being numerically simple, but they may lead to unrealistically high model orders. If, e.g., $Y_{fo}(s)$ is calculated using (3.14), its order is the sum of the orders of $G_{fd}(s)$ and $Y_{fdo}(s)$. This problem is avoided if the *right path* approach is followed, since the desired model order is not specified before the last step of the procedure. However, calculations with frequency-domain samples is time-consuming, especially since the applied estimator (the maximum likelihood estimator described in section 2.4) also requires the variance of the excitation and response data.

The estimation of the transfer functions of the extended set and the internal-machine set requires an additional step: either polynomial calculations have to be carried out, or frequency-domain excitation and response data, including variances, must be manipulated. From comparison of both paths in practical situations, it appears that the route via manipulated frequency-domain data is suitable for all internal-machine transfer functions except for $Y_{fo}(s)$, $L_{qi}(s)$, and $L_{di}(s)$.

For the admittance $Y_{fo}(s)$, data from two direct-axis experiments need to be combined. These experiments usually have different sample rates, and therefore the data may not be available at equal frequencies, which complicates the calculation. For the inductances $L_{qi}(s)$ and $L_{di}(s)$ the right path implies that equation (3.13a&c) must be applied to frequency-domain samples, which is difficult: it requires an accurate, externally determined value of R_a , measured at the winding temperature which occurred during the test.

The other internal-machine transfer functions ($G_{fd}(s)$, $sG_{fd}(s)$, $Y_{fo}(s)$, $Z_{qi}(s)$, and $Z_{di}(s)$) may be identified using manipulated frequency-domain data.

Summary of the internal-machine transfer function estimation procedures

We may now complete the discussion of data-processing by specifying the estimation procedure to follow for each of the transfer functions of the internal-machine set (see figure 5.1).

As concluded above, the impedances $Z_{qi}(s)$ and $Z_{di}(s)$ are estimated using manipulated frequency-domain data. From the parameters of $Z_{qi}(s)$ and $Z_{di}(s)$, the parameters of the inductances $L_{qi}(s)$ and $L_{di}(s)$ are calculated using equations (3.22), (3.23), and (3.13a).

The transfer functions $G_{fd}(s)$ and $sG_{fd}(s)$ only differ a factor s . Since $sG_{fd}(s)$ is part of the basic set, it may be estimated directly using measured data, but in this way a part of the transfer function is estimated which is already known: the factor s , which represents a zero at 0 rads^{-1} . The estimation will probably give a zero near, but not equal to, 0 rads^{-1} , which is unwanted. Therefore, $G_{fd}(s)$ is estimated, after a factor s has been removed from the frequency-domain data (I_f and I_d), and the parameters of $sG_{fd}(s)$ follow from multiplying $G_{fd}(s)$ by s .

Since $Y_{fo}(s)$ cannot be estimated directly, it must be calculated using (3.14) from the estimated parameters of $G_{fd}(s)$ and $L_{fdo}(s)$. The estimation of $G_{fd}(s)$ has just been discussed, and $L_{fdo}(s)$ is estimated after a factor s has been removed from the frequency-domain data I_d and U_f . As with $G_{fd}(s)$, for estimation $L_{fdo}(s)$ is preferred over $Y_{fdo}(s)$. Table 5.1 lists the results.

Table 5.1

Transfer function	Estimated using manipulated frequency-domain data	Derived from
$L_{fdo}(s)$ (from extended set)	x	
$Z_{qi}(s)$	x	
$Z_{di}(s)$	x	
$L_{qi}(s)$		$Z_{qi}(s)$
$L_{di}(s)$		$Z_{di}(s)$
$G_{fd}(s)$	x	
$sG_{fd}(s)$		$G_{fd}(s)$
$Y_{fo}(s)$		$G_{fd}(s)$ and $L_{fdo}(s)$

The internal-machine transfer functions estimation procedure





6

THEORETICAL ANALYSIS OF THE EXCITATION SOURCE AND OF TEMPERATURE INFLUENCES

In chapters 4 and 5 a technique for the identification of a synchronous machine has been described, which has been called the modified step-response test (MSR). In this chapter two important aspects of the MSR test are analysed theoretically.

6.1 Aims of this chapter

In this chapter two topics related to the MSR test are analysed using simulated experiments and analytical techniques. In section 6.2 the focus is on the choice of the *excitation source*. In section 6.3, the effects of *winding resistance changes* during the measurement (due to heating) are analysed.

By using analytical techniques and simulated step-response data to address these topics, the complexity of the system of the synchronous machine with rectifier is avoided, and:

- 'true' system characteristics (such as the model parameters) are known, which enables direct evaluation of identification results;
- experiments are possible which are not so easily carried out under real circumstances (e.g. varying noise level, or non-linearities);
- it is relatively easy to determine the source of inaccuracies
- the analysis and experiments are inexpensive and flexible.

6.2 The choice of the excitation source

The excitation source used in the MSR test is usually a set of batteries, possibly with a series resistor. The question is how the characteristics of this excitation source affect the identification results. The question is analysed below, taking into consideration the effects of noise and aliasing (see section 4.2).

Idealised MSR-test excitation source

Consider an idealised excitation source which is connected to an impedance Z (see figure 6.1):

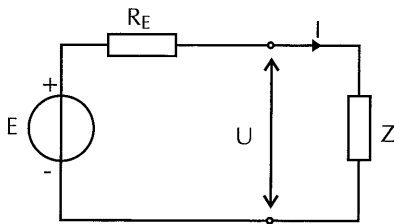


Figure 6.1
Idealised step-excitation source and impedance

$$Z(s) = R + sL \quad (6.1)$$

where R and L are a (constant) resistance and a (constant) inductance. The impedance $Z(s)$ is to be identified. The source voltage E is given in the frequency domain by:

$$E(s) = S(s) \quad (6.2)$$

where $S(s)$ is the Laplace-transform of the unit-step $s(t)$ and R_E is the internal resistance of the excitation source.

By choosing $R_E \gg R$, the excitation source approximates a current source: the current I is close to an ideal step. By choosing $R_E \ll R$, the excitation source approximates a voltage source, and the voltage U is close to an ideal step. By varying R_E/R , both the current-source and voltage-source excitation are approximated. It should be noted, that when R_E increases, the current amplitude of the test decreases. Since a test is usually designed with the current amplitude given, this implies that a current-step excitation requires a much larger voltage source than a voltage-step excitation. This is an important practical advantage of the voltage step over the current step.

Given the circuit of figure 6.1, from (6.2) and (6.1) the response current and voltage may be calculated:

$$I(s) = \frac{1}{R_E + R + sL} S(s) \quad (6.3a)$$

$$U(s) = \frac{R + sL}{R_E + R + sL} S(s) \quad (6.3b)$$

For $s \neq 0$, $S(s)$ equals:

$$S(s) = \frac{1}{s} \quad (6.4)$$

Theoretical spectra of the MSR-test signals

Using (6.3a) and (6.4), with $R = 1 \Omega$, $L = 0.1 \text{ H}$, and four different values of R_E ($1 \text{ m}\Omega$, 1Ω , 10Ω and $1 \text{ k}\Omega$), theoretical spectra of U and I are calculated, and drawn in figures 6.2 (the solid lines). The spectra are normalised with respect to their lowest frequency; the actual spectra become smaller with increasing R_E . As expected, the signal spectra are roughly inversely proportional to the frequency squared. The larger R_E , the larger the high-frequency energy in the voltage and current spectra. The current-source excitation therefore results in signals with a broader frequency band, which is advantageous. Actual limitations, however, cannot be observed considering the theoretical spectra only. More realistic spectra have to be determined, which include the effects of noise and aliasing.

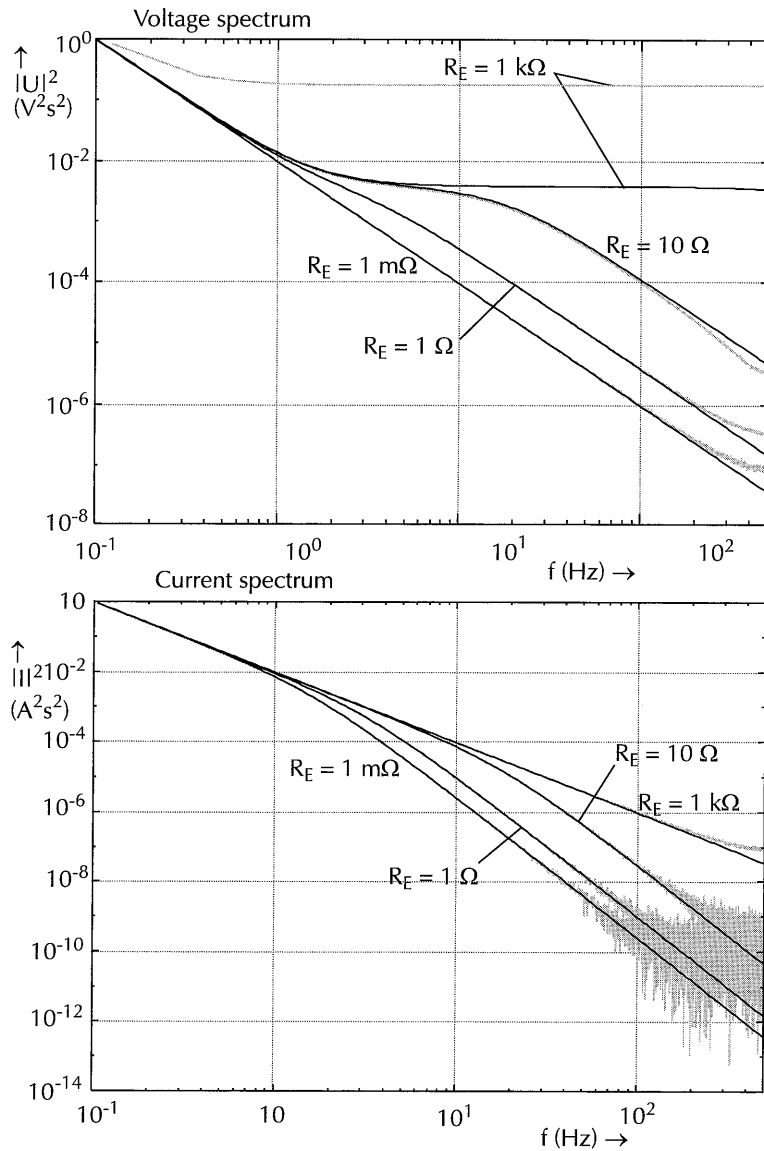


Figure 6.2
 Step-signal spectra for different values of R_E (1 m Ω , 1 Ω , 1, 10 Ω , k Ω).
 Solid lines: theoretical value; shaded or dotted lines: simulated, including the effects of noise at -70 dB
 and aliasing

More realistic spectra of the MSR-test signals

More realistic spectra of the step-response signals are obtained using numerically simulated time-domain step-response data using the model of figure 6.1 (4096 samples at a sample period of 1 ms). White noise is added at a level of -70 dB (a level which is attainable in an actual measurement). The simulated signals also allow for the analysis of the aliasing effect, the sampling phenomenon that the high-frequency content of a signal (frequencies higher than half the sample



frequency) distorts the low-frequency content. Commonly, before being sampled, signals are low-pass filtered to remove most of the frequency content above half the sample frequency, so that aliasing will not occur. But since step-response spectra exhibit a natural decrease of high-frequency content with increasing frequency, it is interesting to check whether this eliminates the need for anti-aliasing filters. The simulated signals therefore remain unfiltered, so when sampled, their high-frequency content introduces aliasing.

The simulated signals are transformed into the frequency domain, and their (normalised) spectra are displayed shaded (dotted) in figure 6.2. The normalised noise spectral density is about 10^{-10} .

The influence of the excitation source on the MSR-test bandwidth

Figure 6.2 shows that noise and aliasing cause two important differences compared to the theoretical spectra. The first difference is that the simulated spectra do not continue to decrease with increasing frequency: there is a certain frequency above which the spectrum becomes dominated by the noise, and the spectrum becomes ragged. This signal/noise intersection frequency may be used as a measure of the signal bandwidth. With increasing R_E/R , the signal/noise intersection frequency increases, which implies that with a larger R_E/R , the test may accommodate the identification of a wider range of systems. The voltage spectrum for $R_E = 1 \text{ k}\Omega$ even becomes flat at frequencies above circa 3 Hz.

The theoretical and simulated spectra also show differences which cannot be attributed to noise: for $R_E = 1 \text{ m}\Omega$ and $1 \text{ }\Omega$, the simulated voltage spectrum slightly curves upward at the high end of the frequency axis; for $R_E = 10 \text{ }\Omega$, the voltage spectrum slightly drops below the theoretical value for high frequencies; for $R_E = 1 \text{ k}\Omega$ the simulated and theoretical spectra even differ over the full frequency range shown. For the current spectra, there is an upward curve for $R_E = 1 \text{ k}\Omega$. The cause of these differences is aliasing, the amount of which increases with larger values of R_E .

From figure 6.2 the conclusion may be drawn that with a *voltage-source-like* excitation, it is possible to refrain from using anti-aliasing filters, at the expense of a smaller signal bandwidth. In case of a *current-source-like* excitation anti-aliasing filters are required.

From figure 6.2 it may also be concluded that the current is the quantity which determines the actual bandwidth of the step-response signals.

(This of course depends on the kind of system being identified. The conclusion holds for inductive systems such as a machine.) Before drawing more detailed conclusions considering the bandwidth, the signal/noise intersection frequency f_i of the current spectrum is calculated for a larger range of situations (for the calculation see Appendix A1). Figure 6.3 shows the location of f_i as a function of R_E/R , with four parameters: N , T_s , L , and the noise level. The Nyquist frequency ($1/2f_s$, $f_s = 1/T_s$) is also shown, since this is an additional limiting factor on the signal (and identification) bandwidth.

From figure 6.3 it may be concluded that the difference in f_i between a voltage-source excitation (small R_E/R) and a current-source excitation (large R_E/R) is about 2 decades (10^2 Hz versus 10^4 Hz), but this difference is neutralised to a large extent by the bandwidth limit imposed by the sample frequency. At most, the difference is somewhat less than a decade (10^2 Hz versus 10^3 Hz).

It also follows from figure 6.3 that the intersection frequency f_i decreases with increasing N , with increasing T_s , with increasing L , and with increasing noise level. Of these four parameters, the noise level has the most significant influence on the bandwidth. When using a voltage-source excitation (a small R_E/R), all variations result in an upper limit of the test bandwidth in the order of 100 Hz.

Conclusions

The following conclusions may be drawn with respect to the excitation source. Taking noise into consideration, a *current-source-like* excitation results in an MSR test with the largest bandwidth. When using a current-source-like excitation, anti-aliasing filters are required. A practical disadvantage of current-source excitation is that in its usual construction (a voltage source with a large series resistance) a much larger power source is needed than would be necessary when applying a voltage-source excitation. Furthermore, a current-source excitation may result in high induced voltages, which may harm the machine.

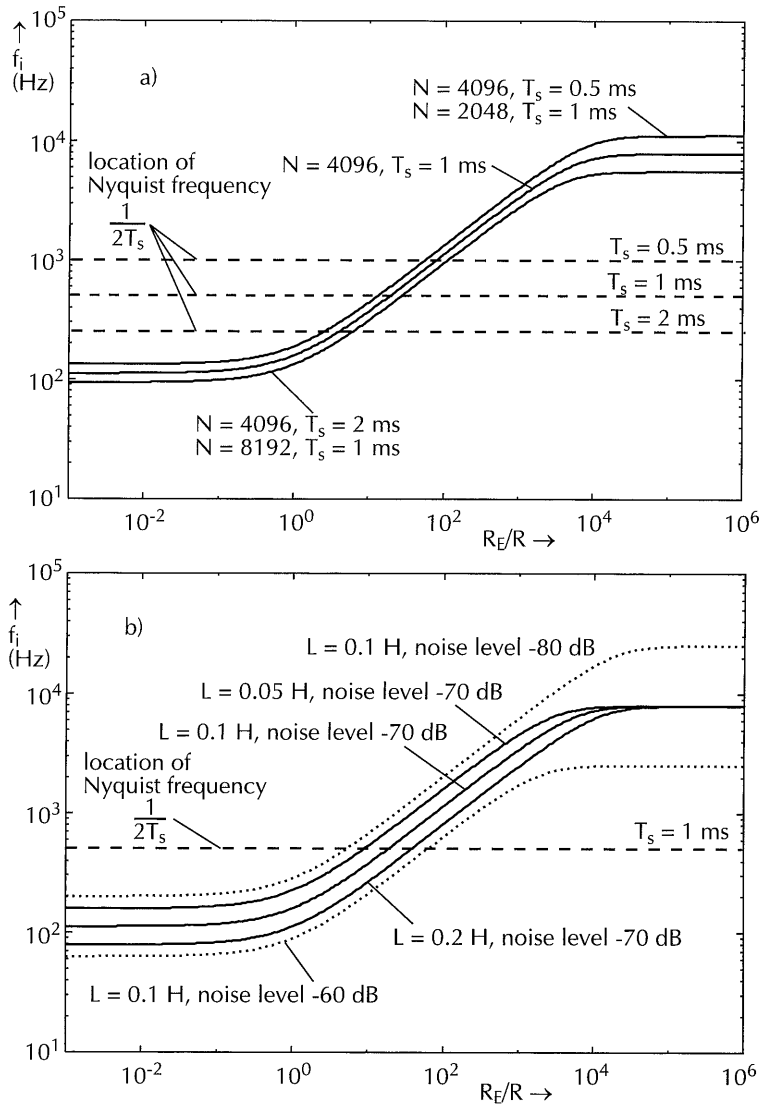


Figure 6.3
Signal/noise intersection frequency f_i of the MSR-test response current I as a function of R_E/R .

a) parameters N and T_s
b) parameters L and the noise level

When using a *voltage-source*-like excitation, the test bandwidth is smaller, but no anti-aliasing filters are required as long as the internal resistance is not larger than the winding resistance: $R_E/R \leq 1$). Under practical circumstances, where the internal resistance R_E is formed by a battery and a thyristor, this criterion will usually be met. At a noise level of -70 dB, the upper limit of the test bandwidth will be approximately 100 Hz.



6.3 The effect of winding resistance changes

The second topic to be discussed in this chapter is the effect of winding resistance changes on the identification results. Although there are other physical phenomena which also have an adverse effect on the identification of the machine (e.g. hysteresis), the literature concerning synchronous-machine identification (see section 2.3) specifically mentions changes of the stator winding resistance (R_a) as a cause of identification errors. If there are changes in R_a during the measurement, and if these are neglected in the processing of the step-response data as described in section 4.1 (i.e. the resistance R_a is supposed to be constant), then the system is outside of the model-set, which results in identification errors. In this section the effect of changes in R_a on the identification results is investigated, and in particular the effect on errors made in the identification of other parameters of the system under test.

Winding resistance changes: analysis and experiments

Step-response data are simulated as in section 6.2, but now the resistance R is not constant. In the simulations, its value is defined as:

$$R(t) = R_0 + \frac{dR}{dt} t \quad (6.5)$$

If R_0 and dR/dt are constant, then R changes as a linear function of time, which is an acceptable assumption considering the fact that heating and cooling are relatively slow processes compared to electrical phenomena (see [Dir92]).

A simple model is chosen to model the armature circuit: as a series connection of a resistance as given by (6.5), with a (frequency-dependent) self-inductance L as given by:

$$L(s) = L(0) \frac{\prod_{\mu=1}^m (1 - sz_{\mu}^{-1})}{\prod_{v=1}^n (1 - sp_v^{-1})} \quad (6.6)$$

where z_{μ} and p_v are the poles and zeros of $L(s)$.

Table 6.1 lists parameter values which describe four models which are representative for the machines we have tested (appr. 30 kVA).



Table 6.1

model name	C1	C2	C3	C4
R_0	0.25	0.25	0.25	0.25
m	2	3	2	3
n	1	2	2	2
$L(0)$	0.035	0.035	0.035	0.035
zeros of $L(s)$	-80, -0.89	-86, -7.4, -0.89	-14, -0.89	-173, -19, -0.89
poles of $L(s)$	-1	-9, -1	-20, -1	-1, -20
zeros of $R_0+sL(s)$	-10	-27, -3	-4.5	-10, -40
poles of $R_0+sL(s)$	-1	-9, -1	-20, -1	-1, -20

Four representative models of the machine armature circuit

Simulations of MSR experiments have been carried out for different values of dR/dt , and for a single value of N , namely 4096. T_s is chosen according to the criterion (4.11). From these simulated MSR data, armature circuit models are identified, using the model according to (6.5) and (6.6) as model-set, with dR/dt taken equal to zero, and with m and n chosen as specified in table 6.1. Only for model C4, $m = 2$ and $n = 1$ were used, to simulate the effect of a disturbing, unidentified pole/zero pair.

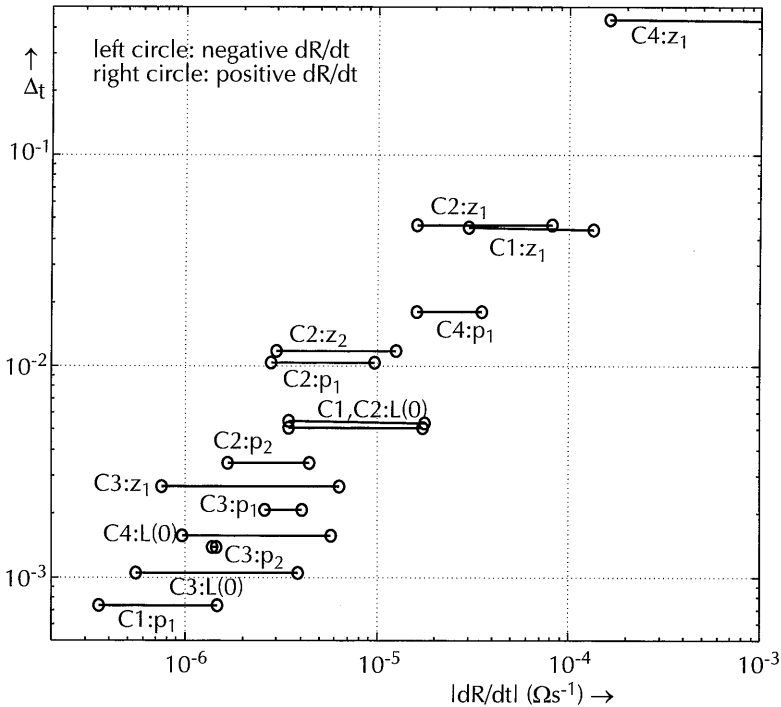


Figure 6.4
The threshold value of dR/dt and the threshold error Δ_t for $L(0)$ and the poles and zeros of models C1 - C4.



For each of the estimated parameters of models C1 - C4 (R_0 , $L(0)$), and the poles and zeros of $L(s)$, the relative estimation error is determined (e.g. for R_0 the relative estimation error $\Delta_{R_0} = |R_{0,est} / R_0 - 1|$, where $R_{0,est}$ is the estimated value of R_0). It appears that for all parameters, the relative estimation error is constant for low values of dR/dt . At a certain value of dR/dt , which is different for every parameter, the relative estimation error begins to increase. Finally, the error increases approximately linearly with dR/dt .

This behaviour of the relative estimation error as a function of dR/dt may be described by the dR/dt *threshold value*, which is defined as the value of dR/dt which doubles the error made with a constant R . Below the threshold value of dR/dt the relative estimation error is constant (the *threshold error* Δ_t), above the value the error increases approximately linearly with dR/dt .

Figure 6.4 shows, for $L(0)$ and for the poles and zeros of models C1 - C4, the dR/dt threshold value and threshold error. The dR/dt -threshold value appears to be different for negative and positive values of dR/dt : the identification is more sensitive to negative values of dR/dt . The two distinct dR/dt values for each model are indicated by a horizontal line with a circle at each end: the left circle corresponds to a negative slope, and the right circle to a positive slope.

From figure 6.4 it follows, that if a pole (or zero) is estimated with a high relative estimation error, then the estimation of this pole (or zero) is also indifferent to changes in R .

Conclusion

If errors of 1% are acceptable, dR/dt -values below $10^{-5} \Omega s^{-1}$ may be neglected. When using the MSR test, actually observed rates of changes have always been below this value (see [Hoe90]). If dR/dt -values are observed which are not negligible, the procedure outlined in Appendix A2 may be followed to eliminate the contribution of a time-varying stator winding resistance from the step-response data. This procedure presupposes that the stator resistance is known as a function of time with sufficient accuracy. This is a topic which still remains to be investigated more closely.



EVALUATION OF THE MODIFIED STEP-RESPONSE TEST BY MEASUREMENTS

In chapters 4 and 5 a technique for the identification of a synchronous machine has been described, which has been called the modified step-response test (MSR). In chapter 6 two topics of specific importance to the MSR test have been analysed, using simulated experiments. In this chapter the test is evaluated using measurements.

To enlarge the readability of the text, the figures of this chapter have been kept separate. They may be found in Appendix A4.

7.1 Aims of this chapter

The MSR test has been designed to identify a synchronous-machine model for use in the simulation of the synchronous machine with rectifier (SM/R). Therefore, a straightforward way to evaluate the test would be to ask whether identification of the synchronous machine by the MSR test enables a sufficiently accurate simulation of the synchronous machine with rectifier, compared to actual measurements. This question is difficult to answer:

- there are no clear criteria for 'sufficiently accurate';
- only a small number of machines can be measured, each under a limited number of operating conditions.

Differences between measurement and simulation will therefore be a limited basis for the evaluation of the procedure followed to simulate the machine with rectifier. And whether the MSR test, which is only a part of the procedure, performs well, will be even more difficult to establish.

More decisive MSR-test evaluation results may be obtained by identifying the machine by a number of parallel tests. Simulation results obtained via the MSR test may thus be compared to simulation results obtained via other tests, as well as to measurements. If, in the process of simulating the machine with rectifier, the only difference is the applied identification technique, then simulation differences may be attributed to the identification technique, and by comparison to measurements the techniques may be ranked.

We have chosen two identification techniques to be compared to the MSR test:

- the standstill frequency-response test (SSFR), since it is a standstill test which has acquired the status of a *de facto* standard [IEE87];
- the DC-decay test, since it is similar to the MSR test but much more involved [IEC85].

These two tests will further be called the *reference tests*. Both tests have already been introduced in section 2.3.

The two reference tests and the MSR test have been applied to two machines: a Siemens 24 kVA machine, which had already been used for similar experiments in 1989 [Hoe90], and a Heemaf 65 kVA machine. The machines have also been subjected to two standard steady-state tests which involve a rotating machine:

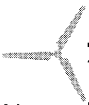
- the *steady-state no-load test* [IEC85, clause 25];
- the *steady-state sustained short-circuit test* [IEC85, clause 26].

The steady-state tests provide a couple of important synchronous-machine parameters, and prevent us from relying solely on standstill tests for the identification of the machines.

The following list summarises the evaluation activities performed for both machines:

- name plate data are gathered;
- the two steady-state tests are carried out;
- the MSR test and the two reference tests are performed;
- the two machines are identified using the test data;
- the identification results are analysed;
- representative dynamic behaviour of the two machines with rectifier are measured;
- using the identified models, the behaviour of the machines in combination with a rectifier are also simulated;
- the differences between the simulated and measured behaviour are analysed.

In the following four sections (7.2 - 7.5) the identification measurements and their results are described and discussed: the steady-state tests and their results in section 7.2, the dynamic tests (the MSR test and the two reference tests) and their results in sections 7.3 - 7.5. In section 7.6 the SM/R measurements are described and discussed. Based on the identification results, in section 7.7 simulations of the SM/R are carried out and compared to the measured behaviour, and the differences are analysed.



7.2 Standard machine data and steady-state tests

Name-plate data

The Siemens machine is a 4-pole 24 kVA inverted machine (type F 1292-4), star-connected for 400V/35A, 20 kW at $\cos(\varphi) = 0.8$. Its rated speed is 1500 min^{-1} , and its rated excitation-winding current 7A at 95V. The armature winding resistance equals 0.228Ω , the excitation-winding resistance 4.45Ω . The machine has a cage damper winding with solid cylindrical conductors lying in semi-closed slots in the laminated stator.

The Heemaf machine is a 65 kVA machine (type DG 82-4), delta-connected for 380V/98A, 65 kW at $\cos(\varphi) = 1.0$. Its rated speed ranges from 1500 min^{-1} (with rated excitation-winding current of 3.6 A) to 1800 min^{-1} (with rated excitation-winding current 3.1 A). The armature winding resistance is $88 \text{ m}\Omega$, the excitation-winding resistance 31Ω . Concluding from the delta connection, the rated phase current equals $98/\sqrt{3} = 57 \text{ A}$.

Since the SM/R measurement set-up was able to accommodate currents up to 60 A, it was decided to operate the Heemaf machine in a star-connected configuration. Given the upper limit of the line voltage of approximately 380 V, the maximum power of the machine in this set-up reduces by a factor of $\sqrt{3}$ to 37.5 kW at $\cos(\varphi) = 1.0$.



The no-load test and the sustained short-circuit test

Two common steady-state tests are carried out to gather some more data of the machines: the no-load test and the sustained short-circuit test (see [IEC85], clauses 25-27, and [IEE83], section 4). They have not been described before in this thesis, and will therefore be described here in some more detail. Figure 7.1 shows the measurement set-up. (For the figures of this chapter see appendix A4.)

The tests are relatively easy to perform, and they provide two major parameters, namely the direct-axis synchronous inductance $L_{do}(0)$ and the stator-to-field inductance $L_{fdo}(0)$. Both quantities include '(0)', to stress their constancy; they are the DC-values of the transfer functions $L_{do}(s)$ and $L_{fdo}(s)$ which appear in (3.10). Both tests require a machine which rotates at a constant speed. In figure 7.1 the machine under test, SMx, is driven by a DC-machine (GMx) which is fed by a Ward-Leonard set (AM+GMa). The no-load test determines the dependency of the open-circuit induced RMS line-voltage $u_{ab,RMS}$ on the excitation-winding current i_f . In figure 7.1 the measurement of $u_{ab,RMS}$ is indicated by the open arrows pointing at the stator terminals. The sustained short-circuit test gives the relationship between the short-circuit RMS line-current $i_{a,RMS}$ and the excitation-winding current. The measurement of $i_{a,RMS}$ is indicated by the filled arrows pointing at the stator terminals.

For both tests an amplitude of 1.2 times the rated excitation-winding current has been used (as in [IEE83]). For the no-load test, the rotor speed should be taken equal to the rated speed, which is equal for both machines (1500 min^{-1}). Since it is difficult to keep the rotor speed perfectly constant, the rotor speed was measured along with i_f and $u_{ab,RMS}$ (using a tacho). The maximum measured speed variation was about 3 %. Since variable-speed operation is a crucial aspect of the study in this thesis, the measurements have been repeated at 0.8 and 0.5 times rated speed.

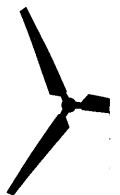
Analysis of the steady-state test data

From the constant-speed synchronous-machine equations (3.10), the Park-transformation (3.1) and (3.2), and the relationship between a sinusoidal time-domain signal and its RMS-value, it follows that:

$$\frac{u_{ab,RMS}}{p\omega_m} = L_{fdo}(0) i_f \quad (7.1)$$

$$i_{a,RMS} = \frac{1}{3} \sqrt{3} \frac{L_{fdo}(0)}{L_{do}(0)} i_f$$

where R_a has been neglected with respect to $p\omega_m L_d(0)$ and $p\omega_m L_d(0)$. Equation (7.1) implies, that (ideally) the measured data of both tests follow a straight line through the origin. The slopes of the lines are measures of the parameters mentioned above. The measured relationships, however, show saturation and hysteresis (see figure 7.2). The fact that the Heemaf machine saturates at a higher value of $u_{ab,RMS}/p\omega_m$, is caused by the fact that the Heemaf machine was star-connected during the measurement, while it is designed to operate delta-connected. For the determination of the approximate slope of these curves several approaches are given in the literature. Figure 7.3 shows two approaches for an example no-load curve. For approach A, a certain portion of the curve is considered 'straight'. The extent of this 'straight' region is determined by inspection, i.e. more or less arbitrarily, and the slope of this 'straight' portion ($O_d S_d$ or $O_u S_u$) is given as appro-



ximate slope of the curve [IEC85, IEE83]. An alternative approach (B) is to determine the slope of the curve at $i_f = 0$. For this approach a polynomial of high order (7 or 9) is fitted to the full curve ($O_d S_d T$ or $O_u S_u T$) [Hoe89b], and the value of its first derivative at $i_f = 0$ is taken for the slope. Figure 7.3 also illustrates that approach A usually leads to a lower slope value than approach B.

For the first approach, the linear parts have been determined by inspection: the no-load curves of both machines are considered straight for $i_f < 0.3 * i_{f, rated}$, and the short-circuit curves for $i_f < 0.5 * i_{f, rated}$. The slope of the linear parts of the curves is found by a 1st-order polynomial least-squares fit. For the second approach, a 7th-order polynomial least-squares fit was applied to the full curve. For the final slope-value the values of a number of curves are averaged.

The results of both steady-state tests are given in table 7.1. The no-load-test tables give values for $L_{fdo}(0)$ and its standard deviation σ over the number of curves measured.

The Siemens-machine $L_{fdo}(0)$ -values differ 6%, those of the Heemaf machine 1%. The value of $L_{fdo}(0)$ of the Siemens machine, as determined by the 7th-order estimator, is within 1.5% of the value determined in [Hoe84a].

Given $L_{fdo}(0)$ and the short-circuit test results, for the Siemens machine $L_{do}(0)$ becomes 35.7 mH or 37.4 mH, depending on the approach: a difference of 5%. For the Heemaf machine the values are 26.7 mH and 26.9 mH, a difference of less than 1%.

Table 7.1

Approach	Siemens (27 curves)		Heemaf (26 curves)	
	$L_{fdo}(0)$ (H)	3σ (%)	$L_{fdo}(0)$ (H)	3σ (%)
A (1 st order)	0.424	0.8	0.953	0.2
B (7 th order)	0.448	0.7	0.965	0.4

Approach	Siemens (25 curves)		Heemaf (21 curves)	
	$L_{do}(0)$ (H)	3σ (%)	$L_{do}(0)$ (H)	3σ (%)
A (1 st order)	$35.7 \cdot 10^{-3}$	0.8	$26.66 \cdot 10^{-3}$	0.6
B (7 th order)	$37.4 \cdot 10^{-3}$	0.8	$26.88 \cdot 10^{-3}$	0.8

Steady-state test results: $L_{fdo}(0)$ and $L_{do}(0)$

7.3 Modified step-response test

Summary of the MSR-test procedure

The three dynamic standstill tests which have been carried out, are described in sections 7.3 to 7.5, and have rather similar details. In this section the MSR test is described, as a summary of topics already discussed in detail in chapters 4 and 5. The measurement set-up is drawn in figure 7.4.

As described in section 4.1, the MSR tests consist of three consecutive measurements:

- 1) a measurement with the rotor position such that the quadrature axis is excited;
- 2) a measurement with the rotor positioned for direct-axis excitation, and the excitation winding short-circuited;
- 3) a measurement with the rotor positioned for direct-axis excitation, and the excitation winding open-circuited.

The three measurements are denoted by 'Q', 'D', and 'DO' respectively.

For the 'DO'-measurement we used a 100 k Ω precision resistor to measure the secondary voltage (the excitation-winding voltage), which may be assumed an ideal open circuit. For the 'D'-measurement, however, shunts of 1 Ω and 10 Ω were used. These are all but ideal short-circuits, and therefore, the identified transfer functions may have to be corrected for the effect of the load resistor (see Appendix A3).

The measured quantities (assuming the machine is excited by its a and b terminals) are:

1. the excitation voltage u_{ab} ;
2. the response current i_a ;
3. the response excitation-winding voltage u_f or excitation-winding current i_f (for direct-axis measurements only);
4. the temperature T_c of the machine housing.

The excitation amplitude for the MSR test is chosen as 10% of rated stator current. The remagnetising current amplitude is chosen equal to the rated amplitude. The sample rate and the number of samples are determined as suggested by (4.11). The fast measurement is carried out at a 50 μ s sample rate, as described at the end of section 4.2. For the measurement protocol of the MSR test, see section 4.3.

Experiments carried out

Table 7.2 lists the MSR measurements carried out for the Siemens machine and the Heemaf machine. None of the measurements incorporated anti-aliasing filters. The 'D'-measurements have a larger sample period because short-circuiting the excitation winding enlarges the largest time-constant of the system.

The measurements are given a name which starts with an 'M' to indicate the MSR test. The next letters indicate the machine ('S' for Siemens, 'H' for Heemaf) and the measurement ('Q', 'D' or 'DO'). A trailing number completes the name.

All measurements have been preceded by remagnetising the system by a large negative current, which is generated by the lower battery in figure 7.4 (40 A for the Siemens machine, 60 A for the Heemaf machine). Each measurement is repeated at least once.

Table 7.2

Meas. type	$i_{a,end}$ (A)	R_{as} (Ω)	R_{fs} (Ω)	N	T_s (ms)	T_c ($^{\circ}$ C)	Run name
Q	4	0.1		4096	1	23	MSQ1,2
DO	4	0.1	1 10^5	4096	1	23	MSDO1,2,3
D	4	0.1	1	4096	2	23	MSD1,2

Meas. type	$i_{a,end}$ (A)	R_{as} (Ω)	R_{fs} (Ω)	N	T_s (ms)	T_c ($^{\circ}$ C)	Run name
Q	6	0.1		4096	1	24	MHQ1,2
DO	6	0.1	1 10^5	4096	1	24	MHDO1,2
D	6	0.1	1	4096	2	24	MHD1-5

Modified step-response test overview

$i_{a,end}$ = approximate stator-current end-value

R_{as} = value of the stator current shunt

R_{fs} = value of the excitation-winding current or voltage shunt

N = number of samples acquired

T_s = sample period used

T_c = housing temperature



Figure 7.5 shows the measured signals of the measurements listed in table 7.2. To distinguish the curves, the measurement names are given (except for the first two letters, which are obvious). The two upper graphs show the stator voltage and current. The voltage peaks at $t = 0$ and then drops to its end-value; the current reaches its end-value without overshoot. By comparing peak-value and end-value of the excitation voltage in figure 7.5, it follows that the internal resistance of the source is larger than the winding resistance: the quotient R_E/R (introduced in section 6.2) equals 1.4 for the Siemens machine, and 3.5 for the Heemaf machine. These values exceed the value of 1, so the measurements are unsafe with respect to aliasing (see section 6.2). In section 7.7 some simulation errors will be described which are related to aliasing, indicating that these values of R_E/R may be a little too large.

The lower two graphs show the measured excitation-winding quantities, the induced voltage for the 'DO'-measurement, and the induced current for the 'D'-measurement. Both quantities peak, the voltage sharply, the current more gradually. After reaching their peak-value, their value decreases to zero.

Preliminary evaluation of the measurements

First, the noise level in the signals is estimated. Table 7.3 lists the noise level in the measured signals (u_{ab} , i_a , u_f and i_f , see figure 7.4), which are calculated from the final 400 samples of the signal. The noise level is expressed in dB with respect to the maximum value of the signal.

For both machines the noise level of the induced excitation voltage u_f is relatively high, and the noise level of the induced excitation-winding current i_f is extremely low. The noise-values listed in table 7.3 should also be related to the quantisation error level, which is approximately -85 dB of full scale (a 14 bit D/A-converter has been used). Since the noise levels are approximately the same as those used in the simulations in chapter 6, the conclusions drawn there are expected to be valid here also.

Table 7.3

Run set	noise in u_{ab}	noise in i_a	noise in u_f or i_f
MSQ	-85	-75	
MSDO	-65	-75	-55
MSD	-85	-75	-85

Run set	noise in u_{ab}	noise in i_a	noise in u_f or i_f
MSQ	-70	-60	
MSDO	-70	-65	-55
MSD	-70	-65	-85

Noise level in the MSR data (in dB)

Next, the signals are transformed into the frequency domain (see section 5.1). Figures 7.6 and 7.7 show Bode-diagrams of several frequency-domain quantities deduced from the signals of figure 7.5.



Figure 7.6a shows Bode-diagrams of the frequency transforms of the measured voltages and currents of the Siemens machine, calculated using the equations of section 5.1. The data are shown up to the Nyquist frequency. The step-like character is clear. The noise content of the data is indicated by the shaded background, which ranges from -3σ to $+3\sigma$ relative to the data value, where σ is the calculated standard deviation of the noise in the data.

The effect of the noise which is present in the MSR-test data, is apparent at the high-frequency end of the curves: the higher the frequency, the lower the signal content at that frequency, and gradually the signal becomes noisier and therefore more uncertain.

Also, the effect of aliasing may be observed in figure 7.6a: the amplitudes of the frequency transforms tend to proceed horizontally (compare to figure 6.2, section 6.2), and the phase difference between the measured voltages and currents exhibit large drifts above circa 100 Hz. Given the noise and the aliasing, the upper bandwidth limit is roughly 100 Hz.

Figure 7.6b shows the admittances $Y_d(s)$, $Y_{do}(s)$, $Y_q(s)$ of the Siemens machine and the associated inductances $L_d(s)$, $L_{do}(s)$, $L_q(s)$, as calculated from the voltage and current transforms using equations (4.5), (4.6a), (4.7a) and (3.13). Generally, for all derived transfer functions the relative error increases with increasing frequency. For the inductances, however, there are also large errors for low frequencies. These errors are not essential: they originate from the fact that for the calculation of the inductances using (3.13), a value of R_a is needed. A value is obtained from the two DC-measurements which are carried out before and after each MSR test to monitor changes in the stator winding resistance. For the test data shown here, the two values differ more than 1%. The resulting standard deviation is used in the calculation of the transfer functions, resulting in high uncertainties at low frequencies.

The use of a measured R_a -value is also responsible for another effect: the inductances $L_d(s)$ and $L_{do}(s)$ do not appear to tend to the steady-state value $L_{do}(0)$ as determined in section 7.2. This is caused by the small difference between the measured R_a (shown as $1/R_a$ in the Y-graph) and the limit value of the admittances for low frequencies.

Figure 7.6c shows the inductance $L_{fdo}(s)$ and the gain $sG_{fd}(s)$. Although the minimum frequency is not very low, the $L_{fdo}(s)$ -data seem to be in correspondence with the steady-state value of $L_{fdo}(s)$ determined in section 7.2.

Figure 7.6d shows $Y_{fo}(s)$ and the reciprocity calculated from (4.10), which is denoted here by $C(s)$. (Both quantities are shown here for reference and completeness only, no further analysis will be based on them.) In the Y_{fo} -graph also the value of $1/R_f$ is given, which should equal $Y_{fo}(0)$. The calculated $Y_{fo}(s)$, however, does not appear to tend to this value. The reason for this lies in the calculation of $Y_{fo}(s)$ using (3.14), $L_{fdo}(s)$ and $G_{fd}(s)$: due to the fact that the 'D'- and 'DO'-measurements are carried out at different sample rates, $L_{fdo}(s)$ is calculated at different frequencies than $G_{fd}(s)$, and consequently (3.14) can only be applied after frequency-domain interpolation of one of the two quantities. The interpolation for the lowest frequency-setpoints is rather inaccurate, and causes $Y_{fo}(s)$ to appear to have no low-frequency limit.

The reciprocity $C(s)$ is expected to equal 1. At frequencies above 0.5 Hz, $C(s)$ shows an increasing uncertainty, but 1 is within the range of possible values. For frequencies lower than 0.5 Hz, however, the calculated value of $C(s)$ clearly deviates from 1. As with the inductances of figure 7.6b, this is caused by using measured values of R_a in the calculation. The term between brackets in the denominator of (4.9) and (4.10) should ideally approach zero when the frequency approaches zero, since at DC $Y_d(s)^{-1}$ and $Y_{do}(s)^{-1}$ both equal R_a . However, both transfer functions



follow from different measurements, and therefore have slightly different values of R_a . These small differences cause $C(s)$ to differ from 1 at low frequencies. Whether the deviation of $C(s)$ from the ideal value of 1 has any consequences, has not been investigated.

Figure 7.7 gives identical data for the Heemaf machine, which show a similar behaviour.

Identification results

After transforming the measured data into the frequency domain, *order test* are performed, i.e. appropriate model orders (i.e. values for m and n in (2.2)) are determined for the transfer functions to be identified (see section 5.1). Figure 7.8 shows the results for both machines. For each machine the transfer functions listed in table 5.1 are tested ($Z_{qi}(s)$, $Z_{di}(s)$, $G_{fd}(s)$, and $L_{fdo}(s)$). Also, the basic set transfer functions $Y_q(s)$, $Y_{do}(s)$, and $Y_d(s)$ are tested, because of their general importance. The results for each transfer function are displayed in one graph. As described in section 5.1, both the *locations and standard deviations of the estimated poles and zeros* and the logarithm of the *minimal value of the loss E* are given as a function of the model order. All order tests given in figure 7.8 follow the same pattern: with increasing model order $\min(E)$ decreases, and the standard deviation of the estimated poles and zeros becomes wider.

The internal-machine impedances $Z_{di}(s)$ and $Z_{qi}(s)$ are derived using a value of the commutation self-inductance L_c , which is determined by (3.26) from L_d'' and L_q'' . These two quantities are determined via a MSR test with high sample rate (described in section 4.2). Table 7.4 lists the values of the subtransient self-inductances for both machines. The order-test results of $Z_{qi}(s)$ and $Z_{di}(s)$ are not sensitive to the value of the subtransient self-inductance used. The graphs present the order-test results for the L_c -value given in table 7.4.

Table 7.4

	Siemens	Heemaf
L_q''	3.7 mH	2.5 mH
L_d''	3.5 mH	2.9 mH
L_c	3.6 mH	2.7 mH

Subtransient self-inductances of the Siemens machine and the Heemaf machine, determined by an MSR test, and the resulting commutation self-inductance.

Table 7.5 lists the optimal orders as deduced from figure 7.8. In figure 7.8 they are indicated by a box around the optimal order. Not all order tests are equally clear, especially those for $L_{fdo}(s)$ and $Y_{do}(s)$. Considering the restriction of equal numerator and denominator order (see section 3.4), a choice for $Z_{qi}(s)$ and $Z_{di}(s)$ is difficult: the 1-1-option is clearly not the best, but the 2-2-configuration includes a rather high zero. The estimations were all based on frequency-domain samples with a frequency up to 30 Hz. The inclusion of samples at higher frequencies sometimes prevents the estimator from finding a proper fit at the lower end of the spectrum. The choice is analysed in more detail in section 7.7.

The results shown in figure 7.8 are based on only one of the available measurements for each transfer function. If the order tests for a given transfer function are repeated using other available measurement data, the order-test results are similar, and lead to the same choice of the model order.

Table 7.5

	Siemens		Heemaf	
	numer.	denom.	numer.	denom.
$Y_q(s)$	1	2	2	3
$Y_{do}(s)$	2	3	2 or 3	3 or 4
$L_{fdo}(s)$	3	4	3	4
$Y_d(s)$	1	2	2	3
$G_{fd}(s)$	2	3	2	3
$Z_{qi}(s)$	2	2	1	1
$Z_{di}(s)$	2	2	2	2

Order-test results of the MSR test: orders of transfer functions

Using the order-test results, the parameters of the transfer functions are estimated, and the estimation results are checked (as described in section 5.1). A small excerpt from the available results is given in table 7.6. This table gives a number of estimated steady-state values, some of which may be compared to table 7.1 in section 7.2. The stator resistance R_a follows from $Y_q(s)$, $Y_{do}(s)$ and $Y_d(s)$, using (3.13a-c). The steady-state inductances $L_q(0)$, $L_d(0)$ and $L_{do}(0)$ also follow by application of (3.13a-c). From $L_{fdo}(s)$ and $G_{fd}(s)$ the admittance $Y_{fo}(s)$ may be calculated using (3.14). The field winding resistance R_f and the steady-state inductance $L_{fo}(0)$ follow from $Y_{fo}(s)$ using (3.13d).

Table 7.6

	Siemens			Heemaf		
	value	$3\sigma_m$ (%)	$3\sigma_e$ (%)	value	$3\sigma_m$ (%)	$3\sigma_e$ (%)
R_a	0.237 Ω	0.7	0.04	94.3 m Ω	0.4	0.02
R_f	5.47 Ω	0.2	0.03	34.8 Ω	0.3	0.003
$L_q(0)$	20.3 mH	3	0.3	15.9 mH	4	0.06
$L_{do}(0)$	37.2 mH	5	0.4	28.6 mH	2	0.15
$L_d(0)$	37.3 mH	7	0.7	28.6 mH	6	0.1
$L_{fdo}(0)$	0.446 H	0.4	0.02	1.038 H	0.03	0.003
$L_{fo}(0)$	6.33 H	2	0.03	44.1 H	0.9	0.004
$G_{fd}(0)$	0.0816	0.3	0.001	0.0297	0.9	0.002

MSR estimation results: steady-state values

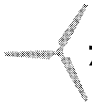
The table gives multiple standard deviation values for a parameter: σ_m is calculated using the parameter values of different measurements, and σ_e is the standard deviation as calculated by the estimator. Although some of the values of σ_m are based on only two measurements, their overall value is at least an order of magnitude larger than the values of σ_e . The uncertainty of the estimated values therefore depends primarily on uncontrolled measurement factors, which may change from one measurement to another. The noise level is of less importance, and the meaning of the estimated standard deviation is therefore limited.



Conclusions

A number of conclusions may be drawn for the MSR test:

- a) Without much effort a noise level of -70 dB can be reached.
- b) At this noise level, and without the use of anti-aliasing filters, the upper bandwidth limit is roughly 100 Hz; for the estimation, it is optimal to include samples up to 30 Hz.
- c) Calculations using samples of frequency-transformed MSR-test data may be very sensitive to errors in the stator resistance R_a .
- d) Order tests based on MSR-test data give clear results for all transfer functions except for the direct-axis quantities $L_{fd0}(s)$ and $Y_{do}(s)$. The order restriction posed upon $Z_{di}(s)$ and $Z_{qi}(s)$ (that the impedance models should be proper) results in a non-ideal compromise.
- e) For steady-state parameters, the uncertainty of the estimate depends primarily on uncontrolled measurement factors, not on the noise level; variances calculated by the estimator coincide in magnitude with error-values obtained from simulated MSR tests, but are much too small to be used as a measure for parameter uncertainty.



7.4 Reference test: the DC-decay test

Description of the DC-decay test

Both the SSFR test and the DC-decay test resemble the MSR test in many ways, since they are all standstill tests. The derivation in section 4.1 applies to all three of them. The DC-decay test measurement set-up is sketched in figure 7.9, which is an elaboration on the DC-decay principle already given in figure 2.5. Its protocol is similar to the MSR-test protocol described in section 4.3, except for the remagnetisation. Instead of a large *negative* current, a large *positive* current is applied, which is decreased gradually using a controlled voltage source (the Ward-Leonard set in figure 7.9), until the winding current reaches the final measurement level. The current now flows from the battery, and the switch S may be switched to the middle position without affecting the system. Finally, S is switched to the right position, thus short-circuiting the machine terminals and creating the DC-decay transient, which is recorded.

For the actual short-circuiting, the literature warns against bouncing switches. This is prevented by replacing the connection between terminals 3 and 6 of S with a diac or a sliding switch, which becomes responsible for short-circuiting the machine terminals. The switching behaviour of a diac and a sliding switch is different (see figure 7.10), but since the transition time stays below 0.5 ms, no effect on the identification is expected.

The DC-decay test description in the IEC-standard [IEC85] does not suggest how to process the measured data. Therefore, the MSR procedure described in chapter 5 is also used for the DC-decay test. The first step in the MSR procedure, which is offset removal, is also applied for the DC-decay test to remove the DC-levels from the measured signal.

For the DC-decay test, the settings of current and voltage amplitudes, of N and of T_s are chosen as for the MSR test.

Measurement protocol

The measurement protocol of the DC-decay test is identical to the protocol of the MSR test, except for the remagnetisation. As with the MSR test, each measurement is preceded and followed by a low-amplitude DC-measurement to monitor stator resistance changes. Refer to section 4.3 for more details.



Experiments carried out

Table 7.7 lists the DC-decay measurements carried out for the Siemens machine and the Heemaf machine. The measurements have been carried out under the same conditions as the MSR tests described in section 7.3. For more details, refer to that section.

Table 7.7

Meas. type	$i_{a,end}$ (A)	R_{as} (Ω)	R_{fs} (Ω)	N	T_s (ms)	T_c ($^{\circ}\text{C}$)	Run name
Q	6	0.1		4096	1	21	DSQ1,2,3
DO	6	0.1	$1 \cdot 10^5$	4096	1	21	DSDO1,2
D	6	0.1	1	4096	2	22	DSD3,4

Meas. type	$i_{a,end}$ (A)	R_{as} (Ω)	R_{fs} (Ω)	N	T_s (ms)	T_c ($^{\circ}\text{C}$)	Run name
Q	6	0.1		4096	1	23	DHQ1,2
DO	6	0.1	$1 \cdot 10^5$	4096	1	23	DHDO1,2
D	6	0.1	1	4096	2	23	DHD1,3

DC-decay test overview

$i_{a,end}$ = approximate stator-current end-value

R_{as} = value of the stator current shunt

R_{fs} = value of the excitation-winding current or voltage shunt

N = number of samples acquired

T_s = sample period used

T_c = housing temperature

Figure 7.11 shows the measured signals of the measurements listed in table 7.7. From figure 7.11 it follows that the internal resistance of the source approximately equals the winding resistance: $R_E/R \approx 0.8$ for the Siemens machine, and 1.3 for the Heemaf machine. With respect to avoiding aliasing, the DC-decay measurement set-up performs better than the MSR-test set-up.

Preliminary evaluation of the measurements

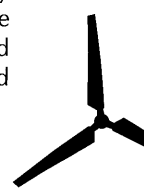
The noise content of the DC-decay data is slightly larger than that of the MSR-test data, but the differences are not large enough to warrant a special table. Figures 7.12 and 7.13 show the same Bode-diagrams as figures 7.6 and 7.7, deduced from the signals of figure 7.11. As expected, the DC-decay transformed data are very similar to those resulting from the MSR test. For the calculation of $L_q(s)$, $L_d(s)$ and $L_{do}(s)$, a value of R_a is needed, which is obtained as in the MSR test, with similar consequences for the uncertainty in the calculated data (see section 7.3).

Identification results

As for the MSR test, order tests have been carried out to obtain proper model orders for 7 transfer functions: $Y_q(s)$, $Y_{do}(s)$, $L_{fdo}(s)$, $Y_d(s)$, $G_{fd}(s)$, $Y_{di}(s)$, and $Y_{qi}(s)$. Figure 7.14 shows the results as figure 7.8 does for the MSR-test data.

Again, the differences between several measurements of the same transfer function are small, and lead to the same order choices.

Table 7.8 lists the optimal orders as deduced from figure 7.14. In figure 7.14 they are indicated by a box around the optimal order. Again, for $L_{fdo}(s)$ and $Y_{do}(s)$ there is no clear statement to be made about the best order. For the Siemens $Y_d(s)$ and the Heemaf $Y_q(s)$ transfer functions the order choice differs from what is deduced



using the MSR test, but the differences are subtle. Also, the Siemens $Z_{di}(s)$ impedance is judged to be of different order. In this case, the order-test results for the 3/3-configuration are quite different.

Table 7.8

	Siemens		Heemaf	
	numer.	denom.	numer.	denom.
$Y_q(s)$	1	2	1	2
$Y_{do}(s)$	2	3	2 or 3	3 or 4
$L_{fdo}(s)$	3	4	3	4
$Y_d(s)$	2	3	2	3
$G_{fd}(s)$	2	3	2	3
$Z_{qi}(s)$	2	2	2	2
$Z_{di}(s)$	3	3	2	2

Order-test results of the DC-decay test: orders of transfer functions

Table 7.9 gives estimated steady-state values (cf. table 7.6). The values obtained via the DC-decay test differ only slightly from those obtained by the MSR test. The same conclusion may be drawn with respect to the meaning of the estimated standard deviation of the parameters.

Table 7.9

	Siemens			Heemaf		
	value	$3\sigma_m$ (%)	$3\sigma_e$ (%)	value	$3\sigma_m$ (%)	$3\sigma_e$ (%)
R_a	0.236 Ω	1	0.01	94.5 m Ω	0.6	0.009
R_f	5.464 Ω	0.08	0.02	34.8 Ω	0.4	0.003
$L_q(0)$	20.1 mH	2	0.02	15.8 mH	0.9	0.006
$L_{do}(0)$	36.9 mH	0.5	0.09	28.5 mH	2	0.06
$L_d(0)$	35.8 mH	2	0.2	27.9 mH	1	0.5
$L_{fdo}(0)$	0.442 H	0.1	0.02	1.038 H	0.7	0.005
$L_{for}(0)$	6.39 H	0.5	0.02	44.4 H	1	0.005
$G_{fd}(0)$	0.08098	0.02	0.001	0.02983	0.2	0.004

Estimation results of the DC-decay test: steady-state values

Conclusions

The conclusions drawn for the MSR test also apply here. In fact, the results of the MSR test and the DC-decay test are very similar. The main difference between the two is the less elaborate measurement set-up of the MSR test, which will therefore be an attractive alternative for the DC-decay test.

7.5 Reference test: the standstill frequency-response test

Description of the standstill frequency-response test

The SSFR-test description of the IEE-standard [IEE87] is used, with some minor changes. Instead of using a dedicated frequency-response analyser, the sine-wave excitation and the responses are simply recorded and stored for each frequency

setpoint, and analysed using discrete Fourier transforms in Matlab. At every frequency set-point, the (complex) amplitudes of the excitation and responses are calculated, and also their variances. These data are then processed as if they were MSR frequency-domain data (see section 5.1). Figure 7.15 shows the measurement set-up, the principle of which has been sketched in figure 2.3.

To monitor stator resistance changes due to heating, the measurements at varying frequencies are alternated with DC-measurements at a low current. A personal computer controls the data acquisition and the frequency of the sine-wave generator, and also instructs it to switch from AC to DC and back.

SSFR-test settings

The excitation is a sine-wave voltage, generated by a signal generator and amplified. Recommendations with respect to the stator current amplitude in [IEE87] and [IEC85] are not consistent. We have chosen a current level of 5 A (approximately 10% of the rated stator current of both machines), so that the SSFR test is comparable to the MSR test and DC-decay test with respect to excitation signal power.

The amplifier is connected to the machine through a series resistor R_p , in order to keep the current relatively constant over a wide frequency range. The low-current DC-measurements to monitor the stator resistance, are carried out at 10% of the AC-amplitude.

The appropriate frequency-range of the test is found experimentally, by carrying out the test at various frequencies until all interesting parts of the transfer function appear to be covered. For both machines under test, the resulting frequency range is 1.5 mHz to 50 Hz.

By measuring at 5 frequencies per decade, and by fixing the sample rate to 0.5 Hz for frequencies below 25 mHz, the overall measurement length became 22 hours. During this period of time, approximately 3 Mb of data is acquired, which is about 10 times more than that of the other two standstill tests.

Measurement protocol

The actual SSFR measurements are prefaced by a manual run in which the following questions are resolved:

1. What is the interesting frequency range?
 2. What are appropriate signal amplitudes given the measuring instrument ranges?
- Based on this information the proper measurement shunts are determined. Then for three machine configurations (the 'Q', 'DO' and 'D' configurations as used also by the MSR test and DC-decay test, see section 4.1 or 7.3) the following measurement steps are executed:

1. Fix the rotor in the proper position with respect to the windings used for excitation;
2. If necessary, open-circuit or short-circuit the excitation-winding terminals;
3. Insert the correct measurement shunts;
4. Check (and if necessary adjust) the main excitation current level;
5. Check (and if necessary adjust) the DC-current level;
6. Acquire data at each frequency set-point (automated).

Experiments carried out

Table 7.10 lists the SSFR measurements carried out for the Siemens machine and the Heemaf machine. Due to problems with the sine-wave generator, each of the measurements 'Q', 'D', and 'DO' has only been carried out once for the Siemens machine, so for this machine the repeatability of the test cannot be checked.



Table 7.10

Meas. type	$i_{a,top}$ (A)	R_{as} (Ω)	R_{fs} (Ω)	T_c ($^{\circ}\text{C}$)	Run name
Q	5	0.1		20-21	FSQ1
DO	5	0.1	$1 \cdot 10^5$	21-22	FSDO1
D	5	0.1	1	19-20	FSD1

Meas. type	$i_{a,top}$ (A)	R_{as} (Ω)	R_{fs} (Ω)	T_c ($^{\circ}\text{C}$)	Run name
Q	5	0.1		21-25	FHQ1,2
DO	5	0.1	$1 \cdot 10^5$	19-22	FHDO2,3
D	5	0.1	1	23-24	FHD1,2

SSFR-test overview $i_{a,top}$ = approximate stator-current amplitude R_{as} = value of the stator current shunt R_{fs} = value of the excitation-winding current or voltage shunt T_c = housing temperature

After the calculation of the excitation and response amplitude and phase at all frequency set-points, the same Bode-diagrams can be generated as displayed in figures 7.6, 7.7, 7.12 and 7.13. The spectra of figures 7.16 and 7.17 are quite different from the MSR and DC-decay spectra. The system is excited more uniformly across the frequency band of interest, and instead of at high frequencies, the uncertainty now concentrates at low frequencies (see the graphs of the self-inductances $L_d(s)$, $L_q(s)$, $L_{do}(s)$, and $L_{dq}(s)$ and of the reciprocity).

Identification results

As for the MSR test and the DC-decay test, order tests have been carried out to obtain appropriate model orders for the following 7 transfer functions: $Y_q(s)$, $Y_{do}(s)$, $L_{fdo}(s)$, $Y_d(s)$, $G_{fd}(s)$, $Z_{qi}(s)$, and $Z_{di}(s)$. Figure 7.18 shows the results as figure 7.8 does for the MSR-test data and figure 7.14 for the DC-decay data.

Since the Siemens machine measurements have not been repeated, we cannot check the influence of repeating the measurements on the order tests. For the Heemaf machine, repeated measurements lead to identical results, except for $G_{fd}(s)$. For $Y_{do}(s)$ and $Y_d(s)$ the location of high zeros must be taken into consideration in order to arrive at consistent orders. For $G_{fd}(s)$ there is no obvious compromise. The time-domain data look similar, but an order test on measurement FHD1 leads to numerator and denominator orders of respectively 1 and 2, and an unstable model for orders 2 and 3. Measurement FHD2 gives the opposite result. I have not found an explanation for this difference.

Table 7.11 lists the optimal orders as deduced from figure 7.18. In figure 7.18 they are indicated by a box around the optimal order. There is a number of differences between the SSFR-test results and the orders determined by the MSR test and DC-decay test. The Siemens $Y_{do}(s)$ admittance numerator and denominator order both increase by one, and the orders of $L_{fdo}(s)$ and $Z_{qi}(s)$ decrease by one. For the Heemaf machine, differences are observed for $L_{fdo}(s)$ and $Z_{qi}(s)$.

To a certain extent, these differences may be caused by the fact that the value of the stator resistance R_a changes from one frequency set-point to the next. From the intermittent DC-measurements it appears that the R_a -variations correlate with night and day temperature changes, and result in a maximum variation of about 1%. If

the data are used to identify a model with constant R_a , the identification results may be affected as discussed in section 6.3.

Table 7.11

	Siemens		Heemaf	
	numer.	denom.	numer.	denom.
$Y_q(s)$	1	2	1	2
$Y_{do}(s)$	3	4	2 or 3	3 or 4
$L_{fdo}(s)$	2	3	2	3
$Y_d(s)$	2	3	2	3
$G_{fd}(s)$	2	3	2*	3*
$Z_{qi}(s)$	1	1	1	1
$Z_{di}(s)$	2	2	2	2

SSFR order-test results: orders of transfer functions

*) based on FHD2

Table 7.12 gives estimated steady-state values similar to table 7.6 and 7.9. Compared to the MSR-test and DC-decay test results, the values of $L_q(0)$, $L_{do}(0)$, $L_d(0)$, $L_{fdo}(0)$, $L_f(0)$ and $G_{fd}(0)$ are all lower, varying from 7% for $L_q(0)$ to 30% for $L_d(0)$. The most probable explanation for these differences is that the minor hysteresis loops which are being travelled at a stator current level of 5A, still differ in slope from the major hysteresis loop travelled by the MSR-test and DC-decay test signals (see section 2.3).

Table 7.12

	Siemens			Heemaf		
	value	$3\sigma_m$ (%)	$3\sigma_e$ (%)	value	$3\sigma_m$ (%)	$3\sigma_e$ (%)
R_a	0.230 Ω	1.4	0.02	92.9 m Ω	2	0.01
R_f	5.71 Ω		0.0007	36.3 Ω	3	0.006
$L_q(0)$	18.6 mH		0.3	14.3 mH	5	0.2
$L_{do}(0)$	32.2 mH		0.009	23.7 mH	10	0.07
$L_d(0)$	25.6 mH		0.2	23.2 mH	9	0.08
$L_{fdo}(0)$	0.371 H		0.0007	0.872 H	2	0.006
$L_{fo}(0)$	5.77 H		0.001	38.2 H	0.9	0.006
$G_{fd}(0)$	0.0649		0.0004	0.02399	4	$5 \cdot 10^{-5}$

SSFR order-test results: steady-state values

Conclusions

A number of conclusions may be drawn for the SSFR test, some of which apply to the MSR test and the DC-decay test as well:

- As expected, the SSFR test provides much better high-frequency data;
- Order-test results differ slightly from the order-test results of the other two tests; the order tests for $L_{fdo}(s)$ and $Y_{do}(s)$ are rather indeterminate, but the problem is smaller than for the MSR test and DC-decay test. A possible cause for these differences may be the fact that the stator resistance is not constant during the SSFR measurement.
- As with the MSR test and DC-decay test, for steady-state parameters the uncertainty of the estimate depends primarily on uncontrolled measurement



factors, not on the noise level; variances calculated by the estimator coincide in magnitude with error-values obtained from simulated MSR tests, but are much too small to be used as a measure for parameter uncertainty.

- d) For low frequencies, the SSFR test performs significantly worse than the MSR test and DC-decay test (see section 7.3 and 7.4), which is caused by the fact that the SSFR-test signals travel minor hysteresis loops whereas the MSR-test and DC-decay test signals travel the major hysteresis loop.

7.6 Measured dynamic behaviour of the synchronous machine with rectifier

Dynamic behaviour to be investigated

The specific dynamic behaviour of the synchronous machine with rectifier (SM/R) to be analysed, is the electrical and mechanical transient which is observed in the system when it is excited by a sudden change of the DC-voltage u_g or the excitation-winding voltage u_f . A measurement set-up to generate this transient is described below, and is depicted in figure 7.19. It has been described earlier in [Hoe90].

Measurement set-up

The synchronous machine with rectifier is driven by a DC-machine (GMx), and the generated power is delivered to a DC-voltage source. This source is the DC-machine (GMb) of a double Ward-Leonard set (GMb, AM, GMa). Machine GMb functions as a motor, machine GMa as a generator. The asynchronous machine AM is connected to the mains.

In two locations step-like disturbances have been generated: in the DC-circuit and in the excitation-winding circuit. To generate the excitations, small resistances with a parallel thyristor are inserted in the DC-circuit and in the excitation-winding circuit. By triggering the thyristor, the resistances are short-circuited, which results in a step-like excitation.

In [Hoe90] the system is also excited from the mechanical side, but this excitation did not give much additional information and has therefore not been included here. For validation purposes, the steady-state situation is also measured (see later in this section).

Step-like disturbances are used because they are generated easily and because their bandwidth is sufficiently wide to excite responses in the interesting bandwidth (around 1 Hz, see section 1.1).

Figure 7.19 shows the complete measurement set-up. Except for the rotor speed, the quantities are measured using a TMSC30-based digital signal processing (DSP) system with 8 analogue inputs (-10/10 V, 12 bits A/D-conversion, 2nd order anti-aliasing filters with cut-off at 1.5 kHz). For each signal a total of 4096 samples are recorded at a rate of 4 kHz.

The rotor speed ω_m is determined using a 4000 pulses-per-revolution encoder which is mounted on the rotor axis. For the Siemens machine, the torque T_m is measured by a 250 Nm torque transducer with matched amplifier. The Heemaf set-up did not have enough space to accommodate the torque-transducer.

Experiments carried out

For both machines measurements are carried out under 12 different sets of operating conditions. At each set of operating conditions, two events are measured:

- the response to a step-like change in the DC-circuit voltage;
- the response to a step-like change in the excitation-winding voltage.



The 12 operating conditions are chosen with DC-output power p_{DC} ($= u_g i_g$) ranging from approximately 50 % to 100 % of the rated power of the machine (see table 7.13). The output power may be reached at different values of the DC-output current i_g and voltage u_g , and at different values of the rotor speed ω_m . The 6th column in table 7.13 gives the field current which is necessary to reach the specific point of operation.

For the Siemens machine, the last two columns give the measured mechanical input power p_{mech} and the quotient p_{DC}/p_{mech} , which indicates the conversion efficiency. For the Heemaf machine, no torque has been measured. The mechanical input power is therefore unavailable, so the last two columns are empty.

Table 7.13

Run name	p_{DC} (kW)	i_g (A)	u_g (V)	ω_m (rads ⁻¹)	i_f (A)	p_{mech} (kW)	p_{DC}/p_{mech}
Siemens machine							
RS2	19.3	45	434	157	6.8	22.2	86.9
RS3	10.8	251	431	126	6.8	12.2	88.4
RS5	19.0	44	431	168	6.5	21.8	87.3
RS6	13.9	32	434	157	5.4	15.8	88.2
RS7	6.8	162	430	126	6.6	7.6	88.6
RS8	13.8	32	432	168	5.1	15.7	87.8
RS9a	13.2	42	312	157	5.6	15.5	85.4
RS10	13.3	42	313	126	6.3	15.4	85.9
RS11	12.9	42	310	168	5.4	15.2	84.9
RS12	9.6	31	309	157	4.4	11.2	86.4
RS13	9.6	31	309	126	5.0	11.0	87.2
RS14	9.6	31	309	168	4.2	11.2	85.6
Heemaf machine							
RH1a	26.7	61	437	157	2.9		
RH2a	26.2	60	437	126	3.2		
RH3a	26.3	60	438	168	2.8		
RH4a	17.9	41	437	157	2.2		
RH5	18.8	43	438	126	2.5		
RH6	18.4	42	438	168	2.1		
RH7	18.8	60	313	157	2.6		
RH8	19.5	62	314	126	2.9		
RH9	18.8	60	314	168	2.6		
RH10	13.1	42	313	157	2.0		
RH11	13.3	43	313	126	2.2		
RH12	12.8	41	313	168	1.9		

Operating conditions of synchronous machine with rectifier measurements

Remarks:

- 1) The intended value of 45 A could not be reached.
- 2) =70% of the value of measurement RS3.



The measured quantities all form pairs, and each pair represents a port through which energy is transported. These ports are:

- the mechanical port (rotor speed ω_m and torque T_m);
- the AC-port (stator line voltage u_{ab} and phase current i_a);
- the DC-port (rectified voltage u_g and current i_g);
- the excitation-winding port (excitation-winding voltage u_f and current i_f).

Measurement protocol

The protocol for the dynamic measurement of the synchronous machine with rectifier is as follows (refer to figure 7.19):

1. Set the excitation-winding current i_f globally with the machine at rated speed;
2. Adjust the machine speed until the DC-current i_g attains the desired value;
3. Check the machine speed ω_m ;
4. Adjust the excitation-winding current i_f and the speed ω_m until the desired operating point is reached;
5. Carry out the u_g -step-measurement and store the data;
6. Decrease the excitation-winding current i_f to zero and bring it back up to its original value (thyristor T_2 blocks);
7. Carry out the u_f -step-measurement and store the data;
8. Decrease the excitation-winding current i_f to zero and bring it back up to its original value (thyristor T_1 blocks);
9. Prepare the measurements at the next operating point.

Although previous experiences with the measurement set-up have shown the effect of hysteresis [Hoe90], the protocol does not take measures to deal with this phenomenon.

Measurement results

Figure 7.20 shows the data of measurement set no. 12 of the Siemens machine, with u_g -excitation and u_f -excitation (measurement RS12-g and RS12-f) and the corresponding Heemaf measurement set no. 10 (RH10-g and RH10-f). For each of the four measurements the inputs (u_g , u_f and ω_m) and outputs (i_g , i_f and for the Siemens machine also T_m , the mechanical torque) are given as a function of time. The various output signals respond similarly to an excitation via u_g : after a transient, the signals more or less return to their original levels. The system appears to be damped subcritically. When excited through u_f , the output signals gradually rise to a new level: the system is damped supercritically.

Voltages and currents

Due to the commutation in the rectifier, the measured voltages and currents contain a 300 Hz ripple, which makes the signals appear as areas (shown shaded in figure 7.20). These fast commutation phenomena (300 Hz and up) are not modelled by the SM/R model described in chapter 3, and they are removed from the signals (by an 8th-order zero-phase Butterworth filter with a cut-off frequency of 100 Hz) before being used as input-signals for simulations. The filter attenuates the commutation phenomena by at least 80 dB, while leaving the lower frequency band (up to 50 Hz) intact. The filtered signals are also shown in figure 7.20, as solid lines.

The measured speed

The measured speed ω_m shows the effects of quantisation, which are removed with the same filter as used above (see figure 7.20). The filtered signal, however, shows an unexpected 25 Hz ripple, which is analysed more conveniently in the frequency domain: in figure 7.21 the frequency transforms of the unfiltered signals



of figure 7.20 are shown. The signals show numerous 25 Hz-harmonics. As expected, the largest of these, at 300 Hz, is present in u_g , i_g , and i_f and corresponds to the commutation in the rectifier. In the measured speed ω_m unexpected harmonics are present at 25 Hz, 50 Hz, up to at least 200 Hz. Although much smaller, a 25-Hz component is also observed in the currents I_f and I_g , and in the voltage U_g . If measurements are carried out at other than rated speed, the frequencies of the harmonics change correspondingly, and therefore the phenomenon is related to the mechanical speed of the machine.

Similar observations are reported by Gorter [Gor97], who used the same encoder in a different set-up. He concludes that the signal (including harmonics) originates from misalignment of the rotation axes of the synchronous machine, the driving DC-machine and the encoder used to measure the rotor speed: if the DC-machine speed is constant, then misalignment causes the synchronous-machine speed and the encoder speed to vary. The synchronous machine and the DC-machine have been aligned previous to the measurements, and therefore, the effect of misalignment on the quantities I_f , I_g , and U_g is expected to be small. The encoder, however, has been mounted on the DC-machine shaft without paying attention to alignment, using a flexible coupling, so that the effect of misalignment on the speed measurement is much larger, which corresponds to the observations.

Concluding from this discussion, the 25-Hz component in the speed signal is an unmodelled measurement error, and should therefore be removed from the measured speed data before using it as a simulation input signal. The applied filter should also leave the frequency band up to 10 Hz intact. A compromise between these two demands is found in an 8th order zero-phase Butterworth filter with a cut-off frequency of 20 Hz, which gives an attenuation of 16 dB at 25 Hz. The resulting signal is shown in the four speed-graphs of figure 7.20 by a second solid line, and is used as input signal for the simulations of section 7.7.

The torque measurement

Finally, also the torque signal measured at the Siemens machine has an unexpected harmonic somewhat above 40 Hz. This frequency does not appear in any of the other measured signals and its frequency does not depend on the rotational frequency of the machine. It probably originates from the torque transducer, and should also be removed from the measured data. The torque-signal will not be simulated in the next section, and therefore no additional filtering has been performed.

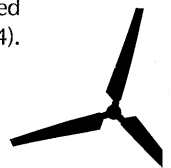
Analysis of the steady-state measurements

As a last topic before turning to the simulation of the dynamic behaviour of the system (the synchronous machine with rectifier), the steady-state data are analysed. The reasons to do this are:

- steady-state errors sometimes become large;
- the analysis is relatively easy to be carried out.

The steady-state description of the machine with rectifier (which follows from the model described in section 3.2) consists of the following equations: (3.6) with di_g/dt taken equal to zero, (3.7), (3.31) with γ_0 equal to 0, and (3.25) evaluated at $s = 0$ (and transformed into the time domain).

These 11 equations contain 14 unknown quantities, of which u_g , u_f and ω_m are input quantities (and the remaining 11 may be calculated). The equation parameters (L_c , R_a , R_f , $L_d(0)$, $L_q(0)$, $L_{fd0}(0)$) are known: L_c is determined using the procedure described in section 4.2 (Siemens machine: 3.6 mH; Heemaf machine: 2.7 mH; see table 7.4). The other parameters follow from the synchronous-machine identification.



The measurements provide steady-state data of the input quantities u_g , u_f and ω_{mr} of the DC-current i_g and of excitation-winding current i_f . From the measured AC-voltage and current, the angle of overlap μ may be determined. Thus, we have three quantities which may be used to check the steady-state correspondence between the system and the model of the machine with rectifier.

An important source of steady-state errors is *the value of the excitation-winding resistance* R_f : the identified value of R_f will not equal the value of R_f during the actual measurement, due to the fact that the identification test is carried out at room temperature, and not at a common operating temperature. This causes large steady-state differences between measurement and simulation. Since the actual value of R_f during the measurement is known (u_f as well as i_f have been recorded), it is possible to correct the model for this error: in the direct-axis model the R_f -value is changed from the identified value into the actual value during the measurement (see Appendix A3).

Having eliminated this error, figure 7.22 shows the remaining differences between measured and calculated i_g and μ , for the Siemens machine and the Heemaf machine. Each calculated value has been obtained in three ways, namely by using the three models identified by each of the three identification procedures described before. (Considering the R_f -correction, comparison of the measured and calculated steady-state value of i_f is rather meaningless, and has therefore been omitted.)

The differences between measured and calculated i_g and μ follow the same pattern. Especially for the Siemens machine the errors may become large, but also for the Heemaf machine differences up to 10 % occur. The large errors for measurements RS7 and RS3 are probably caused by saturation: both are reduced speed measurements (-20 %), with rated excitation-winding current and relatively low stator currents. Also, the differences may be related to hysteresis.

The Siemens machine and Heemaf machine steady-state errors only depend marginally on the kind of identification procedure used (a few percent at most).

Additional experiments show that to decrease the Siemens machine errors to the level of the Heemaf machine (see figure 7.22), L_c needs to be reduced by 15%, $L_d(0)$ or $L_q(0)$ increased by 15%, or $L_{fd0}(0)$ reduced by 5%. For $L_d(0)$ and $L_{fd0}(0)$, these changes exceed the error margins of both quantities (see section 7.2, page 80, and section 7.3, page 87). For L_c , a change of 15% may be motivated by the empirical nature of (3.26).

As mentioned above, the steady-state differences are mainly caused by the inaccurate identification of R_f . For the remaining steady-state differences, some possible explanations are given below (without going into further detail):

- saturation and hysteresis;
- the voltage drop across the diodes in the rectifier (1.8 V) has been neglected;
- the rectified current i_g is assumed to be constant, but the measured current contains a ripple of up to 15% of the average current value;
- the effect of the brushes of the Siemens machine (a voltage drop of approximately 2 V) has been neglected;
- the internal-machine voltage source (equation (3.5)) may not be exactly sinusoidal, but may include higher harmonics, e.g. due to saturation.

Both voltage drops (across the diodes of the rectifier and the brushes of the Siemens machine) have been taken into consideration in the simulations described in the next section.



7.7 Simulated dynamic behaviour of the synchronous machine with rectifier

Simulation model

The system of the synchronous machine with rectifier and load has been simulated using Matlab/Simulink. Figure 3.5 shows a general block-diagram of the model, and gives references to the equations which are used.

For the internal-machine direct-axis and quadrature-axis models, the transfer functions listed in table 3.1 and figure 5.1 need to be identified, for example in the way described in section 5.1. The individual direct-axis SISO-models of the individual transfer functions are combined into a state-space version of the MIMO direct-axis model (3.25a) (see table 3.1), and its order is reduced using standard routines (*modred* in Matlab). Similarly, from the SISO-model of $Z_{qi}(s)$, a state-space version of the MIMO quadrature-axis model (3.25b) is created.

Simulations carried out

The remaining part of this chapter is dedicated to the comparison of simulations of the SM/R with the measurements described in section 7.6. For each machine, four measurements are selected: the measurement at maximum power (RS2, RH1a), and three measurements at half the maximum power, with reduced DC-voltage and current, at three different speeds (RS12, RS13, RS14, RH10, RH11 and RH12). For each measurement two sets have been considered: the set with DC-circuit excitation (denoted by a suffix '-g') and the set with field-winding excitation (denoted by suffix '-f').

Each set of measurement data contains 5 (Heemaf) or 6 (Siemens) quantities. Three of these (the rectified DC-voltage u_g , the excitation-winding voltage u_f and the machine speed ω_m) are used as inputs of the SM/R model. The signals are filtered as described in section 7.6. Using these filtered signals, the model responses (i_g and i_f) are simulated.

Figures 7.23 and 7.24 show the measured quantities i_g and i_f for these eight SM/R measurements (filtered like the input quantities), and compare them to the simulated quantities. Each quantity is simulated three times, using the synchronous-machine models as identified by the three identification tests described earlier in this chapter (the MSR test, the DC-decay test, and the SSFR test). The model orders are as determined by these tests, see tables 7.5, 7.8, and 7.11. For L_c the values of table 7.4 are used. The measured data are shown dotted, the MSR-test simulations are shown dashed.

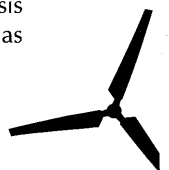
Evaluation of the simulation results

Within the context of this thesis, no criteria have been formulated to decide whether the quality of simulation results is sufficient or insufficient. Evaluation of the simulation results will therefore be restricted to comparisons and observations without an absolute quality judgement.

Steady-state differences

The most prominent difference between the measured quantities and their simulated counterparts is their steady-state value. In section 7.6 it has already been concluded that steady-state values may be simulated inaccurately.

With respect to simulating the *steady-state*, the Heemaf machine results are better than those of the Siemens machine, and the SSFR test gives the smallest steady-state differences between measurement and simulation. In the steady-state analysis of section 7.6 it is concluded that the choice of the identification technique has only minor impact on steady-state errors.



the model of the machine with rectifier. On the other hand, if the impact of the variations is considerable, then refinement of the identification procedure may also be an option when the simulation results need to be enhanced.

The following variations of the identification procedure are analysed below:

- variations concerning the identification procedure in a *general* sense;
- variations concerning the identification procedure in *detail*.

General variations of the identification procedure

The following general variations of the identification procedure are considered:

- repeating the identification experiment;
- using different model-orders for the individual transfer functions;
- applying different weighting factors for the estimation (for the identification carried out in sections 7.3 - 7.5 only samples up to 30 Hz were used, see section 7.3 under Identification results).

From these variations, the effect of repeating the experiments is particularly important, since it may show how sensitive the procedure is to uncontrolled or random changes, which inevitably affect the measurement set-up and equipment.

Variations of details of the identification procedure

The identification procedure can also be varied in details, e.g. by using external values of parameters. Since alternative values of $L_d(0)$ and $L_{fd0}(0)$ are available from the steady-state tests (see section 7.2), one may identify the machine under the condition of given $L_d(0)$ and $L_{fd0}(0)$. We shall consider the effect of varying $L_d(0)$ and $L_{fd0}(0)$, since it may be an option to enhance the SSFR-test identification. Similarly, variations of $L_q(0)$ and L_c are considered. For the commutation self-inductance L_c other values are conceivable, due to the empirical nature of (3.26).

Analysis of the impact of the variations

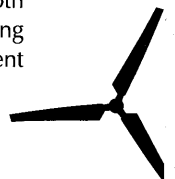
The effects of these variations are presented in the figures below (figures 7.25 - 7.29). Only the MSR test is used for identification, and from the simulation data only the rectifier DC-current response i_g is shown. Simulations are carried out for two SM/R experiments: experiment RS12-g and RH10-g at half the maximum power, rated speed, and with DC-circuit excitation.

These limitations are motivated as follows:

- The DC-current response and the field-current response are very similar in shape (cf. figure 7.23 and 7.24).
- The dynamic character of the measurements with DC-circuit excitation is more pronounced. Especially the response peak value is interesting since it has consequences for designing the system (maximum currents and forces, need for measures to keep these quantities within limits). The SM/R measurements with field-winding excitation do not exhibit overshoot, and their general effect may be predicted using steady-state calculations only.
- For the reference tests no results are presented because they are similar to the results from the MSR test.

Repeating the identification experiment

To check the sensitivity of the MSR identification procedure to repeating the step-response measurements, for each of the MSR measurements 'Q', 'DO', and 'D' two realisations are considered. All possible combinations of these measurements, $2 \times 2 \times 2 = 8$ in total, have been submitted to the identification procedure. For both machines, the largest difference in the identification results originates from repeating the 'D'-measurement. In figure 7.25, the differences in the simulated DC-current



i_g are shown. The second experiment (MSD2 for the Siemens machine, and MHD4 for the Heemaf machine) leads to a slightly smaller i_g -peak-value than the first (MSD1, MHD3). Furthermore, the second Siemens experiment gives a subcritically damped transient, much like the DC-decay simulations in figure 7.23.

A closer analysis shows that the only transfer function of the internal-machine set which changes significantly, is the direct-axis internal impedance $Z_{di}(s)$. Figure 7.26 shows Bode-diagrams of the identified $Z_{di}(s)$. The differences between the two are concentrated in the region above 10 Hz. Figure 7.26 also shows the frequency-domain data which were used to identify $Z_{di}(s)$. For both machines, repeated experiments lead to differences in the experimental data above approximately 10 Hz (with large uncertainties). The amplitude data of the Siemens machine curve downward, and the phase increases rapidly with increasing frequency. At higher frequencies than those shown in figure 7.26, the amplitude increases again. In both Siemens measurements and in the MHD3-measurement, the value of $Z_{di}(s)$ becomes large and negative at the Nyquist frequency ($1/2T_s$).

The differences are caused by the unobtrusive fact that within the sample interval which surrounds the step-moment, the *actual instant* of the step varies. This is in fact a case of aliasing: the measured voltage signal high-frequency content is too large in relation to the sample frequency. As has been observed in sections 7.3 and 7.4, the problem results (at least partly) from using an excitation source with an internal resistance which is too large.

Choosing different model orders for the individual transfer functions

To check the sensitivity of the MSR identification procedure to the choices of the model orders of the internal-machine transfer functions, four quantities ($Z_{qi}(s)$, $Z_{di}(s)$, $G_{fd}(s)$ and $L_{fdo}(s)$) are re-identified using both numerator and denominator order one less than determined by the MSR order tests (see table 7.5). Sixteen additional simulations are carried out (for each of the four transfer functions there are two possible model choices, one of the original order, and one with lowered order).

Again, the only notable difference originates from the identification of $Z_{di}(s)$, see figure 7.27. The use of the reduced model-orders leads to a considerably larger i_g -peak-value than the use of the original values, and the transient is subcritically damped.

In [Hoe90], a direct-axis model for the Siemens machine has been identified which incorporated a 3rd-order $Z_{di}(s)$ (numerator and denominator order equal to 3). The model was adjusted manually to enhance the fit in the region of 0.5 to 5 Hz. With our present data, a 3rd-order $Z_{di}(s)$ cannot be identified except by using *ad-hoc* techniques (e.g. interactively changing the parameters until a good fit is reached), and has therefore not been used in simulations.

Using weighting factors in the estimator

To check the sensitivity of the MSR identification procedure to changes of the frequency band of the samples which are used for the identification, the upper limit of this frequency band is changed. It appears that varying the upper limit from 30 Hz to 75 Hz does not result in significant simulation changes. Below 30 Hz the estimator behaves increasingly troublesome.

Weighting the frequency band from 1 to 10 Hz, an option originally envisioned to create a model which would correctly predict the system behaviour in this frequency range, does not result in significant simulation changes. If the weight of this frequency range is increased too far, then the identification results at DC deteriorate.

Using external values for $L_d(0)$, $L_{fd0}(0)$, $L_q(0)$ and L_c

The values of $L_d(0)$ and $L_{fd0}(0)$ as determined by the MSR test differ from those determined by the steady-state tests (see section 7.2, and table 7.6), by $\pm 2\%$ and $\pm 3\%$ respectively. Figure 7.28 shows the effect of fixing the value of $L_d(0)$ and $L_{fd0}(0)$ during the identification, at 30% below and 30% above the originally estimated value (the deviation is chosen relatively high to create visible changes in the dynamic simulation results).

It appears that changes in $L_d(0)$ and $L_{fd0}(0)$ primarily affect the steady-state. Changes of approximately -5% in $L_{fd0}(0)$ and 10% in $L_d(0)$ neutralise the steady-state differences between measured and simulated i_g . The simulated transients are not very sensitive to changes in $L_d(0)$ and $L_{fd0}(0)$. Therefore, the use of externally determined values of $L_d(0)$ and/or $L_{fd0}(0)$ seems important mainly for the SSFR-test identification (see section 7.5, page 90). For the other two tests, it may improve the steady-state simulation.

Variations of $L_q(0)$ have been analysed but not shown in figure 7.28, since there is no externally supplied value available for this quantity. The effect of variations in $L_q(0)$ is comparable to that of $L_d(0)$.

Parameter L_c is varied from 30% below to 30% above their original value. In figure 7.29 the simulated DC-current i_g is shown resulting from the applied variations. Variations of L_c have considerable impact on the DC-current response, for the steady-state as well as the shape of the transient.

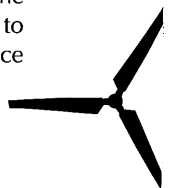
Conclusions

In this section the MSR-test identification results of section 7.3 have been used to create dynamic models of the Siemens machine with rectifier, and of the Heemaf machine with rectifier. The behaviour of these models has been compared to measurements, and also to the behaviour simulated by models built by two other identification techniques (the DC-decay test and the Standstill Frequency-Response test). In general, the three ways of identifying the machine lead to similar results. There is not one technique which clearly performs better than the others.

With respect to the differences between measurement and simulation, several sources have been indicated. A source of large differences is the value of R_f , the excitation-winding resistance, which is identified at room temperature, but attains a different value at operating temperature. Furthermore, steady-state differences are probably caused by the rectifier model (see section 7.6), in relation to saturation and hysteresis. Both are also probable causes for differences between simulated and measured end-levels after a transient.

The identification via the MSR test has been submitted to some additional analysis, from which the following conclusions have been drawn.

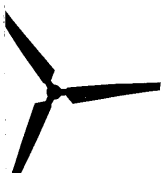
- Repeating the identification measurements leads to similar identification results for all transfer functions, and consequently, to small simulation differences. The impedance $Z_{dq}(s)$ shows the largest variation, which is caused by the fact that the stator voltage of the 'D'-measurement is affected by aliasing (in the set-up used, the internal resistance of the battery was too high).
- Order choices of the transfer functions of the internal-machine set (see figure 5.1) are not critical, except for $Z_{di}(s)$.
- Different weighting factors have been applied in the estimation of the transfer functions of the internal-machine set, using the orders which followed from the order tests. The behaviour of the synchronous machine with rectifier appears to be rather insensitive to the weighting applied in these estimations. The impedance

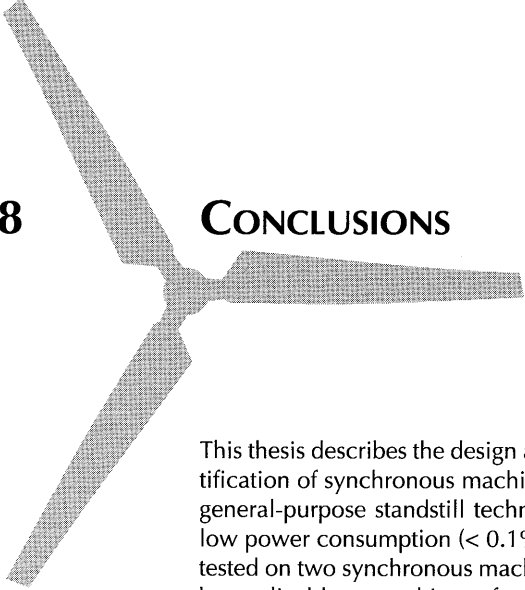


$Z_{dij}(s)$ may be an exception, if it is re-identified using measurement data which are not affected by aliasing.

- The use of externally determined values of $L_d(0)$, $L_{fd0}(0)$, and L_c may improve the simulation results, in particular the calculation of the steady-state, but it is not the prime solution for the differences which are observed between simulations and measurements

Apparently the procedure to identify the machine using MSR-test data is not very crucial for the simulation of the system of a synchronous machine with rectifier. If a more accurate match between this system and its model is necessary, the identification procedure may be improved by including anti-aliasing filters into the measurement set-up (or by using a battery with a sufficiently low internal resistance). Simultaneously, attention should be directed to the refinement of the model, e.g. with respect to saturation and hysteresis.





This thesis describes the design and evaluation of a simple technique for the identification of synchronous machines, the *modified step-response (MSR) test*. It is a general-purpose standstill technique which has a very simple test set-up, and a low power consumption ($< 0.1\%$ of the rated power of the machine). It has been tested on two synchronous machines of approximately 30 kVA, but is expected to be applicable to machines of a wide power range.

The test has originally been designed as an aid for modelling the system of a synchronous machine with rectifier, a system which was to be incorporated in a variable-speed wind-energy system. For the design a number of criteria has been formulated (see chapter 1), which may be summarised as follows: a simple technique was required, which would allow identification of (essentially linear) models of the machine. The existing experience in the field of synchronous machine identification, as described in the literature, has been reviewed (chapter 2) and been used as a basis for the test design, which has resulted in a modification of an existing technique (chapters 3 - 6).

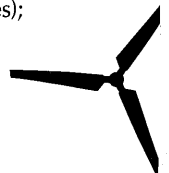
The test has been evaluated under practical circumstances (chapter 7) within the context of the system of the synchronous machine with rectifier. The dynamic behaviour of the synchronous machine with rectifier has been measured, and also simulated, using synchronous machine models identified by the MSR test and two reference tests: the DC-decay test and the Standstill Frequency-Response (SSFR) test. The evaluation has been based on comparison of measurements and simulated results. The evaluation result may be summarised as follows: the MSR test enables a simple identification procedure, especially with respect to the identification experiment. The quality of the identification is comparable to that of the DC-decay test. The SSFR test has a larger bandwidth, but also needs significantly larger excitation signals to match the MSR test at low frequencies.

Below, the conclusions which have already been given at the end of the successive chapters, are recapitulated.

Conclusions from the literature on synchronous machine identification

There are many publications on synchronous machine identification, but only very few cover the full identification procedure, which consists of:

- the choice of a set or class of possible models;
- the choice of the identification experiment (test signal, set-up);
- the choice of a specific model from the model-set, using measurement data from the system under test (which includes the determination of parameter values);
- the validation of the results.



Many publications limit themselves to simulations, which makes it difficult to judge the quality of the applied identification technique. Furthermore, most of the existing identification techniques are outdated, at least in their official form, and although efforts are being made in modernising them, the assimilation of results from the field of identification theory and control is progressing slowly.

Concerning the machine model, it is concluded that Park's theory remains an indispensable tool. Network models appear to hamper the identification. Instead, transfer-function representations of Park's axis models are preferred.

Considering the necessary identification experiment, most techniques disqualify because of the cost, size, or weight of the equipment, or because of the fact that the equipment cannot be installed easily. The least practical obstacles are to be expected from standstill tests using terminal measurements only.

A step signal is chosen to excite the machine. Although a step excitation is much less persistent than e.g. a range of sine-waves (the SSFR test) or a (binary) noise signal, it has the advantage of allowing excitation at a low power level. Contrary to many other excitation signals, an identification experiment using a low-amplitude step excitation is not adversely affected by the hysteresis of the magnetic circuit of the machine.

Existing step-response tests try to approach an ideal step excitation, which leads to complicated measurement set-ups. Non-ideal steps, however, are equally well suited for identification, and generated much more easily. This measurement set-up advantage outweighs the disadvantage of the less persistent excitation, and therefore the standstill test with non-ideal step excitation has been adopted as identification experiment.

For the estimation, a frequency-domain estimator is preferred, for two reasons: it easily allows stressing model accuracy in the frequency band around 1 Hz; it allows monitoring of the effects of the unbalanced energy density spectrum of the step signal.

Advantages and disadvantages of the MSR test

The Modified Step-Response test has the following advantages:

- it needs a small amount of standard equipment;
- it is safe for the machine;
- it is fast: the preparations of the machine under test are limited, the measurement set-up is simple, and the tests themselves are a matter of seconds;
- the necessary identification calculations are carried out using standard software;
- it allows identification of models valid in a large range of operating conditions.

The fact that the measurements require the machine to be at standstill, is usually also considered an advantage, but this depends on the situation.

Its main disadvantages are:

- the test has a small identification bandwidth compared to other techniques;
- within its bandwidth, the excitation energy is not spread evenly, but concentrated at low frequencies.

Characteristics of the MSR test

The upper limit of the test bandwidth is approximately 100 Hz, at a noise level of -70 dB. This noise level is achievable without specific measures, except that it requires a 14 bit D/A-conversion. The lower bandwidth limit is related to the measurement length, which should equal 2 to 5 times the largest time-constant of the machine.

If a current-source-like excitation is used, the bandwidth is maximal, but it requires a larger excitation signal power source, and may pose a risk to the machine (high induced voltages).

With a voltage-source excitation, the bandwidth is smaller, but the required power source is small. Furthermore, anti-aliasing filters are not strictly necessary. Winding resistance changes due to temperature effects during the measurements may be neglected for the identification.

The performance of the MSR test, as compared to two reference tests

The identification results of the MSR test (order tests and estimated parameters) are compared to results of two reference tests (the DC-decay test and the Standstill Frequency-Response test). Two machines have been identified using the three techniques mentioned: a rather uncommon inverted machine and a regular machine, both rated about 30 kVA.

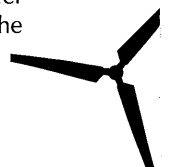
From the identification results it is concluded that the performance of all three tests is rather similar. The same conclusion also follows from using the identified machine models to simulate the system of the synchronous machine with rectifier: from comparison of the simulation results to actual measurements, it may be concluded that the choice of the identification technique is of secondary importance. The correspondence between the MSR test and the DC-decay test is expected since they both use a step excitation. The tests provide usable frequency-domain data up to approximately 30 Hz, given a signal-to-noise ratio of 70 dB. The main difference between the two is the more elaborate measurement set-up of the DC-decay test. The MSR test will therefore be an attractive alternative for the DC-decay test.

Also as expected, the SSFR test provides much better high-frequency data (i.e. with less variance) than the MSR test. But at comparable excitation signal levels the low-frequency data of the SSFR test are significantly worse than those of the MSR test and DC-decay test, which is caused by the fact that the SSFR-test signals travel minor hysteresis loops whereas the MSR-test and DC-decay test signals travel the major hysteresis loop. This may be corrected, but considering the equipment and time needed for an SSFR test, in many cases the MSR test will be preferable. The performance of the combination of the MSR test and the model of the synchronous machine with rectifier, in predicting the behaviour of this system Using the identified machine models, the system of the synchronous machine with rectifier is simulated, and the simulations are compared to the measured behaviour.

The largest differences between measurement and simulation occur for the steady-state of the system. A source of large differences is the value of R_f , the excitation-winding resistance, which is identified at room temperature, but attains a different value at operating temperature. After correcting for this error, still some steady-state differences remain. Compared to the steady-state differences, the differences between dynamic simulation results and measurements are smaller. The dynamics are simulated equally well for both considered machines.

Possible causes of the observed differences are unmodelled system characteristics (hysteresis, saturation, neglected DC-circuit voltage drops), and the identification procedure (too low model order, repeatability of the test, weighting). The topics related to the identification procedure have been checked and may be eliminated as possible cause for errors:

- Repeating the identification measurements leads to similar identification results for all transfer functions, and consequently, to small simulation differences. The impedance $Z_{di}(s)$ shows the largest variation.
- The orders of the transfer functions of the machine are not critical, except for $Z_{di}(s)$.
- Different weighting factors have been applied in the estimation of the transfer functions of the internal machine set, using the orders which followed from the



order tests. The behaviour of the synchronous machine with rectifier appears to be rather insensitive to the weighting applied in these estimations. The impedance $Z_{di}(s)$ may be an exception, if it is re-identified using measurement data which are not affected by aliasing.

- The use of externally determined values of $L_d(0)$, $L_{fd0}(0)$, and L_c may improve the simulation results, in particular the calculation of the steady-state, but it is not the prime solution for the differences which are observed between simulations and measurements

Apparently the procedure to identify the machine using MSR-test data is not very crucial for the simulation of the system of a synchronous machine with rectifier. If a more accurate match between this system and its model is necessary, the identification procedure may be improved by including anti-aliasing filters into the measurement set-up (or by using a battery with a sufficiently low internal resistance). Simultaneously, attention should be directed to the refinement of the model, e.g. with respect to saturation and hysteresis.





SUMMARY

This thesis describes the design and evaluation of a simple technique for the identification of synchronous machines: the *modified step-response (MSR) test*. The technique has been evaluated using two synchronous machines of approximately 30 kVA, but is expected to be applicable to machines of a wide power range. Contrary to most standard tests, it is not tied to a specific model of the machine. It is a standstill technique with a very simple test set-up, and a low power consumption (< 0.1% of the rated power of the machine).

The MSR test has been designed as an aid to model the synchronous machine with rectifier, a system which was analysed with respect to its potentials in variable-speed wind-energy systems. Due to this context, the MSR test has been evaluated using the behaviour of the synchronous machine with rectifier as a bench-mark.

Initial design requirements

Originating from the research of the synchronous machine with rectifier, the following requirements for the identification technique have been formulated:

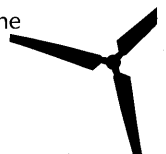
1. It should allow identification of the dynamic behaviour of a synchronous machine of about 100 kVA, in a frequency range of approximately 0.1 Hz - 10 Hz.
2. It should allow determination of the subtransient inductance values of the machine.
3. The measurements should have a low power consumption.
4. The measurement equipment should be compact.
5. Terminal measurements should be sufficient.
6. Measurements should be possible while the machine is at standstill.
7. The number of measurements should be low.

Synchronous machine identification

From the literature on synchronous machine identification, no readily available solution could be obtained. To prepare a customised solution, two essential parts of the identification procedure are discussed in detail: the *model of the system* to be identified (a synchronous machine), and the choice of a *persistent excitation* for the identification experiment. A *step excitation* appears to be a good compromise between persistent excitation and the ability to identify a general-purpose model from relatively low-power signals and a simple measurement set-up.

The modified step-response test

The concept of the step excitation is used as a basis for the *Modified Step-Response (MSR) Test*. Instead of attempting to generate an *ideal* step, which is found in the literature but which is difficult to achieve, an *approximate* step is generated by simply switching on a low-power DC-voltage source (e.g. a battery) which is connected to two stator terminals of the machine. Both the excitation and the



response are measured. The measurement set-up is very simple, which is an important advantage over most other synchronous machine identification techniques. The acquired data are transformed into the frequency domain, and the frequency-domain data are used to identify the transfer functions of the two axis models of the machine.

Evaluation of the MSR test

The MSR test is evaluated in a relative way, by comparison to *two reference tests* (the DC-decay test and the Standstill Frequency-Response test), within the context of the system of a synchronous machine with rectifier. The procedure is as follows. Two 30 kVA machines are identified using the three tests. The machines are incorporated in a set-up with a rectifier, and dynamic measurements are carried out. With the models, the system behaviour is also simulated. From comparisons of simulated and measured behaviour, conclusions are drawn with respect to:

- the performance of the MSR test, as compared to the two reference tests;
- the performance of the combination of the MSR test and the model of the synchronous machine with rectifier, in predicting the behaviour of this system.

It is concluded that the performance of the MSR test, the DC-decay test and the SSFR test is rather similar: it is of relatively minor importance for the simulations which test is used. The first two tests provide usable frequency-domain data up to approximately 30 Hz, given a signal-to-noise ratio of 70 dB. The SSFR-test bandwidth reaches 250 Hz without difficulties, but at comparable excitation levels it has inferior quality at low-frequencies. The main difference between the three tests is the measurement set-up: the MSR-test set-up is the most favourable considering equipment cost and weight, measurement time and complexity.

Comparison of the measurements to simulations mainly shows differences with respect to the steady-state. Dynamic differences are much smaller. Possible causes of these differences are unmodelled system characteristics (hysteresis, saturation, neglected DC-circuit voltage drops), and the identification procedure (too low model order, repeatability of the test, weighting). The topics related to the identification procedure have been checked and may be eliminated as possible cause for errors: the simulation errors appear to be insensitive to repetition of the test, to the actual model-order choice, and to weighting.

The only exception is the stator impedance $Z_{di}(s)$: it is sensitive to variations in the identification procedure, and is also an important factor in the rectified current response. Its sensitivity may be reduced by proper measures against aliasing.





SAMENVATTING

Windmolens zijn onderhevig aan voortdurend wisselende krachten. Hoe beter die krachten in de molen kunnen worden opgevangen, hoe goedkoper dat is, want dat betekent dat de constructie lichter kan worden. Er wordt daarom voortdurend gezocht naar wegen om de krachten in een molen te verkleinen.

Eén van de eenvoudigste manieren is deze: een gewone windmolen die elektriciteit opwekt kan maar op één snelheid draaien, omdat het elektriciteitsnet een vaste frequentie van 50 Hz heeft. Maar voor de krachten in een molen is het veel gunstiger als die zou kunnen versnellen en vertragen alnaargelang de wind harder of zachter waait. Dat kan gerealiseerd worden door de opgewekte elektrische energie eerst gelijk te richten, en daarna pas om te zetten in een 50 Hz wisselspanning.

Aan dit systeem van generator, gelijkrichter en wisselrichter is aan de TUE vanaf de jaren 80 onderzoek gedaan. Dit onderzoek begon eenvoudig, maar gaandeweg werd het veelomvattender, omdat het systeem soms onverwacht gedrag vertoonde (oscillaties), maar ook omdat het steeds belangrijker werd te voorspellen hoe het systeem zich onder bepaalde omstandigheden zou gedragen.

Om dat te kunnen doen, werd er een model (een wiskundige beschrijving) van het systeem gemaakt. Een van de knelpunten van dat model was, dat daarin parameters van de generator (een synchrone machine, of kortweg machine) voorkwamen, die we niet kenden. Daarom zijn we op zoek gegaan naar een eenvoudige techniek om de parameters van een gegeven machine te bepalen, d.w.z. om de machine te *identificeren*.

Dit proefschrift beschrijft het ontwerp en de evaluatie van de gevonden eenvoudige techniek voor de identificatie van synchrone machines: de *aangepaste stap-responsie test*, ofwel in het Engels: *modified step-response (MSR) test*. De techniek wordt in dit proefschrift geëvalueerd aan de hand van twee synchrone machines van ongeveer 30 kVA, maar naar verwachting is hij bruikbaar voor machines van een breed vermogensgebied. In tegenstelling tot de meeste standaardtechnieken, is de MSR test niet gekoppeld aan een specifiek model van de machine. De test gaat uit van een stilstaande machine, heeft een bijzonder eenvoudige meetopstelling en een laag energieverbruik (< 0.1% van het nominale vermogen van de machine).

De MSR test is ontwikkeld als hulp bij het modelleren van de synchrone machine met gelijkrichter, een systeem dat werd onderzocht vanwege zijn mogelijke toepassing in windenergie systemen met een variabel toerental. Vanwege deze context heeft het gedrag van de synchrone machine met gelijkrichter gefungeerd als kapstok voor de evaluatie van de MSR test.



Oorspronkelijke ontwerp-eisen

Vanuit het onderzoek naar de synchrone machine met gelijkrichter zijn de volgende eisen voor de identificatietechniek geformuleerd:

1. De techniek moet identificatie mogelijk maken van het dynamisch gedrag van machines van ongeveer 100 kVA, in een frequentiegebied van ongeveer 0.1 Hz - 10 Hz.
2. Met de techniek moeten de subtransiënte zelfinducties van de machine bepaald kunnen worden.
3. De metingen moeten een laag energieverbruik hebben.
4. De benodigde meetapparatuur moet compact zijn.
5. Metingen aan de klemmen van de machine moeten voldoende zijn.
6. De metingen moeten mogelijk zijn bij stilstaande machine.
7. Het aantal noodzakelijke metingen moet laag zijn.

Identificatie van synchrone machines

Uit de literatuur over identificatie van synchrone machines komt geen kant-en-klare oplossing naar voren. Ter voorbereiding van een oplossing toegesneden op onze eigen situatie, worden twee essentiële kanten van de identificatieprocedure in detail besproken: het *model van het systeem* dat geïdentificeerd moet worden (een synchrone machine), en de keuze van een *persistente excitatie* voor het identificatie-experiment. Een *stap-excitatie* blijkt een goed compromis te zijn tussen enerzijds persistente excitatie en anderzijds de mogelijkheid om algemene modellen te identificeren op basis van relatief kleine signalen en een eenvoudige meetopstelling.

De aangepaste stap-responsie test

Het concept van de stap-excitatie is de basis voor de *Modified Step-Response (MSR) Test*. In plaats van te proberen een *ideale* stap te genereren, wat in de literatuur wordt gepoogd maar wat moeilijk te verwezenlijken is, wordt een benaderde stap gegenereerd door eenvoudigweg een gelijkspanningsbron van laag vermogen (bijvoorbeeld een accu) in te schakelen die verbonden is met twee stator-klemmen. Zowel het excitatie-sigitaal als het responsie-sigitaal worden gemeten. De meetopstelling is erg eenvoudig, wat een belangrijk voordeel is in vergelijking met de meeste andere identificatietechnieken voor synchrone machines.

De meetgegevens worden naar het frequentiedomein getransformeerd, en deze frequentiedomein-gegevens worden gebruikt om de overdrachtsfuncties te identificeren van de modellen van de twee assen van de machine.

Evaluatie van de MSR test

De MSR test wordt geëvalueerd in relatieve zin, door vergelijking met twee *referentie tests* (de DC-decay test en de Standstill Frequency-Response test), binnen de kontekst van het systeem van de synchrone machine met gelijkrichter. De procedure is als volgt. Twee 30 kVA machines worden geïdentificeerd met de drie tests. De machines worden vervolgens ingebouwd in een opstelling met een gelijkrichter, en dynamische metingen worden uitgevoerd. Met de modellen wordt het systeem eveneens gesimuleerd. Door vergelijking van het gesimuleerde met het gemeten gedrag worden conclusies getrokken over:

- het functioneren van de MSR test vergeleken met de referentietests;
- het functioneren van de combinatie van MSR test en het model van de synchrone machine met gelijkrichter, wat betreft het voorspellen van het gedrag van dit systeem.

De conclusie is dat de MSR test, de DC-decay test en de SSFR test alle drie vergelijkbaar functioneren: het is van ondergeschikt belang voor de simulaties welke van de drie tests wordt gebruikt. De eerste twee tests leveren bruikbare meetgegevens tot ongeveer 30 Hz, bij een signaal-ruisverhouding van 70 dB. De SSFR test bereikt met gemak een bandbreedte tot 250 Hz, maar bij vergelijkbare amplitudes van de excitatiesignalen is de kwaliteit van de test bij lage frequenties minder. Het belangrijkste verschil tussen de drie tests is de meetopstelling: de opstelling van de MSR test onderscheidt zich wat betreft kosten en gewicht van de apparatuur, meettijd en complexiteit.

Vergelijking van de metingen met de simulaties laat met name stationaire verschillen zien. Dynamische verschillen zijn veel kleiner. Mogelijke oorzaken voor deze verschillen zijn ongemodelleerde aspecten van het systeem (hysterese, verzadiging, verwaarloosde spanningsvallen in het gelijkstroomcircuit), en de identificatie-procedure (te lage modelordes, de herhaalbaarheid van de test, weging). De onderwerpen die met de identificatieprocedure te maken hebben, zijn gecontroleerd en mogen worden uitgesloten als oorzaak voor fouten: de simulatie is ongevoelig voor herhaald testen, voor de keuze van de modelorde, en voor weging. De enige uitzondering is de stator impedantie $Z_{di}(s)$: die is gevoelig voor variaties in de identificatieprocedure, en is eveneens een belangrijke factor in de respons van het systeem. De gevoeligheid kan worden teruggebracht door juiste maatregelen te nemen tegen aliasing.







REFERENCES

- [Abo88] Abo-Shady, S.E., F.I. Ahmed, S.M. El-Hakim, and M.A. Badr: *Analysis of Self-Dual Excited Synchronous Machine*. IEEE Trans. on Energy Conversion, vol. 3, no. 2, pp. 305-314 (part 1) and 315-322 (part 2), 1988.
- [Alv89] Alvarado, F.L., and C. Cañizares: *Synchronous machine parameters from sudden-short tests by back-solving*. IEEE Trans. on Energy Conv., vol. 4, no. 2, pp. 224-236, 1989.
- [Aui80] Auinger, H., und G. Nagel: *Vom transienten Betriebsverhalten herrührende Schwingungen bei einem über Gleichrichter belasteten Synchrongenerator*. Siemens Forsch. u. Entwickl.-Ber., vol. 9, no. 1, 1980.
- [Bac95] Bacalao U., N.J., P. de Arizon, and R.O. Sánchez L.: *A Model for the Synchronous Machine using Frequency Response Measurements*. IEEE Trans. on Power Systems, vol. 10, no. 1, 1995.
- [Bed88] Bedford, T.J., and A.G. Jack: *A method to compute transients in synchronous generators using frequency domain methods*. IEEE Trans. on Energy Conversion, vol. 3, no. 2, pp. 367-374, 1988.
- [Bey94] Beya, K., e.a.: *Identification of Synchronous Machines Parameters Using Broadband excitations*. IEEE Trans. on Energy Conversion, vol. 9, no. 2, 1994.
- [Bis93] Bissig, H., K. Reichert, and T.S. Kulig: *Modelling and Identification of Synchronous Machines, a New Approach with an Extended Frequency Range*. IEEE Trans. on Energy Conversion, vol. 8, no. 2, pp. 263-271, 1993.
- [Boj90] Boje, E.S., J.C. Balda, R.G. Harley, and R.C. Beck: *Time-domain identification of synchronous machine parameters from simple standstill tests*. IEEE Trans. on Energy Conv., vol. 5, no. 1, pp. 164-175, 1990.
- [Bol76] Bollinger, K.E., R. Winsor, and D. Cotcher: *Power system identification using noise signals*. IEEE PES, summer meeting 1976 record, text 339-2, pp. 1-7, 1976.
- [Bol82] Bollinger, K.E., H.S. Khalil, L.C.C. Li, and W.E. Norum: *A method for on-line identification of power system model parameters in the presence of noise*. IEEE Trans. on Power App. and Systems, vol. PAS-101, no. 9, pp. 3105-3111, 1982.

- [Bon82] Bonte, J.A.N., en M.J. Hoeijmakers: *Windturbinesysteem met variabel toerental*. PT/Elektrotechniek/Elektronika, vol. 37, no. 8, pp. 66-73, 1982.
- [Bon90] Bongers, P., W. Bierbooms, S. Dijkstra, and T. Van Holten: *An Integrated Dynamic Model of a Flexible Wind Turbin*
- [DeM81] De Mello, F.P., and L.H. Hannett: *Validation of Synchronous Machine Models and Derivation of Model Parameters from Tests*. IEEE Trans. on Power Apparatus and Systems, vol. PAS-100, no. 2, pp. 662-672, 1981.
- [DeM83] De Mello, F.P., and L.H. Hannett: *Determination of Synchronous Machine Electrical Characteristics by Test*. IEEE Trans. on Power Apparatus and Systems, vol. PAS-102, no. 12, pp. 3810-3813, 1983.
- [Dir92] Dirven, R.G.C.: *Een model van de korte-termijn temperatuursafhankelijkheid van de weerstand van een machine-wikkeling*. Stageverslag Faculteit Elektrotechniek (EMV 92-11), Eindhoven University of Technology, 1992.
- [ElH89] El-Hakim, S.M.: *Transient performance of the self-dual excited synchronous machine*. etzArchiv, vol. 11, no. 7, pp. 221-230, 1989.
- [ElS92] El-Serafi, A.M., J. Wu, and A.S. Abdallah: *Saturation representation in synchronous machine models*. Electric Machines and Power Systems, vol. 20, pp. 355-369, 1992.
- [ElS93] El-Serafi, A.M., and J. Wu: *Determination of the Parameters Representing the Cross-Magnetizing Effect in Saturated Synchronous Machines*. IEEE Trans. on Energy Conversion, vol. 8, no. 3, 1993.
- [Erl94] Erlich, I.: *Empfindlichkeit elektromechanischer Ausgleichsvorgänge bezüglich der Parameter von Synchronmaschinen*. Elektrie, vol. 48, no. 2/3, pp. 44-48, 1994.
- [Fai90] Fairbairn, R.E., and R.G. Harley: *On-line measurement of synchronous machine parameters*. Conf. Record of the 1990 IEEE Industry Appl. Society Annual Meeting, vol.1, pp. 134-139, 1990.
- [Gor97] Gorter, R.J.: *Grey-box Identification of Induction Machines*. Thesis Eindhoven University of Technology, Eindhoven, 1997.
- [Hoe84a] Hoeijmakers, M.J.: *On the steady-state performance of a synchronous machine with convertor: with special attention to wind energy conversion systems*. Dissertation Eindhoven University of Technology, 1984.
- [Hoe84b] Hoeijmakers, M.J.: *Resultaten van enkele simulaties van overgangsverschijnselen bij een demperloze synchrone machine met gelijkrichter*. Group Electromechanics and Power Electronics, Faculty of Electrical Engineering, Eindhoven University of Technology, Report EMV 84-33, 1984.
- [Hoe88] Hoeijmakers, M.J.: *A Simple Model of the Synchronous Machine with Convertor*. Proc. 8th Int. Conf. on Electrical Machines, Pisa, 12-14 sept. 1988, vol. 2, pp. 237-242, 1988.
- [Hoe89a] Hoeijmakers, M.J., en J.M. Vleeshouwers: *Een model van de synchrone machine met gelijkrichter, geschikt voor regeldoeleinden*. Eindhoven University of Technology, EUT-Report 89-E-215, 1989.
- [Hoe89b] Hoeijmakers, M.J.: *A possibility to incorporate saturation in the simple, global model of a synchronous machine wit rectifier*. Eindhoven University of Technology, EUT Report 89-E-225, 1989.
- [Hoe90] Hoeijmakers, M.J., and J.M. Vleeshouwers: *Derivation and Verification of a Model of the Synchronous Machine with Rectifier with two Damper Windings on the Direct Axis*. Eindhoven University of Technology, EUT-Report 90-E-248, 1990.
- [Hoe96] Hoeijmakers, M.J.: *A simple model of a synchronous machine with rectifier*. Proc. Int. Conf. on Electrical Machines (ICEM '96), Vigo (Spain), vol. 2, pp 57-62, 1996.
- [Hua94] Huang, C.-T., e.a.: *On-line Measurement Based Model Parameter Estimation for Synchronous Generators: Model Development and Identification Scheme*. IEEE Trans. on Energy Conversion, vol. 9, no. 2, pp. 330-336, 1994.
- [IEC85] International Electrotechnical Committee: *IEC Standard 34-4: Rotating Electrical Machines - part 4: Methods for determining synchronous machine quantities from tests*. Geneva: Central Office of the Int. El. Committee, 1985.
- [IEE83] Institute of Electrical and Electronics Engineers: *IEEE Guide: Test Procedures for Synchronous Machines (IEEE Std 115-1983)*. New York: IEEE, 1983.
- [IEE87] Institute of Electrical and Electronics Engineers: *IEEE Standard Procedures for obtaining Synchronous Machine Parameters by Standstill Frequency Response Testing (Supplement to IEEE Std 115-1983)*. New York: IEEE, 1987.
- [Iri86] Iriasa, T., S. Takata, R. Ueda, T. Sonoda, and T. Mochizuki: *A novel approach on a parameter self-tuning method in an ac servo system*. Automatica, vol. 22, no. 3, pp. 287-294, 1986.

- [Jac87] Jack, A.J., and T.J. Bedford: *A Study of the Frequency Response of Turbogenerators with Special Reference to Nanticoke G.S.* IEEE Trans. on Energy Conversion, pp. 496-505, 1987.
- [Jin90] Jin, Y., and A.M. El-Serafi: *A Three Transfer Function Approach for the Standstill Frequency Response Test of Synchronous Machines.* IEEE Trans. on Energy Conversion, vol. EC-5, no. 4, pp. 740-749, 1990.
- [Kam90] Kamwa, I., P. Viarouge, and E.J. Dickinson: *Optimal Estimation of the Generalized Operational Impedances of Synchronous Machines from Short-Circuit Tests.* IEEE Trans. on Energy Conversion, vol. 5, no. 2, pp 401-407, 1990.
- [Kam91] Kamwa, I., P. Viarouge, and E.J. Dickinson: *Identification of generalised models of synchronous machines from time-domain tests.* IEE Proc.-C, vol. 138, no. 6, pp. 485-498, 1991.
- [Kam92] Kamwa, I., P. Viarouge, and J. Dickinson: *A Frequency-Domain Maximum Likelihood Estimation of Synchronous Machine High-Order Models Using SSFR Test Data.* IEEE Trans. on Energy Conversion, vol. 7, no. 3, pp. 525-536, 1992.
- [Kam94a] Kamwa, I., P. Viarouge, and R. Mahfoudi: *Phenomenological Models of Large Synchronous Machines from Short-Circuit Tests During Commissioning - A Classical/Modern Approach.* IEEE Transactions on Energy Conversion, vol. 9, no. 1, pp. 85-97, 1994.
- [Kam94b] Kamwa, I., P. Viarouge, H. Le-Huy, and E.J. Dickinson: *Three-transfer-function approach for building phenomenological models of synchronous machines.* IEE Proc.-Gener. Transm. Distrib., vol. 141, no. 2, 1994.
- [Key89] Keyhani, A., S. Hao, and G. Dayal: *The Effects of Noise on Frequency-Domain Parameter Estimation of Synchronous Machine Models.* IEEE Trans. on Energy Conversion, vol. 4, no. 4, pp. 600-607, 1989.
- [Key92a] Keyhani, A., and S.I. Moon: *Maximum likelihood estimation of synchronous machine parameters and study of noise effect from DC flux decay data.* IEE Proc.-C, vol. 139, no. 1, pp. 76-80, 1992.
- [Key92b] Keyani, A.: *Synchronous Machine Parameter Identification.* Electric Machines and Power Systems, no. 20, pp. 45-69, 1992.
- [Key94] Keyhani, A., H. Tsai, and T. Leksan: *Maximum Likelihood Estimation of Synchronous Machine Parameters from Standstill Time Response Data.* IEEE Trans. on Energy Conversion, vol. 9, no. 1, pp. 98-114, 1994.
- [Kin89] King, R.J.: *A Fourier analysis for a fast simulation algorithm.* IEEE Trans. on Power Electronics, vol. 4, no. 4, pp. 434-441, 1989.
- [Kol94] Kollar, I.: *Frequency Domain System Identification Toolbox for use with MATLAB.* Mathworks Partner Series, Mathworks, Natick Mass., 1994.
- [Lan83] Lang, R.D., M.A. Hutchison, and H. Yee: *Microprocessor-based identification system applied to synchronous generators with voltage regulator.* IEE Proc. part C, vol. 130, no. 5, pp. 257-265, 1983.
- [Lev59] Levy, E.C.: *Complex-Curve Fitting.* IEEE Trans. on Automatic Control, vol AC-4, pp 37-43, 1959.
- [Lju87] Ljung, L.: *System Identification: Theory for the user.* Englewood Cliffs, NJ, Prentice Hall, 1987.
- [Ma_94] Ma, J., B.W. Hogg, N. Zhiyuan and Y. Yihan: *On-line Decoupled Identification of Transient and Sub-T*
- [Par29] Park, R.H.: *Two Reaction Theory of Synchronous Machines, Part I.* Trans. AIEE, 1929 (vol. 48), pp. 716-728.
- [Par33] Park, R.H.: *Two Reaction Theory of Synchronous Machines, Part II.* Trans. AIEE, 1933 (vol. 52), pp. 352-355.
- [Pin90] Pintelon, R. and J. Schoukens: *Robust identification of transfer functions in s- and z- domains.* IEEE Trans. on Instrumentation and Measurement, vol. 39, no. 4, pp. 565-573, 1990.
- [Pin94] Pintelon, R., P. Guillaume, Y. Rolain, J. Schoukens, and H. Vanhamme: *Parametric Identification of Transfer Functions in the Frequency Domain - A Survey.* IEEE Trans. on Automatic Control, vol. 39, no. 11, pp. 2245-2260, 1994.
- [Rak80] Rake, H.: *Step Response and Frequency Response Methods.* Automatica, vol. 16, pp. 519-526, 1980.
- [Rit86] Ritter, C.: *Bestimmung der Parameter einer Synchronmaschine mit Hilfe von Gleichspannungsversuchen im Stillstand.* etzArchiv, vol. 8, no. 6, pp. 189-194, 1986.
- [Ruf92] Ruff, M., J. Wiesing und H. Grotstollen: *Ein automatisiertes Verfahren zur Identifikation der Parameter einer Asynchronmaschine.* Elektromagnetischer Felder, Energiewandlung und -versorgung: 37. Internationales Wissenschaftliches Kolloquium, TU Illmenau, 21-24 september 1992, vol. 1, pp. 234-239.



- [Sau91] Saunders, R.M.: *Synchronous-machine Standstill Frequency-Response Test Data Analysis*. IEEE Trans. on Energy Conversion, vol.6, no. 3, 1991.
- [Ser88] Serrano-Iribarnegaray, L., and A. Cervera-Vicente: *Cylindrical rotor synchronous machine with non-sinusoidal stator currents (part 1)*. etzArchiv, vol. 10, no. 6, pp. 195-200, 1988.
- [Sha74] Shackshaft, G.: *New approach to the determination of synchronous-machine parameters from tests*. Proc. IEE, vol. 121, no. 11, pp. 1385-1392, 1974.
- [Sha77] Shackshaft, G., and A.T. Poray: *Implementation of new approach to the determination of synchronous-machine parameters from tests*. Proc. IEE, vol. 124, no. 12, pp. 1170-1178, 1977.
- [Tou94] Touhami, O., H. Guesbaoui and C. lung: *Synchronous Machine Parameter Identification by a Multitime Scale Technique*. IEEE Trans. on Industry Appl., vol. 30, no. 6, pp. 1600-1608, 1994.
- [Tum95] Tumageanian, A., and A. Keyhani: *Identification of Synchronous Machine Linear Parameters from Standstill Step Voltage Input Data*. IEEE Trans. on Energy Conversion, vol. 10, no. 2, pp. 232-240, 1995.
- [Vle90] Vleeshouwers, J.M., M.J. Hoeijmakers and J.A. Schot: *A practical method of determining quadrature-axis synchronous machine parameters using a least-squares estimator*. Proc. Electrical Drives Symposium, Capri (IT), pp. 125-139, 1990.
- [Vle92a] Vleeshouwers, J.M.: *Experimental Verification of a Simple Dynamic Model of a Synchronous Machine with Rectifier*. Proc. Int. Conf. on Electrical Machines (ICEM), Manchester, vol.3, pp. 1087-1091, 1992.
- [Vle92b] Vleeshouwers, J.M.: *Derivation of a model of the Exciter of a Brushless Synchronous Machine*. Eindhoven University of Technology, EUT Report 92-E-258, 1992.
- [Wan95] Wang, J.-C., H.-D. Chiang, C.-T. Huang, and Y.-T. Chen: *Identification of synchronous generator saturation models based on on-line digital measurements*. IEE Proc.- Generation, Transmission and Distribution, vol. 142, no. 3, pp. 225-232, 1995.
- [Wat73] Watson, W., and G. Manchur: *Synchronous machine operational impedances from low voltage measurements at the stator terminals*. IEEE Trans. on Power App. and Systems, vol. PAS-93, pp. 777-784, 1973.
- [Wil95] Williamson, S., and A.F. Volschenk: *Time-stepping finite element analysis for a synchronous generator feeding a rectifier load*. IEE Proc.-Electr. Power Appl., vol. 142, no. 1, pp. 50-56, 1995.
- [Wri31] Wright, S.H.: *Determination of synchronous machine constants by test*. Trans. AIEE, vol. 50, pp. 1331-1351, 1931.

LIST OF SYMBOLS

Operators

Description

\angle	angle of
*	complex conjugation
–	(bar over symbol) mean
arg min	the function argument which minimises
cov	covariance (function of two arguments)
d	differentiation
Im	imaginary part (function of a complex variable)
min	minimum of
Re	real part (function of a complex variable)
T	transpose

Unit
[deg]

Quantities

Description

γ	synchronous-machine rotor position	Unit [rad]
γ_0	synchronous-machine rotor position at $t = 0$	
Δ	relative estimation error (chapter 6)	[1]
Δ_t	threshold-error (section 6.3)	
ε	phase angle of voltage source (3.5)	[rad]
η	noise-power spectral density (appendix 1)	[Ws]
θ	general vector of parameters	
θ_{\min}	parameters which minimise loss function (section 2.4)	
μ	angle of overlap (commutation angle)	[rad]
μ_c	calculated angle of overlap (section 7.6)	
μ_m	measured angle of overlap (section 7.6)	
σ	standard deviation	[*]
σ^2	variance	
σ_m	standard deviation determined from a number of measurements	
σ_e	standard deviation determined by estimator	
τ	time-constant	[s]
$\tau_d^{(i)}$	direct-axis time-constants, eq. (3.25)	
$\tau_{do}^{(i)}$	direct-axis time-constants, eq. (3.25)	
τ_{\max}	largest time-constant of system under test (section 4.2)	
ψ	flux [Vs]	
ψ_a	stator a-phase flux	
ψ_b	stator b-phase flux	
ψ_c	stator c-phase flux	
ψ_d	direct-axis stator flux	
ψ_{di}	internal direct-axis stator flux (figure 3.5)	
ψ_f	direct-axis excitation-winding flux	
ψ_q	quadrature-axis stator flux	
ψ_{qi}	internal quadrature-axis stator flux (figure 3.5)	
Ψ	flux (frequency domain, Laplace-transformed)	[Vs ²]
Ψ_d	direct-axis stator flux	

	Ψ_{di}	internal direct-axis stator flux	
	Ψ_f	direct-axis excitation-winding flux	
	Ψ_q	quadrature-axis stator flux	
	Ψ_{qi}	internal quadrature-axis stator flux	
ω		angular frequency	[rad s ⁻¹]
	ω_B	noise bandwidth (Appendix 1)	
	ω_m	rotor angular speed	
	ω_{nyq}	Nyquist angular frequency (p/T_s)	
	ω_0	lower bandwidth boundary of frequency transform ($=1/T$)	
Ω		angular frequency (frequency domain, Laplace-transformed)	[rad]
	Ω_m	rotor angular speed	
a		coefficients of numerator polynomial, eq. (2.2a)	[*]
A		denominator polynomial of polynomial fraction (section 2.4)	[*]
A		general amplitude (Appendix 1)	[*]
b		coefficients of denominator polynomial, eq. (2.2a)	[*]
B		numerator polynomial of polynomial fraction (section 2.4)	[*]
C		reciprocity (sections 7.3 - 7.5)	[1]
d		(referring to) synchronous-machine direct-axis	
D		<i>in figures:</i> diode	
D		<i>with respect to MSR-test:</i> direct-axis measurement with short-circuited excitation winding	
DO		<i>with respect to MSR-test:</i> direct-axis measurement with open excitation winding	
e		residual	[*]
e		voltage	[V]
	\hat{e}	amplitude of sinusoidal voltage source (3.5)	
	e_a	a-phase voltage of three-phase symmetrical voltage source	
	e_b	b-phase voltage of three-phase symmetrical voltage source	
	e_c	c-phase voltage of three-phase symmetrical voltage source	
	e_d	(synchronous machine) direct-axis stator internal voltage	
		(3-phase voltage source) direct-axis Park-transformed source voltage	
	e_q	(synchronous machine) quadrature-axis stator internal voltage	
		(3-phase voltage source) quadr.-axis Park-transformed source voltage	
E		voltage (frequency domain, Laplace-transformed)	[Vs]
	E_d	(synchronous machine) direct-axis stator internal voltage	
	E_q	(synchronous machine) quadrature-axis stator internal voltage	
E		loss (to be minimised by estimator)	[*]
f		frequency	[Hz]
	f_s	sample frequency	
	f_i	signal/noise intersection frequency of step-signal spectrum	
	f	(referring to) synchronous machine excitation winding	
G		synchronous machine gain	[1]
	G_{fd}	synchronous-machine gain I_f/sI_d ($U_f=0$)	
H		general transfer function	[*]
i		current	[A]
	i_a	stator a-phase current	
	i_{a1}	fundamental component of stator a-phase current (eq. (3.8))	
	$i_{a,end}$	approximate stator-current end-value (chapter 7)	
	$i_{a,RMS}$	RMS phase current (section 7.2)	
	i_b	stator b-phase current	
	i_c	stator c-phase current	
	i_d	direct-axis stator current	
	i_f	direct-axis excitation-winding current	
	$i_{f, rated}$	rated direct-axis excitation-winding current	
	i_g	rectifier DC-current	
	i_{gc}	calculated rectifier DC-current	
	i_{gm}	measured rectifier DC-current	
	i_q	quadrature-axis stator current	
I		current (frequency domain, Laplace-transformed)	[As]
	I_d	direct-axis stator current	
	I_f	direct-axis excitation-winding current	
	I_q	quadrature-axis stator current	
	j	imaginary constant ($j^2 = -1$)	

L	coefficient of inductance (possibly frequency dependent)	[H]
	L_c rectifier commutation self-inductance	
	L_d synchronous-machine inductance Y_d/I_d ($I_d \neq 0$)	
	L_d' synchronous-machine direct-axis subtransient inductance	
	L_{di} internal synchronous-machine inductance ($L_d(s)-L_c$)	
	L_{do} synchronous-machine inductance Y_d/I_d ($I_d=0$)	
	L_{dfo} synchronous-machine inductance Y_d'/I_f ($I_d=0$)	
	L_{fdo} synchronous-machine inductance Y_f'/I_f ($I_d=0$)	
	L_{fo} synchronous-machine inductance Y_f'/I_f ($I_d=0$)	
	L_{HF} winding inductance for high frequencies (section 4.2)	
	L_q synchronous-machine inductance Y_q/I_q	
	L_q' synchronous-machine quadrature-axis subtransient inductance	
	L_{qi} internal synchronous-machine inductance ($L_q(s)-L_c$)	
m	denominator order	[1]
n	numerator order, or general integer	[1]
N	number of samples	[1]
	N_p number of samples before the instant of the step	
p	number of pole-pairs of the synchronous machine (in pwm)	[1]
p	pole (root of denominator of polynomial fraction)	[rad s ⁻¹]
p	power	[W]
	P_{DC} DC output power of synchronous machine with rectifier	
	P_{mech} mechanical input power of synchronous machine with rectifier	
P	normalised Park-transformation matrix (defined in eq. (3.1))	[1]
	q (referring to) synchronous-machine quadrature axis	
	Q with respect to MSR-test: quadrature-axis measurement	
R	resistance	[W]
	R_a synchronous-machine stator-winding resistance	
	R_0 value of R at $t = 0$ for time-varying R (section 6.3)	
	R_{as} stator-current shunt resistance	
	dR/dt rate of change of R for time-varying R (section 6.3)	
	R_E internal resistance of source E (section 6.2)	
	R_f synchronous-machine excitation-winding resistance	
	R_{fs} excitation-winding current or voltage shunt resistance	
	DR_f change in R_f (appendix 3)	
	R_{HF} winding resistance for high frequencies (section 4.2)	
	R_p SSFR-test resistance (section 7.5)	
s	Laplace-variable	[rad s ⁻¹]
s	ideal step signal (time domain)	[*]
S	ideal step signal (frequency domain)	[*]
	S in figures: switch	
t	time [s]	
T	period of time	[s]
	T measurement time	
	T_s sample period	
T	temperature	[°C]
	T_c machine housing temperature (chapter 7)	
T	torque	[Nm]
	T_m mechanical torque (also used for frequency-domain torque, unit [Nms], in figure 7.21)	
	T in figures: thyristor	
u	voltage	[V]
	u_a stator a-phase voltage	
	$u_{ab,RMS}$ RMS line voltage (section 7.2)	
	u_b stator b-phase voltage	
	u_c stator c-phase voltage	
	u_g rectifier output voltage	
	u_d direct-axis stator voltage	
	u_f direct-axis excitation-winding voltage	
	u_q quadrature-axis stator voltage	
	u_0 homopolar voltage (eq. (3.2))	
U	voltage (frequency domain, Laplace-transformed)	[Vs]
	U_d direct-axis stator voltage	
	U_f direct-axis excitation winding voltage	
	U_g rectifier load voltage	
	U_q quadrature-axis stator voltage	



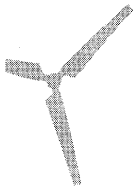
v	state vector (Appendix 1)	[*]
x	general (input) signal (time domain)	[*]
X	general (input) signal (frequency domain)	[*]
y	general output signal (time domain)	[*]
Y	general output signal (frequency domain)	[*]
Y	admittance	[W ⁻¹]
Y_d	synchronous-machine admittance I_d/U_d ($U_f=0$)	
Y_{d0}	synchronous-machine admittance I_d/U_d ($I_f=0$)	
Y_{fd0}	synchronous-machine admittance I_d/U_f ($I_f=0$)	
Y_{f0}	synchronous-machine admittance I_f/U_f ($I_d=0$)	
Y_q	synchronous-machine admittance I_q/U_q	
z	zero (root of numerator of polynomial fraction)	[rad s ⁻¹]
Z	impedance	[W]
Z_d	synchronous-machine impedance U_d/I_d ($U_f=0$)	
Z_{di}	transfer function $-E_d/I_d$ ($U_f=0$), eq. (3.21)	
Z_q	synchronous-machine impedance U_q/I_q	
Z_{qi}	transfer function $-E_q/I_q$, eq. (3.21)	

A unit specification [*] means that several units are possible. For infrequently used symbols, the section or chapter is given in which they appear.





APPENDICES



A1 THE RELATION BETWEEN BANDWIDTH AND NOISE CONTENT OF A STEP SIGNAL

A step signal is known to have most of its energy at the lower part of the frequency band, see e.g. figures 2.6, 7.6 or 7.7. When a step signal is used for identification, a measure for the bandwidth of the signal is desirable, since it indicates the frequency band in which the system under test is excited and may be identified.

The common definition of bandwidth (the frequency region within which the signal deviates less than 3 dB from a given reference level), is inapplicable. An alternative measure may be defined as the frequency above which the step-signal level drops below the level of the noise, which is inevitably present (see figure A1.1). This frequency may serve as an alternative for the upper bound of the signal bandwidth, and will be called the *noise-intersection frequency*. In the remainder of this appendix the noise-intersection frequency will be analysed more closely.

Continuous time-domain signals

Consider the continuous noisy step signal $x(t)$ as sketched in figure A1.2. Its amplitude equals A , and the noise is assumed to be additive and white within a frequency band of $[-\omega_B, \omega_B]$. To determine the noise-intersection frequency of $x(t)$, the energy spectrum of the step-component $x_s(t)$ of the signal is compared to the energy spectrum of the noise-component $x_n(t)$. A limited time interval is considered ($t \in [0, T]$) to limit the signal energy (so $x(t)$ equals 0 outside this interval).

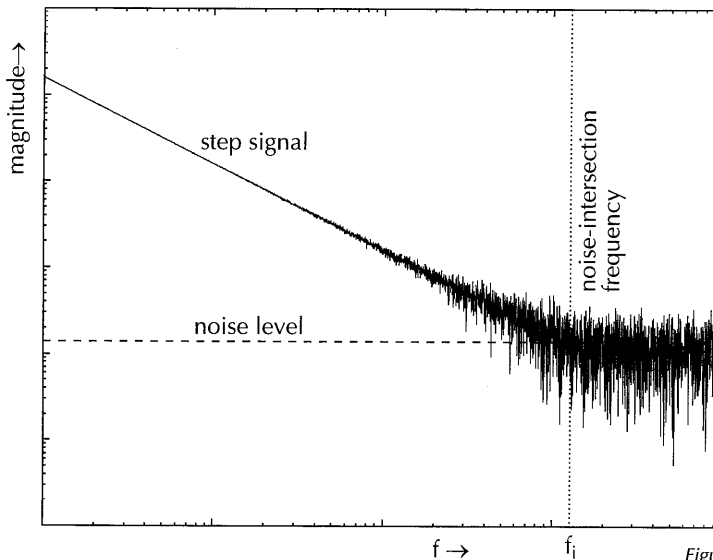


Figure A1.1
Location of the noise-intersection frequency f_i for an arbitrary step signal.

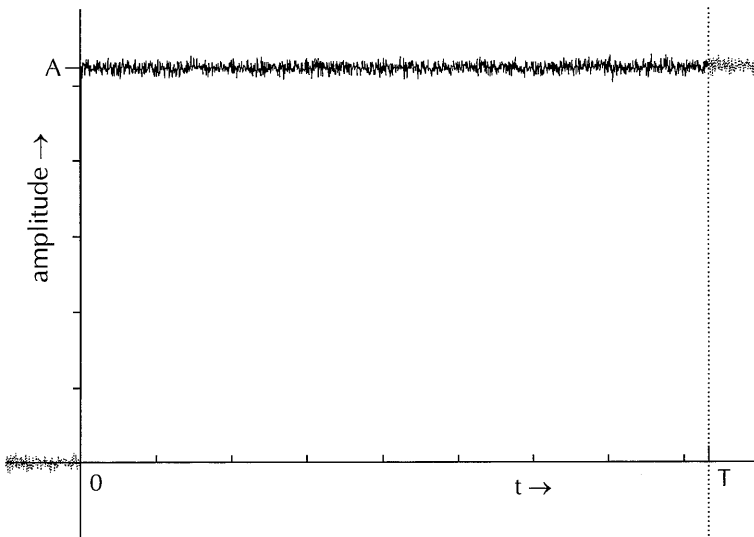


Figure A1.2
A noisy step signal

The Fourier-transform of the step-component $x_s(t)$ equals:

$$X_s(\omega) = \int_{-\infty}^{\infty} x_s(t) e^{-j\omega t} dt = \int_0^T A e^{-j\omega t} dt = \frac{2A}{\omega} \sin\left(\frac{1}{2}\omega T\right) e^{-j\omega T/2} \quad (\text{A1.1a})$$

and therefore its energy spectrum $|X_n(\omega)|^2 = T\eta$ is given by:

$$|X_s(\omega)|^2 = \frac{4A^2}{\omega^2} \sin^2\left(\frac{1}{2}\omega T\right) \quad (\text{A1.1b})$$

For the noise component $x_n(t)$, the assumption of whiteness within frequency band $[-\omega_B, \omega_B]$ implies a constant power spectrum within this frequency band. If this value is called η , then the energy spectrum is:

$$|X_n(\omega)|^2 = T\eta \quad (\text{A1.2})$$

The energy spectrum may also be expressed using σ^2 , the variance of the noise. The full noise energy equals $T\sigma^2$. Using (A1.2), the full noise energy equals $2\omega_B T\eta/2\pi$, so:

$$\sigma^2 = \frac{\omega_B \eta}{\pi} \quad (\text{A1.3})$$

Substituting η from (A1.3) into (A1.2) gives:

$$|X_n(\omega)|^2 = \frac{\pi T \sigma^2}{\omega_B} \quad (\text{A1.4})$$

To find the noise-intersection angular frequency ω_i , ω is solved from (A1.1b) and (A1.2) or (A1.4). Since the spectrum $X_s(\omega)$ is pulsed, many solutions are found, but by taking only the extrema of the pulses into consideration ($\langle ea1_x2 \rangle$), a unique solution is obtained:

$$\omega_i = 2A \sqrt{\frac{1}{\eta T}} = 2A \sqrt{\frac{\omega_B}{\pi \sigma^2 T}} \quad (\text{A1.5})$$

Continuous time-domain signals submitted to the time-transpose technique

For the actual transformation from the time-domain step-response data into the frequency domain, a time-transpose technique is applied as described in section 5.1. The results are only valid at discrete values of ω :

$$\omega_k = \frac{2\pi k}{2T}, \quad (\text{k odd}) \quad (\text{A1.6})$$

By applying the equations of section 5.1, the spectrum of $x_s(t)$ may be calculated:

$$|\tilde{X}_s(\omega_k)|^2 = \frac{A^2}{\omega_k^2} \quad (\text{A1.7})$$

where the tilde indicates the use of the time-transpose technique, and ω_k is given by (A1.6). The spectrum of (A1.7) is equal to that of an ideal time-unlimited step. Due to the time-transpose technique, the measured noise signal is repeated twice within time interval $[0, 2T]$, and its spectrum is no longer white. It may be derived that:

$$|\tilde{X}_n(\omega)|^2 = \frac{1}{4} (2 - 2\cos(\omega T)) |X_n(\omega)|^2 \quad (\text{A1.8a})$$

Using (A1.6) and (A1.2), (A1.8a) simplifies to:

$$|\tilde{X}_n(\omega_k)|^2 = |X_n(\omega_k)|^2 = T\eta \quad (\text{A1.8b})$$

Solving ω_k from (A1.7) and (A1.8b), and using (A1.3) gives:

$$\omega_i = A \sqrt{\frac{1}{\eta T}} = A \sqrt{\frac{\omega_B}{\pi \sigma^2 T}} \quad (\text{A1.9})$$

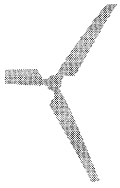
which differs from (A1.5) by a factor of 2: the mean step amplitude has decreased by a factor of 2, while the noise RMS-value has remained the same.

Sampled time-domain signals submitted to the time-transpose technique

The actually measured time-domain data are not continuous but sampled, and after time-transposing the data as described in section 5.1, frequency-domain data are calculated using the Discrete Fourier Transform:

$$\begin{aligned} X_k &= \frac{1}{2} T_s \text{DFT}([x_0, x_1, \dots, x_{N-1}, x_E - x_0, x_E - x_1, \dots, x_E - x_{N-1}]) \\ &= \frac{1}{2} T_s \left(\sum_{i=0}^{N-1} x_i e^{-2\pi j \frac{ki}{2N}} + \sum_{i=N}^{2N-1} (x_E - x_{i-N}) e^{-2\pi j \frac{ki}{2N}} \right) \end{aligned} \quad (\text{A1.10})$$

where x_i , $i = 0 \dots N-1$, are the N signal samples, DFT denotes the discrete Fourier transform, and x_E is the end-value of the step signal. Equation (A1.6) gives the angular frequency which is related to a given k .



Suppose N samples of the noisy step signal $x(t)$ are acquired, at a sample period of T_s , starting at $t = 0$. The step-components $x_{s,0} \dots x_{s,N-1}$ of the samples all equal A , and its spectrum follows from (A1.10) using $x_E = A$:

$$|X_{s,k}|^2 = \frac{1}{4} A^2 T_s^2 \frac{1}{\sin^2\left(\frac{k\pi}{2N}\right)} \quad (\text{A1.11})$$

Assuming $k\pi \ll 2N$, $\sin(k\pi/2N)$ may be approximated by $k\pi/2N$. Using (A1.6) and this approximation, (A1.11) becomes:

$$|X_{s,k}|^2 = \frac{1}{4} A^2 T_s^2 \left(\frac{2N}{k\pi}\right)^2 = \frac{1}{4} A^2 T_s^2 \frac{4N^2}{\omega_k^2 T^2} = \frac{A^2}{\omega_k^2} \quad (\text{A1.12})$$

For the noise-component of the samples of $x(t)$, $x_{n,0} \dots x_{n,N-1}$, application of (A1.10) leads to:

$$\begin{aligned} X_{n,k} &= \frac{1}{2} T_s \left(\sum_{i=0}^{N-1} x_{n,i} e^{-2\pi j \frac{ki}{2N}} + \sum_{i=N}^{2N-1} (x_{n,E} - x_{n,i-N}) e^{-2\pi j \frac{ki}{2N}} \right) \\ &= \frac{1}{2} T_s \sum_{i=0}^{N-1} x_{n,i} \left(e^{-2\pi j \frac{ki}{2N}} - e^{-2\pi j \frac{k(i+N)}{2N}} \right) \\ &= \frac{1}{2} T_s \sum_{i=0}^{N-1} x_{n,i} e^{-2\pi j \frac{ki}{2N}} \left(1 - e^{-\pi j k} \right) \end{aligned} \quad (\text{A1.13})$$

In (A1.13), $x_{n,E}$ is the noise end-value, which equals the mean value of the noise: 0. Since $e^{-\pi j k} = -1$ for odd k , the final result for $X_{n,k}$ is:

$$X_{n,k} = T_s \sum_{i=0}^{N-1} x_{n,i} e^{-2\pi j \frac{ki}{2N}} \quad (\text{A1.14})$$

To determine the noise-intersection angular frequency, the mean value of the energy spectrum $|X_{n,k}|^2$ is calculated, using (A1.4):

$$\begin{aligned} E\{|X_{n,k}|^2\} &= E\{X_{n,k} X_{n,k}^*\} = E\left\{ T_s^2 \sum_{i=0}^{N-1} x_{n,i} e^{-2\pi j \frac{ki}{2N}} \sum_{m=0}^{N-1} x_{n,m} e^{2\pi j \frac{km}{2N}} \right\} \\ &= E\left\{ T_s^2 \sum_{i=0}^{N-1} \sum_{m=0}^{N-1} x_{n,i} x_{n,m} e^{2\pi j \frac{k(m-i)}{2N}} \right\} = E\left\{ T_s^2 \sum_{i=0}^{N-1} x_{n,i}^2 \right\} = T_s^2 N E\{x_{n,1}^2\} = T_s^2 N \sigma^2 \end{aligned} \quad (\text{A1.15})$$

The transition from double to single summation follows under the condition that the noise samples are mutually independent, which is valid if ω_B is large enough (larger than $\omega_{nyq} = \pi/T_s$, the Nyquist angular frequency corresponding to a sampling period of T_s).

To find the noise-intersection angular frequency ω_i , for the sampled data, ω_k is solved from (A1.12) and (A1.15):

$$\frac{A^2}{\omega_k^2} = T_s^2 N \sigma^2 = T_s^2 N \frac{\omega_B}{\pi} \eta = \frac{\omega_B}{\omega_{nyq}} T \eta \quad (\text{A1.16})$$

where the second step follows from (A1.3). Equation (A1.16) gives

$$\omega_i = A \sqrt{\frac{\omega_{nyq}}{\eta T \omega_B}} = A \sqrt{\frac{\omega_{nyq}}{\pi \sigma^2 T}} \quad (\text{A1.17})$$

Discussion

For continuous as well as sampled signals, similar expressions are found for the noise-intersection frequency: it is proportional to the signal amplitude A , and inversely proportional to both the root of the measurement length T and the power spectral density η of the noise. In the sampled case, the noise-intersection frequency is also proportional to the root of ω_{nyq}/ω_B . A logical value of this factor is 1, which results in equal expressions for ω_i in the continuous and the sampled case.

The relationship between the noise-intersection frequency and the signal amplitude A may be expected: the larger this value, the more the intersection point of the step spectrum and the noise spectrum shifts to higher frequencies. A smaller noise spectral density η or variance σ^2 has the same effect.

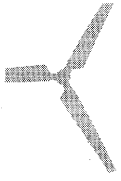
The decrease of ω_i with increasing measurement length T is caused by the fact that a longer measurement increases the noise energy over the whole frequency range, while only increasing the step-signal energy around DC.

In the continuous case (A1.9), a larger noise bandwidth ω_B leads to a larger ω_i , which may be surprising. The reason is that a constant noise variance σ^2 is assumed: with (A1.3) a larger ω_B then leads to a lower noise-energy density ηT , and therefore a smaller ω_i . It is more realistic, however, to assume that the noise-energy density ηT remains constant. Under this condition, an increasing ω_B gives a proportionally larger noise variance σ^2 (see (A1.3)), and the noise-intersection frequency is constant. In the sampled case (A1.17), a larger ω_{nyq} (faster sample rate) causes ω_i to increase. This also is due to the assumption of a constant σ^2 , which is not realistic when the sample rate increases. It is more likely that η is constant and that ω_B increases proportionally with ω_{nyq} , which leaves ω_i unchanged.

Noise-intersection bandwidth

For the sampled case, the lowest angular frequency available is $\omega_0 = 2\pi/2T$, so the noise-intersection bandwidth ω_i/ω_0 becomes:

$$\frac{\omega_i}{\omega_0} = \frac{A}{\sigma} \sqrt{\frac{\omega_{nyq}}{\pi T}} = \frac{A}{\pi \sigma} \sqrt{\frac{T \omega_{nyq}}{\pi}} = \frac{A}{\pi \sigma} \sqrt{N} \quad (\text{A1.18})$$



Using the signal-to-noise ratio $\rho = A/\sigma$, expressed in dB, (A1.18) may be expressed in decades:

$$\log\left(\frac{\omega_i}{\omega_0}\right) = \log\left(\frac{A}{\sigma}\right) + \log\left(\frac{1}{\pi}\sqrt{N}\right) = \frac{\rho}{20} + \log\left(\frac{1}{\pi}\sqrt{N}\right) \quad (\text{A1.19})$$

For a common Modified Step-Response signal with 4096 samples and signal-to-noise ratio of 70 dB, the noise-intersection bandwidth equals 4.8 decades.

Equation (A1.19) shows that a larger number of samples will increase the step-signal bandwidth, but this does not mean that the high-frequency range is extended: both frequency boundaries shift to lower frequencies, but the lower boundary shifts faster.

A2 HANDLING STATOR RESISTANCE CHANGES DUE TO HEATING AND COOLING

If the stator winding temperature changes significantly during the step-response measurement, and consequently the stator resistance is not constant, then the frequency transformation of equations (3.3), which leads to (3.9), is not allowed. All equations which depend on (3.9), including those describing the step-response concept in chapter 4, are invalid.

In this section alternative equations are derived, which do not require a constant stator resistance. Essentially, the contribution of R_a to the measurement data is removed before transforming them into the frequency domain.

Assume that the value of $R_a(t)$ during the measurement is known as a function of time. Using this value, auxiliary voltages u'_q and u'_d are calculated from the time-domain voltages u_q and u_d , which are independent of R_a :

$$u'_d = u_d - R_a(t)i_d \quad (\text{A2.1})$$

$$u'_q = u_q - R_a(t)i_q$$

Substitution of (A2.1) in (3.3) gives:

$$-u'_d = \frac{d\psi_d}{dt} + p \frac{d\gamma}{dt} \psi_q$$

$$u_f = R_f i_f + \frac{d\psi_f}{dt} \quad (\text{A2.2})$$

$$-u'_q = \frac{d\psi_q}{dt} - p \frac{d\gamma}{dt} \psi_d$$

Starting from (A2.2), the derivation of section 3.3 is repeated. Assuming constant angular speed $d\gamma/dt = \omega_m$, (A2.2) may be transformed into the frequency domain:

$$-U'_d = s\Psi_d + p\omega_m \Psi_q$$

$$U_f = R_f I_f + s\Psi_f \quad (\text{A2.3})$$

$$-U'_q = s\Psi_q - p\omega_m \Psi_d$$

Assuming reciprocity, and using (3.4), (A2.3) becomes:

$$\begin{aligned}
 -U'_d &= sL_{do}(s) I_d + sL_{fdo}(s) I_f + p\omega_m L_q(s) I_q \\
 U_f &= sL_{fdo}(s) I_d + (R_f + sL_{fo}(s)) I_f \\
 -U'_q &= sL_q(s) I_q - p\omega_m (L_{do}(s) I_d + L_{fdo}(s) I_f)
 \end{aligned} \tag{A2.4}$$

Taking U_f as input (A2.4) becomes:

$$\begin{aligned}
 -U'_d &= sL_d(s) I_d - sG_{fd}(s) U_f + p\omega_m L_q(s) I_q \\
 I_f &= sG_{fd}(s) I_d + \frac{U_f}{R_f + sL_{fo}(s)} \\
 -U'_q &= sL_q(s) I_q - p\omega_m (L_d(s) I_d - G_{fd}(s) U_f)
 \end{aligned} \tag{A2.5}$$

which is the alternative for equation (3.11). Equation (3.12) still holds to relate $L_d(s)$, $G_{fd}(s)$, $L_{do}(s)$ and $L_{fdo}(s)$.

At standstill, equations (A2.4) and (A2.5) simplify to:

$$\begin{aligned}
 -U'_d &= sL_{do}(s) I_d + sL_{fdo}(s) I_f \\
 U_f &= sL_{fdo}(s) I_d + (R_f + sL_{fo}(s)) I_f \\
 -U'_q &= sL_q(s) I_q
 \end{aligned} \tag{A2.6}$$

and

$$\begin{aligned}
 -U'_d &= sL_d(s) I_d - sG_{fd}(s) U_f \\
 I_f &= sG_{fd}(s) I_d + \frac{U_f}{R_f + sL_{fo}(s)} \\
 -U'_q &= sL_q(s) I_q
 \end{aligned} \tag{A2.7}$$

which are the alternatives for (4.1) and (4.2). From the same three measurements as described in section 4.1, the following basic set of transfer functions may be determined (which replaces the basic set of figure 5.1):

$$sL_q(s) = \frac{-U'_q}{I_q} \tag{A2.8a}$$

$$sL_d(s) = \frac{-U'_d}{I_d} \Big|_{u_f = 0} \tag{A2.8b}$$

$$sG_{fd}(s) = \frac{I_f}{I_d} \Big|_{u_f = 0} \tag{A2.8c}$$

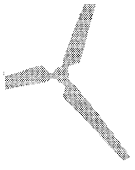
$$s L_{do}(s) = \left. \frac{-U'_d}{I_d} \right|_{i_f = 0} \quad (\text{A2.8d})$$

$$Y_{fdo}(s) = \left. \frac{I_d}{U_f} \right|_{i_f = 0} \quad (\text{A2.8e})$$

where (A2.8a), (A2.8b) and (A2.8d) are alternatives for (4.5), (4.6a) and (4.7a). Equations (A2.8c) and (A2.8e) are identical to (4.6b) and (4.7b).

The relationships between the transfer functions, as displayed in figure 5.1, change only slightly. For $sG_{fd}(s)$, $G_{fd}(s)$, $L_{fdo}(s)$ and $Y_{fo}(s)$ nothing changes. For the other quantities, the relationships given in figure 5.1 are reversed. The admittances $Y_q(s)$, $Y_d(s)$ and $Y_{do}(s)$ now follow from $L_q(s)$, $L_d(s)$ and $L_{do}(s)$ respectively, using (3.13c), (3.13a) and (3.13b) and an additional value of R_a . The internal-machine impedances $Z_{qi}(s)$ and $Z_{di}(s)$ follow from $L_q(s)$ and $L_d(s)$ using (3.13) and (3.22).

Equation (A2.1) presupposes that the value of $R_a(t)$ during the measurement is known. In [Dir92] it is concluded that for the duration of the step-response measurement, $R_a(t)$ may be approximated as a linear function of time, due to the fact that the thermal time-constants are considerably larger than the electrical ones. The topic of how to determine R_a and its change during the MSR test still remains to be investigated more closely.



A3 HANDLING EXCITATION-WINDING RESISTANCE CHANGES DUE TO HEATING AND COOLING

The excitation-winding resistance R_f may have a different value during the MSR test than during actual machine operation, caused by temperature differences: the step-response test will usually be carried out with the machine at ambient temperature, whereas the common operating temperature of the machine may be higher by 50 °C. Therefore, in a simulation, a value of R_f may have to be used which differs from the identified value.

The value of R_f may also have to be corrected, if the MSR 'D' measurement is carried out with an excitation-winding shunt which is not negligible with respect to the actual winding resistance R_f .

For both reasons, in this appendix equations are derived to alter the R_f -value of a given direct-axis state-space model. Suppose the identified internal-machine direct-axis model is given in standard state-space form:

$$\begin{aligned} \dot{\underline{v}} &= \mathbf{A}\underline{v} + \mathbf{B}\underline{x} \\ \underline{y} &= \mathbf{C}\underline{v} + \mathbf{D}\underline{x} \end{aligned} \tag{A3.1a}$$

with states \underline{v} , input vector \underline{x} and output vector \underline{y} according to table 3.1:

$$\underline{x} = \begin{pmatrix} i_d \\ u_f \\ p\omega_m \psi_{qi} \end{pmatrix}, \quad \underline{y} = \begin{pmatrix} -e_d \\ i_f \\ \psi_{di} \end{pmatrix} \tag{A3.1b}$$

Now suppose the identified value of R_f needs to be altered by ΔR_f , so the new excitation-winding resistance R_f' equals:

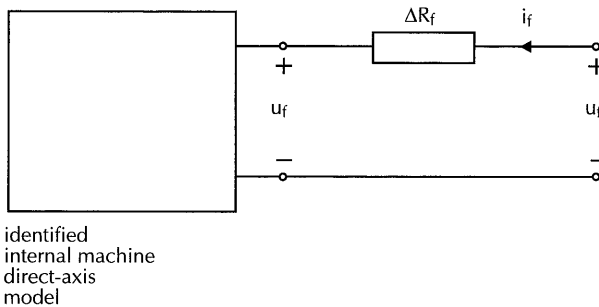
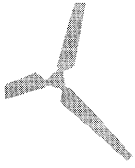


Figure A3.1
Altering R_f by addition of ΔR_f to the identified model.



$$\mathbf{R}_f' = \mathbf{R}_f + \Delta\mathbf{R}_f \quad (\text{A3.2})$$

We may picture this change as in figure A3.1.

We shall now derive state-space model-equations of the altered direct-axis model. For the excitation-winding voltage u_f' of the altered model, the following equation holds:

$$u_f' = \Delta R_f i_f + u_f \quad (\text{A3.3})$$

Substitution of (A3.3) into (A3.1) gives:

$$\dot{\underline{y}} = \underline{\mathbf{A}}\underline{y} + \underline{\mathbf{B}} \begin{pmatrix} i_d \\ u_f' \\ p\omega_m \Psi_{qi} \end{pmatrix} - \Delta R_f \underline{\mathbf{B}} \begin{pmatrix} 0 \\ i_f \\ 0 \end{pmatrix} \quad (\text{A3.4a})$$

$$\begin{pmatrix} -e_d \\ i_f \\ \Psi_{di} \end{pmatrix} = \underline{\mathbf{C}}\underline{y} + \underline{\mathbf{D}} \begin{pmatrix} i_d \\ u_f' \\ p\omega_m \Psi_{qi} \end{pmatrix} - \Delta R_f \underline{\mathbf{D}} \begin{pmatrix} 0 \\ i_f \\ 0 \end{pmatrix} \quad (\text{A3.4b})$$

The last term in (A3.4a) may be written as:

$$\Delta R_f \underline{\mathbf{B}} \begin{pmatrix} 0 \\ i_f \\ 0 \end{pmatrix} = \Delta R_f (\underline{b}_1 \mid \underline{b}_2 \mid \underline{b}_3) \begin{pmatrix} 0 \\ i_f \\ 0 \end{pmatrix} = \Delta R_f \underline{b}_2 i_f = (\underline{0} \mid \Delta R_f \underline{b}_2 \mid \underline{0}) \begin{pmatrix} -e_d \\ i_f \\ \Psi_{di} \end{pmatrix} \quad (\text{A3.5})$$

Similarly, the last term in (A3.4b) may be written as:

$$\Delta R_f \underline{\mathbf{D}} \begin{pmatrix} 0 \\ i_f \\ 0 \end{pmatrix} = (\underline{0} \mid \Delta R_f \underline{d}_2 \mid \underline{0}) \begin{pmatrix} -e_d \\ i_f \\ \Psi_{di} \end{pmatrix} \quad (\text{A3.6})$$

Substitution of (A3.6) into (A3.4b) gives:

$$\left\{ \mathbf{I} + (\underline{0} \mid \Delta R_f \underline{d}_2 \mid \underline{0}) \right\} \begin{pmatrix} -e_d \\ i_f \\ \Psi_{di} \end{pmatrix} = \underline{\mathbf{C}}\underline{y} + \underline{\mathbf{D}} \begin{pmatrix} i_d \\ u_f' \\ p\omega_m \Psi_{qi} \end{pmatrix} \quad (\text{A3.7})$$

where \mathbf{I} is the identity-matrix. Define matrix \mathbf{K} as

$$\mathbf{K} = \mathbf{I} + (\underline{0} \mid \Delta R_f \underline{d}_2 \mid \underline{0}) \quad (\text{A3.8})$$

Using the definition of \mathbf{K} , equation (A3.7) may be rewritten as:

$$\begin{pmatrix} -e_d \\ i_f \\ \Psi_{di} \end{pmatrix} = \mathbf{K}^{-1} \mathbf{C}_v + \mathbf{K}^{-1} \mathbf{D} \begin{pmatrix} i_d \\ u_f' \\ p\omega_m \Psi_{qi} \end{pmatrix} \quad (\text{A3.9})$$

which is the *output-equation* of the altered model.

Define matrix \mathbf{L} as:

$$\mathbf{L} = (\underline{0} \mid \Delta R_f \underline{b}_2 \mid \underline{0}) \quad (\text{A3.10})$$

Using (A3.10), substitution of (A3.5) into (A3.4a) gives:

$$\dot{\underline{y}} = \mathbf{A}_v + \mathbf{B} \begin{pmatrix} i_d \\ u_f' \\ p\omega_m \Psi_{qi} \end{pmatrix} - \mathbf{L} \begin{pmatrix} -e_d \\ i_f \\ \Psi_{di} \end{pmatrix} \quad (\text{A3.11})$$

which with (A3.9) changes into:

$$\begin{aligned} \dot{\underline{y}} &= \mathbf{A}_v + \mathbf{B} \begin{pmatrix} i_d \\ u_f' \\ p\omega_m \Psi_{qi} \end{pmatrix} - \mathbf{L} \left\{ \mathbf{K}^{-1} \mathbf{C}_v + \mathbf{K}^{-1} \mathbf{D} \begin{pmatrix} i_d \\ u_f' \\ p\omega_m \Psi_{qi} \end{pmatrix} \right\} \\ &= (\mathbf{A} - \mathbf{L} \mathbf{K}^{-1} \mathbf{C}) \underline{y} + (\mathbf{B} - \mathbf{L} \mathbf{K}^{-1} \mathbf{D}) \begin{pmatrix} i_d \\ u_f' \\ p\omega_m \Psi_{qi} \end{pmatrix} \end{aligned} \quad (\text{A3.12})$$

which is the *state-equation* of the altered model.

Summarising, if the internal-machine direct-axis model is described by (A3.1) with model matrices \mathbf{A} , \mathbf{B} , \mathbf{C} , and \mathbf{D} , then the internal-machine direct-axis model with altered R_f may be described by:

$$\begin{aligned} \dot{\underline{y}} &= \mathbf{A}' \underline{y} + \mathbf{B}' \underline{x}' \\ \underline{y} &= \mathbf{C}' \underline{y} + \mathbf{D}' \underline{x}' \end{aligned} \quad (\text{A3.13a})$$

with

$$\underline{x}' = \begin{pmatrix} i_d \\ u_f' \\ p\omega_m \Psi_{qi} \end{pmatrix}, \quad \underline{y} = \begin{pmatrix} -e_d \\ i_f \\ \Psi_{di} \end{pmatrix} \quad (\text{A3.13b})$$

and


$$\mathbf{A}' = \mathbf{A} - \mathbf{L}\mathbf{K}^{-1}\mathbf{C}$$

$$\mathbf{B}' = \mathbf{B} - \mathbf{L}\mathbf{K}^{-1}\mathbf{D}$$

$$\mathbf{C}' = \mathbf{K}^{-1}\mathbf{C}$$

(A3.13c)

$$\mathbf{D}' = \mathbf{K}^{-1}\mathbf{D}$$

Matrices \mathbf{K} and \mathbf{L} are given by (A3.8) and (A3.10).

Figures belonging to chapter 7 "Evaluation of the modified step-response test by measurements".

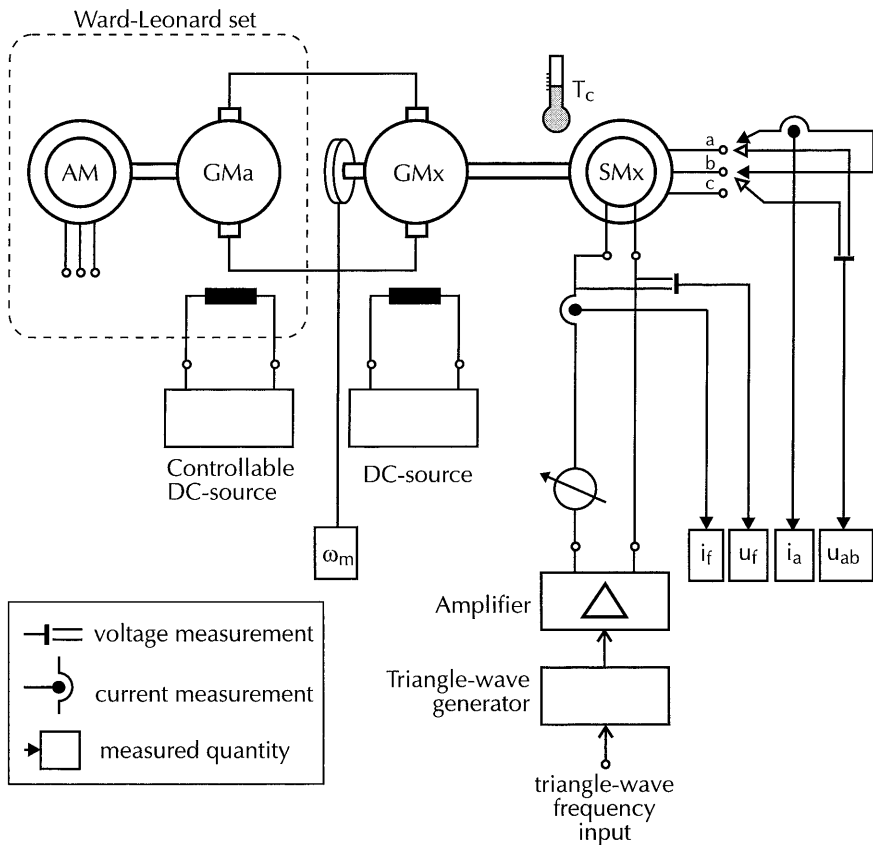


Figure 7.1
Steady-state tests measurement set-ups

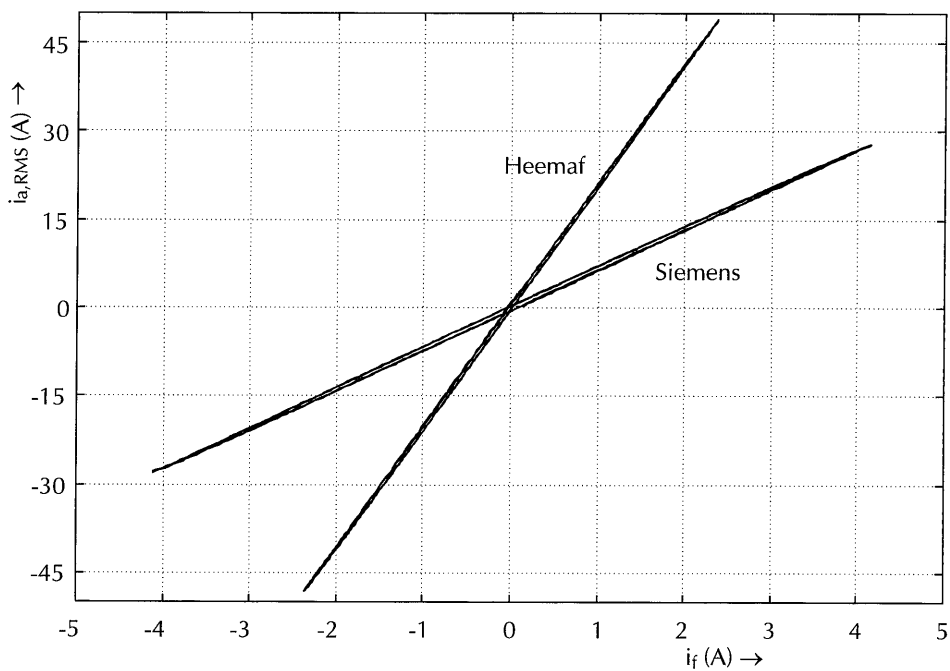
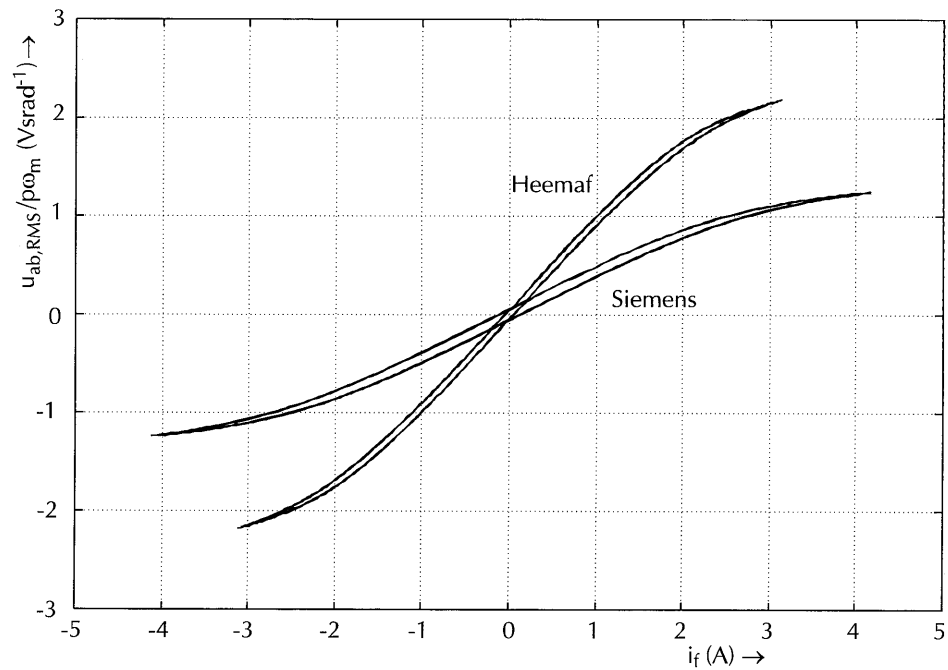
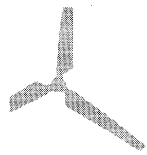


Figure 7.2
Steady-state no-load curve and steady-state short-circuit curve for the Siemens machine and the Heemaf machine.
a) no-load;
b) short-circuit

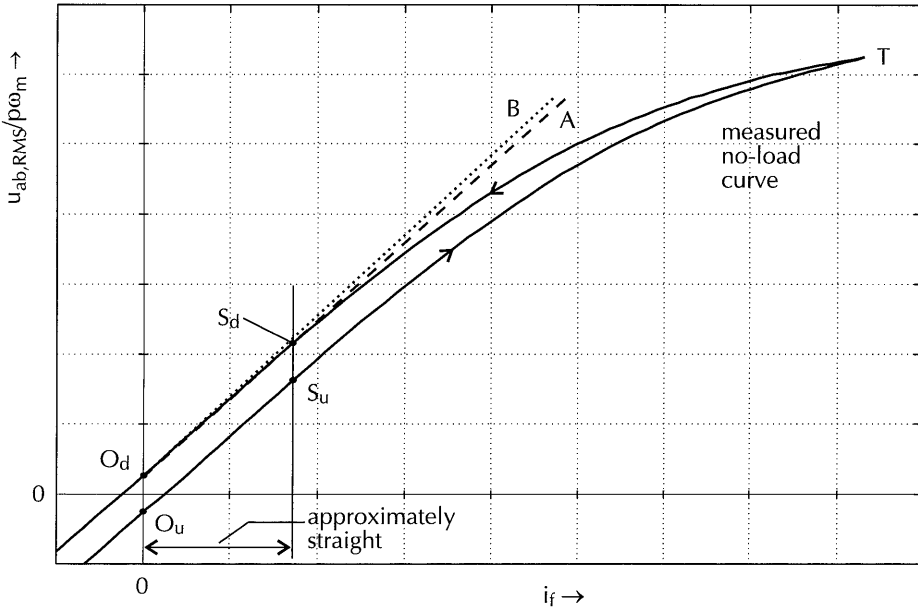


Figure 7.3
Two approaches to determine the slope of a no-load curve.

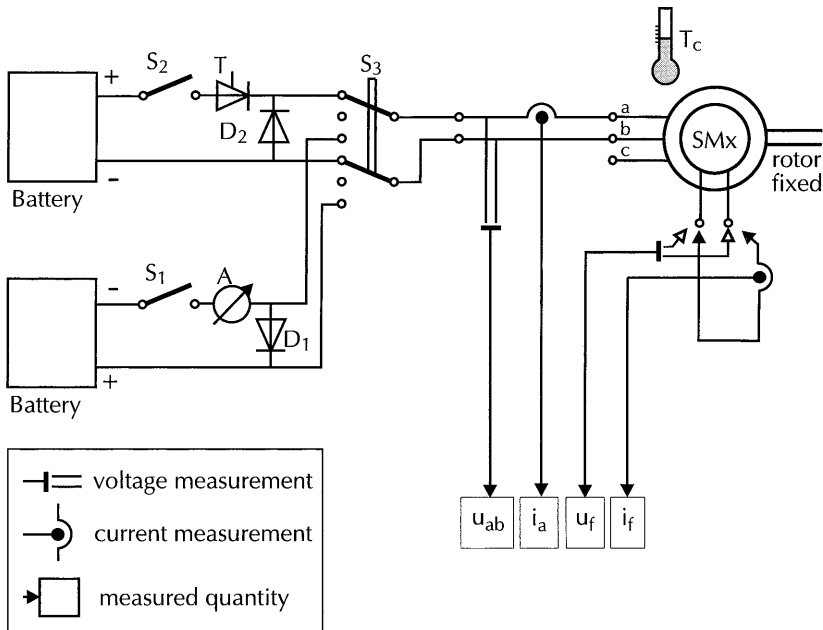


Figure 7.4
Measurement set-up of the modified step-response test

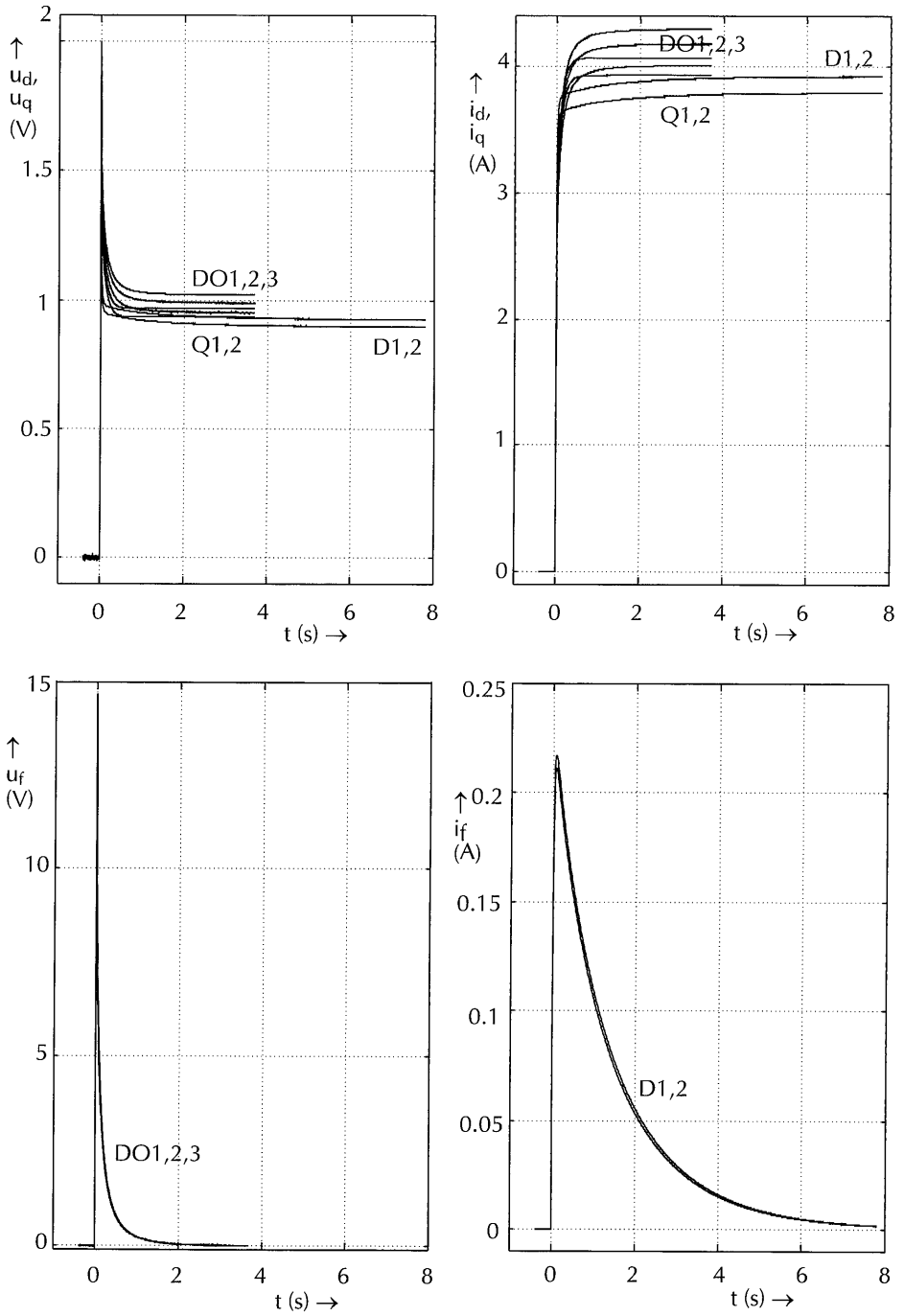
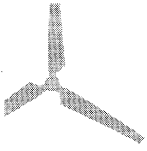


Figure 7.5a
MSR-test measured signals, Siemens machine

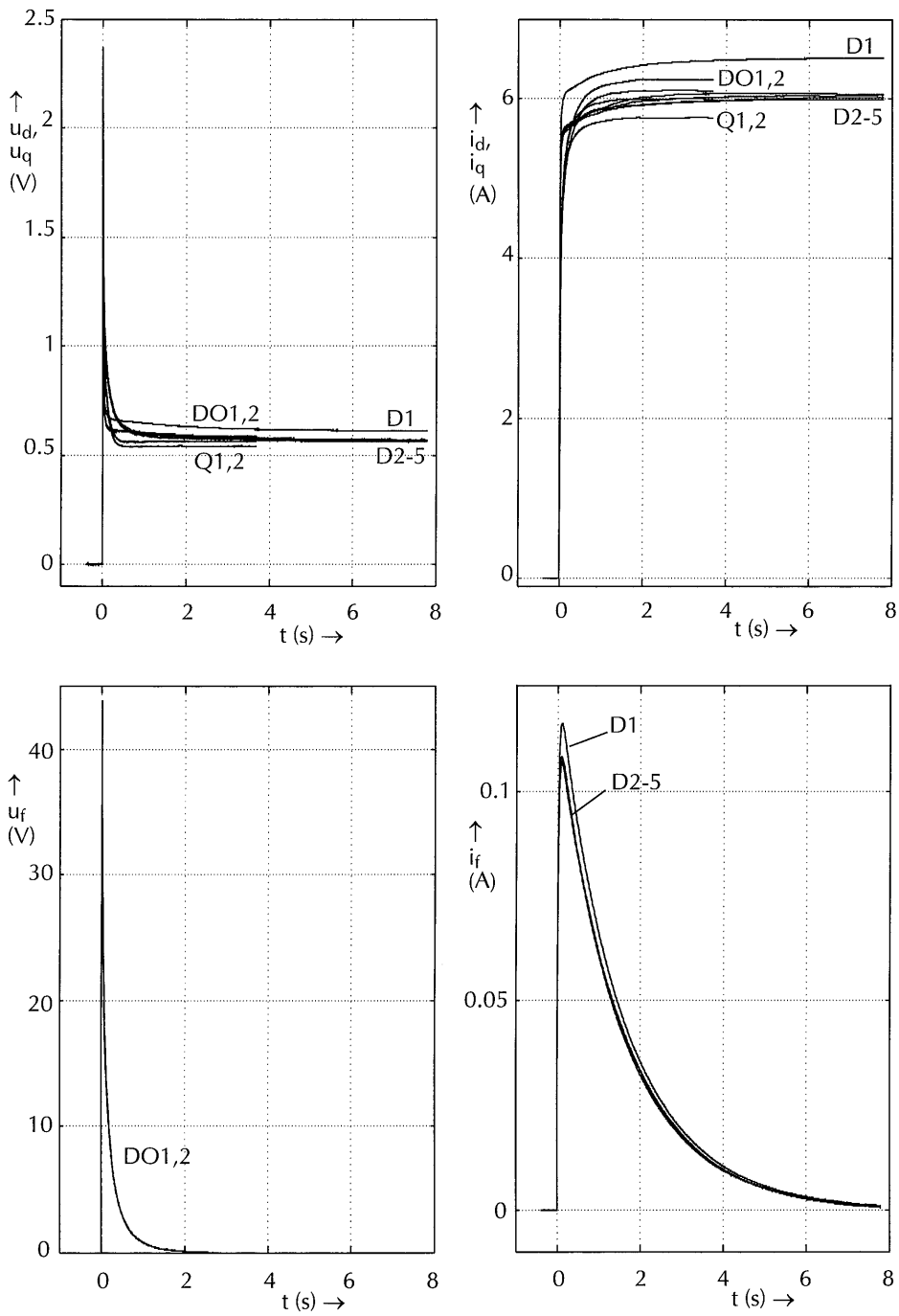
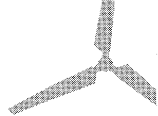


Figure 7.5b
MSR-test measured signals, Heemaf machine

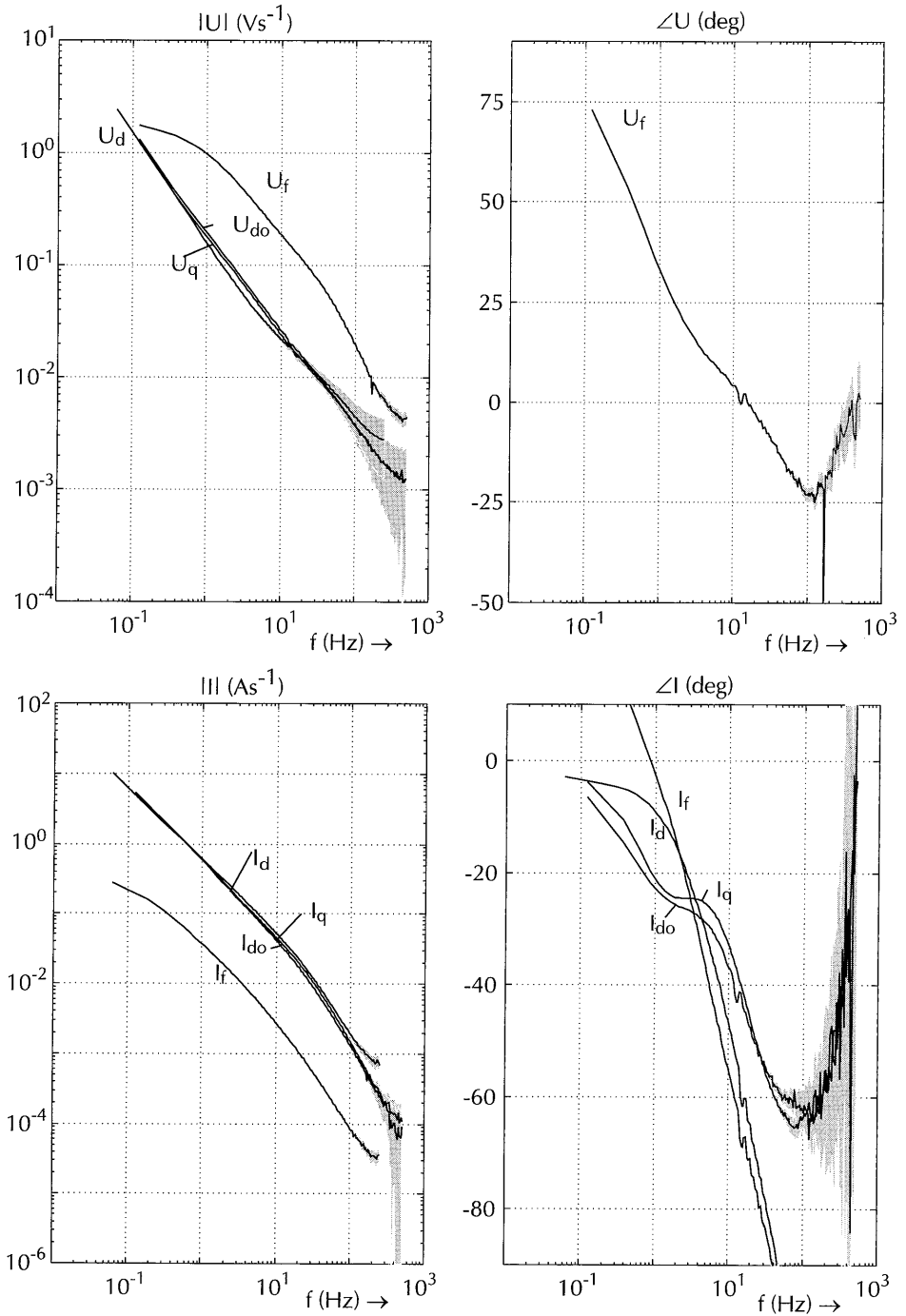
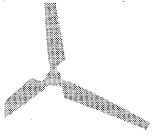


Figure 7.6a
 Frequency transforms of Siemens MSR-signals and derived transfer functions: U_d , U_q , U_{do} , U_f , I_d , I_q , I_{do} , I_f

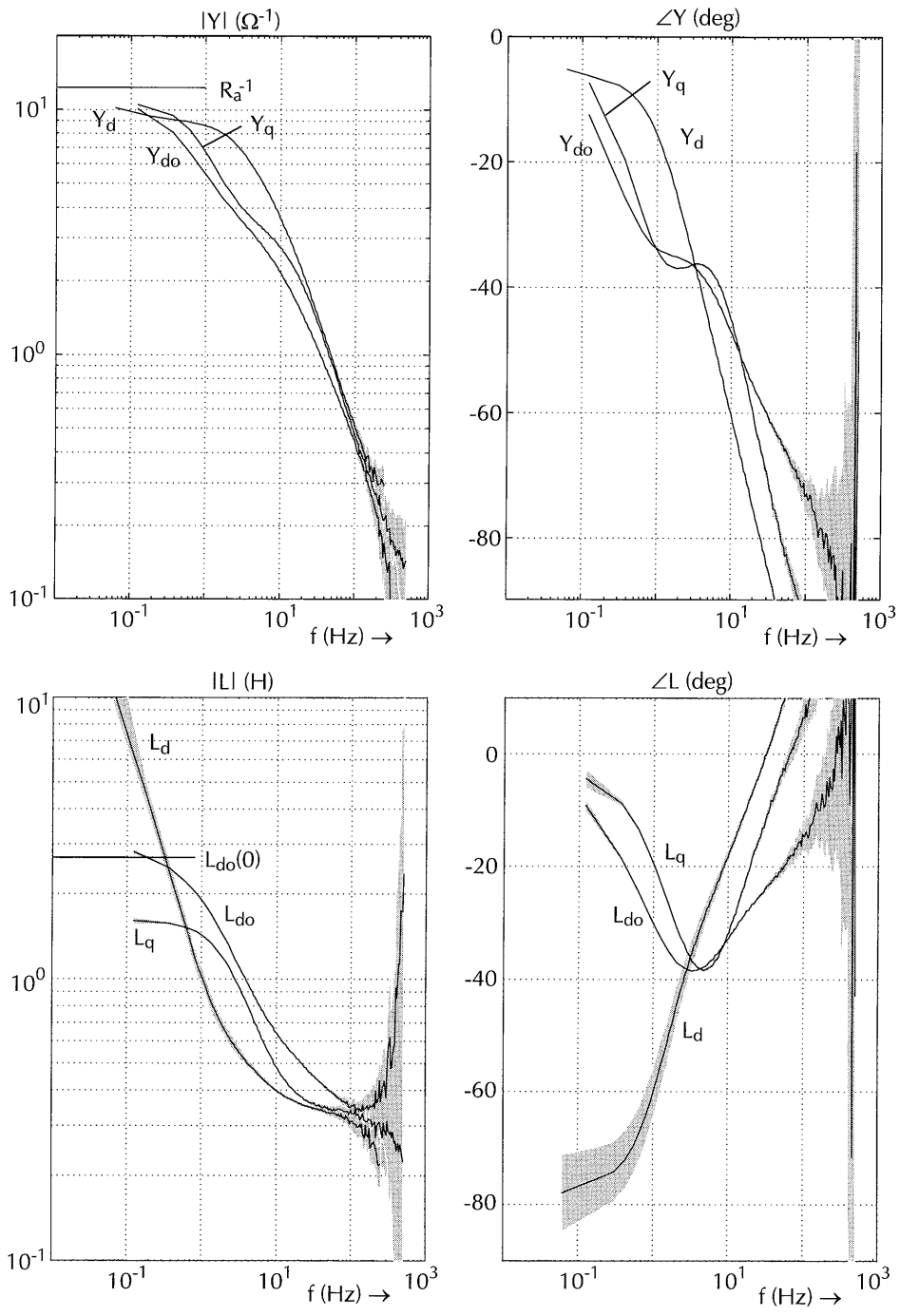
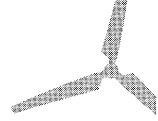


Figure 7.6b
Frequency transforms of Siemens MSR-signals and derived transfer functions: $Y_d(s)$, $Y_{do}(s)$, $Y_q(s)$, $L_d(s)$, $L_{do}(s)$, $L_q(s)$

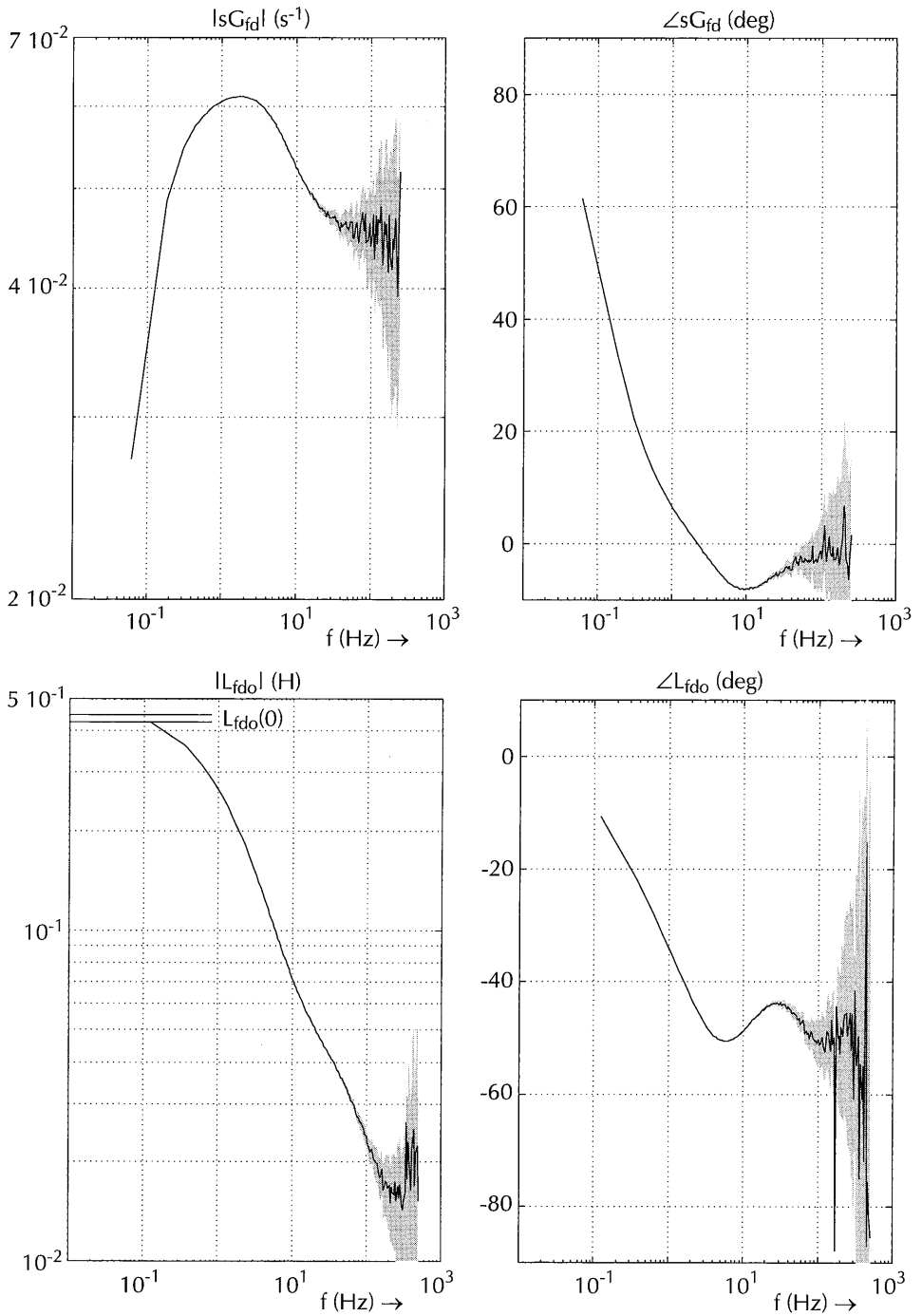
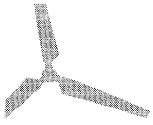


Figure 7.6c
Frequency transforms of Siemens MSR-signals and derived transfer functions: $sG_{fd}(s)$, $L_{fdo}(s)$

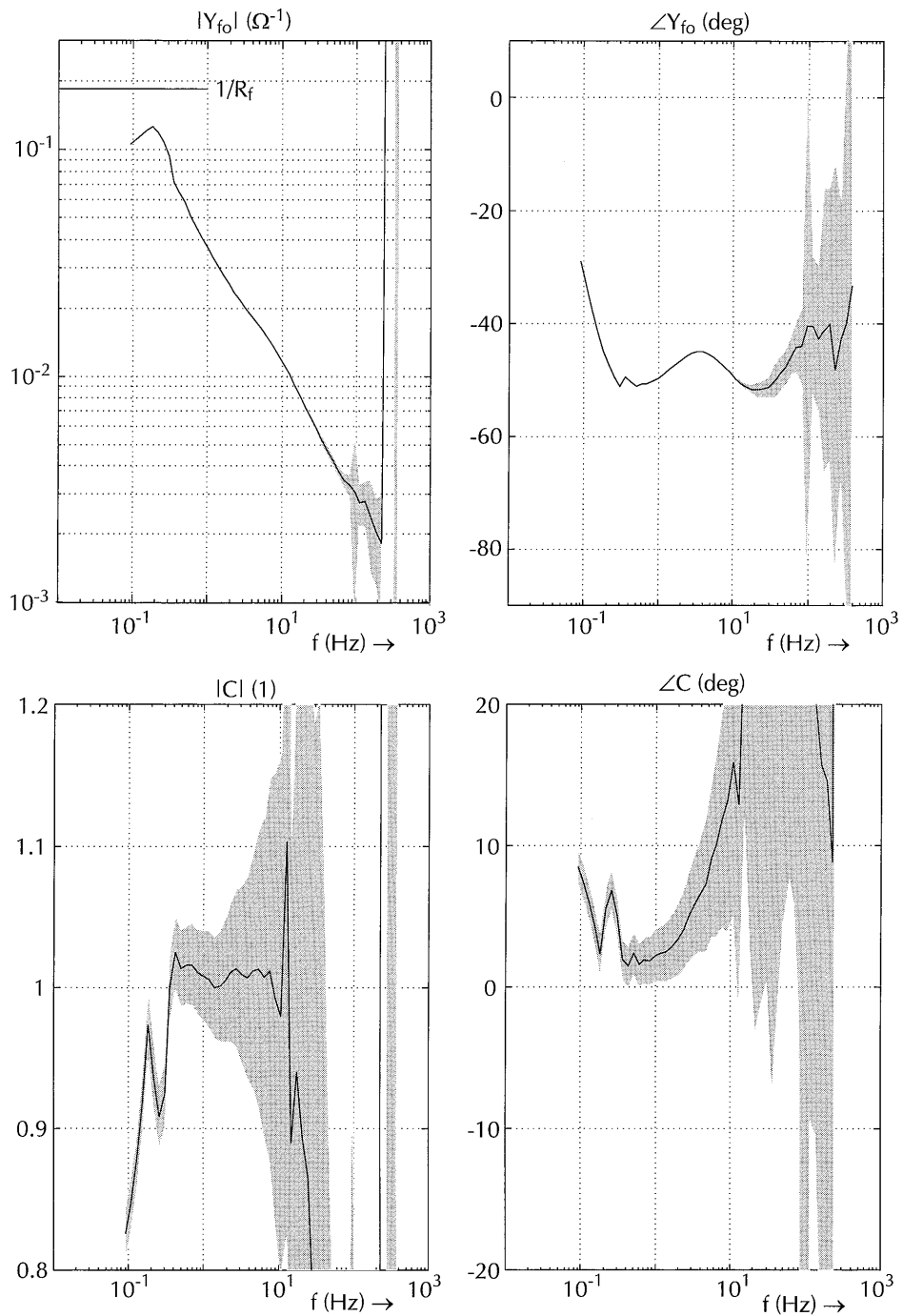
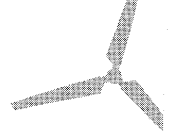


Figure 7.6d
Frequency transforms of Siemens MSR-signals and derived transfer functions: $Y_{fo}(s)$, $C(s)$

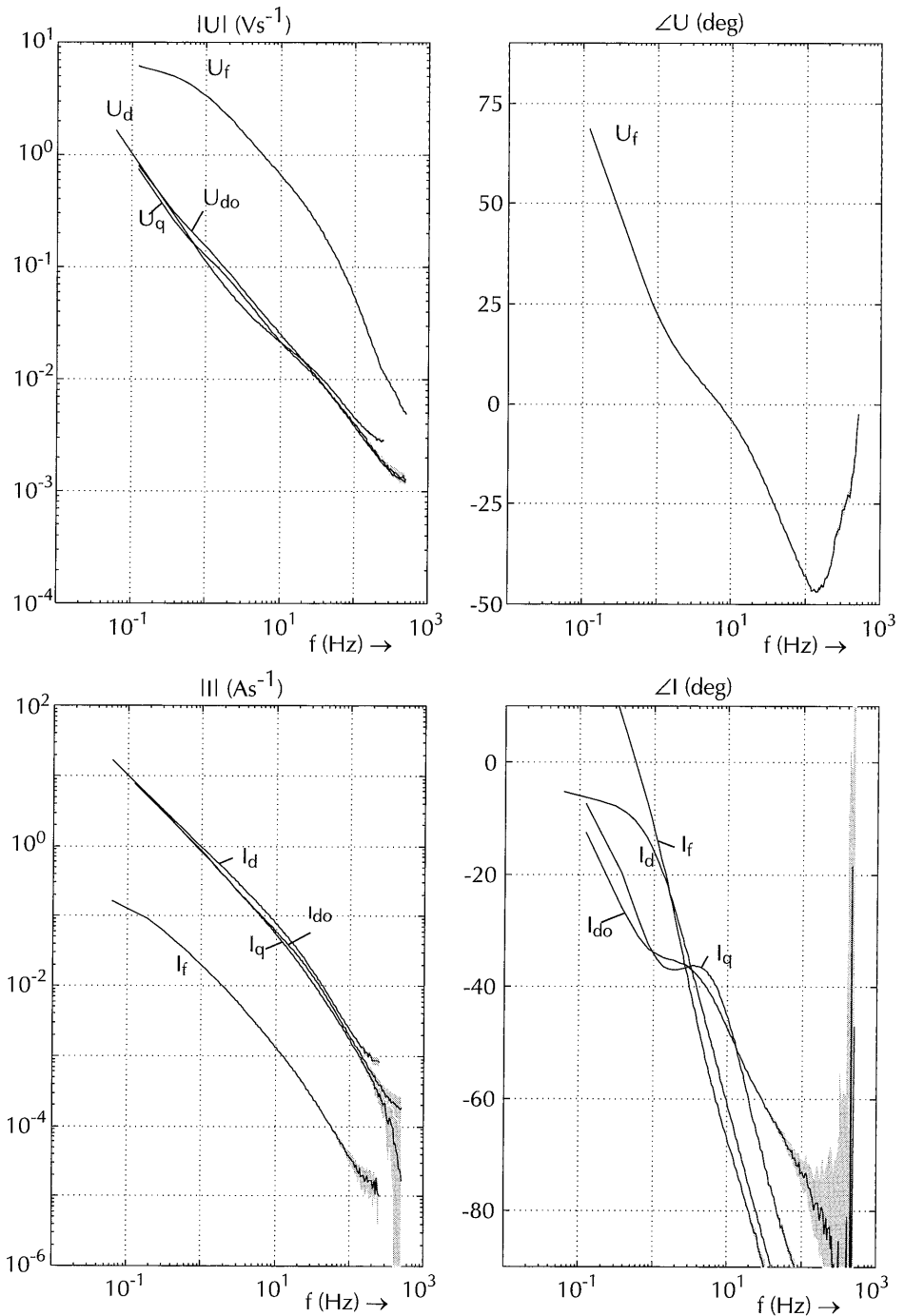
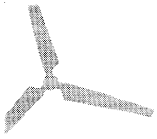


Figure 7.7a
 Frequency transforms of Heemaf MSR-signals and derived transfer functions: U_d , U_q , U_{do} , U_f , I_d , I_q , I_{do} , I_f

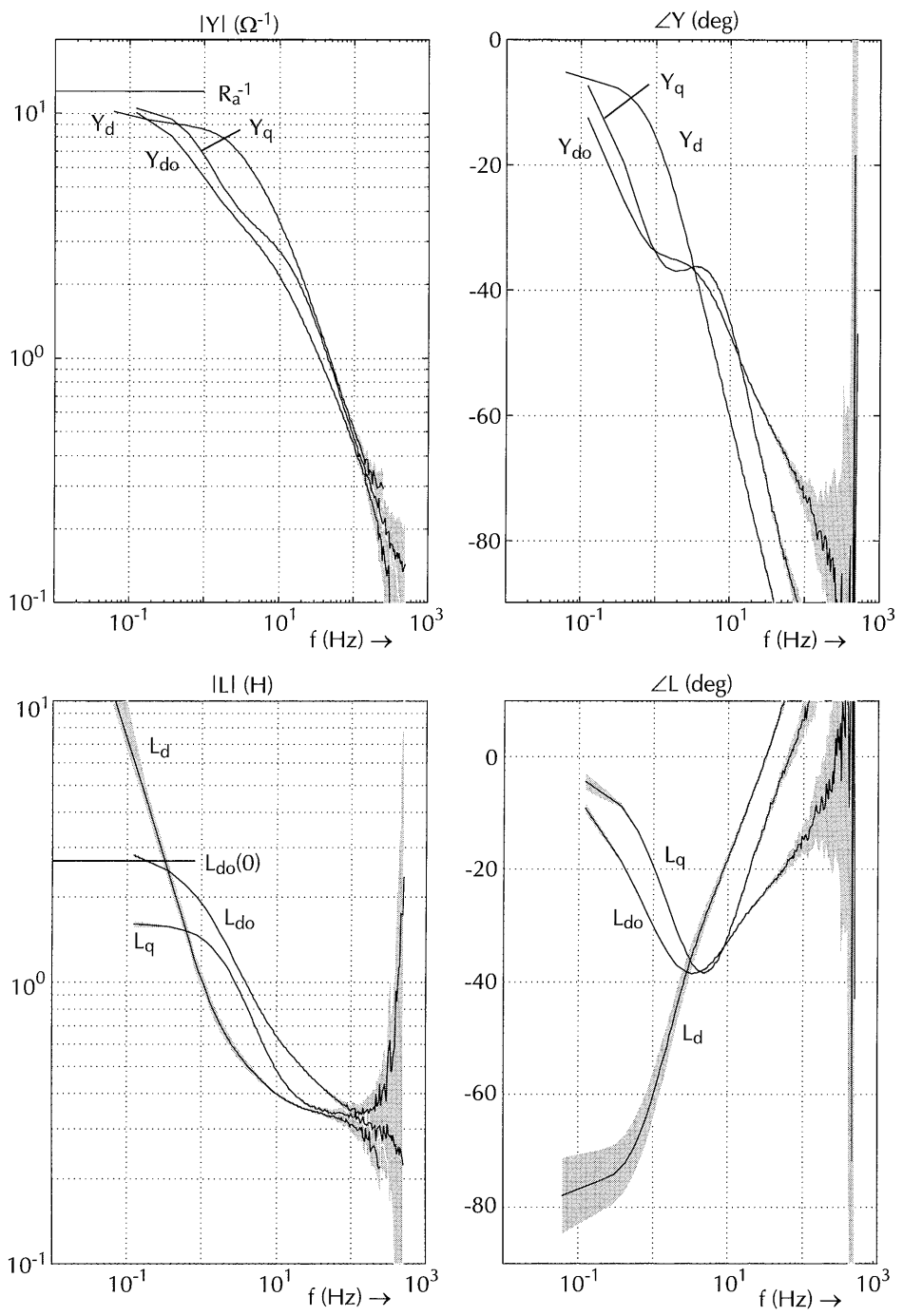


Figure 7.7b
Frequency transforms of Heemaf MSR-signals and derived transfer functions: $Y_d(s)$, $Y_{do}(s)$, $Y_q(s)$, $L_d(s)$, $L_{do}(s)$, $L_q(s)$

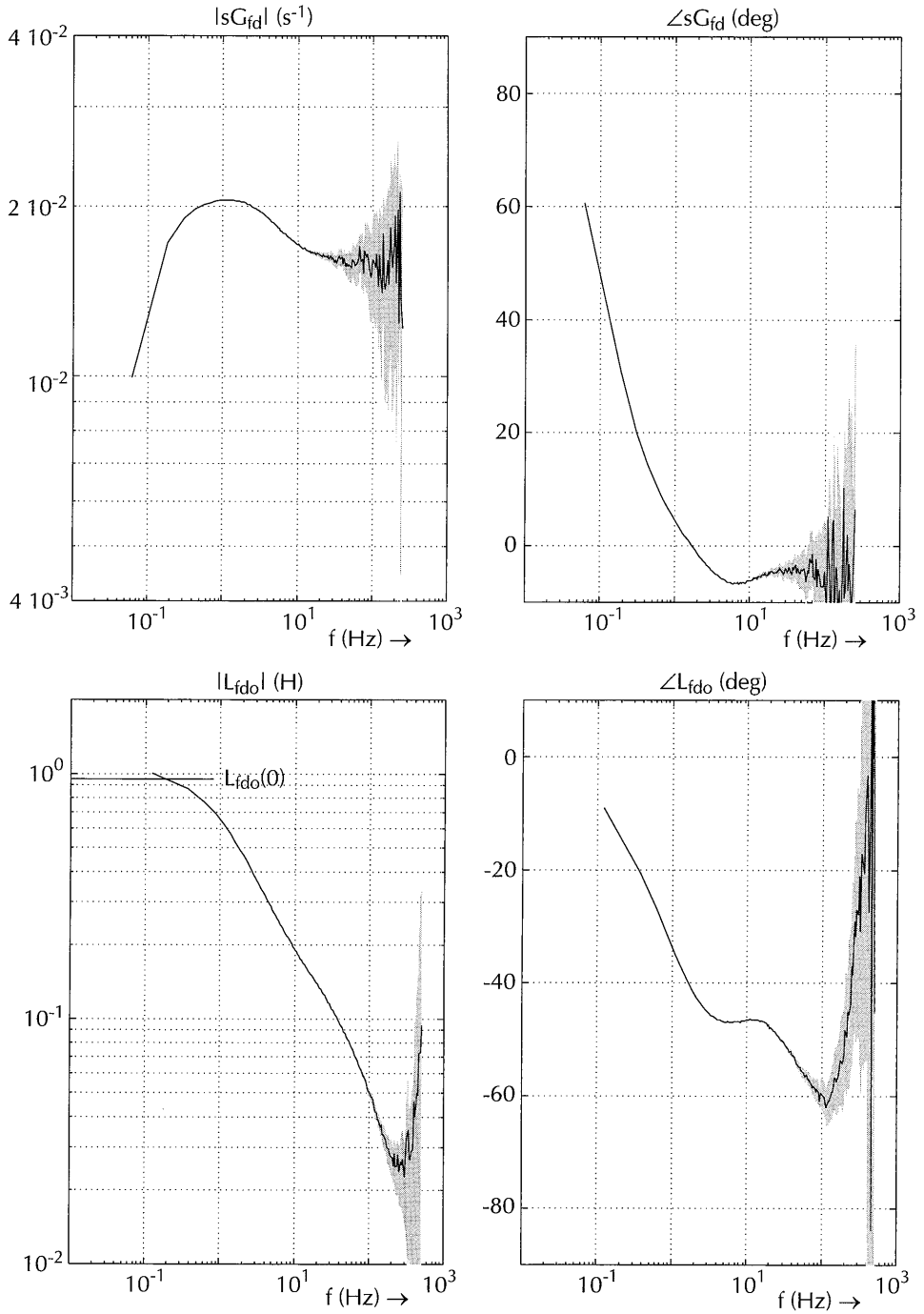
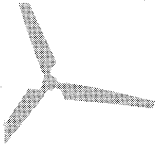


Figure 7.7c
Frequency transforms of Heemaf MSR-signals and derived transfer functions: $sG_{fdl}(s)$, $L_{fdol}(s)$

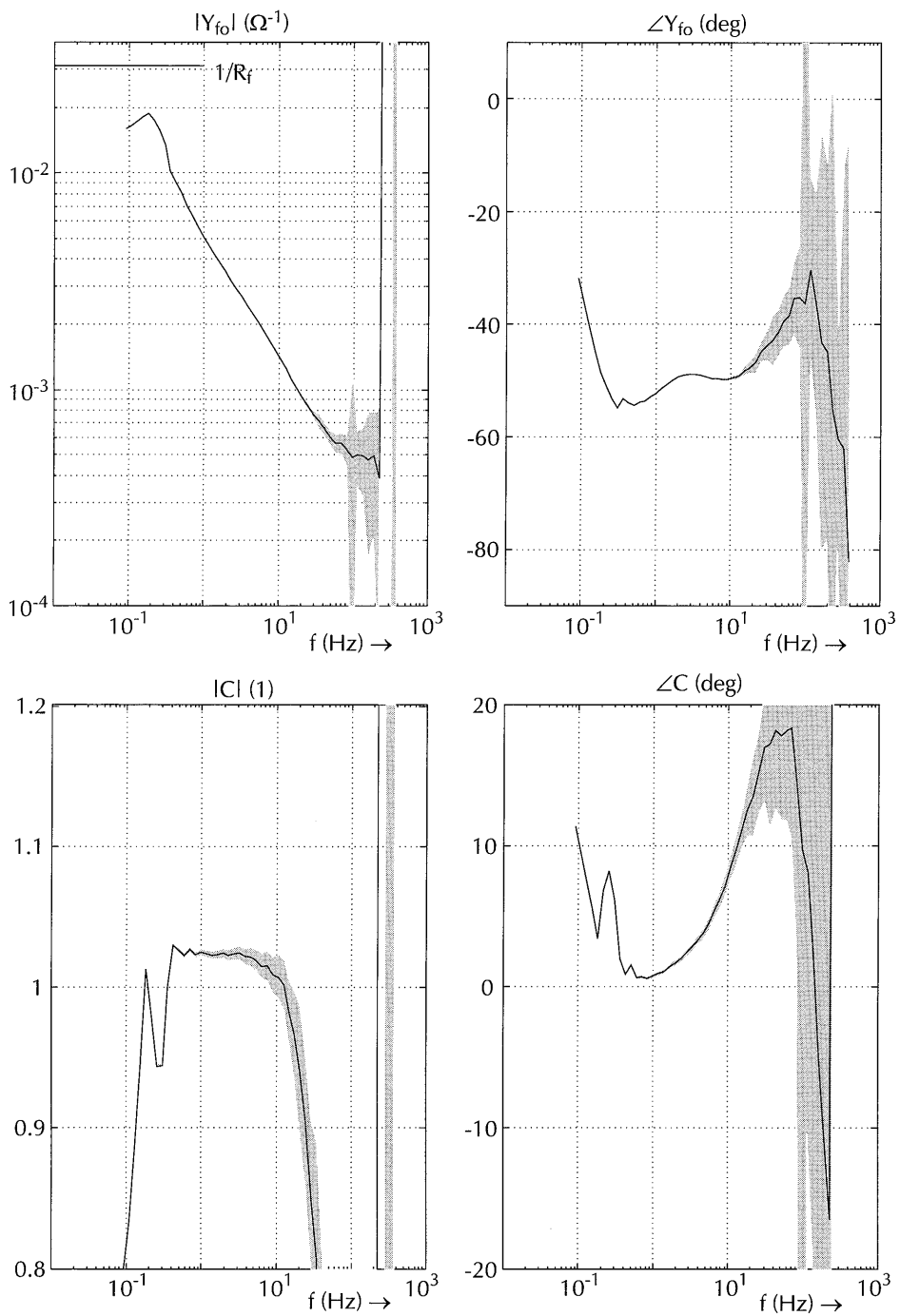
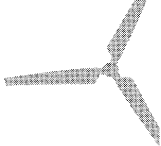


Figure 7.7d
Frequency transforms of Heemaf MSR-signals and derived transfer functions: $Y_{fo}(s)$, $C(s)$

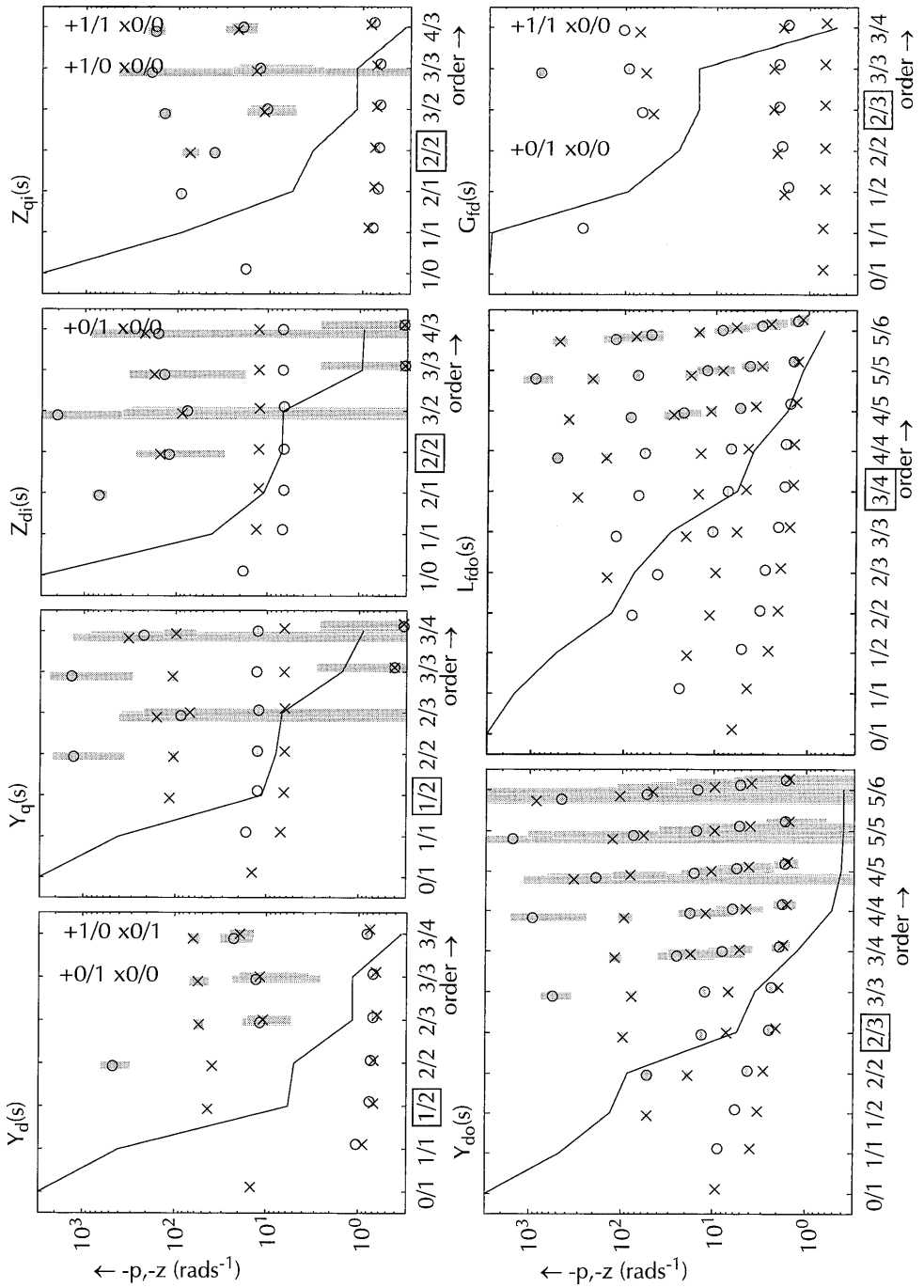
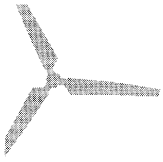


Figure 7.8a
Order-test results of the MSR test for the Siemens machine

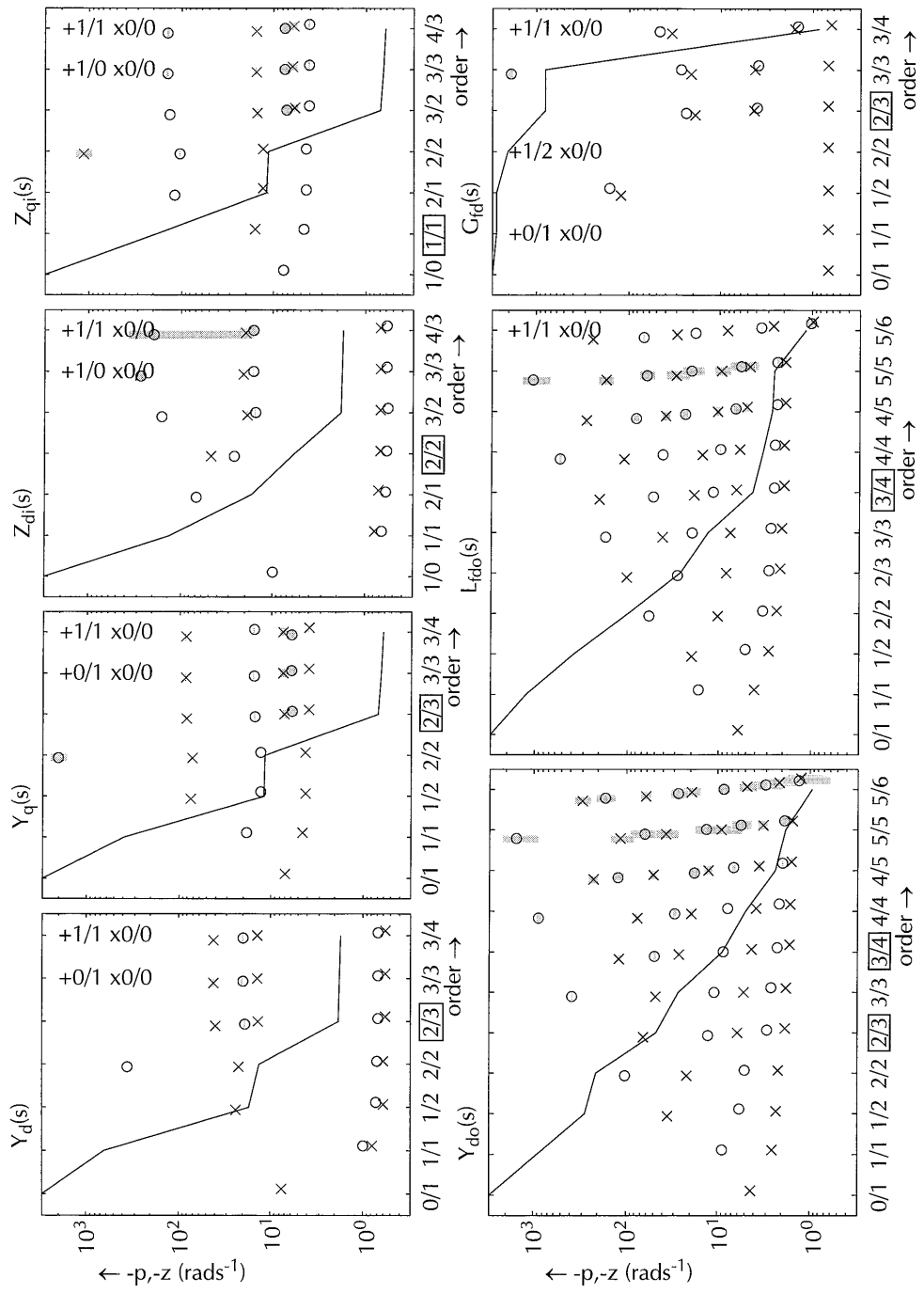
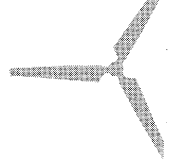


Figure 7.8b
Order-test results of the MSR test for the Heemaf machine

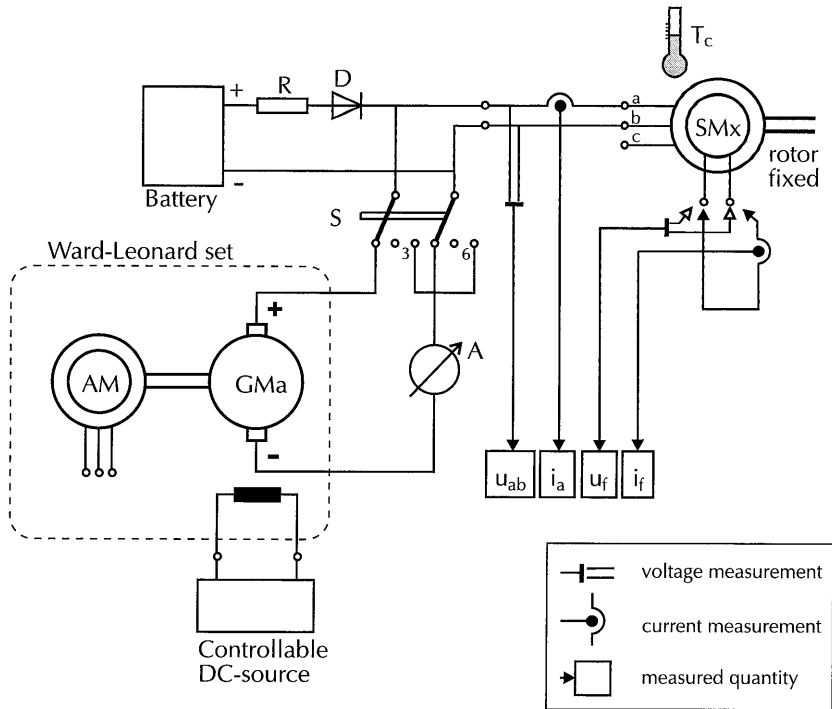
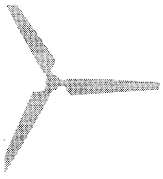


Figure 7.9
DC-decay test measurement set-up

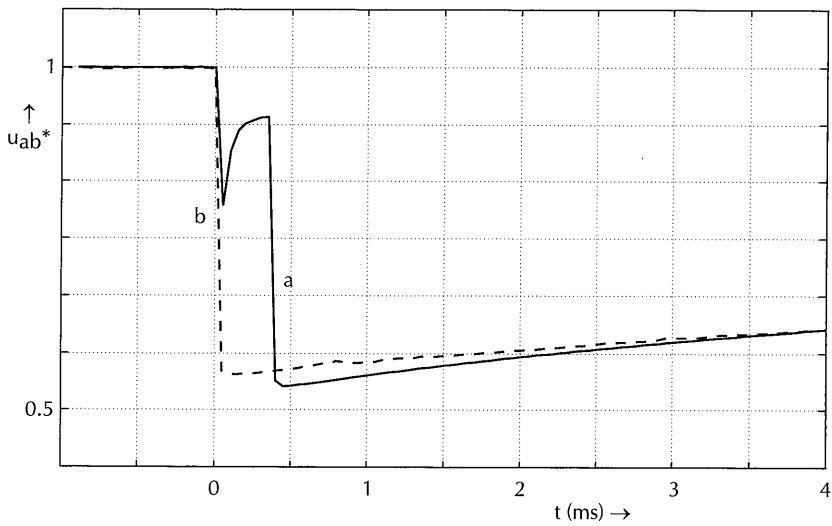


Figure 7.10
DC-decay primary voltage u_{ab} (normalised) at the step-moment, as a function of time:
a) Siemens machine, using a diac switch
b) Heemaf machine, using a mechanical sliding switch

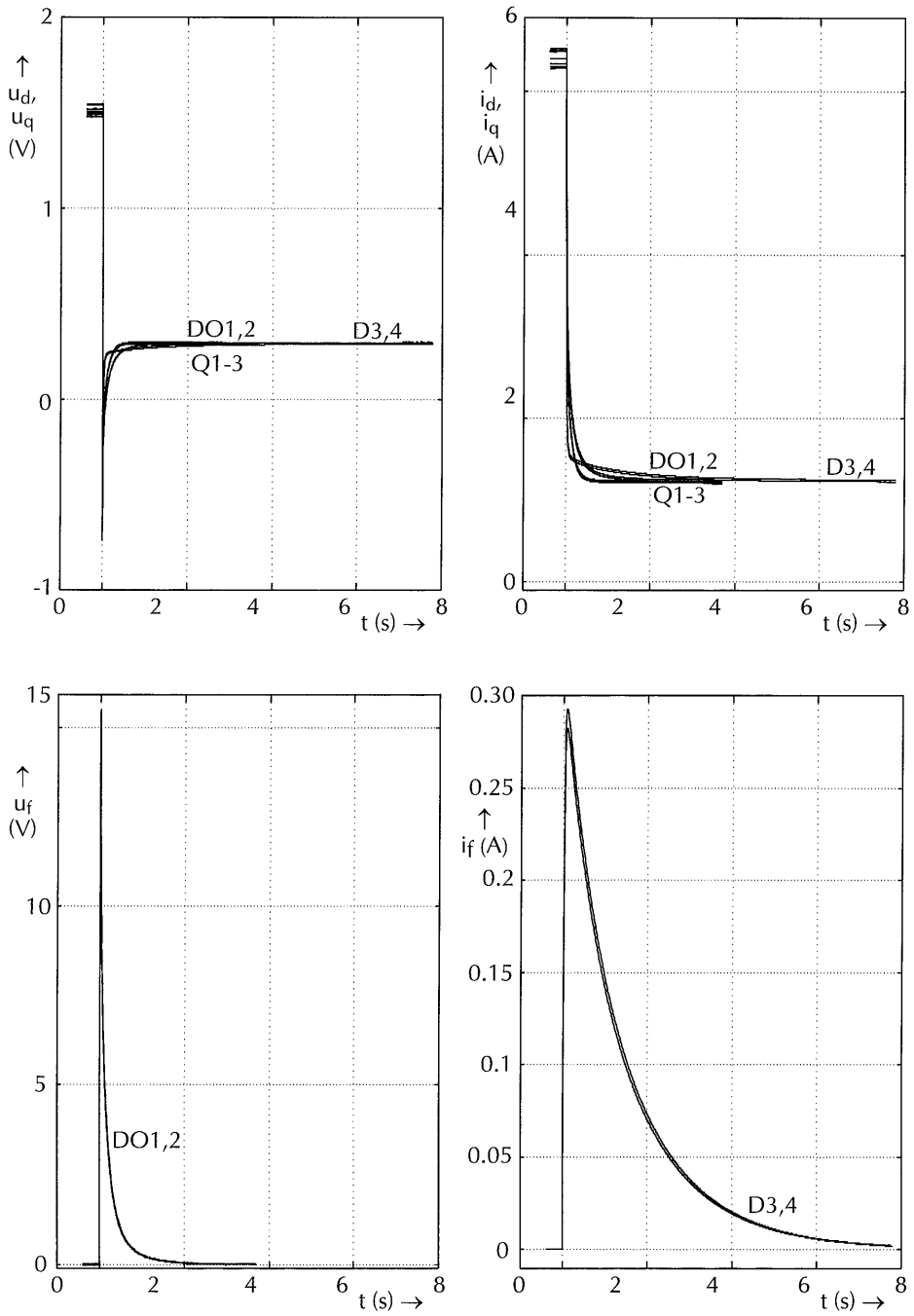
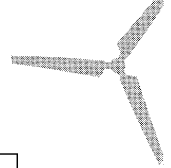


Figure 7.11a
DC-decay test measured signals, Siemens machine

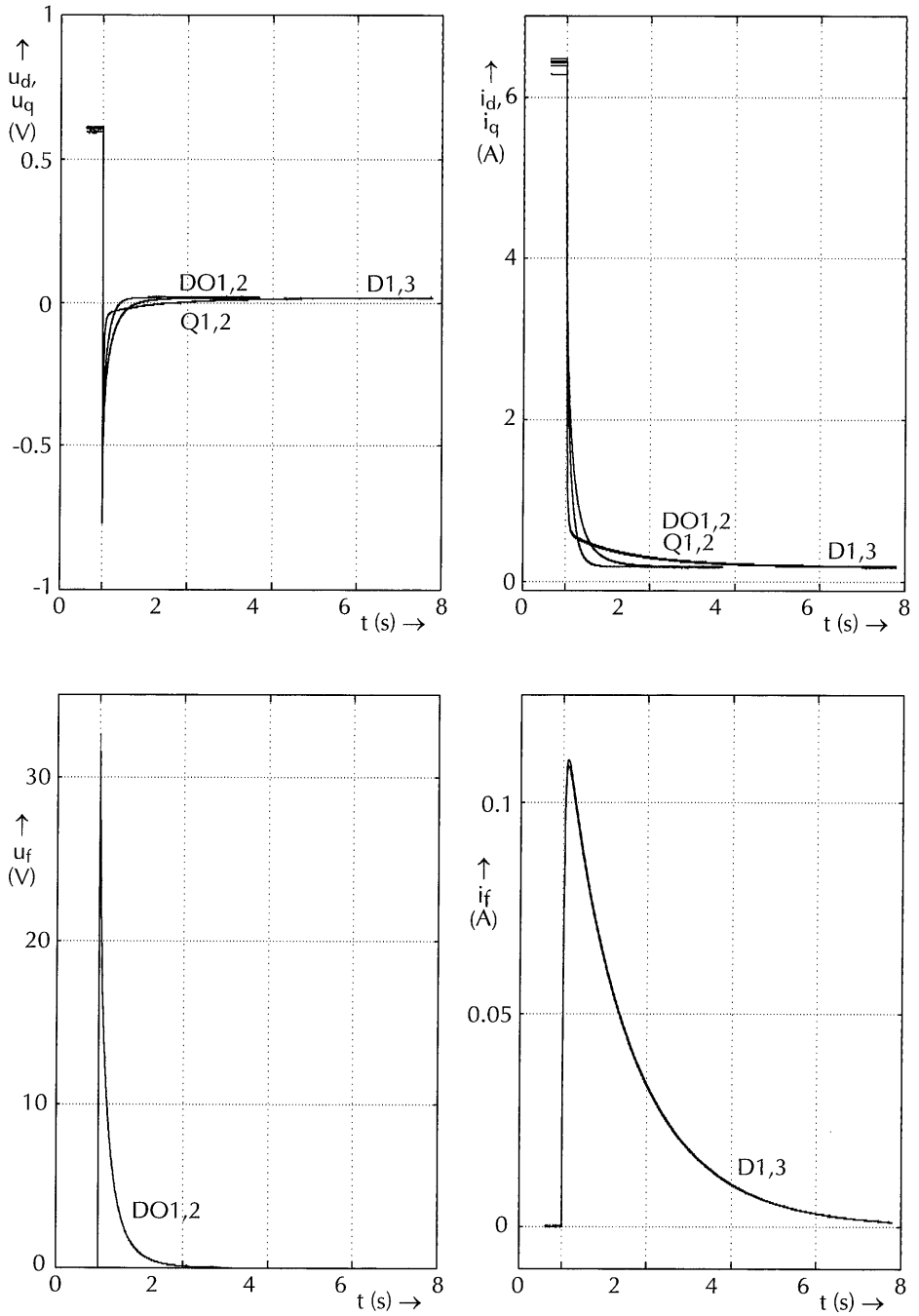
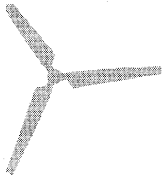


Figure 7.11b
DC-decay test measured signals, Heemaf machine

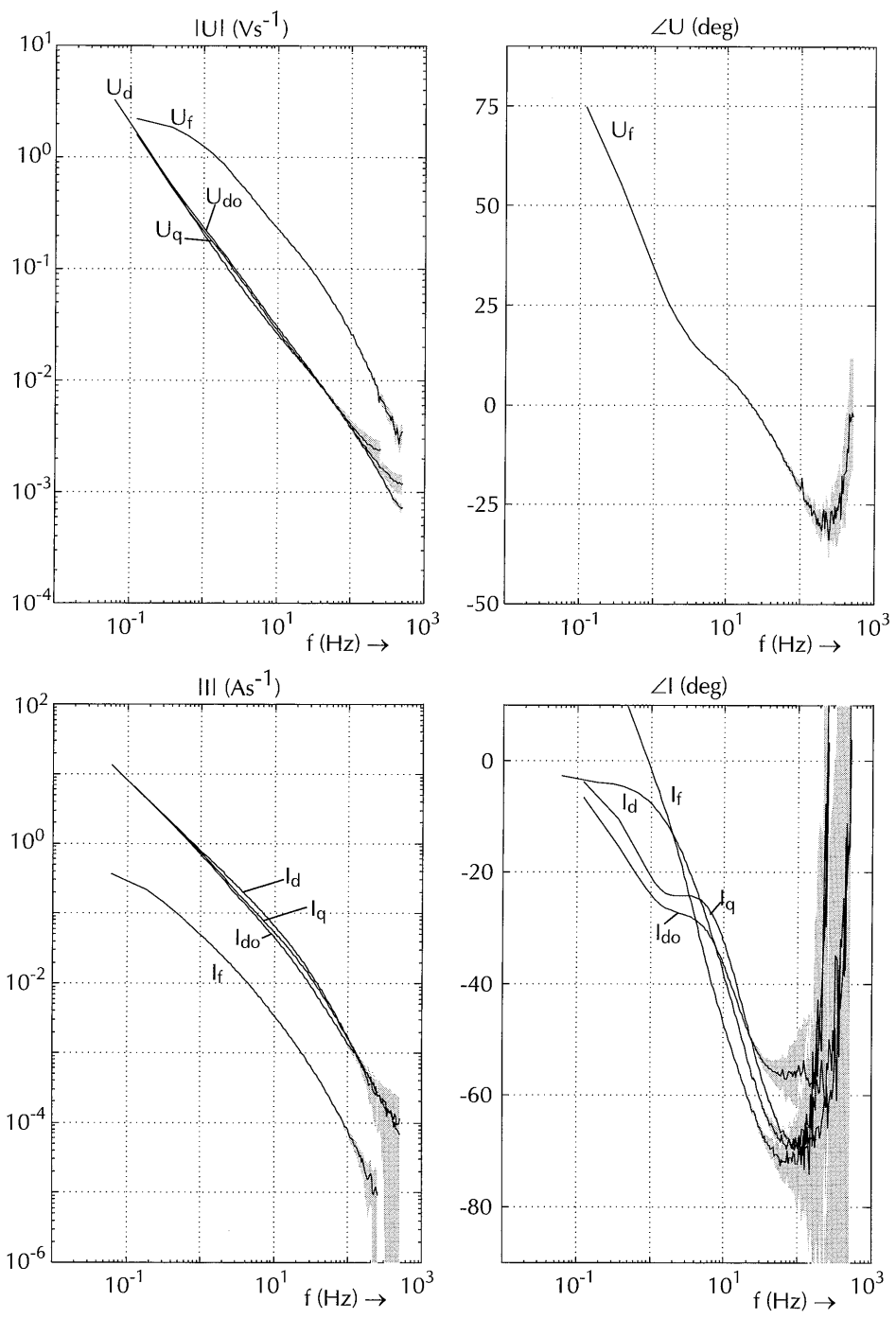
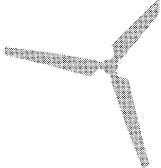


Figure 7.12a
Frequency transforms of Siemens DC-decay signals and derived transfer functions: U_d , U_q , U_{do} , U_f , I_d , I_q , I_{do} , I_f

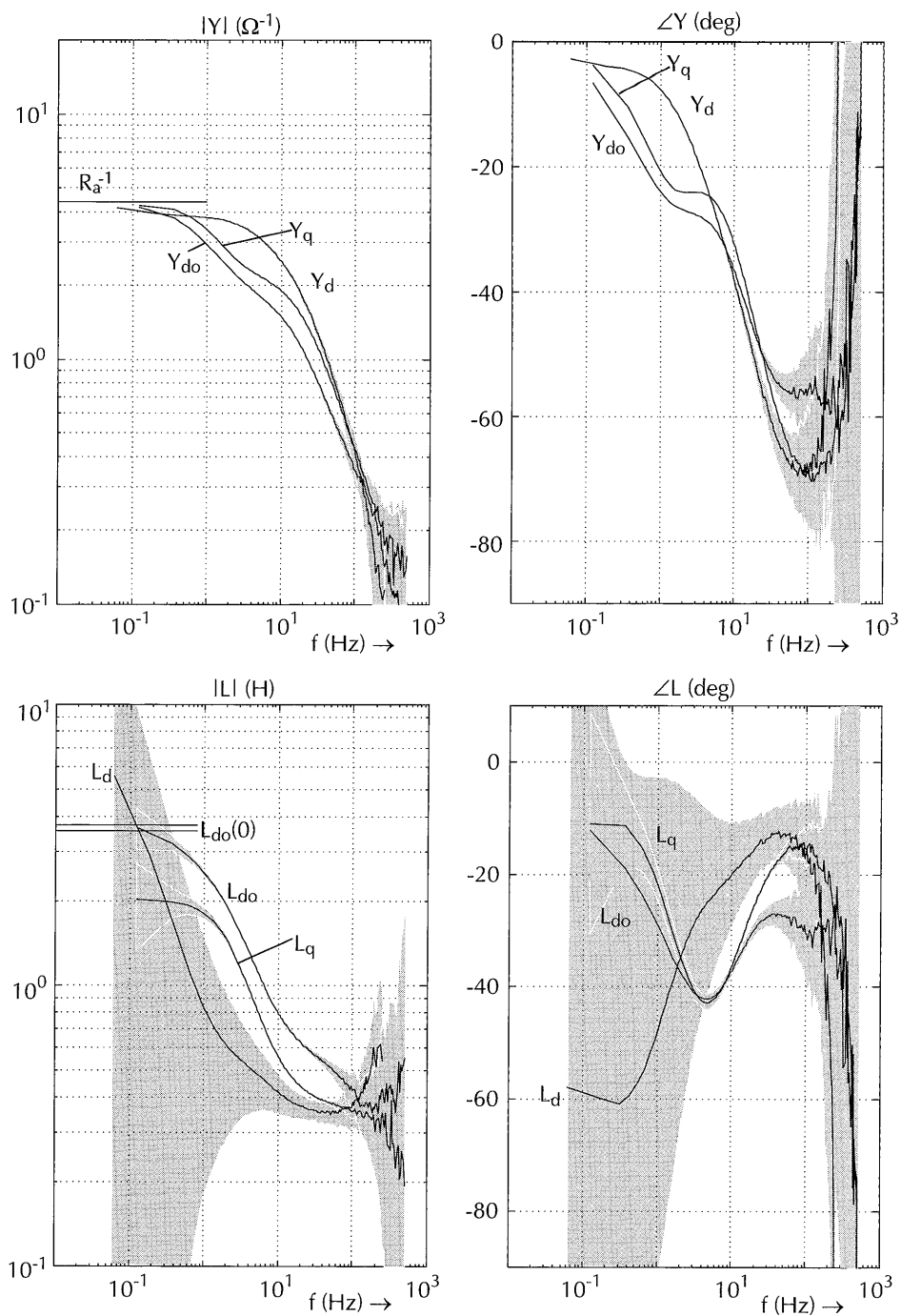
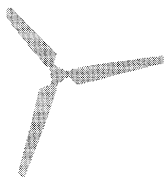


Figure 7.12b
 Frequency transforms of Siemens DC-decay signals and derived transfer functions: $Y_d(s)$, $Y_{do}(s)$, $Y_q(s)$, $L_d(s)$, $L_{do}(s)$, $L_q(s)$

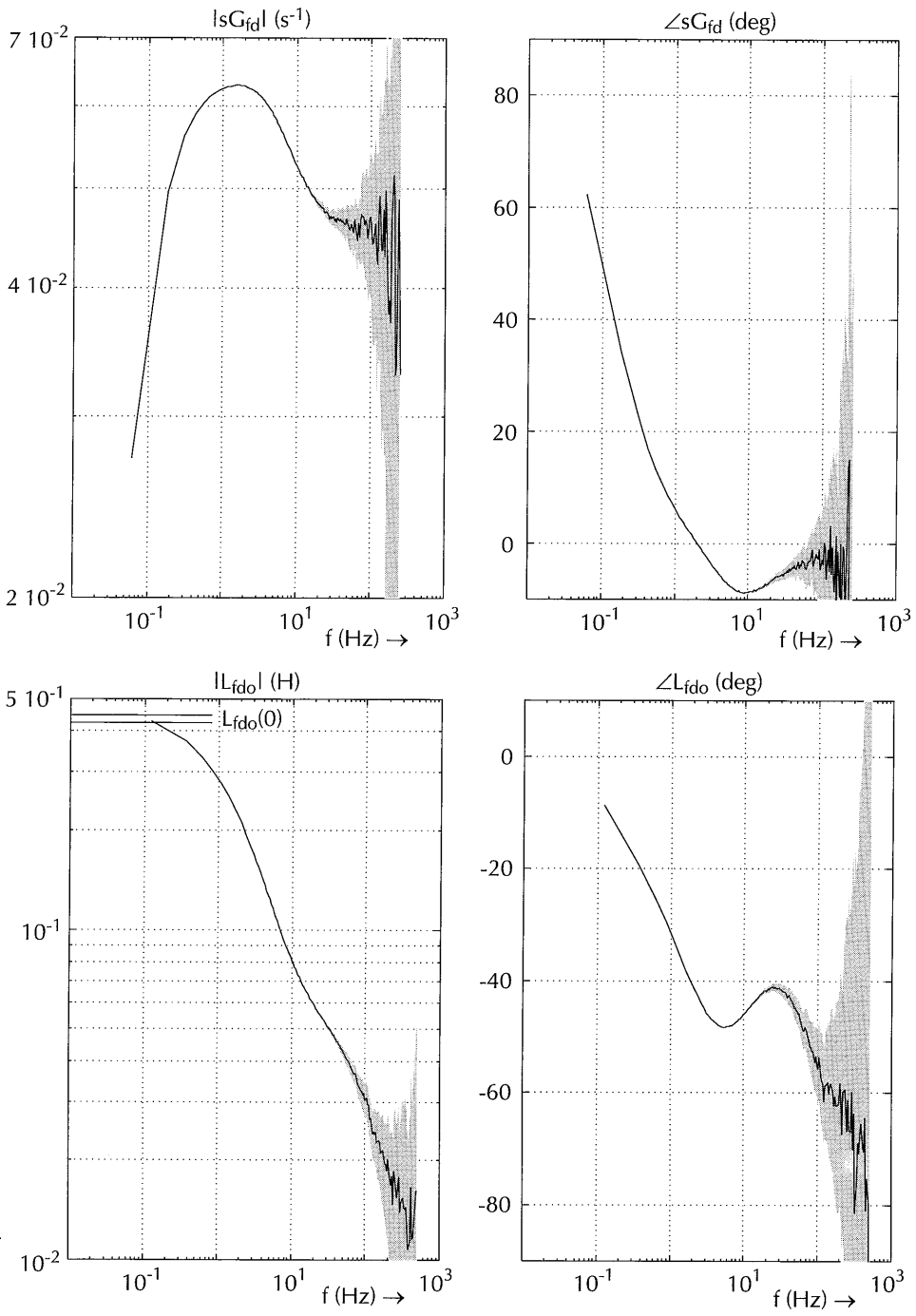
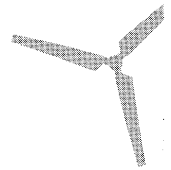


Figure 7.12c
Frequency transforms of Siemens DC-decay signals and derived transfer functions: $sG_{fd}(s)$, $L_{fdo}(s)$

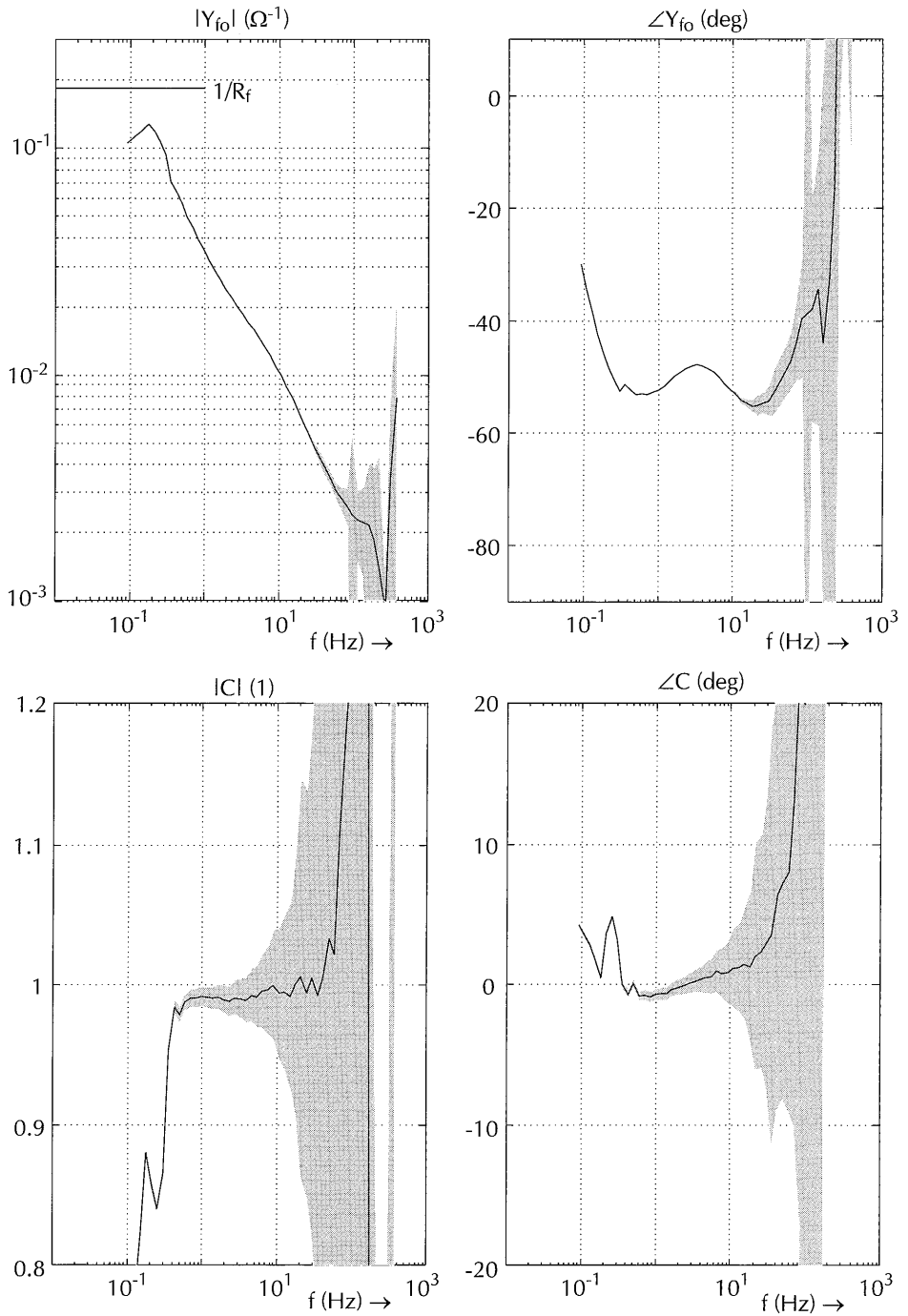


Figure 7.12d
Frequency transforms of Siemens DC-decay signals and derived transfer functions: $Y_{fo}(s)$, $C(s)$

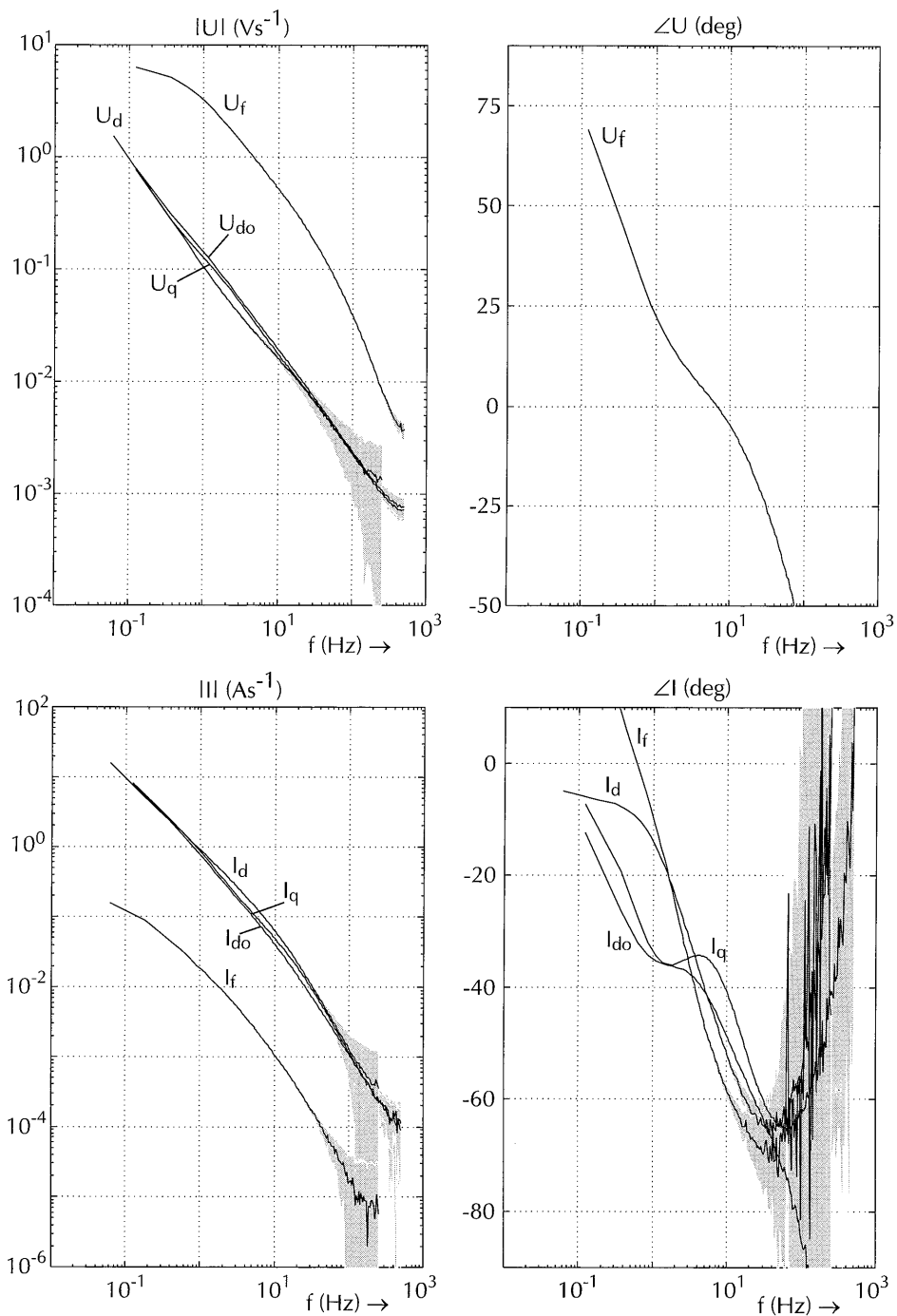
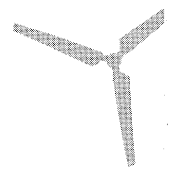


Figure 7.13a
Frequency transforms of Heemaf DC-decay signals and derived transfer functions: U_d , U_q , U_{do} , U_f , I_d , I_q , I_{do} , I_f

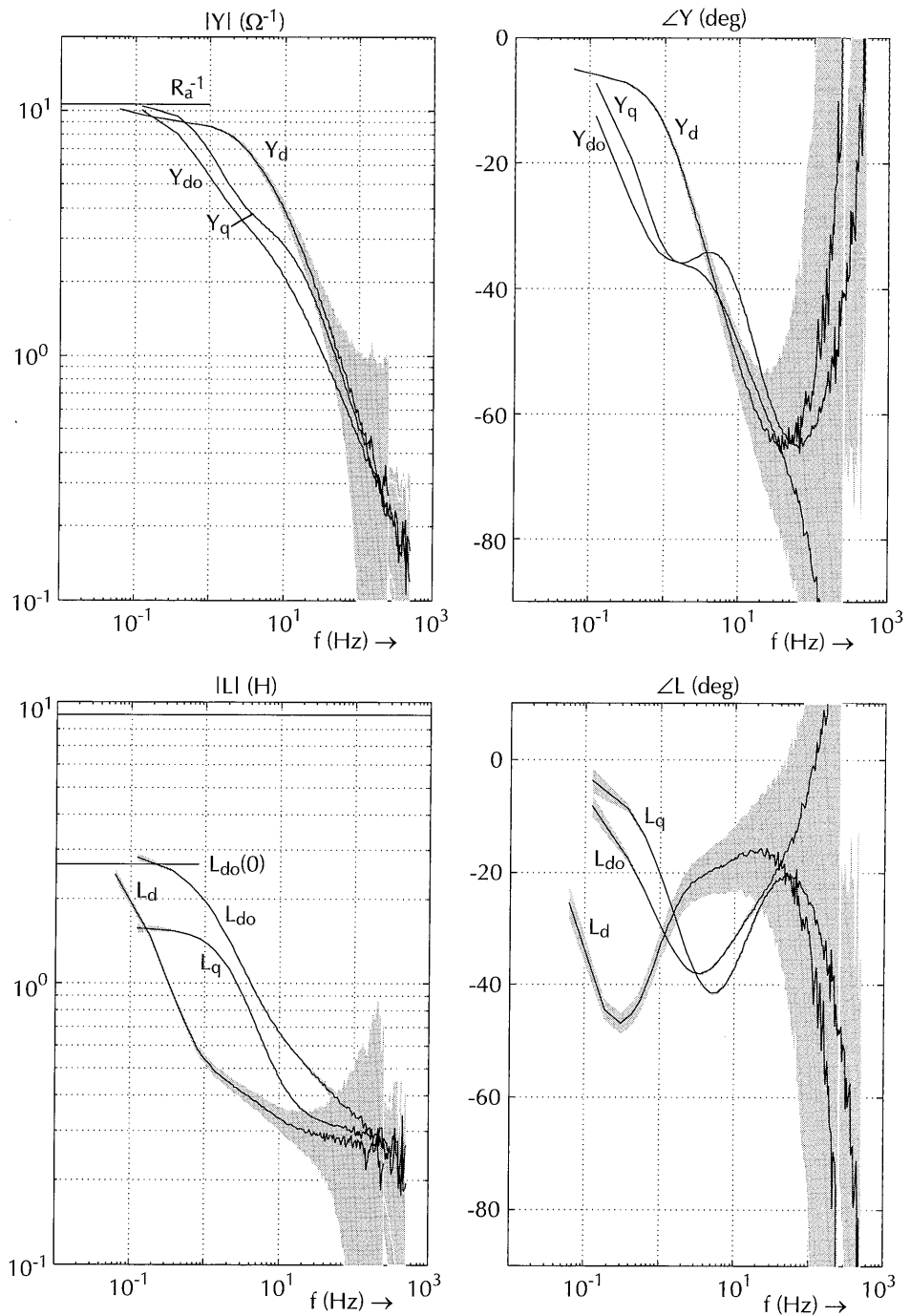


Figure 7.13b
 Frequency transforms of Heemaf DC-decay signals and derived transfer functions: $Y_d(s)$, $Y_{do}(s)$, $Y_q(s)$, $L_d(s)$, $L_{do}(s)$, $L_q(s)$

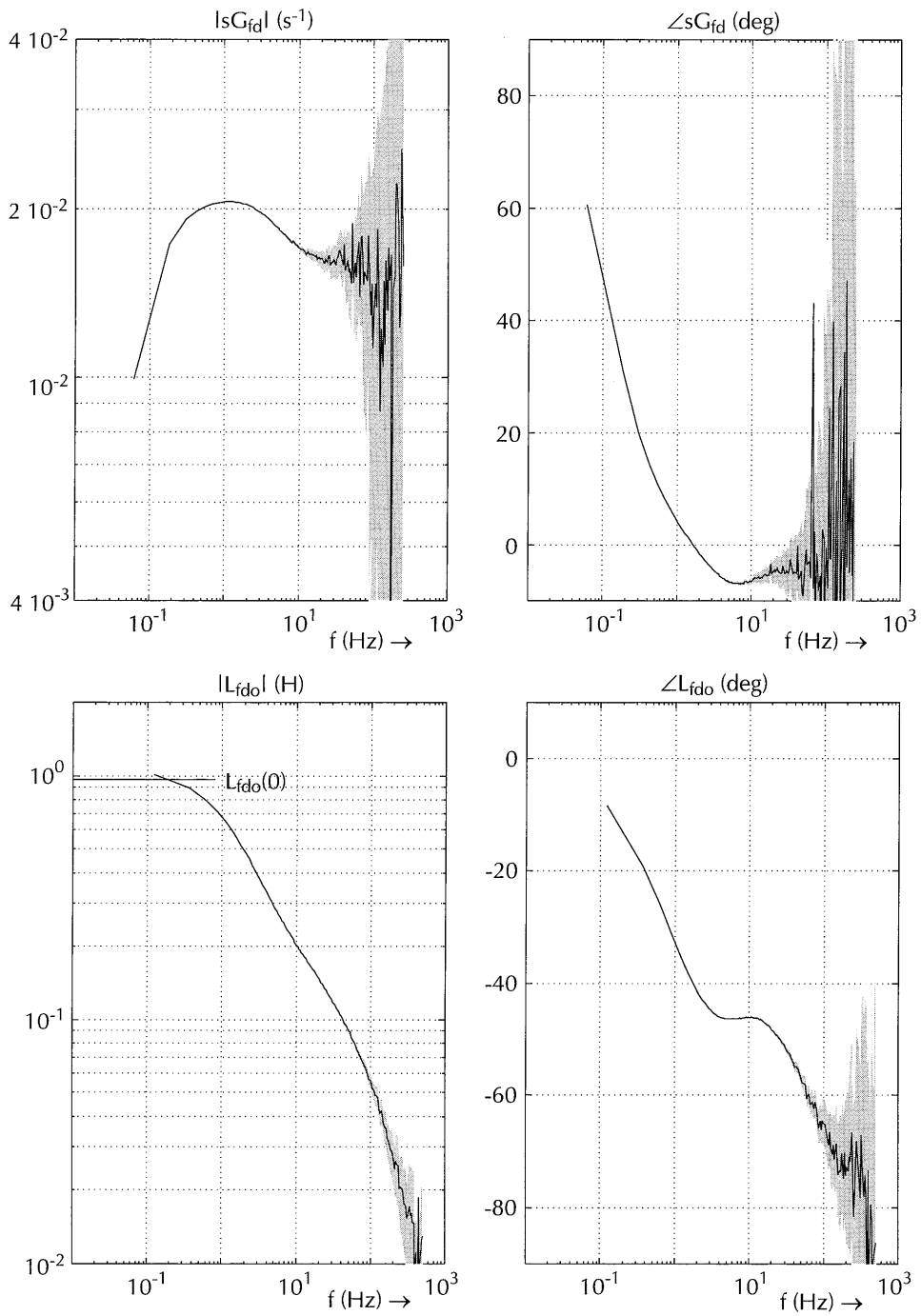
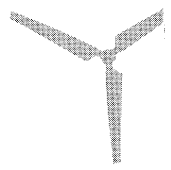


Figure 7.13c
Frequency transforms of Heemaf DC-decay signals and derived transfer functions: $sG_{fd}(s)$, $L_{fdo}(s)$

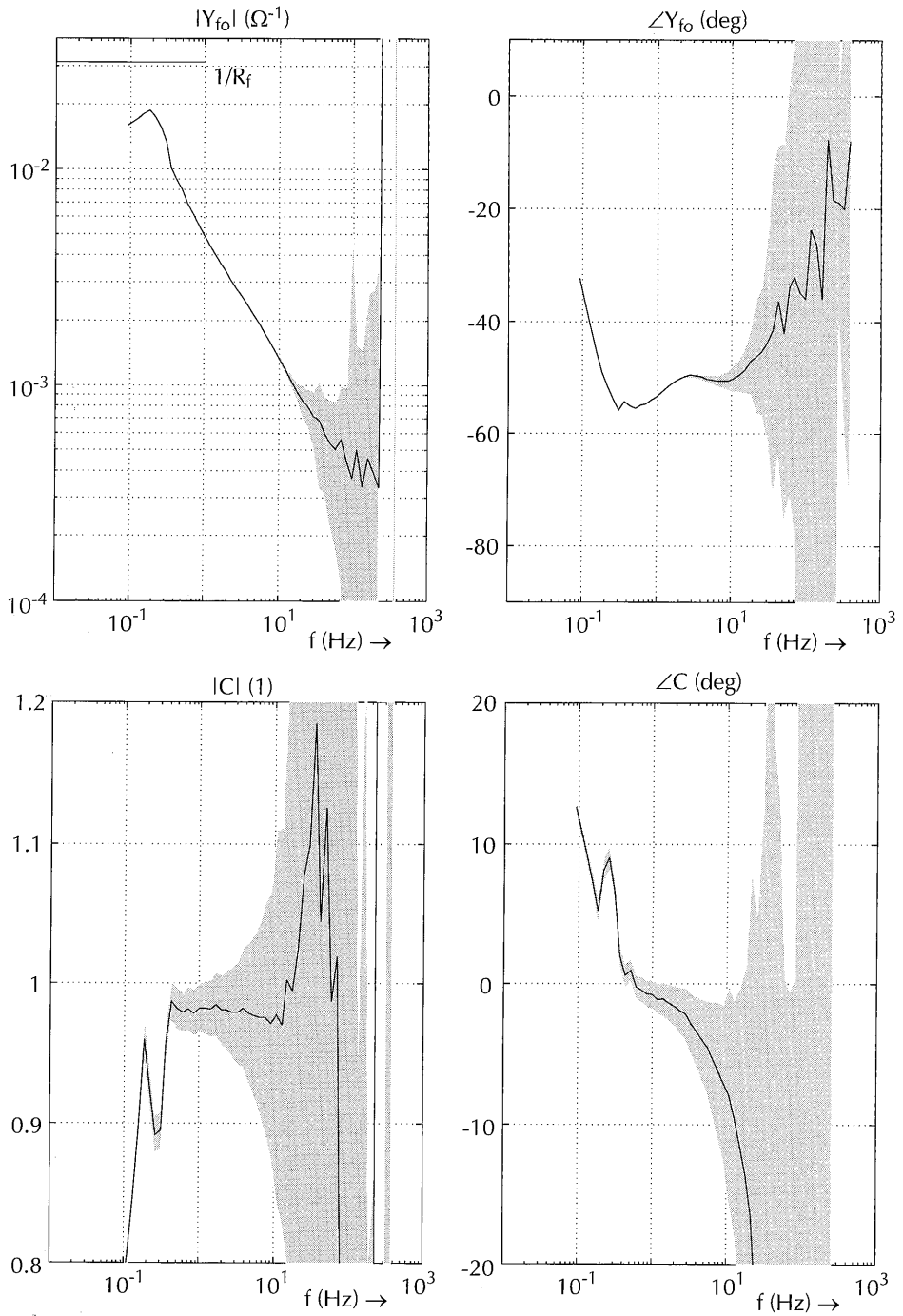
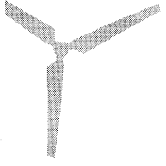


Figure 7.13d
Frequency transforms of Heemaf DC-decay signals and derived transfer functions: $Y_{f_0}(s)$, $C(s)$

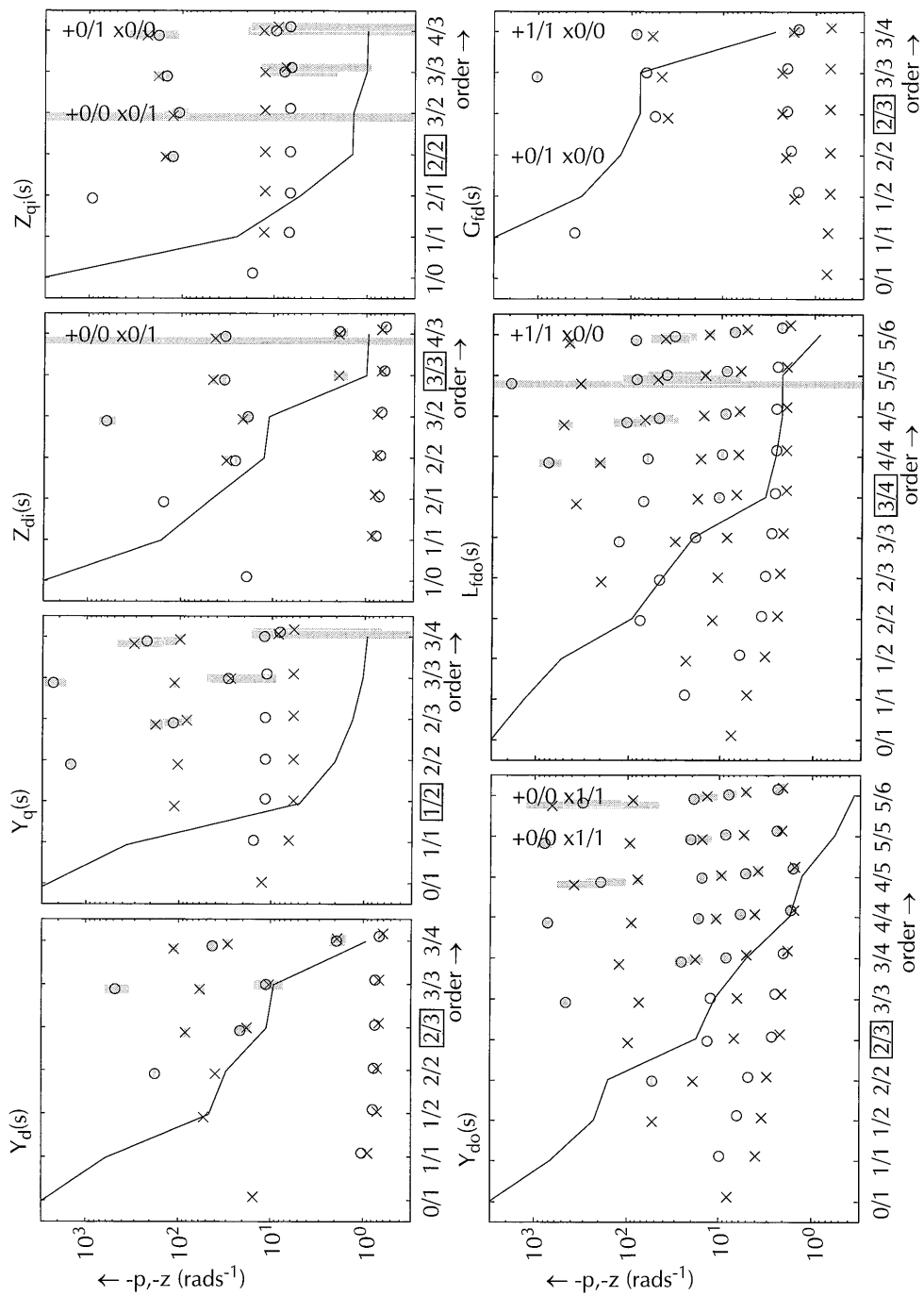
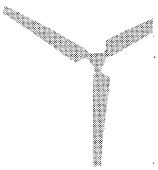


Figure 7.14a
Order-test results of the DC-decay test for the Siemens machine

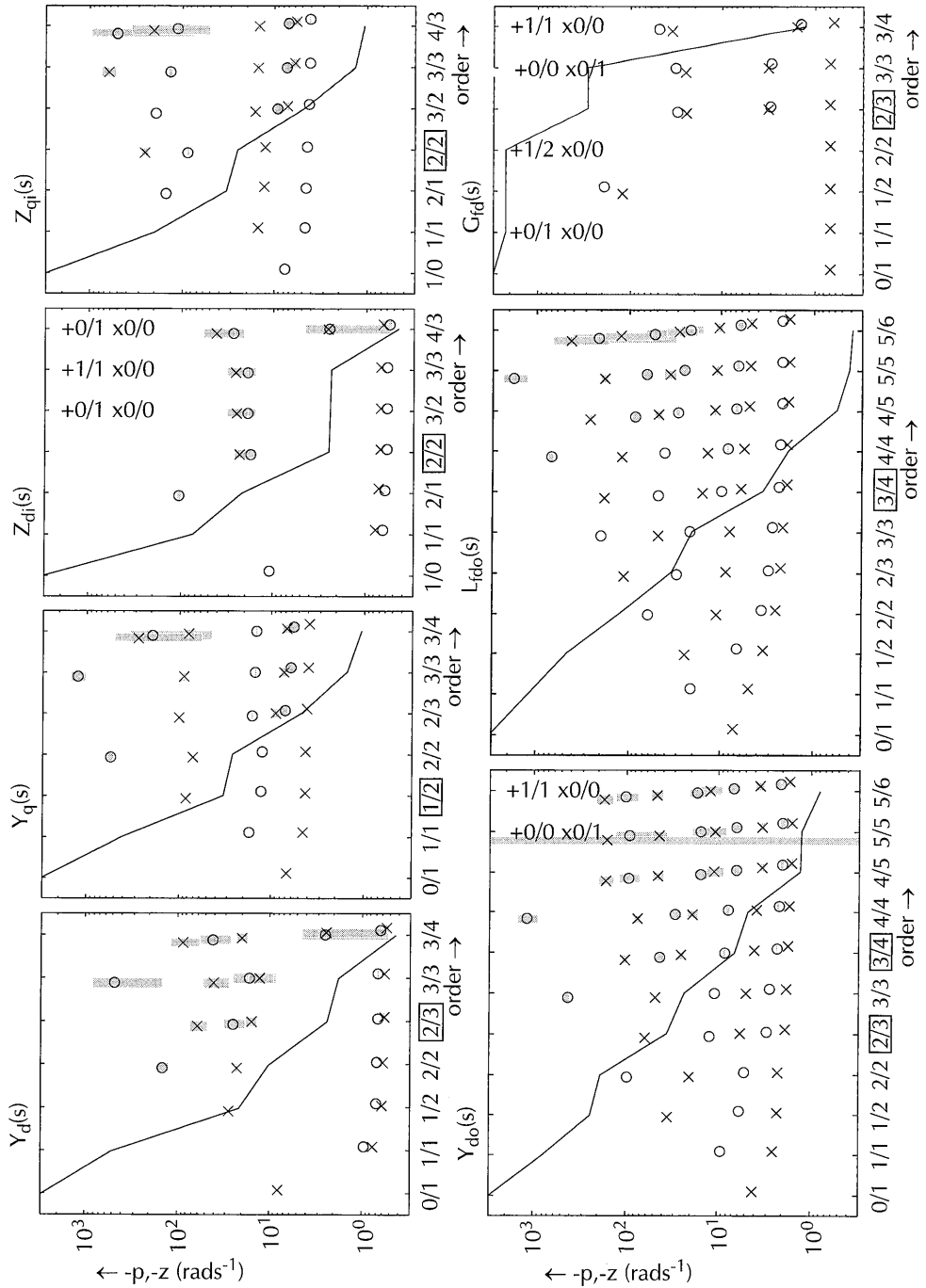
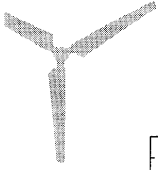


Figure 7.14b
Order-test results of the DC-decay test for the Heemaf machine

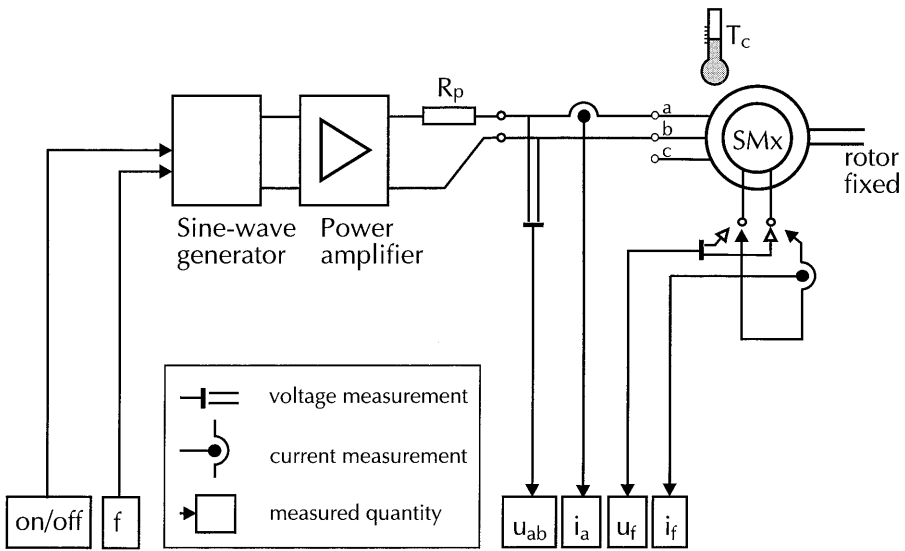


Figure 7.15
SSFR-test measurement set-up

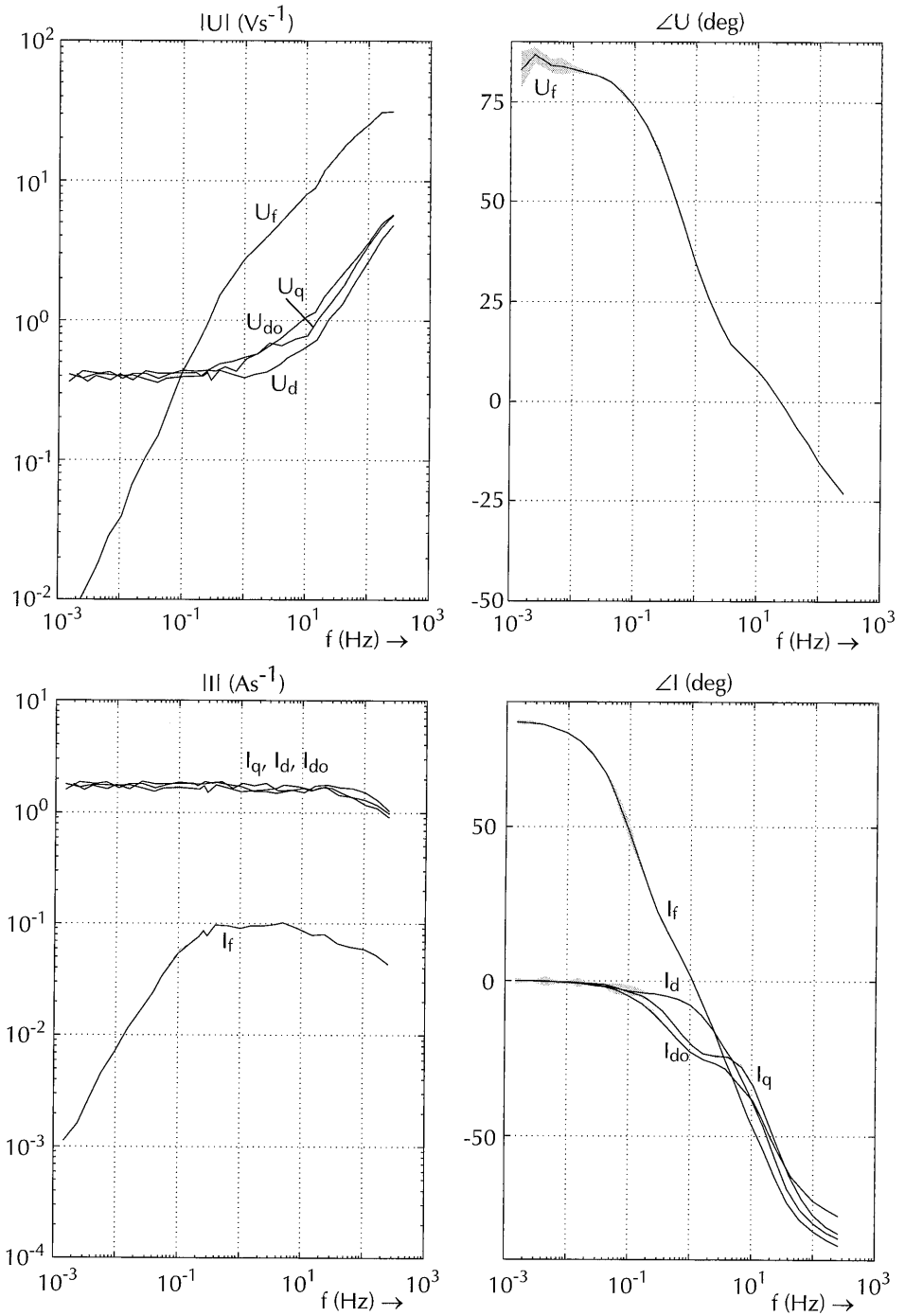
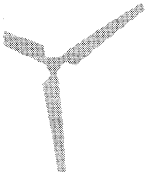


Figure 7.16a
 Frequency transforms of Siemens SSFR signals and derived transfer functions: U_d , U_q , U_{do} , U_f , I_d , I_q , I_{do} , I_f

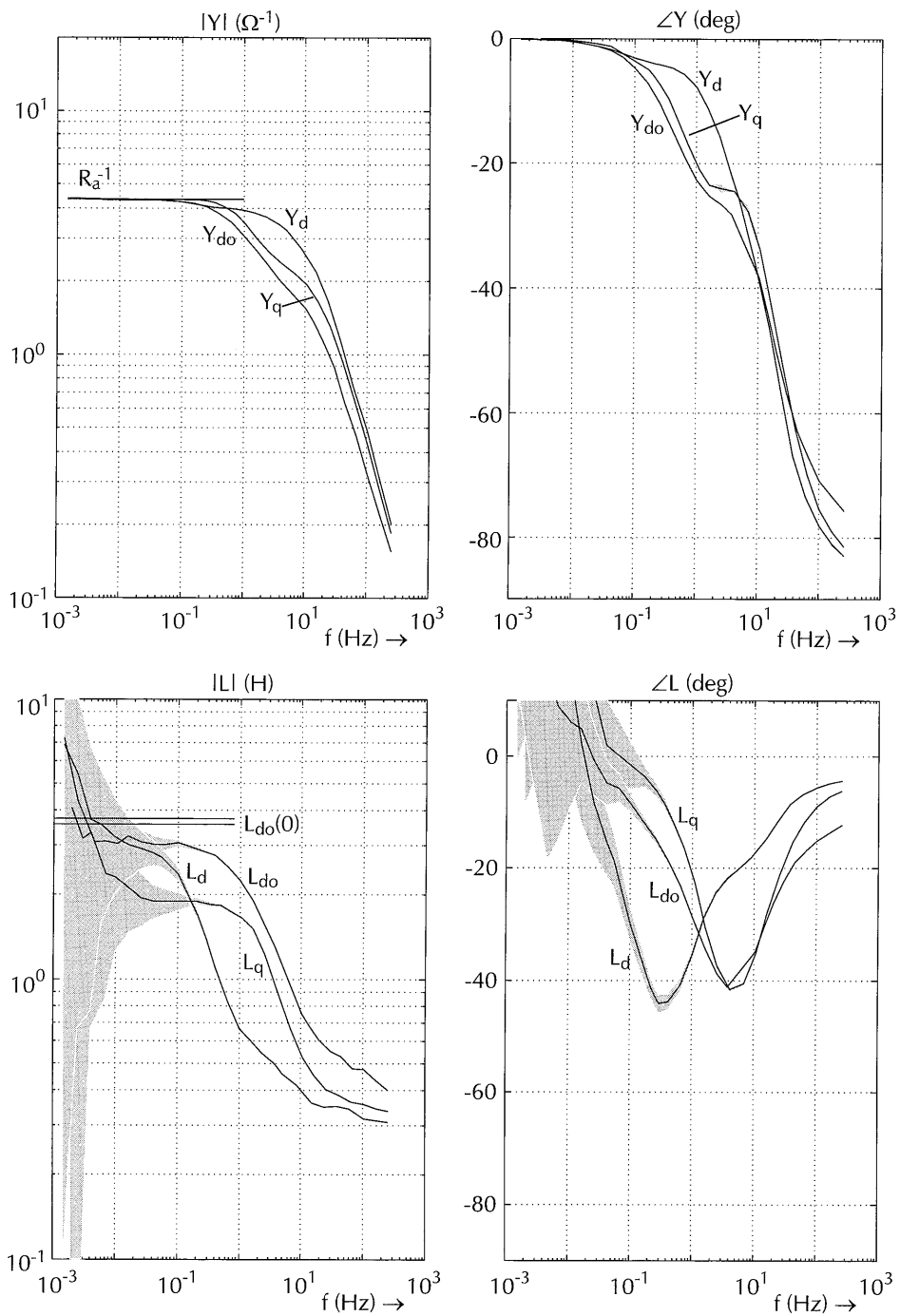


Figure 7.16b
 Frequency transforms of Siemens SSFR signals and derived transfer functions: $Y_d(s)$, $Y_{do}(s)$, $Y_q(s)$, $L_d(s)$, $L_{do}(s)$, $L_q(s)$

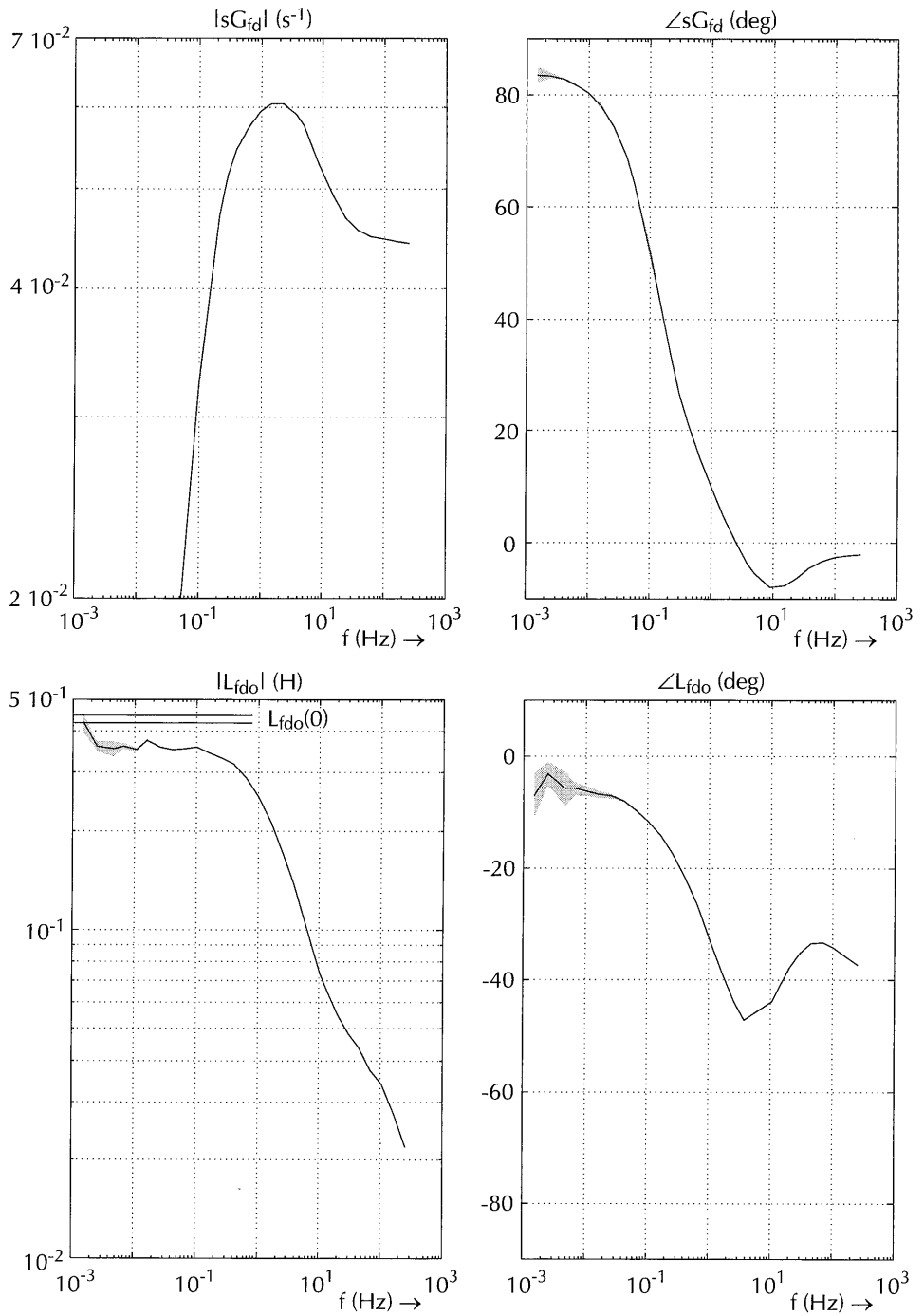
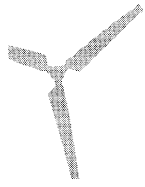


Figure 7.16c
Frequency transforms of Siemens SSFR signals and derived transfer functions: $sG_{fd}(s)$, $L_{fdo}(s)$

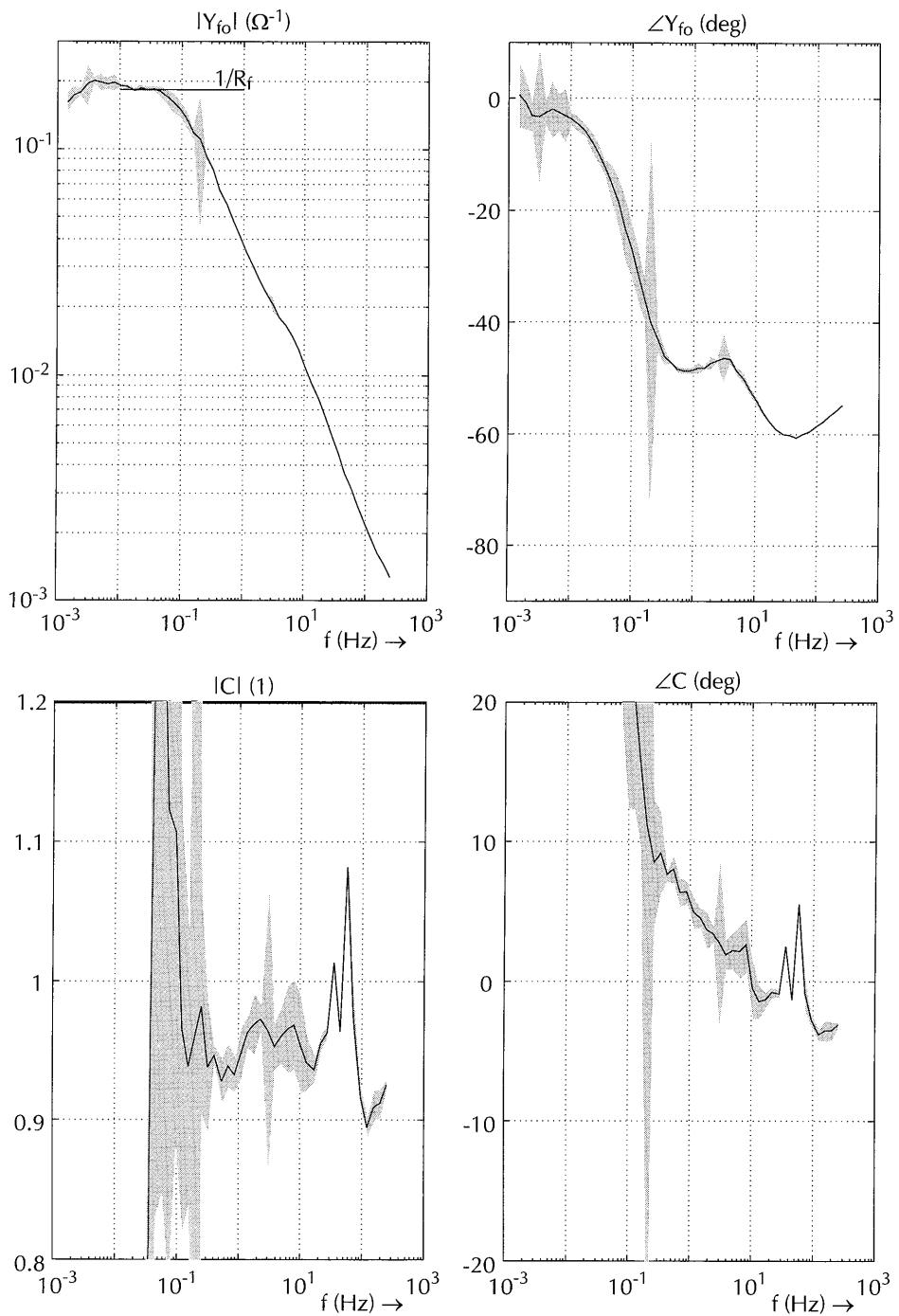


Figure 7.16d
Frequency transforms of Siemens SSFR signals and derived transfer functions: $Y_{fo}(s)$, $C(s)$

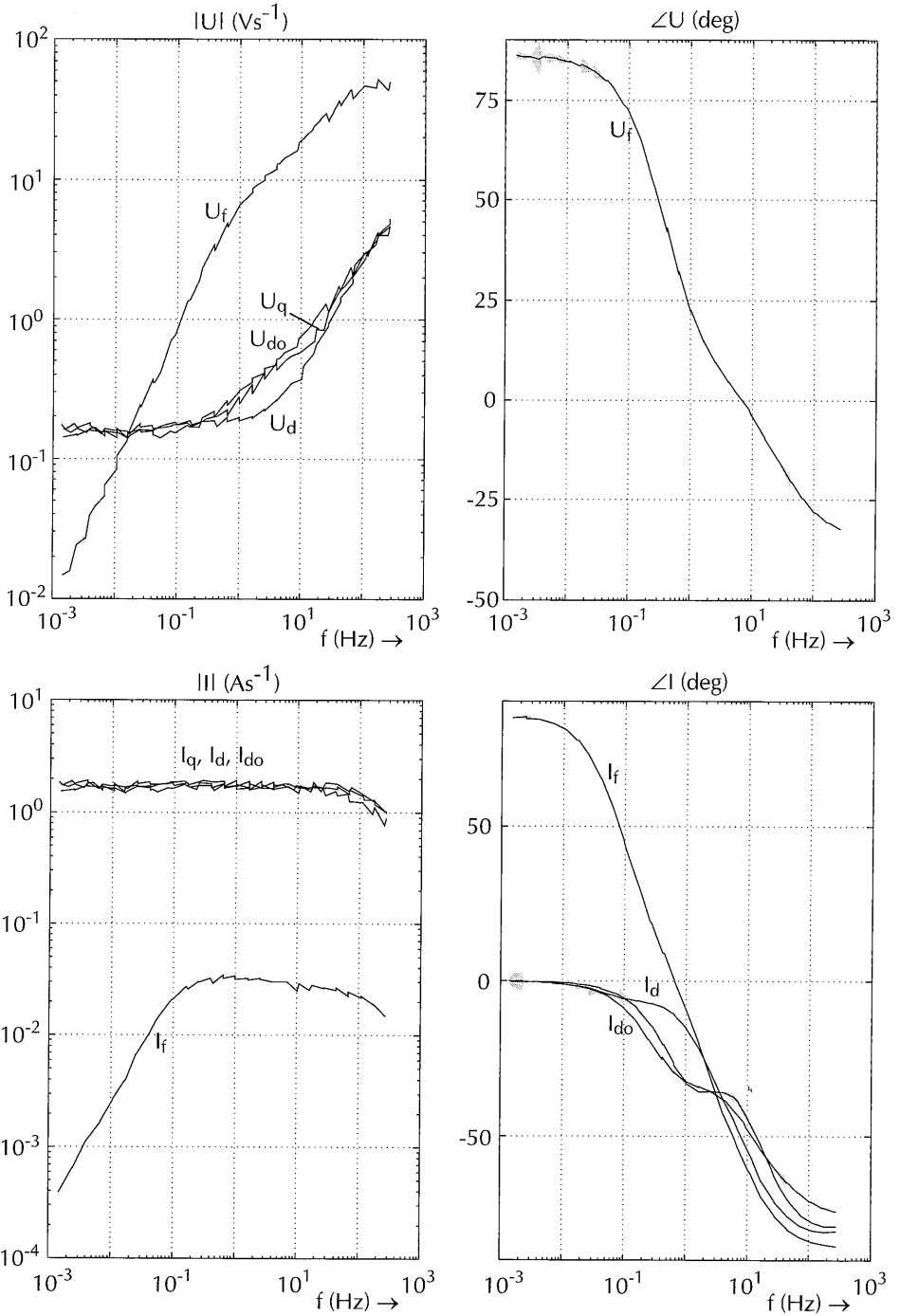
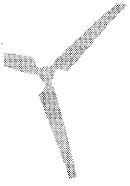


Figure 7.17a
 Frequency transforms of Heemaf SSFR signals and derived transfer functions: $U_d, U_q, U_{do}, U_f, I_d, I_q, I_{do}, I_f$

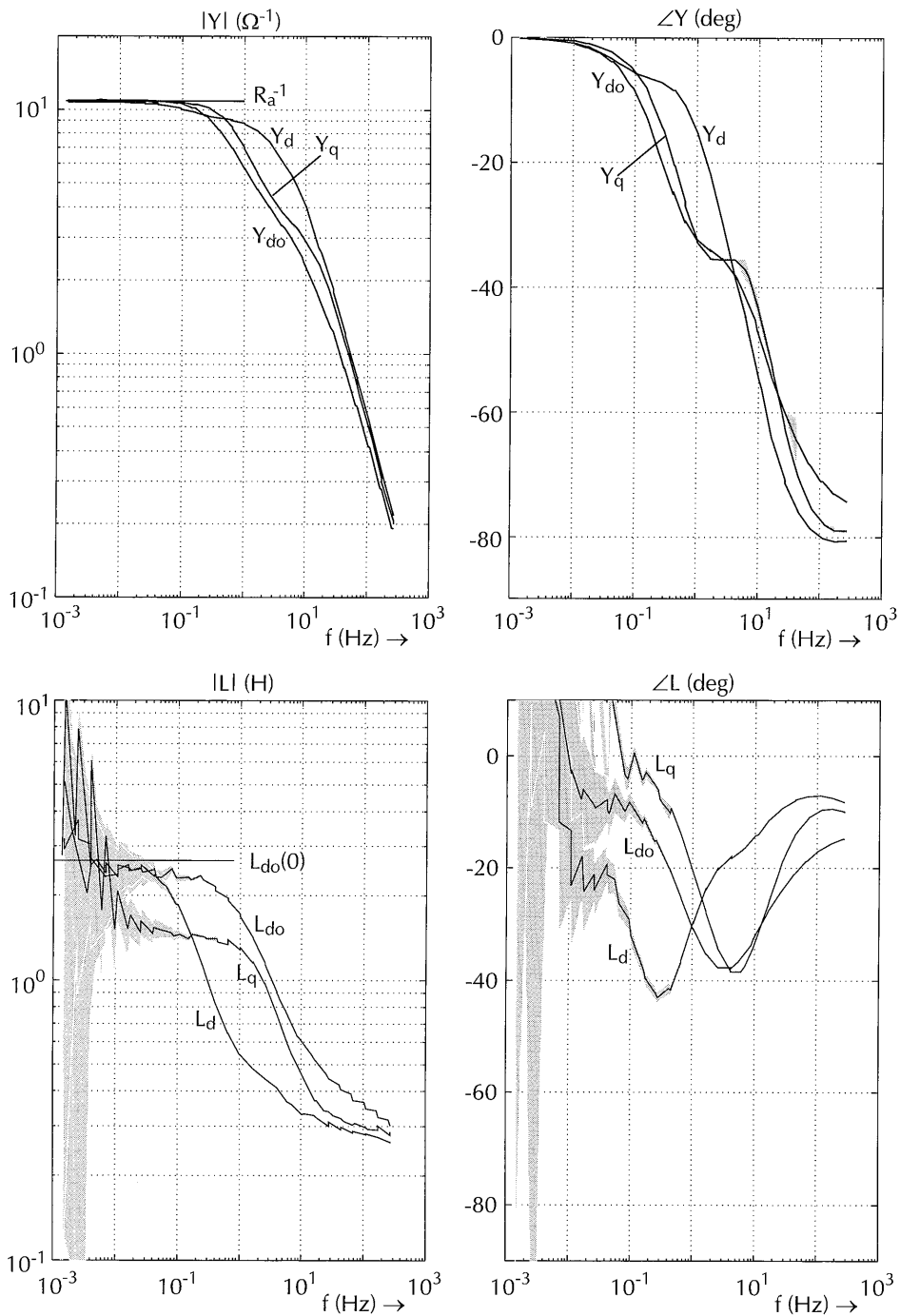


Figure 7.17b
 Frequency transforms of Heemaf SSFR signals and derived transfer functions: $Y_d(s)$, $Y_{do}(s)$, $Y_q(s)$, $L_d(s)$, $L_{do}(s)$, $L_q(s)$

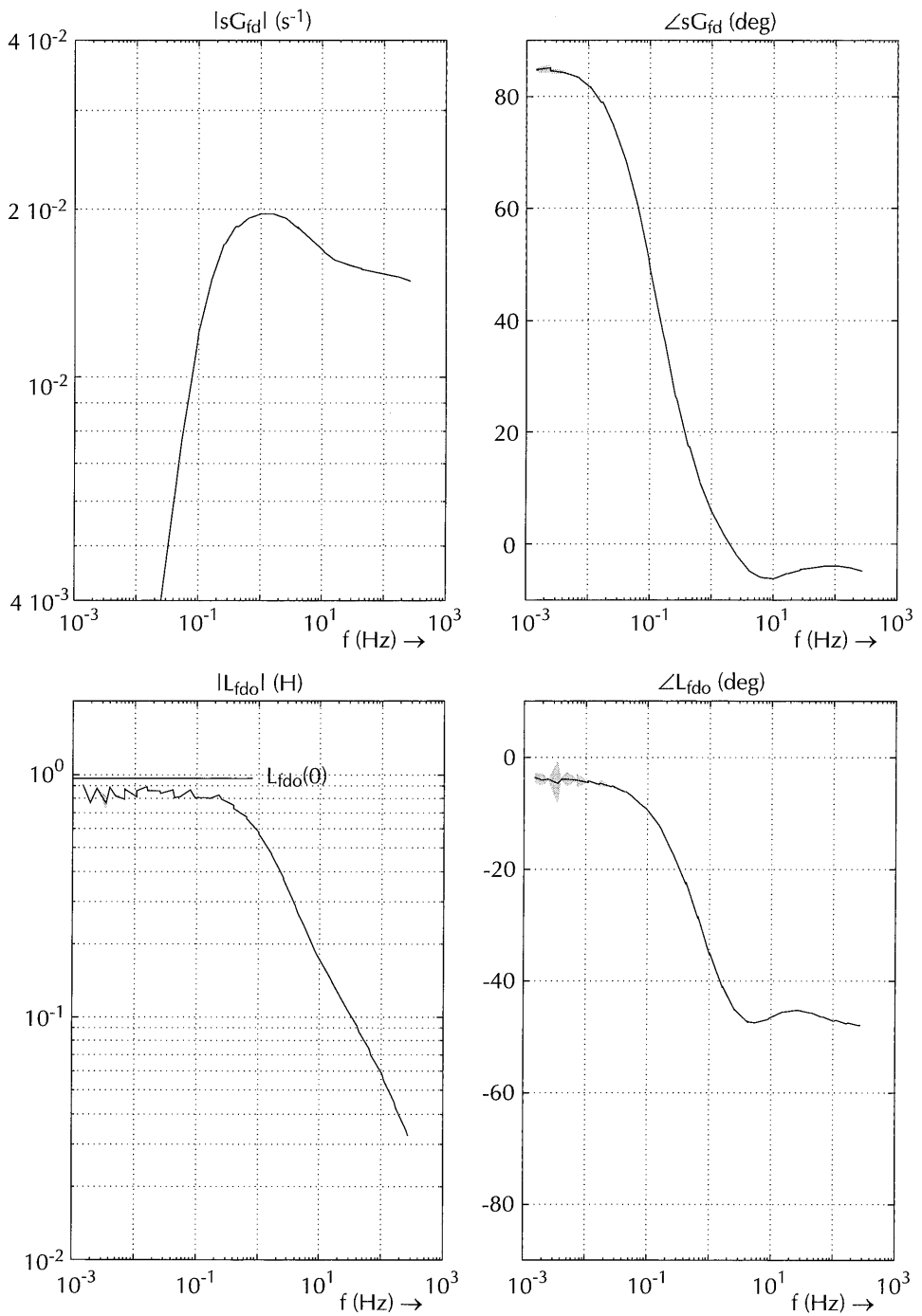
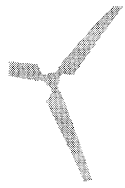


Figure 7.17c
Frequency transforms of Heemaf SSFR signals and derived transfer functions: $sG_{fd}(s)$, $L_{fdo}(s)$

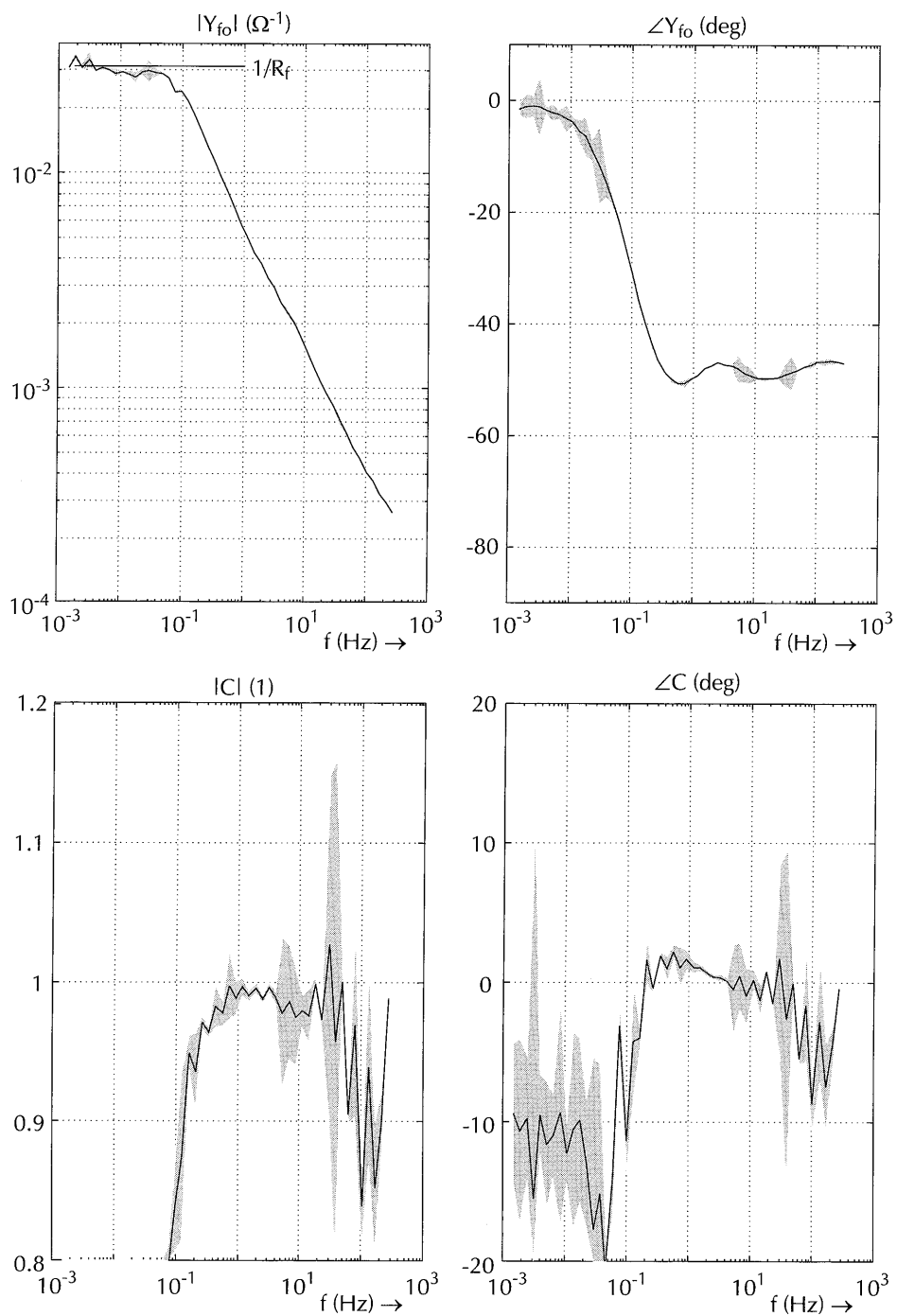


Figure 7.17d
 Frequency transforms of Heemaf SSFR signals and derived transfer functions: $Y_{fo}(s)$, $C(s)$

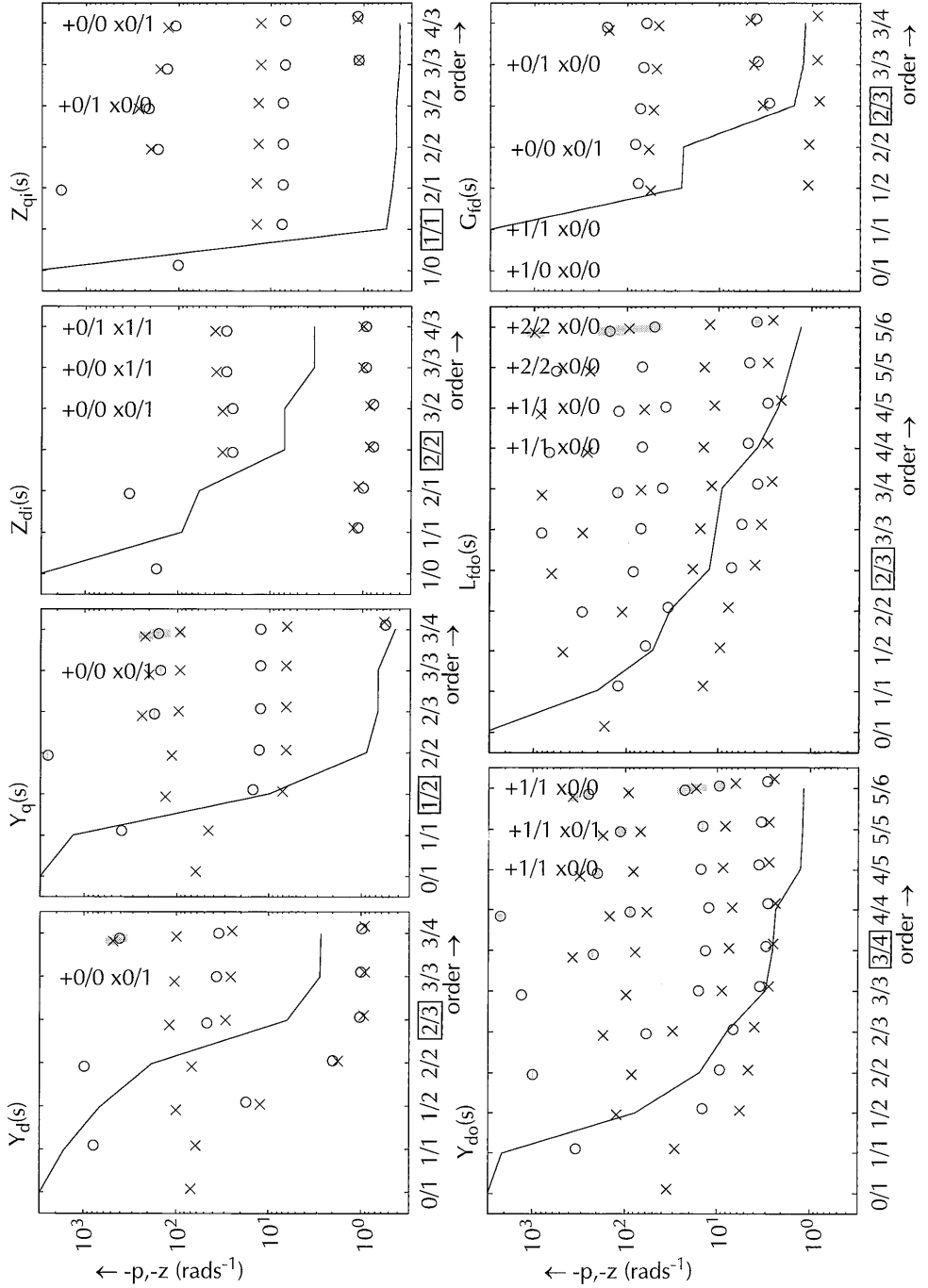
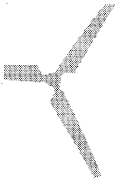


Figure 7.18a
Order-test results of the SSFR test for the Siemens machine

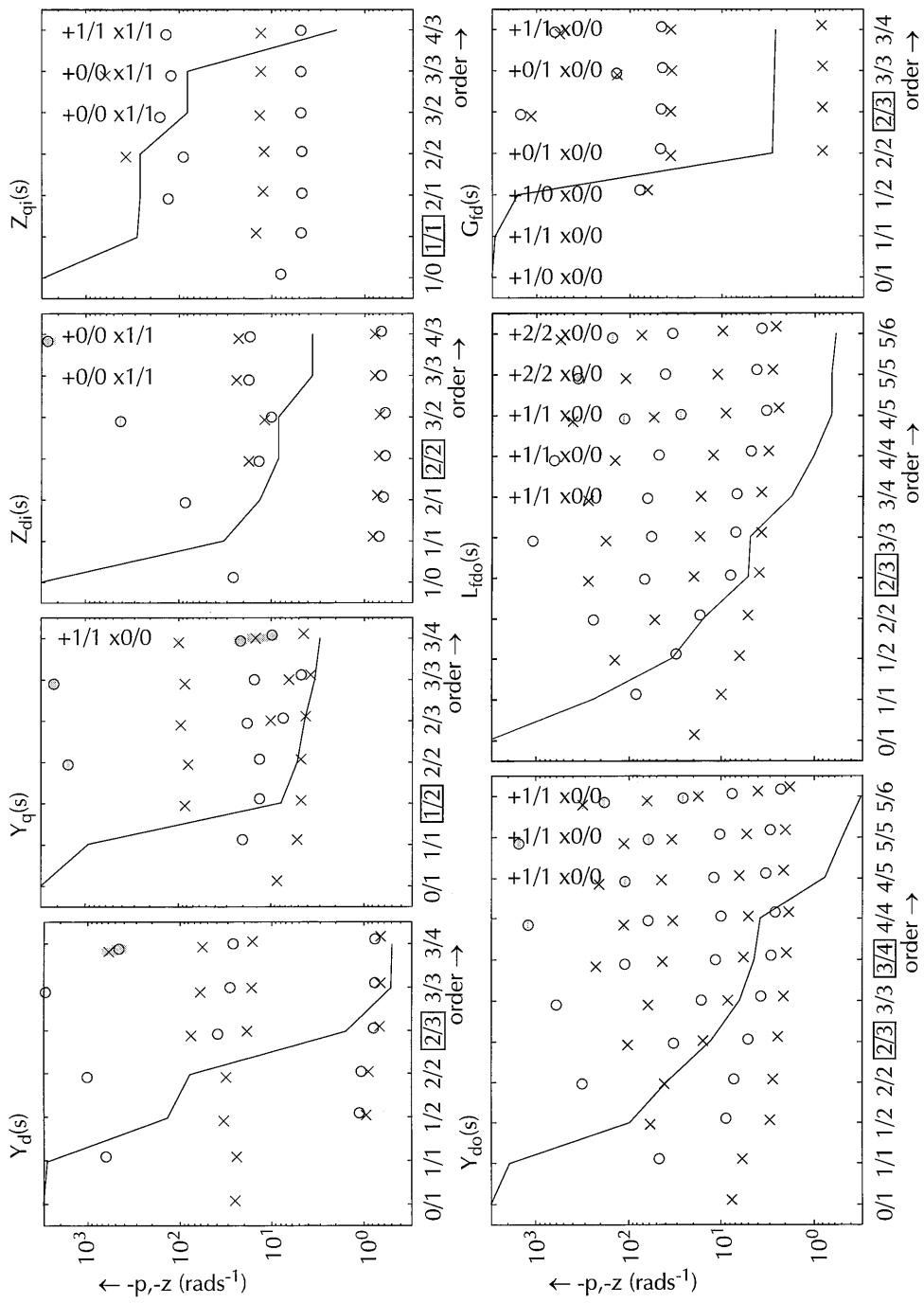
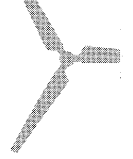


Figure 7.18b
Order-test results of the SSFR test for the Heemaf machine

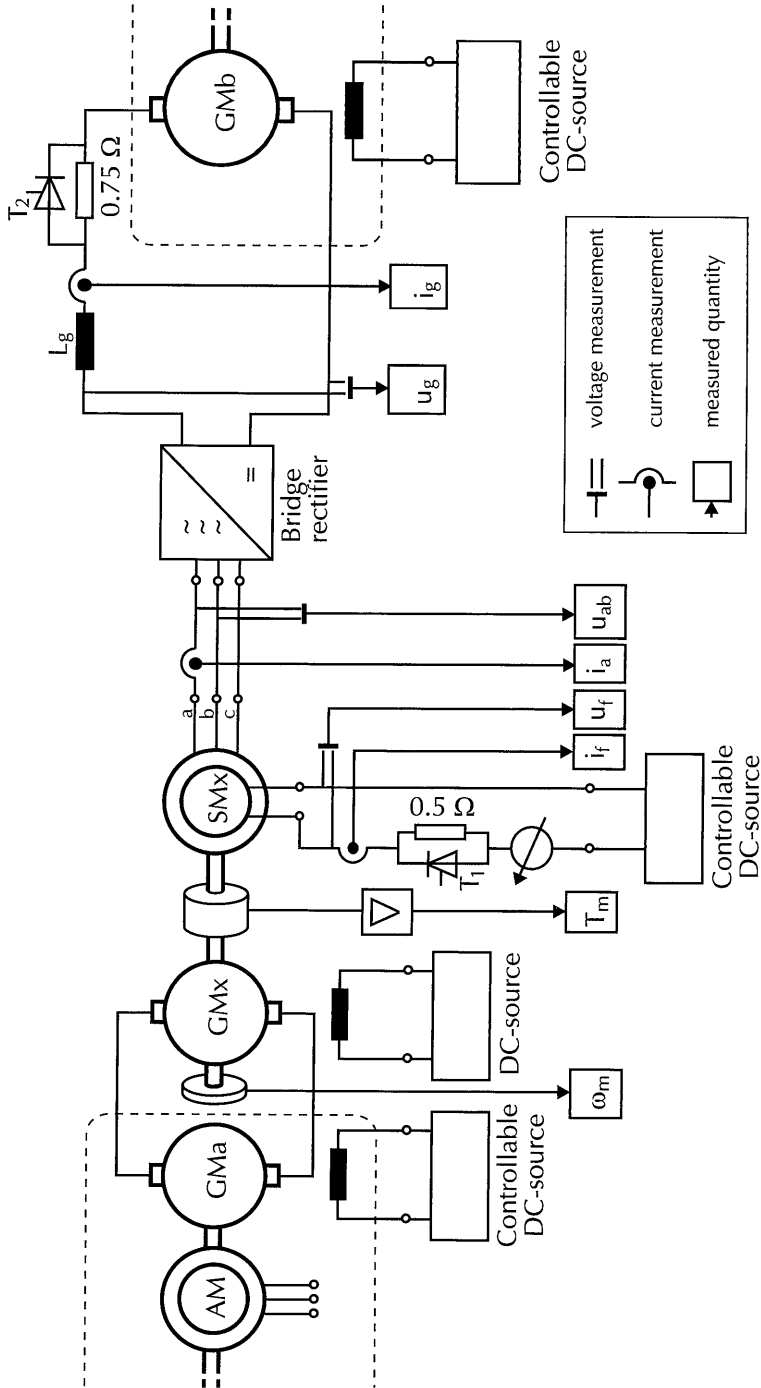
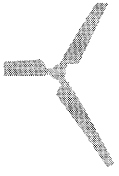


Figure 7.19
Synchronous machine with rectifier measurement set-up

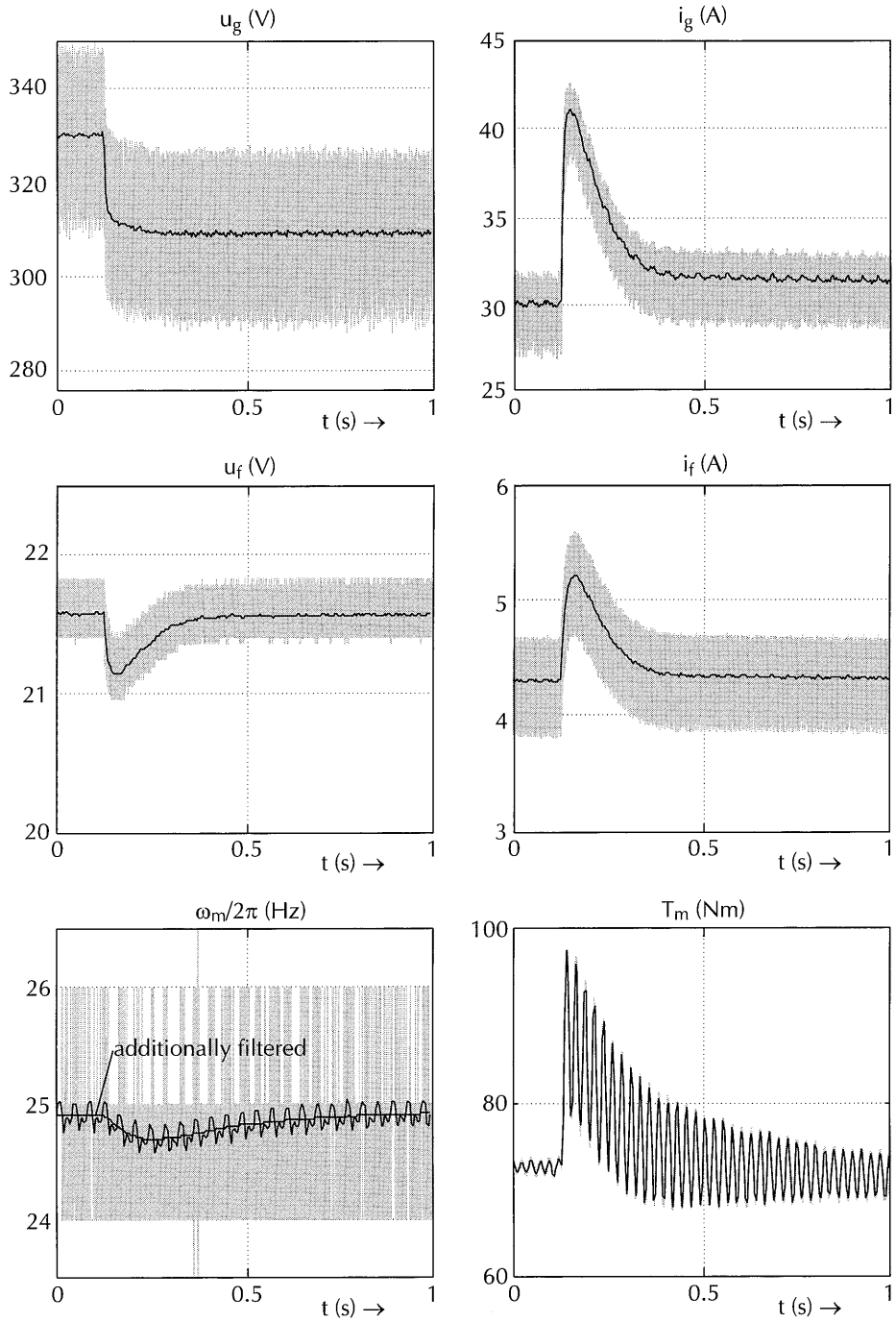


Figure 7.20a
 Dynamic measurement of the synchronous machine with rectifier,
 measurement RS12-g (time-domain signals)

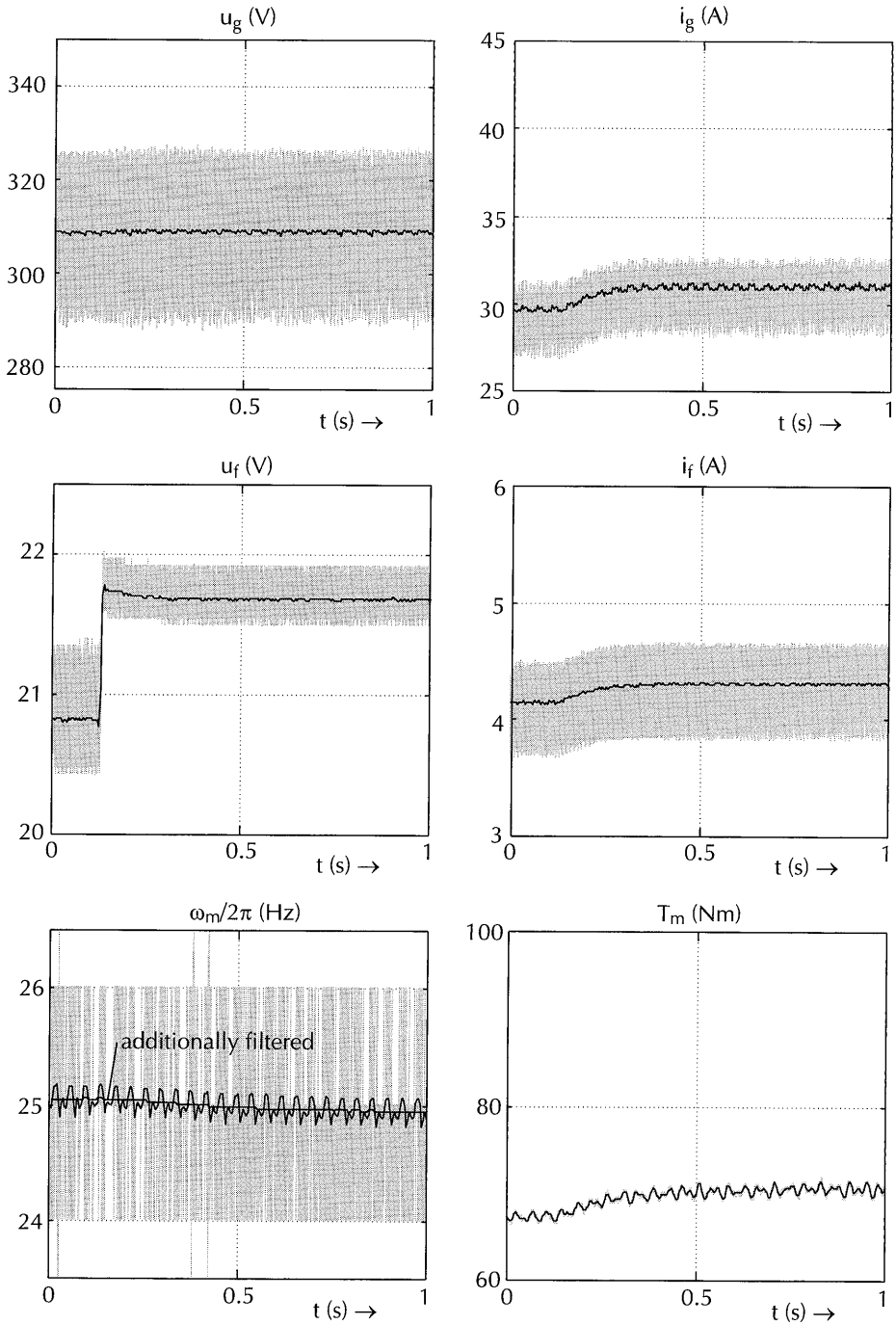
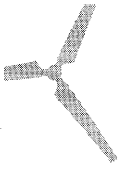


Figure 7.20b
Dynamic measurement of the synchronous machine with rectifier, measurement RS12-f (time-domain signals)

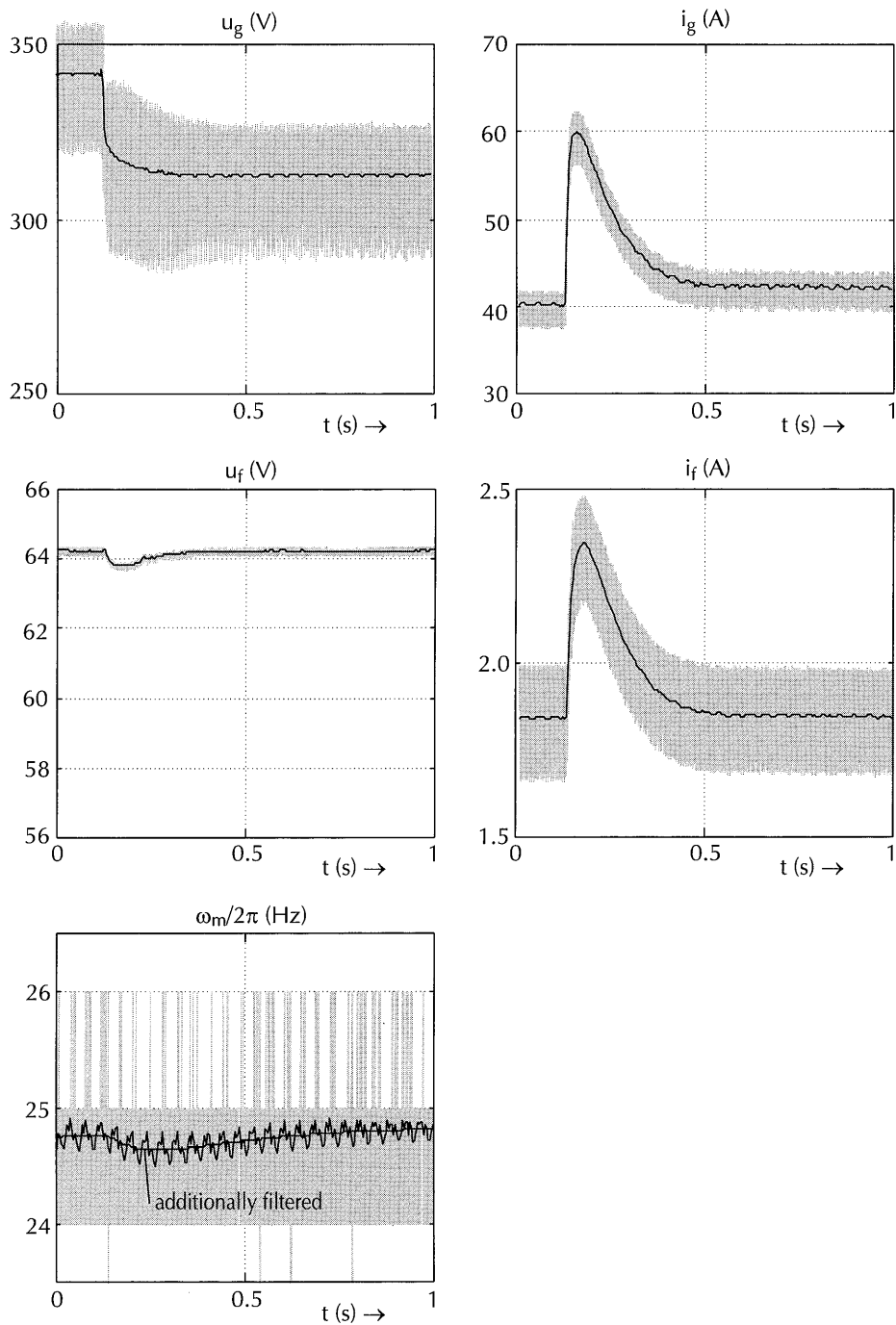
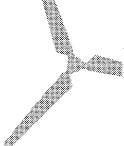


Figure 7.20c
Dynamic measurement of the synchronous machine with rectifier, measurement RH10-g (time-domain signals)

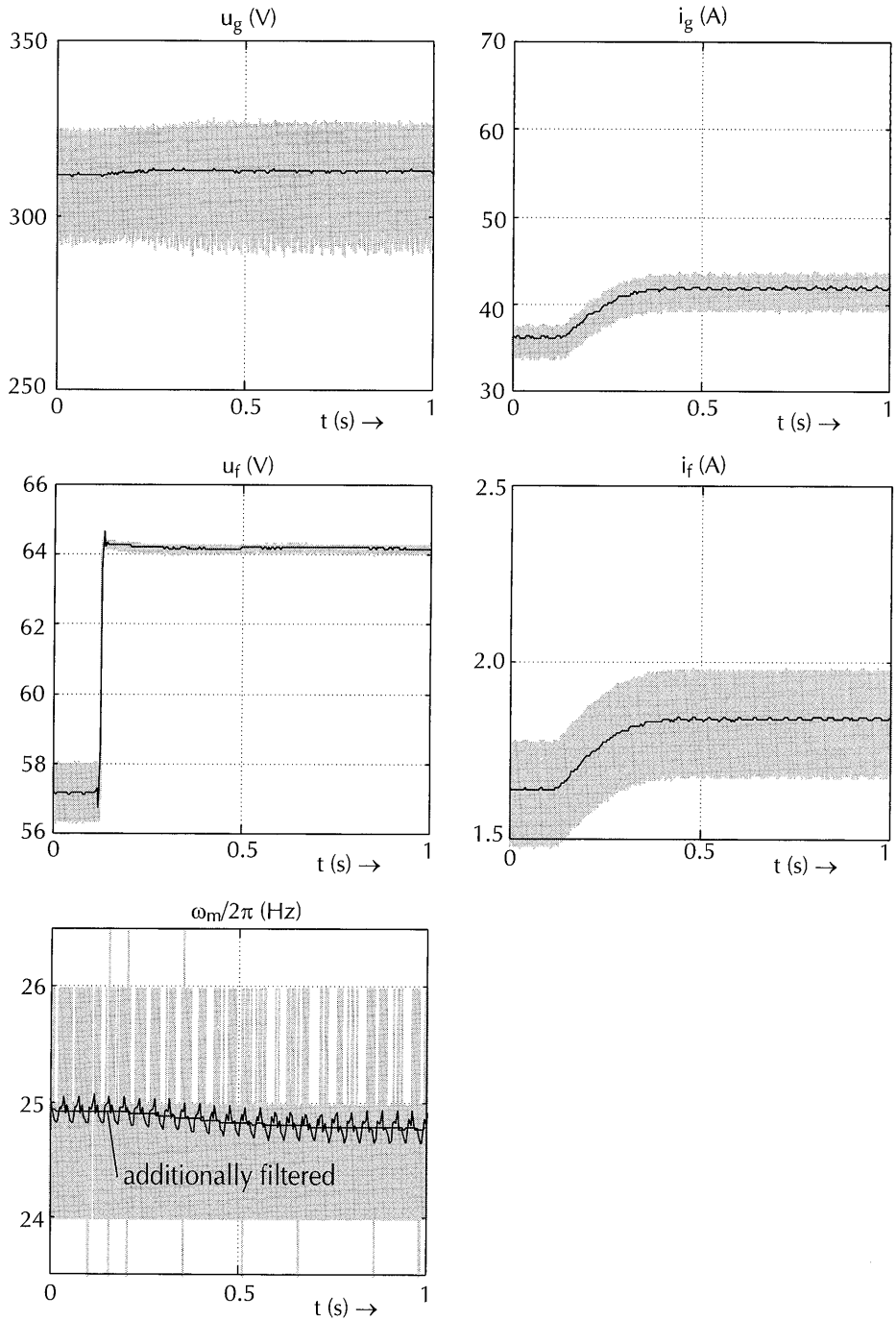
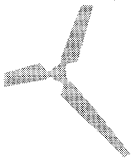


Figure 7.20d
Dynamic measurement of the synchronous machine with rectifier, measurement RH10-f (time-domain signals)

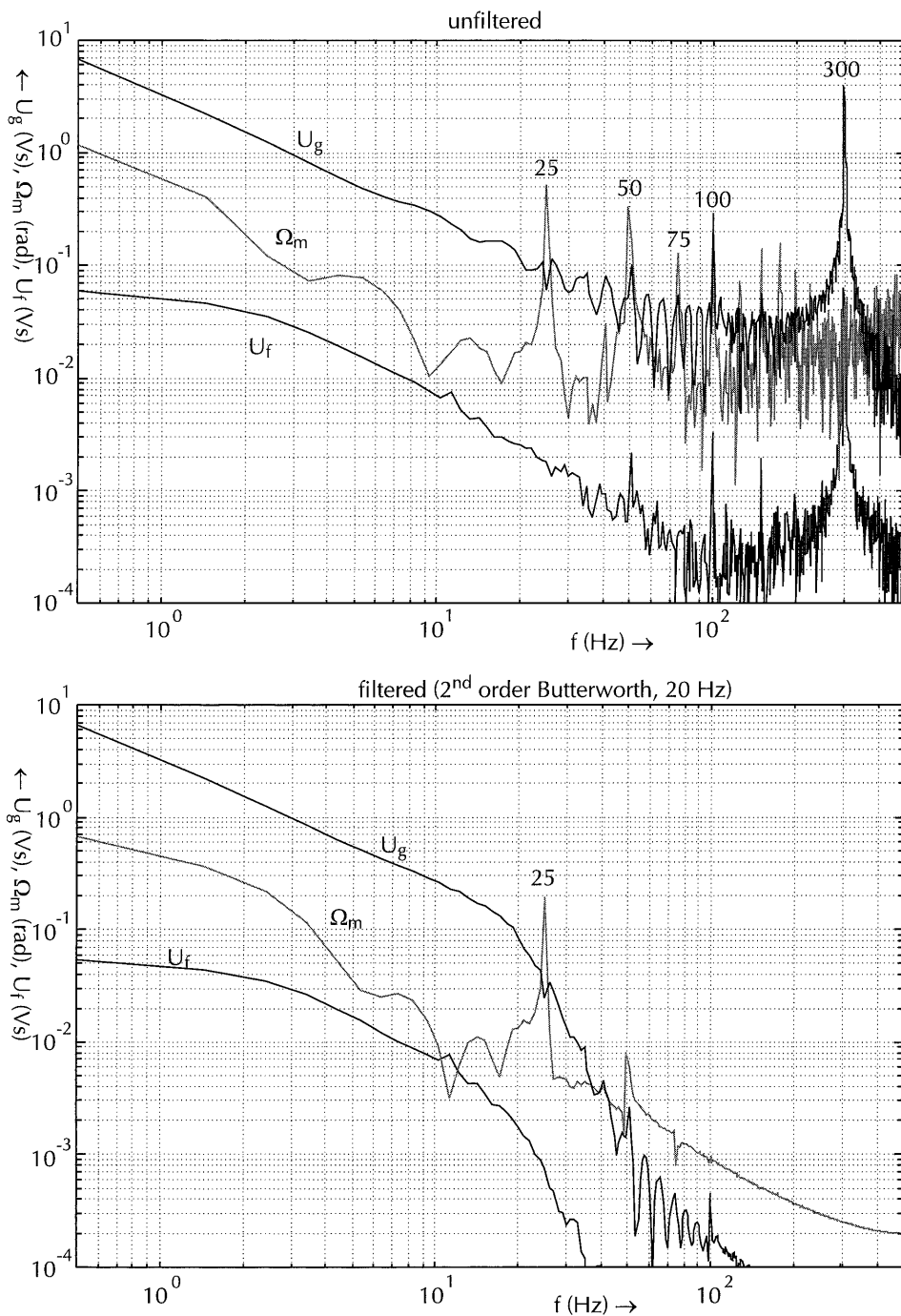


Figure 7.21a
Dynamic measurement of the synchronous machine with rectifier, measurement RS12-g (frequency-transformed signals)

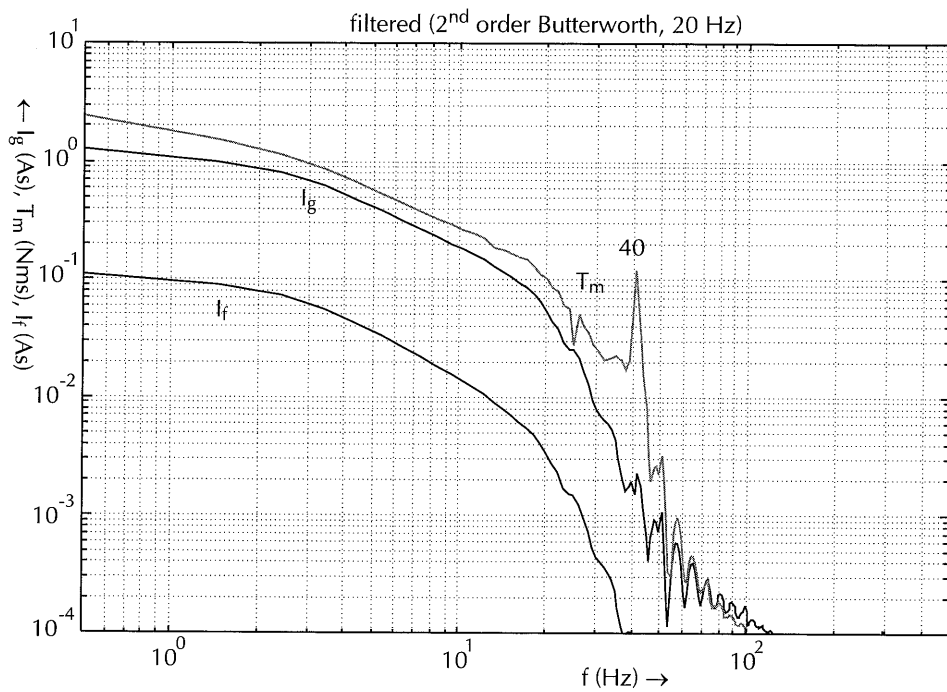
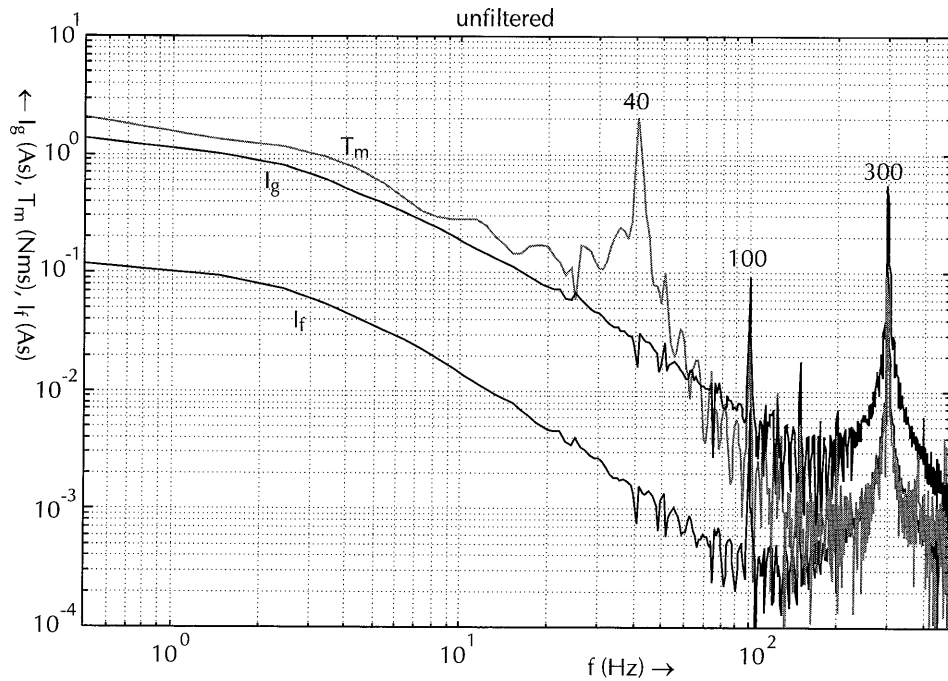
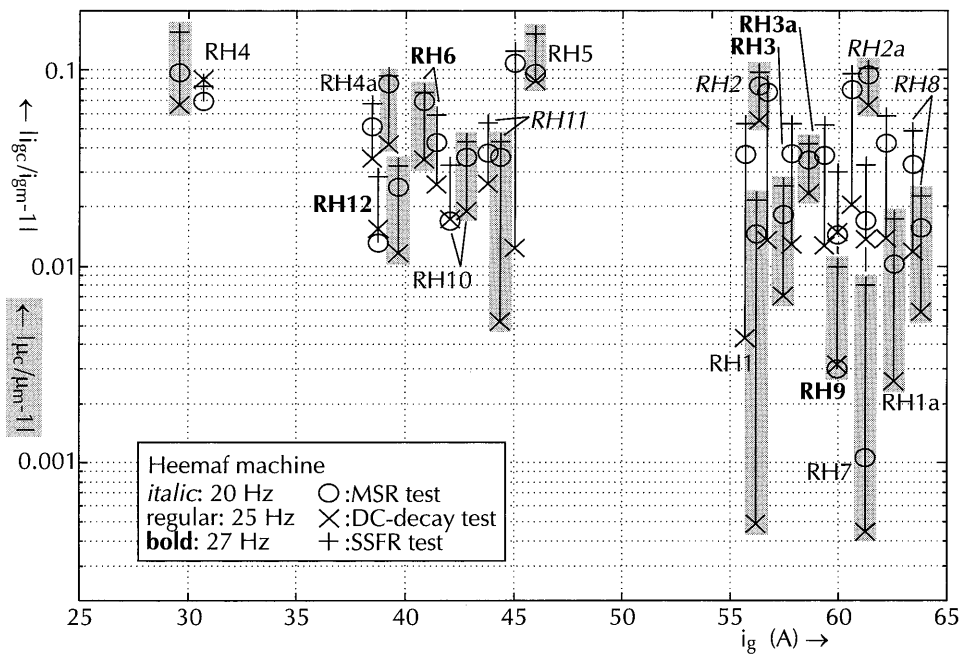
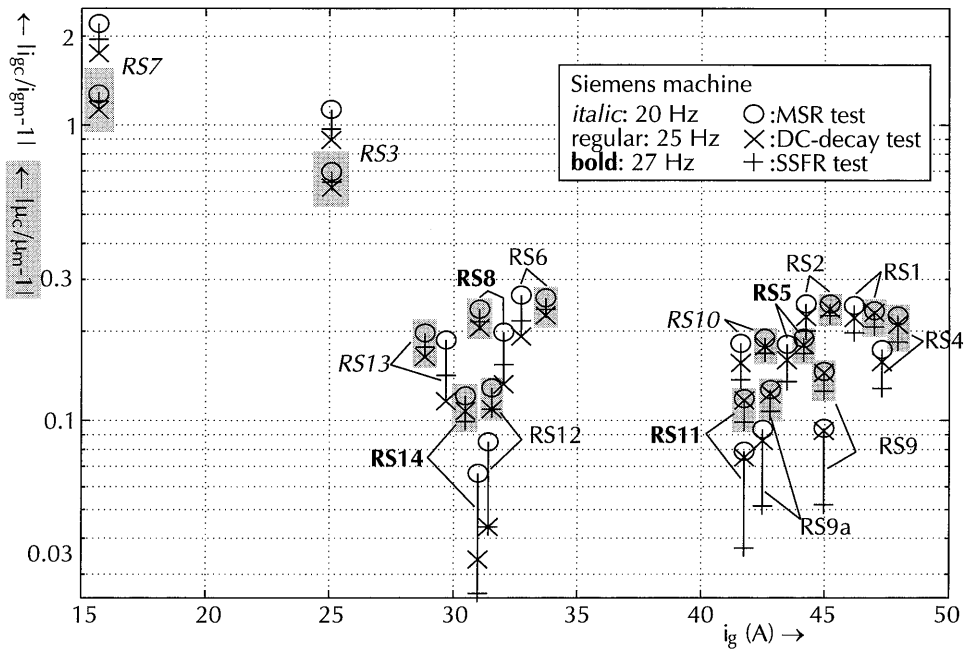


Figure 7.21b
Dynamic measurement of the synchronous machine with rectifier,



measurement RH10-g (frequency-transformed signals)

Figure 7.22
 Steady-state differences between measured (index *m*) and calculated (index *c*) DC-current i_g and angle of overlap μ ,
 as a function of the DC-current i_g for the Siemens machine and for the Heemaf machine

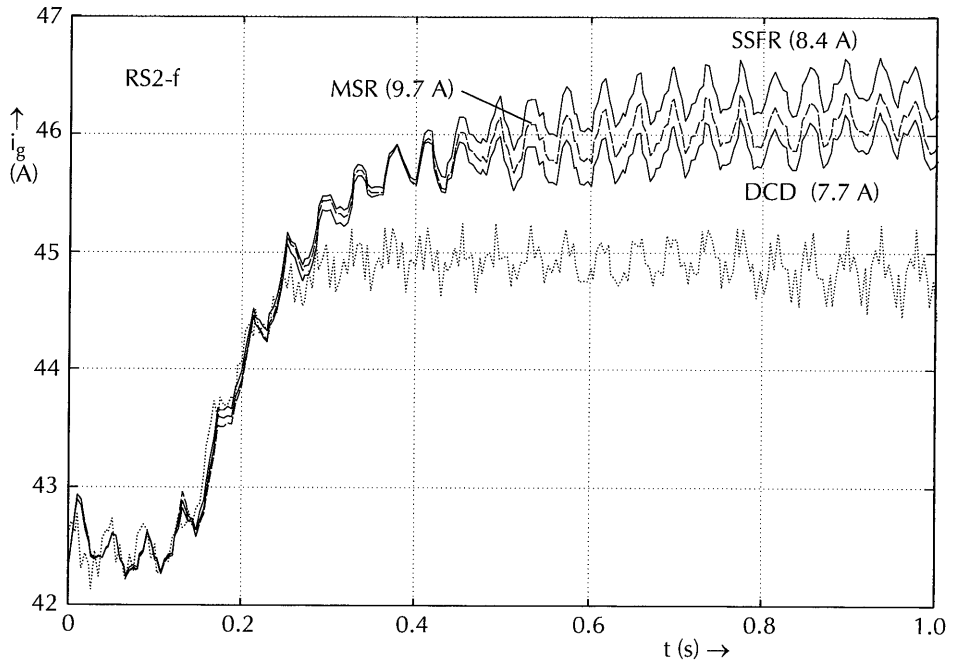
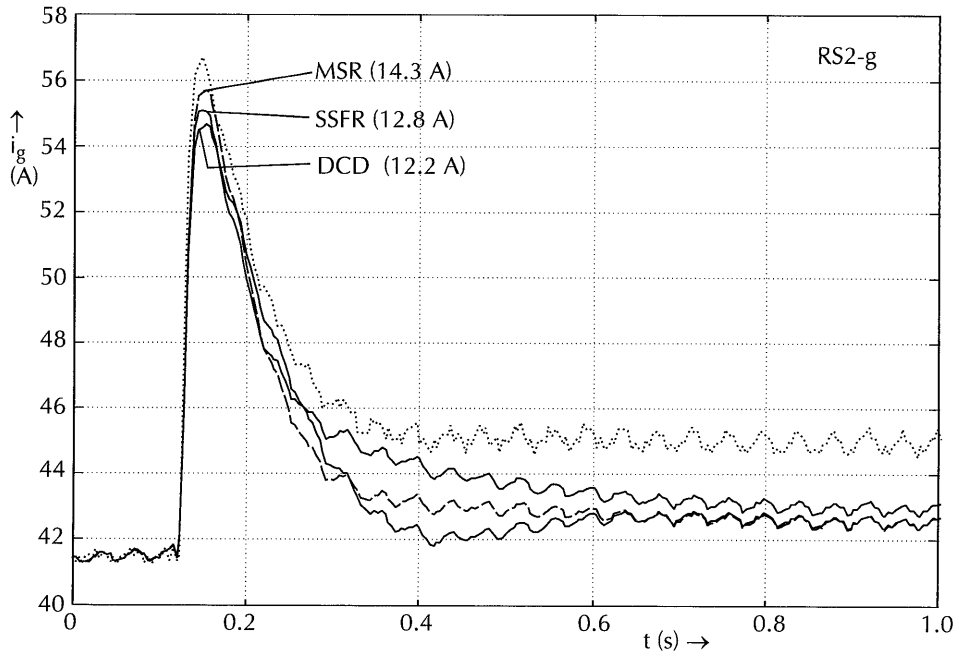
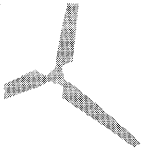


Figure 7.23a
Measured and simulated SM/R quantities
Siemens measurements RS2-g and -f: rectifier DC-current i_g

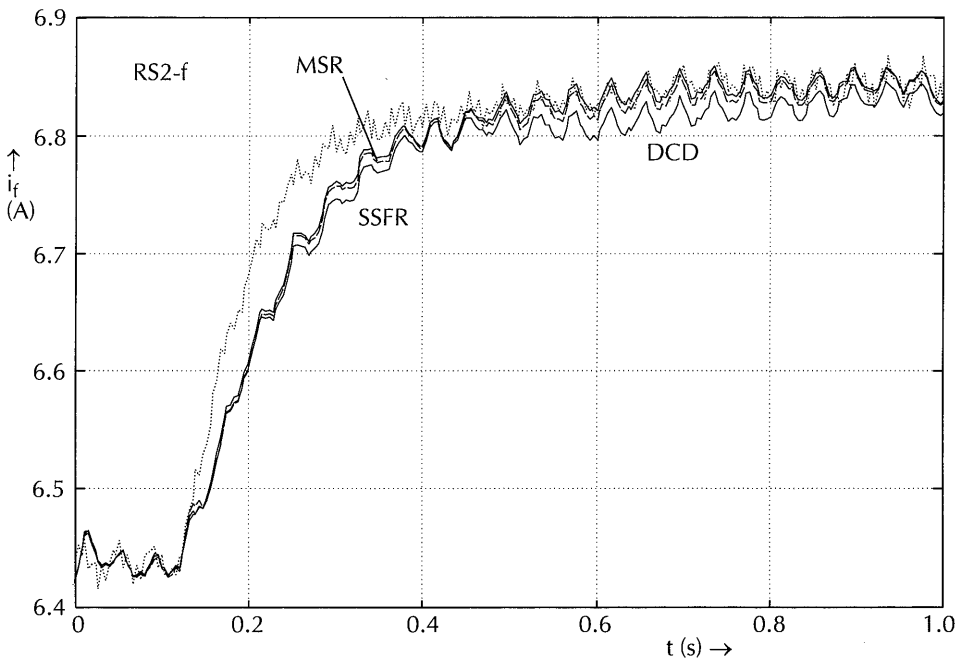
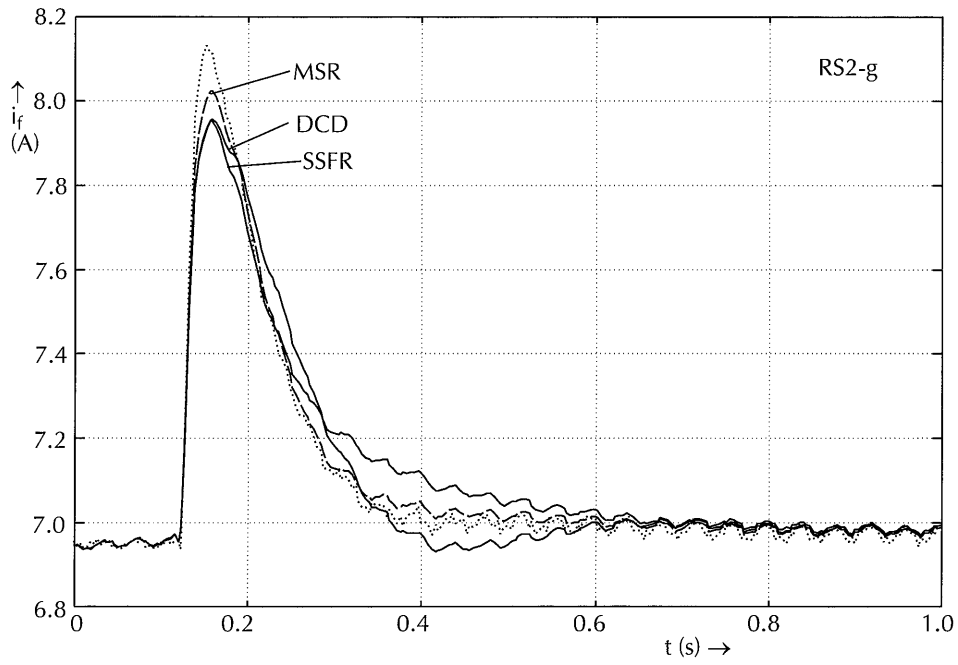
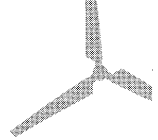


Figure 7.23b
Measured and simulated SM/R quantities
Siemens measurements RS2-g and -f: excitation-winding current i_f

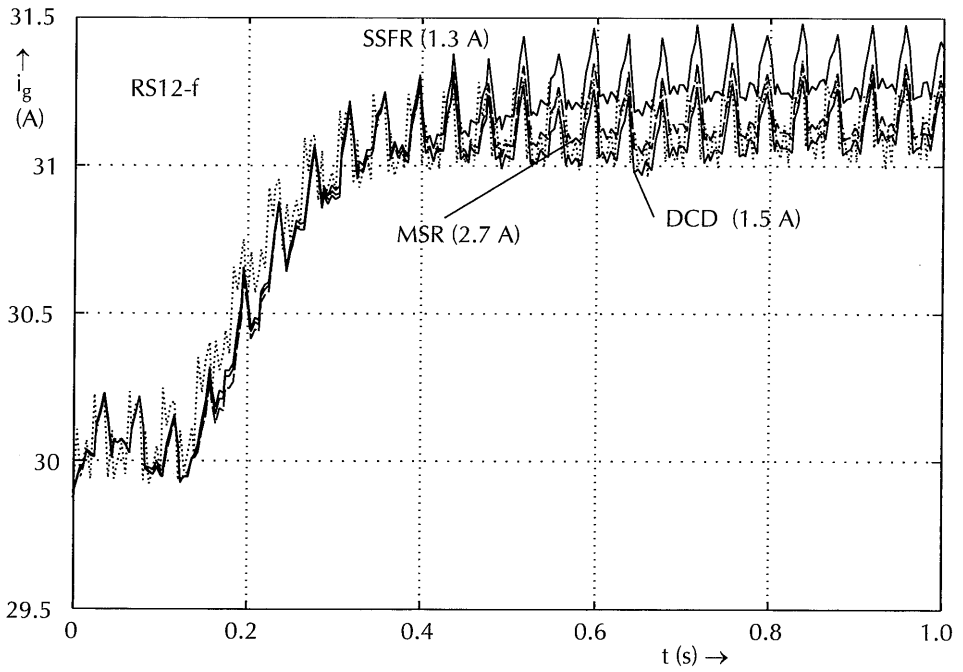
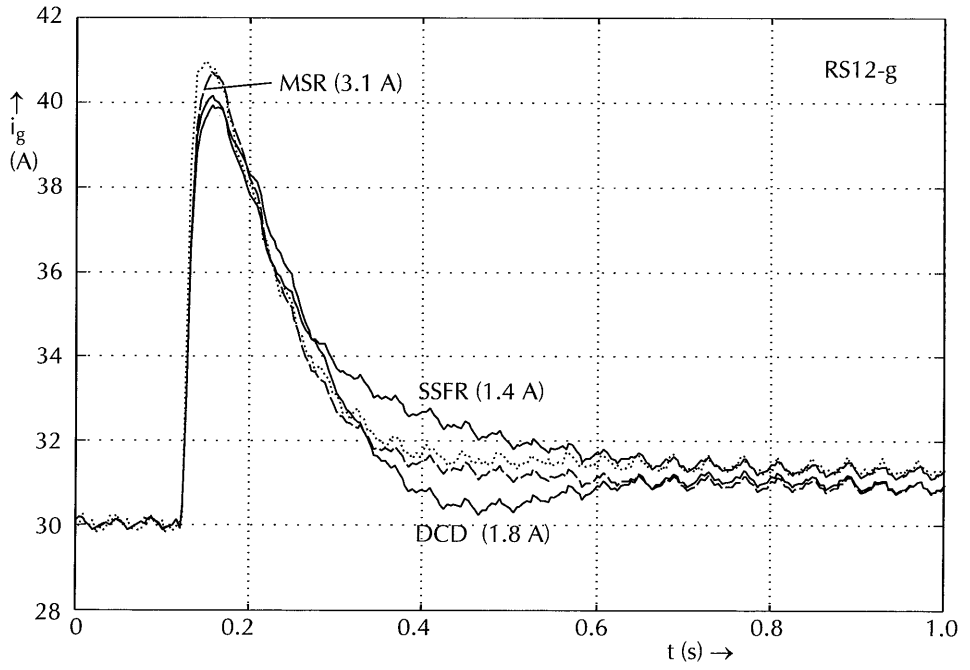
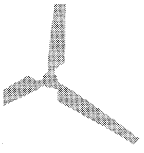


Figure 7.23c
Measured and simulated SM/R quantities
Siemens measurements RS12-g and -f: rectifier DC-current i_g

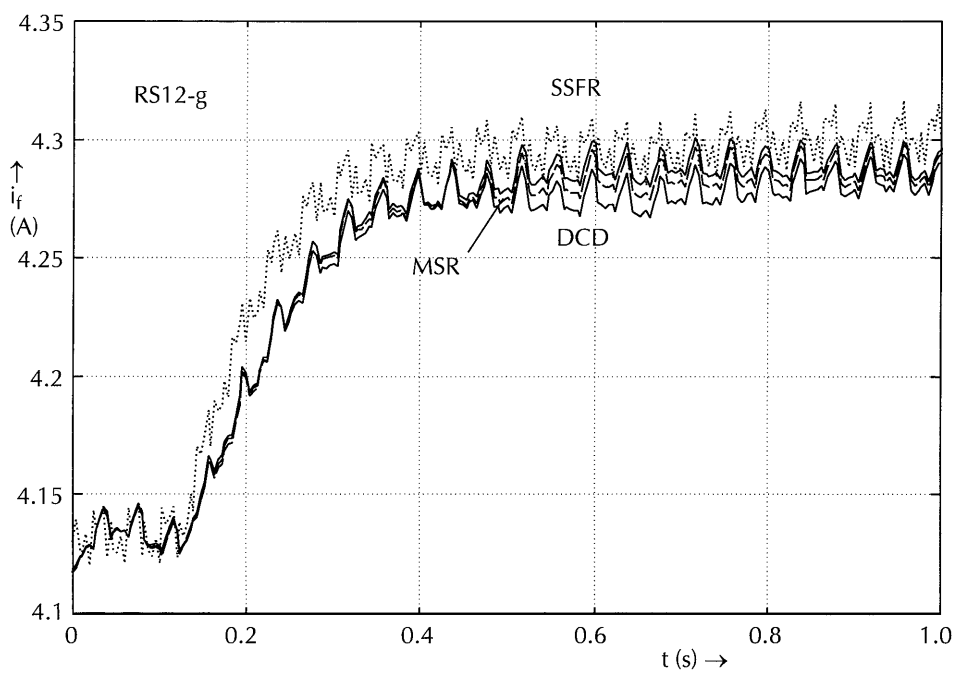
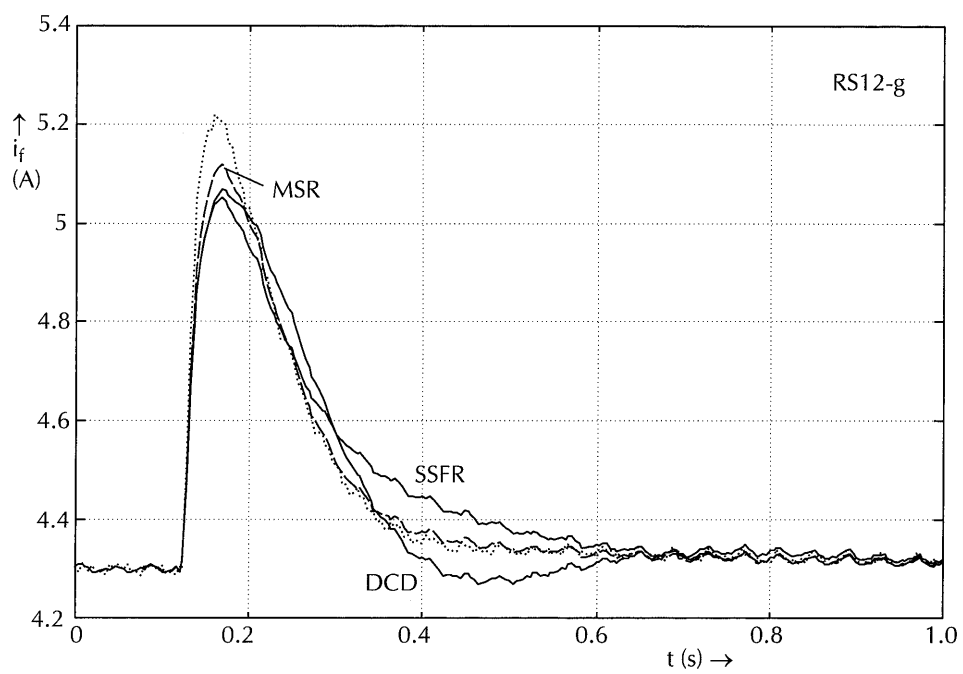
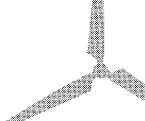


Figure 7.23d
Measured and simulated SM/R quantities
Siemens measurements RS12-g and -f: excitation-winding current i_f

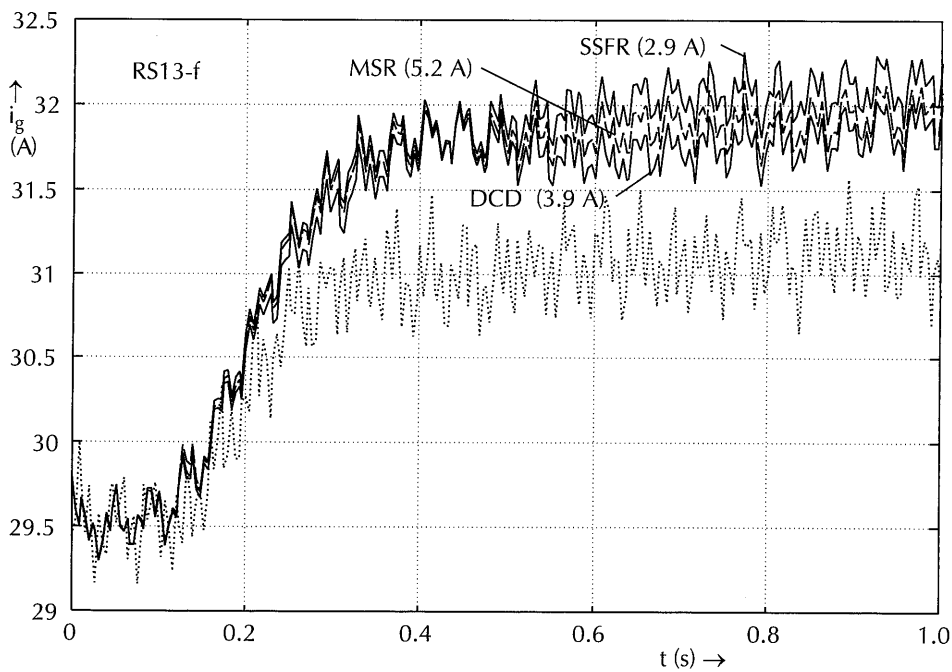
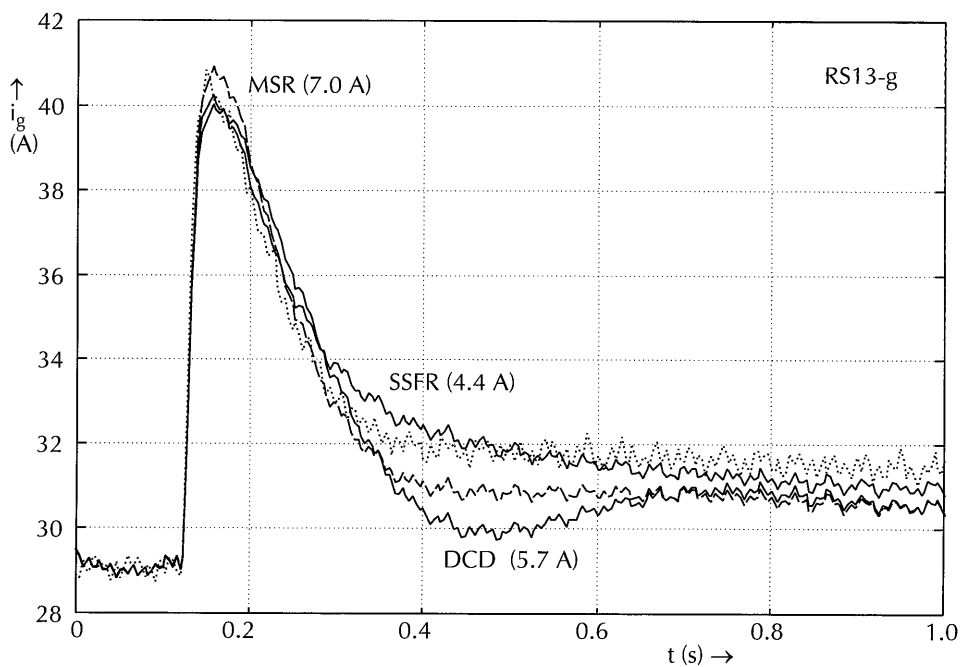
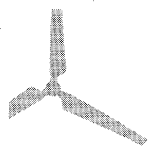


Figure 7.23e
Measured and simulated SM/R quantities
Siemens measurements RS13-g and -f: rectifier DC-current i_g

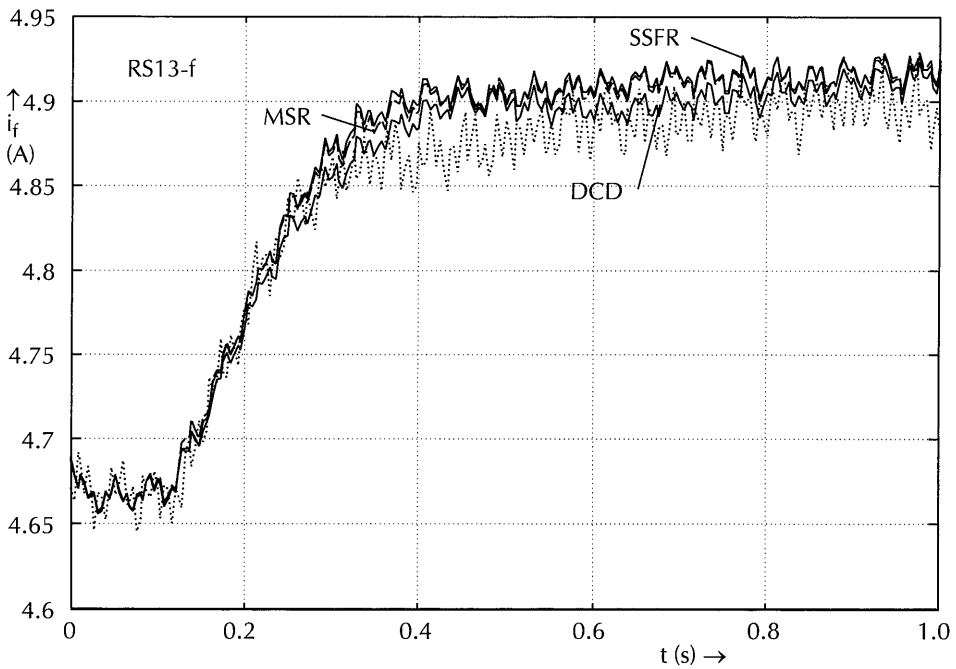
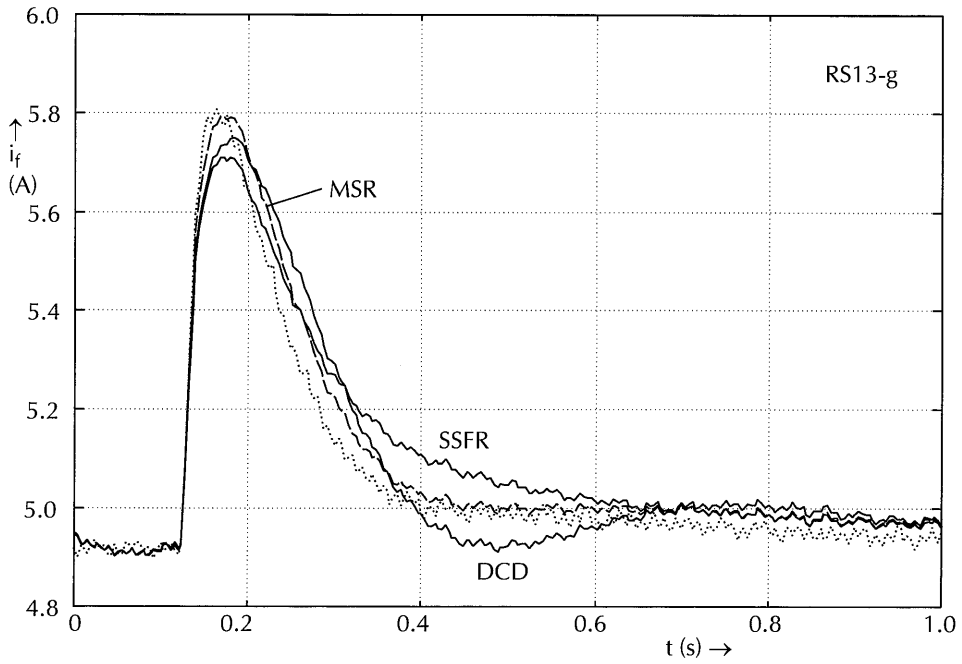
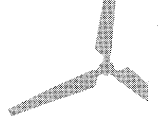


Figure 7.23f
Measured and simulated SM/R quantities
Siemens measurements RS13-g and -f: excitation-winding current i_f

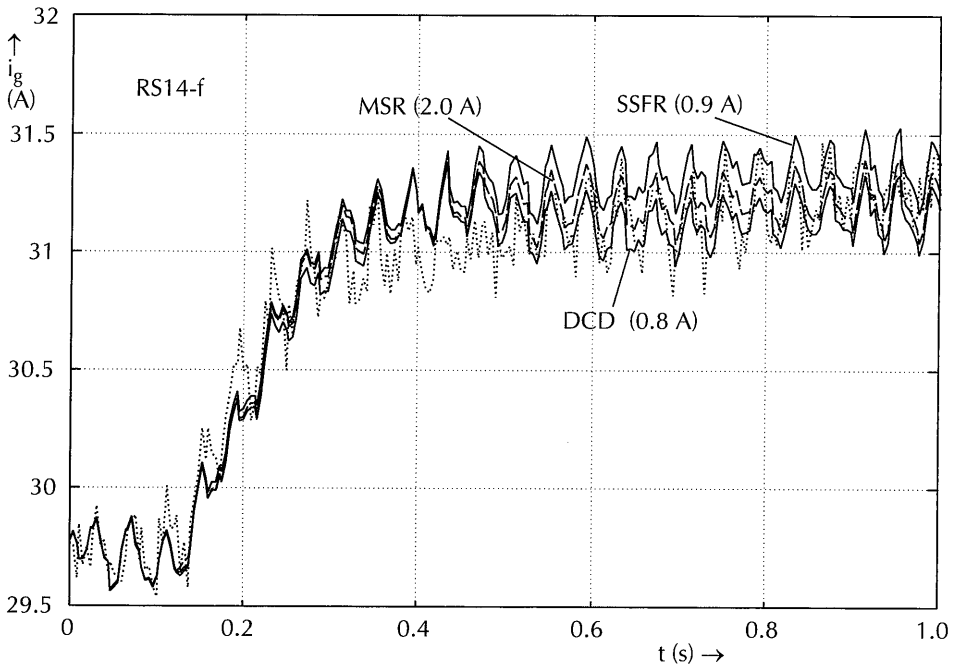
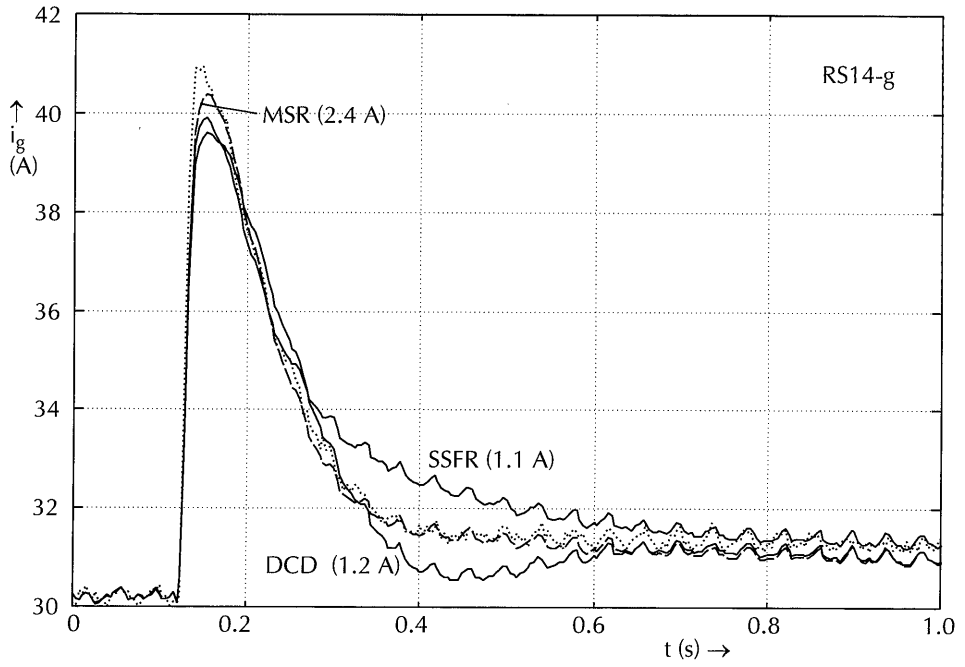
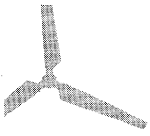


Figure 7.23g
Measured and simulated SM/R quantities
Siemens measurements RS14-g and -f: rectifier DC-current i_g

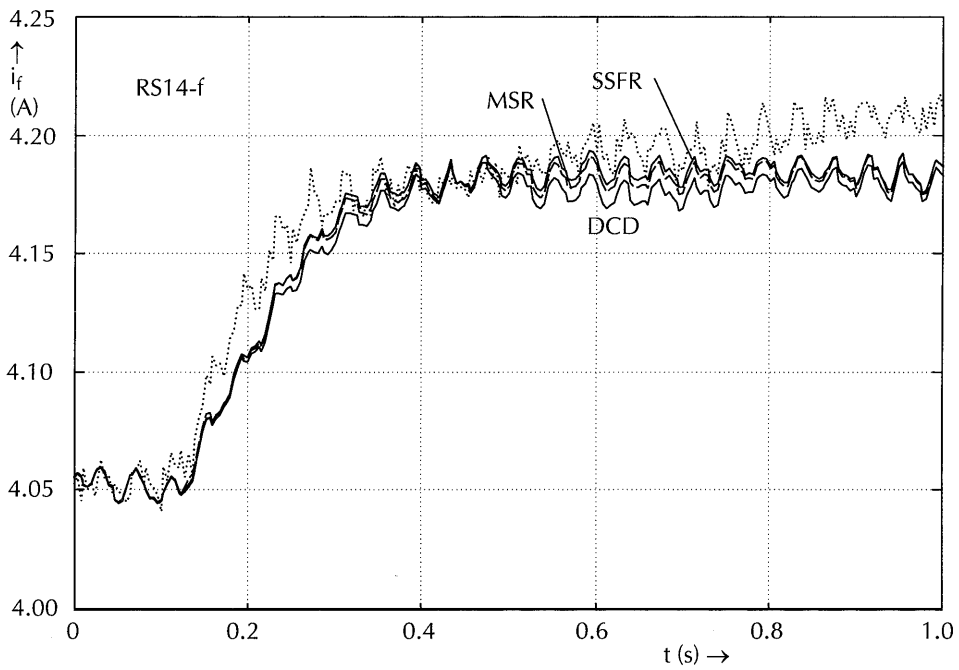
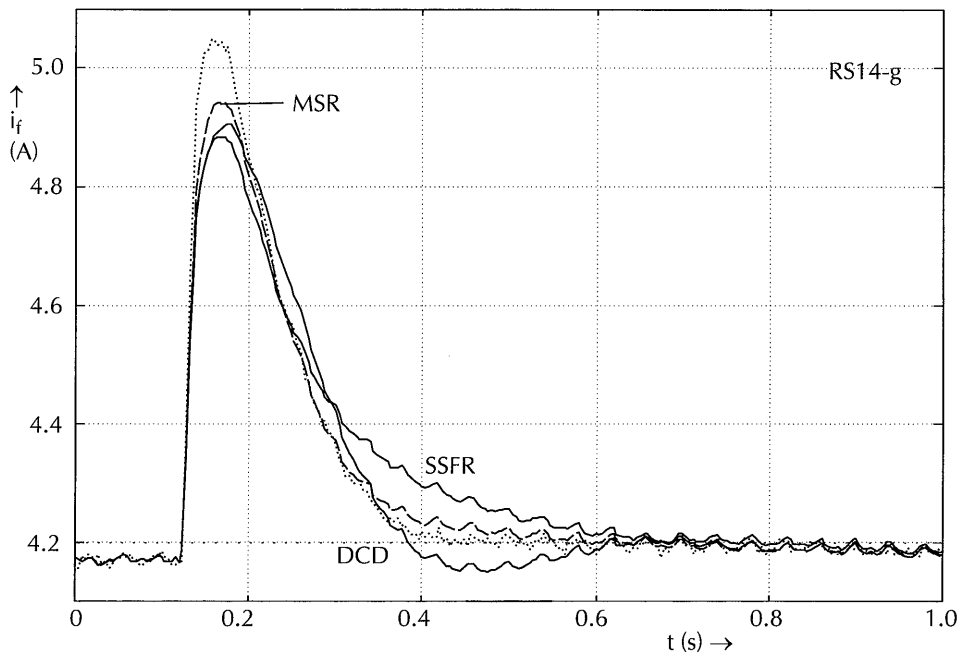
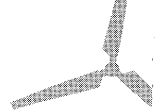


Figure 7.23h
Measured and simulated SM/R quantities
Siemens measurements RS14-g and -f: excitation-winding current i_f

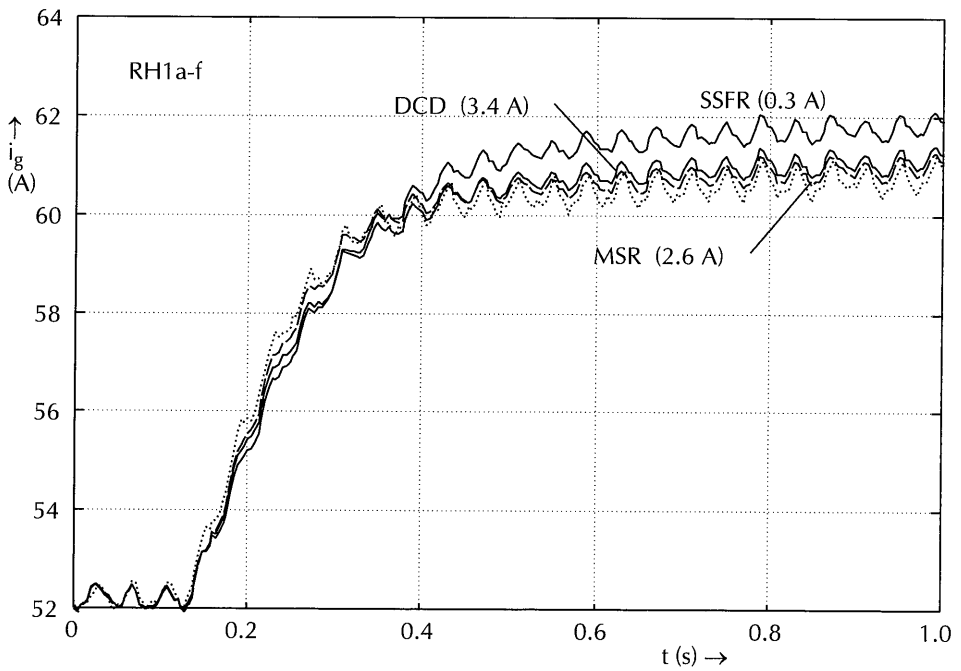
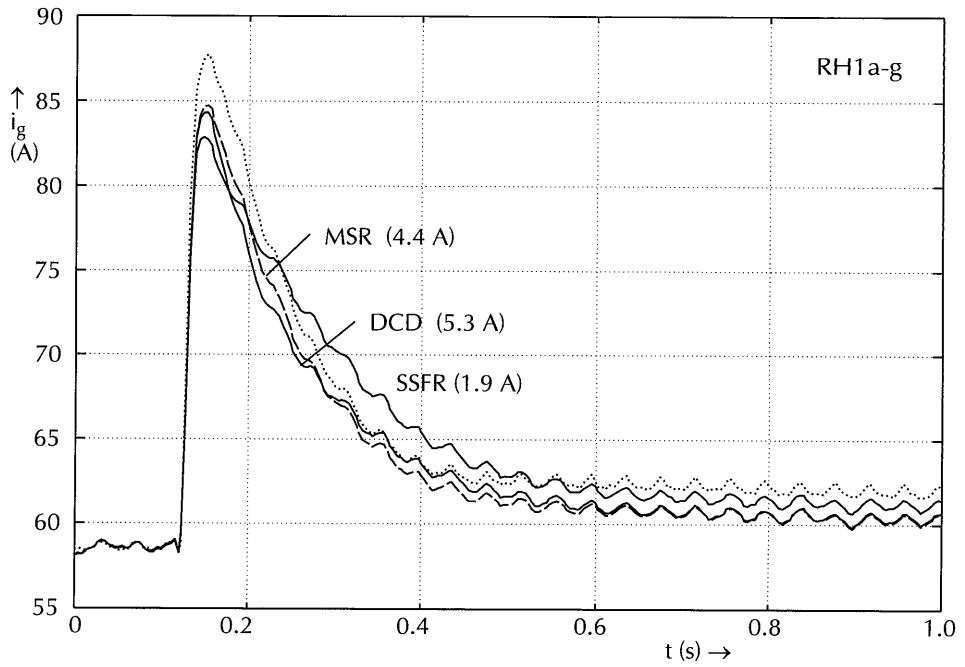
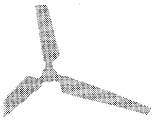


Figure 7.24a
Measured and simulated SM/R quantities
Heemaf measurements RH1a-g and -f: rectifier DC-current i_g

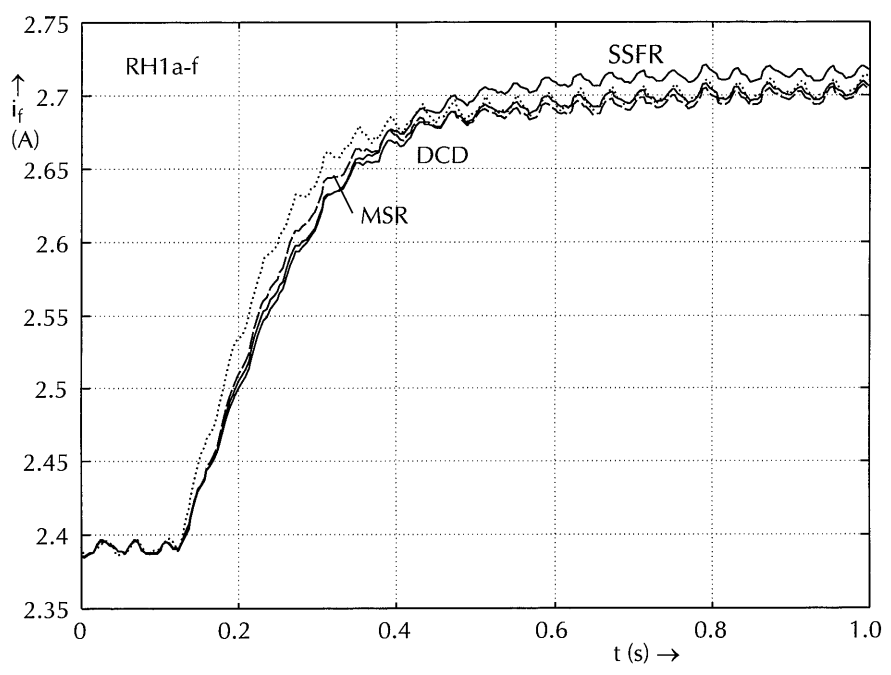
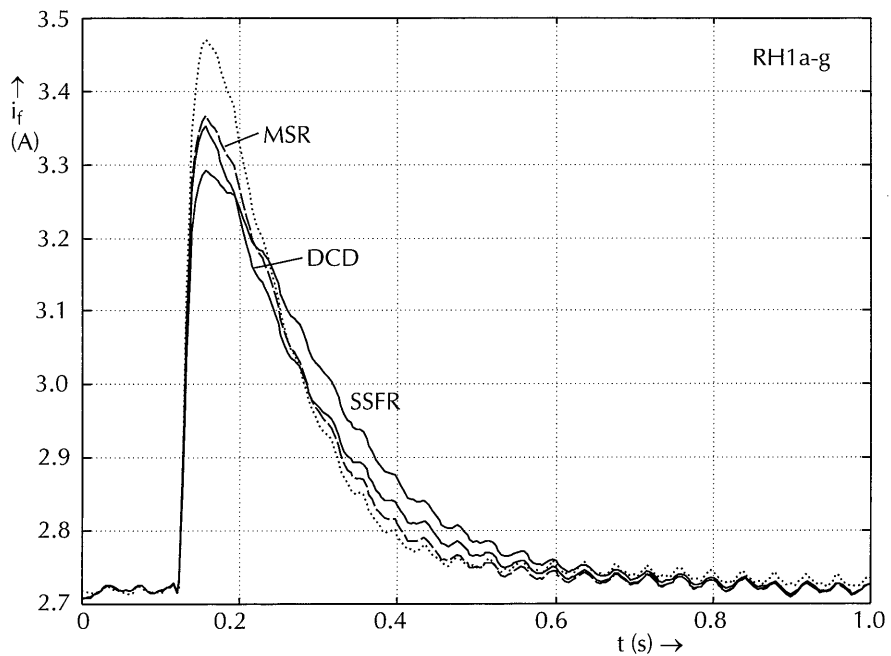
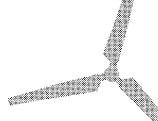


Figure 7.24b
Measured and simulated SM/R quantities
Heemaf measurements RH1a-g and -f: excitation-winding current i_f

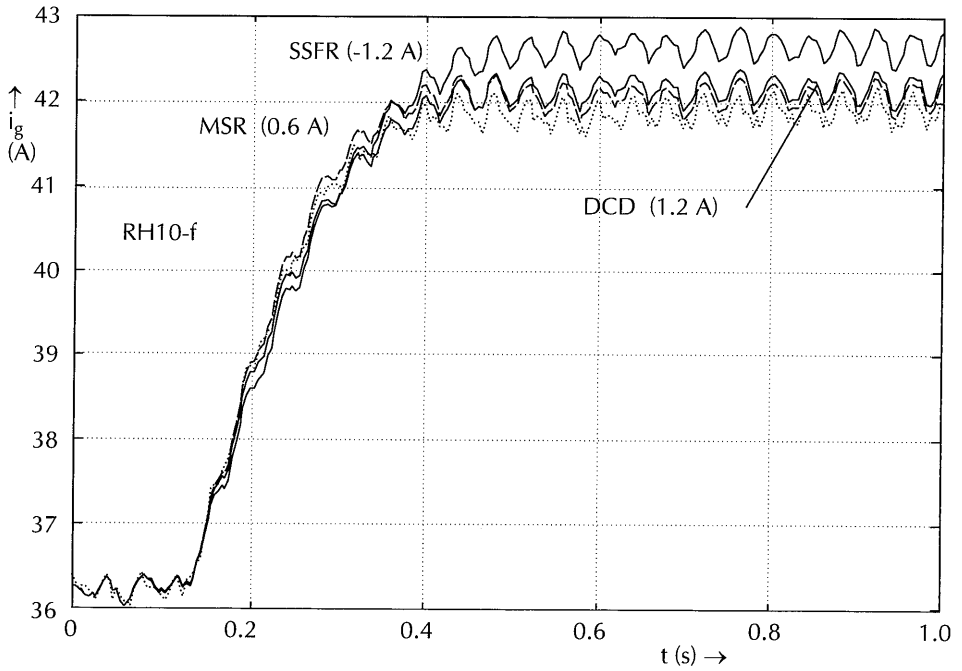
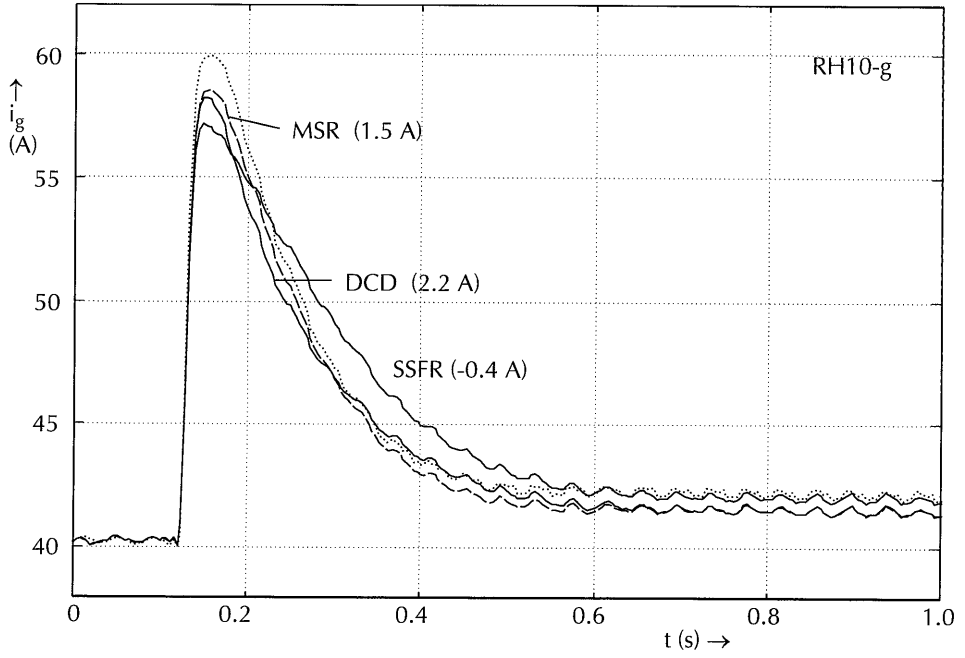
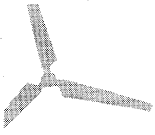


Figure 7.24c
Measured and simulated SM/R quantities
Heemaf measurements RH10-g and -f: rectifier DC-current i_g

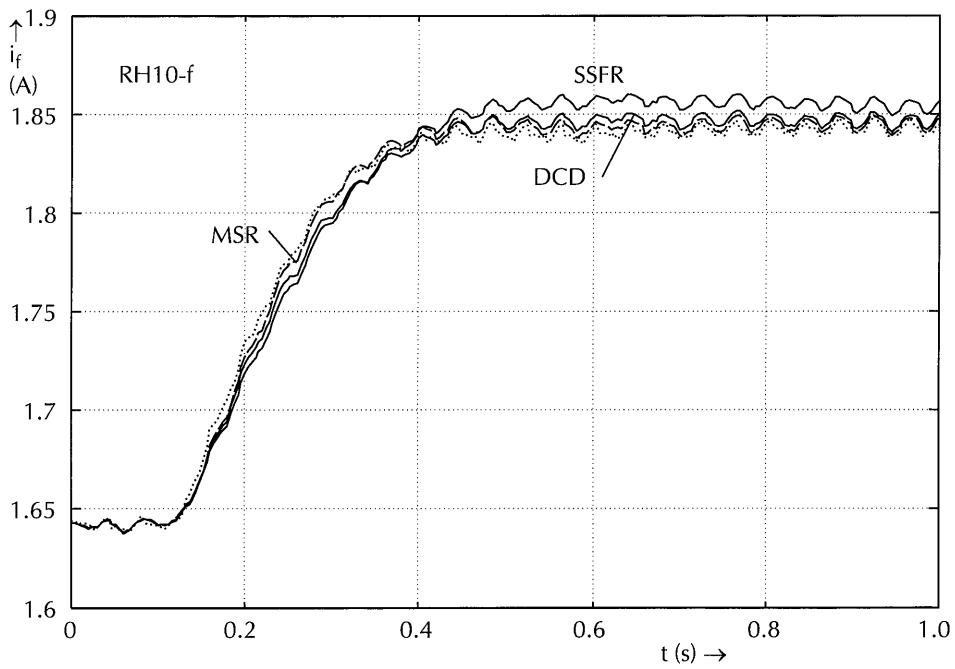
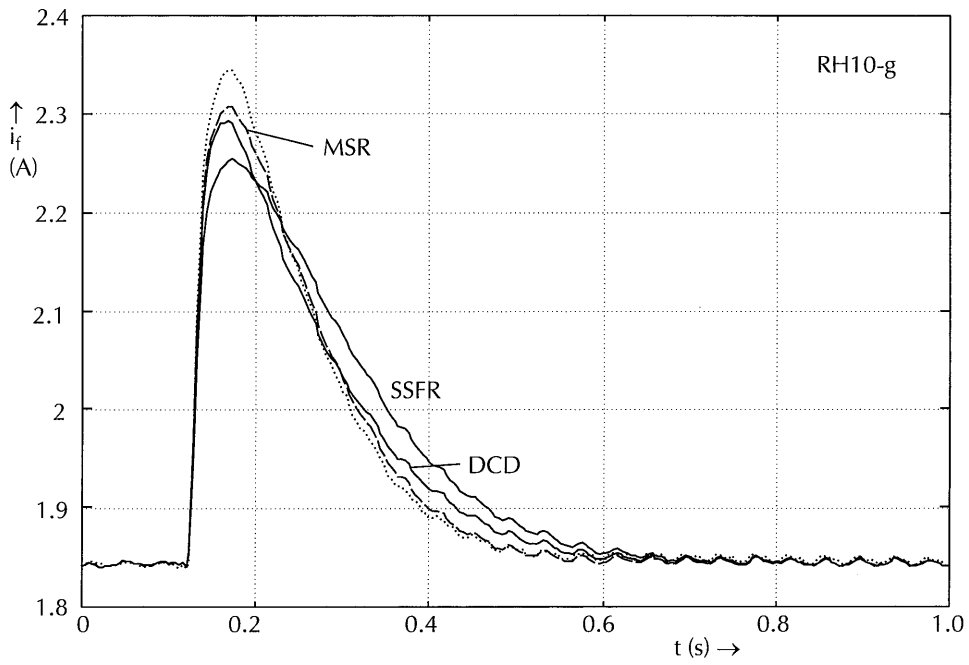
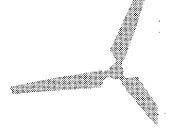


Figure 7.24d
Measured and simulated SM/R quantities
Heemaf measurements RH10-g and -f: excitation-winding current i_f

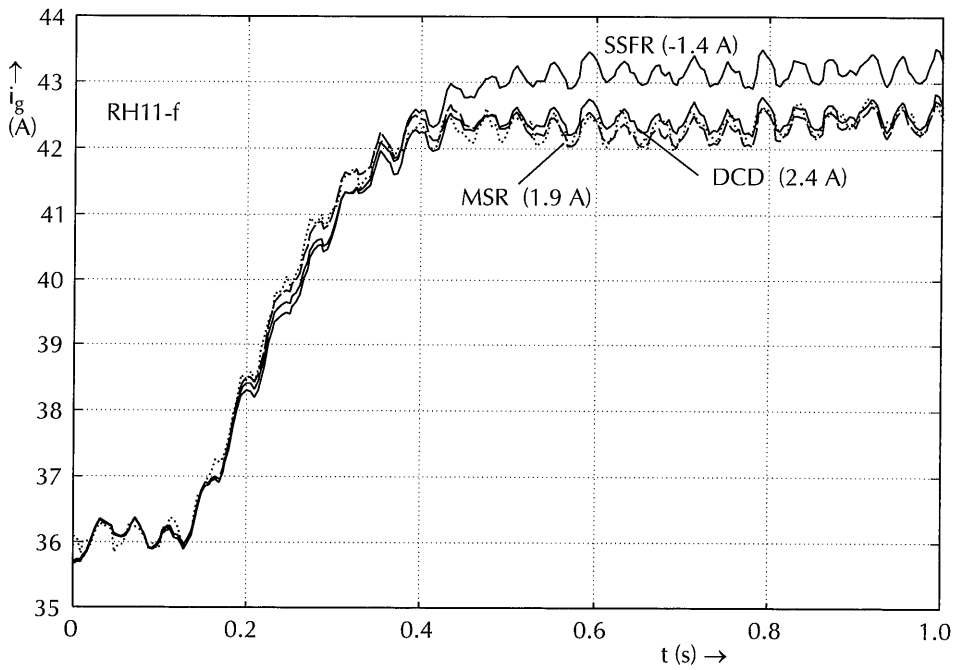
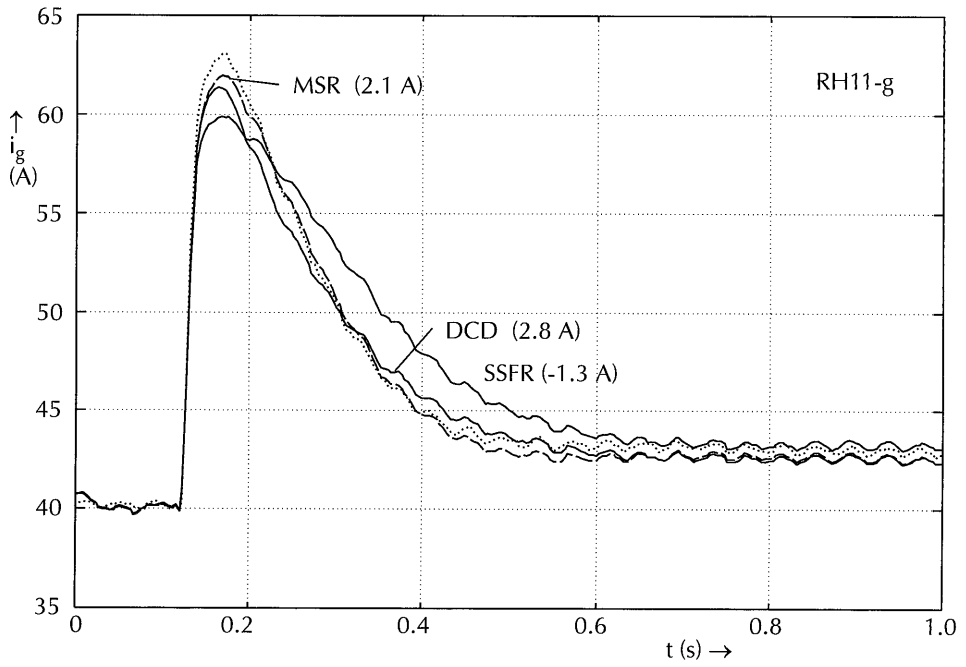


Figure 7.24e
Measured and simulated SM/R quantities
Heemaf measurements RH11-g and -f: rectifier DC-current i_g

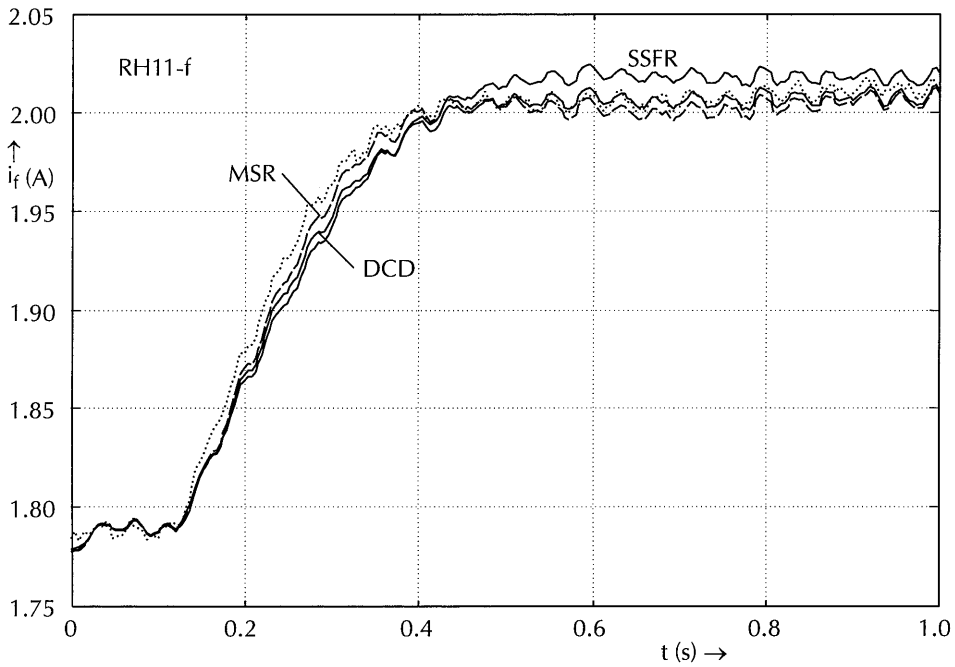
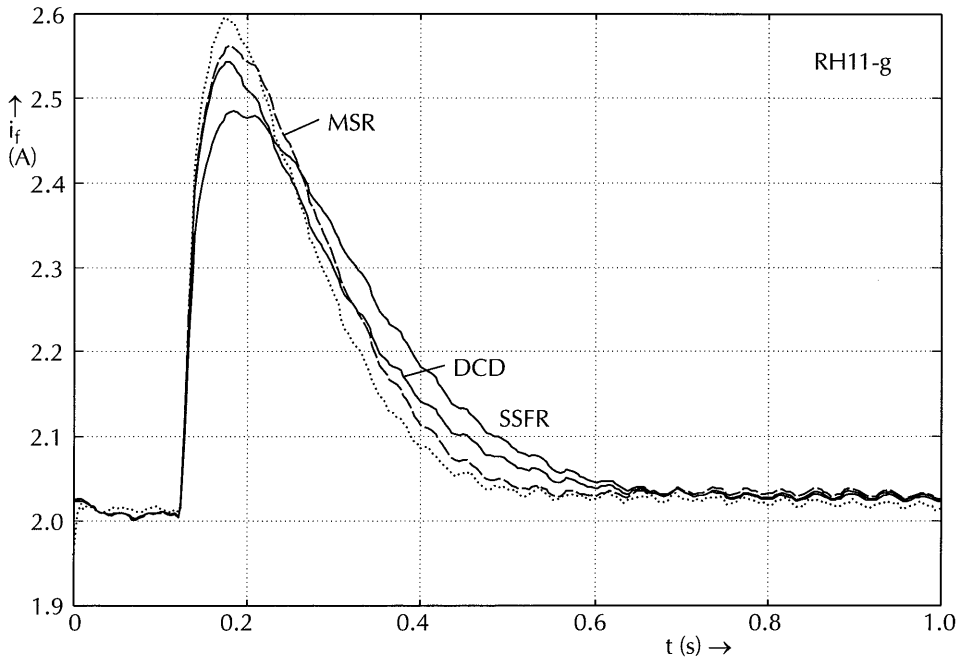
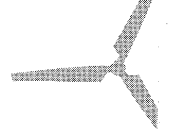


Figure 7.24f
Measured and simulated SM/R quantities
Heemaf measurements RH11-g and -f: excitation-winding current i_f

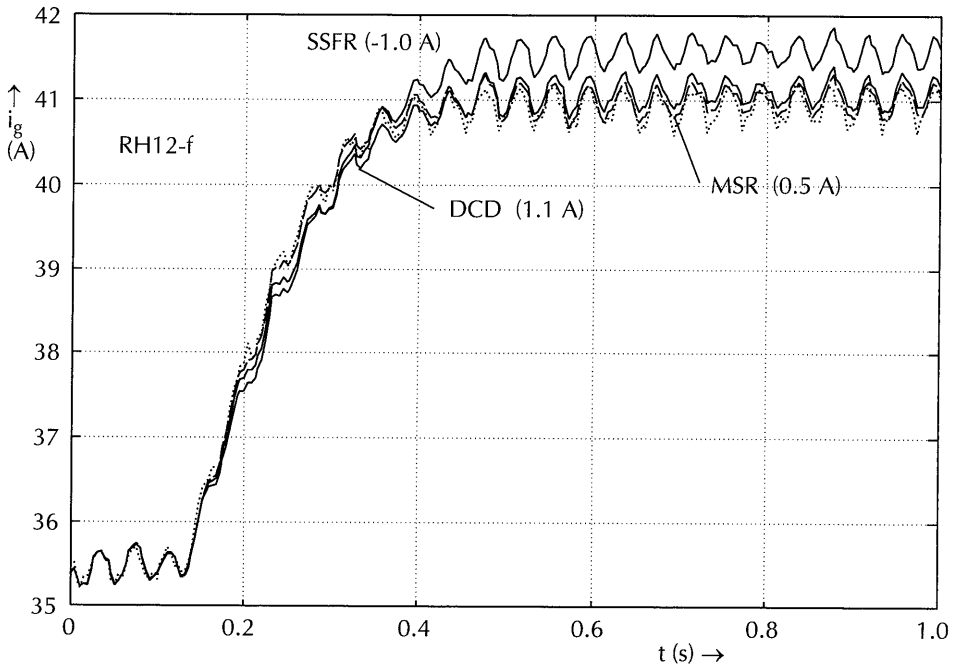
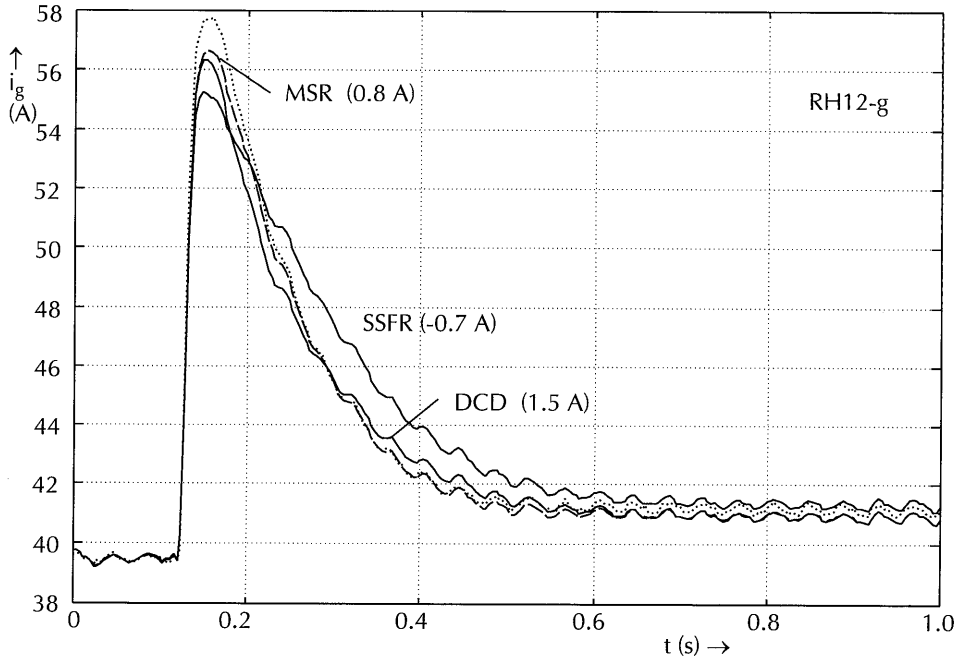
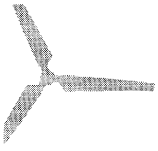


Figure 7.24g
Measured and simulated SM/R quantities
Heemaf measurements RH12-g and -f: rectifier DC-current i_g

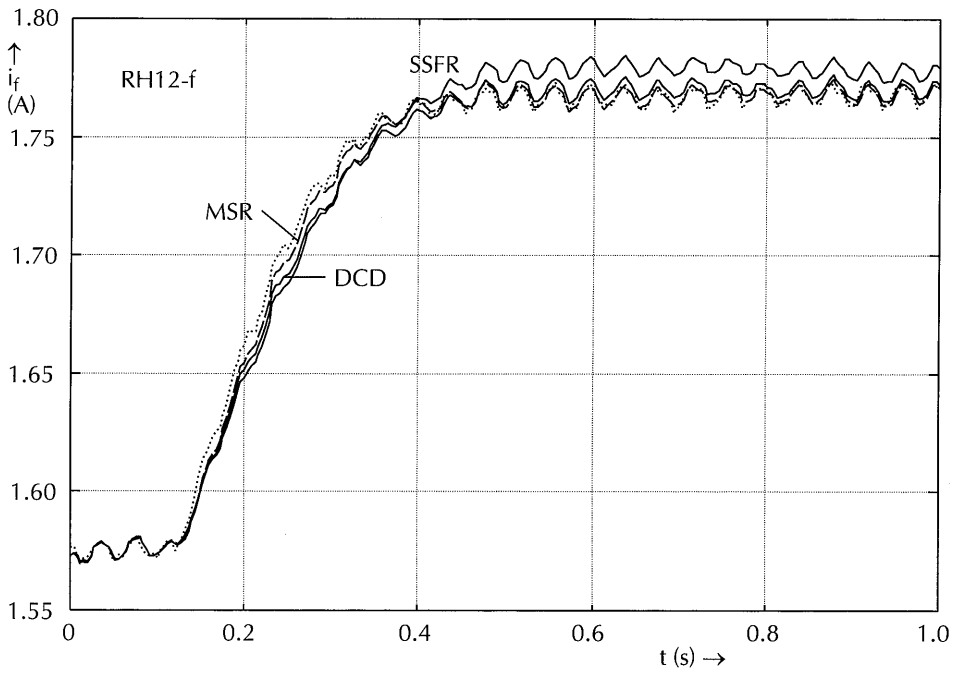
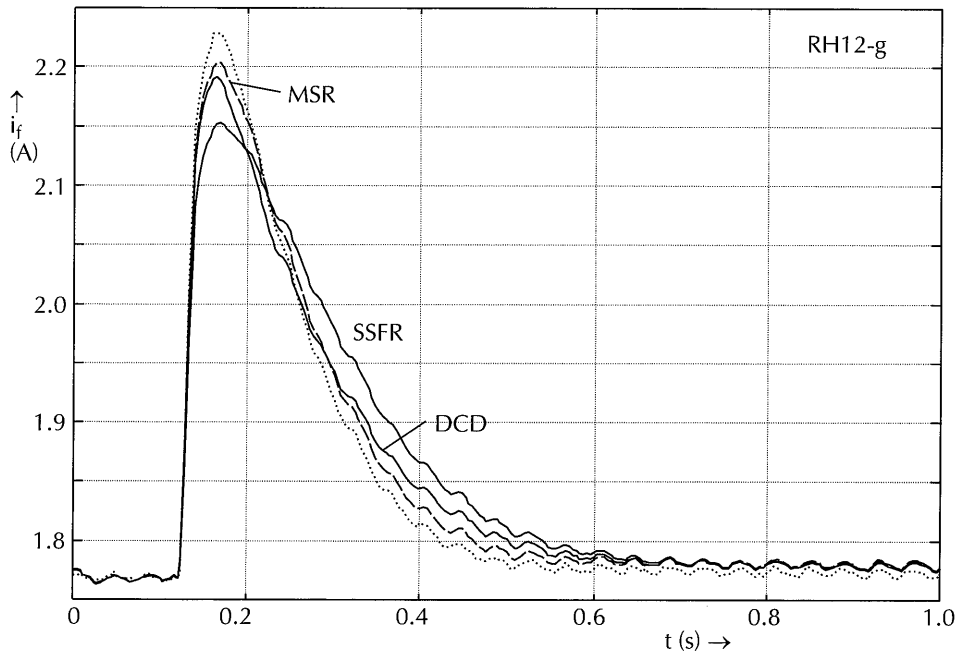
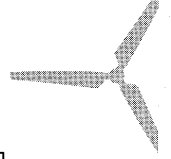


Figure 7.24h
Measured and simulated SM/R quantities
Heemaf measurements RH12-g and -f: excitation-winding current i_f

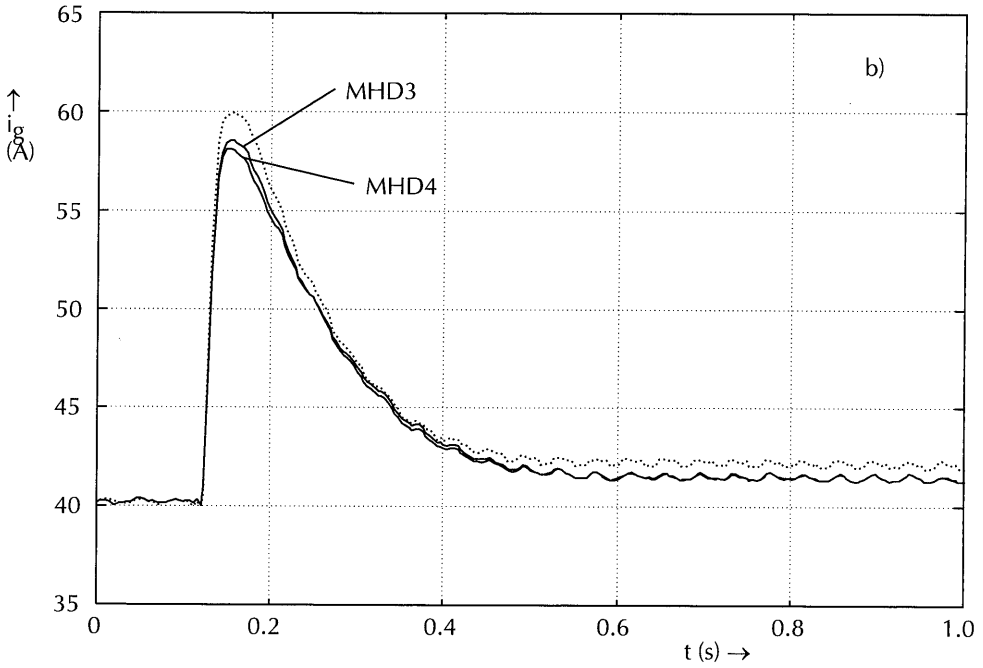
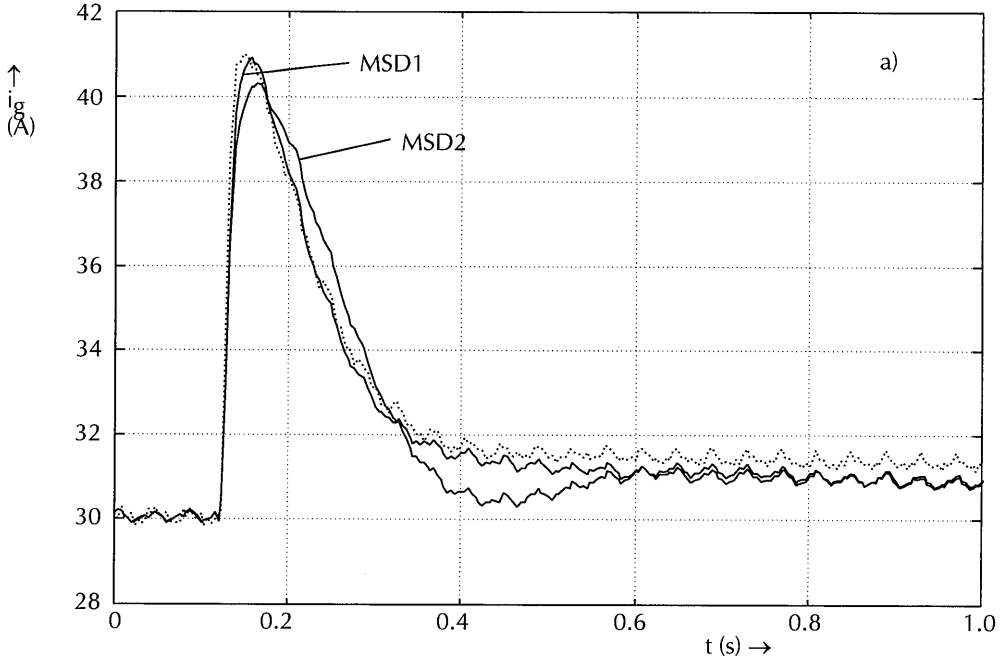
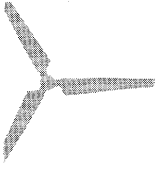


Figure 7.25
Variations in the simulated DC-current i_g , as a result of using different sets of MSR-test data; simulations based on:
a) Siemens measurement RS12-g
b) Heemaf measurement RH10-g

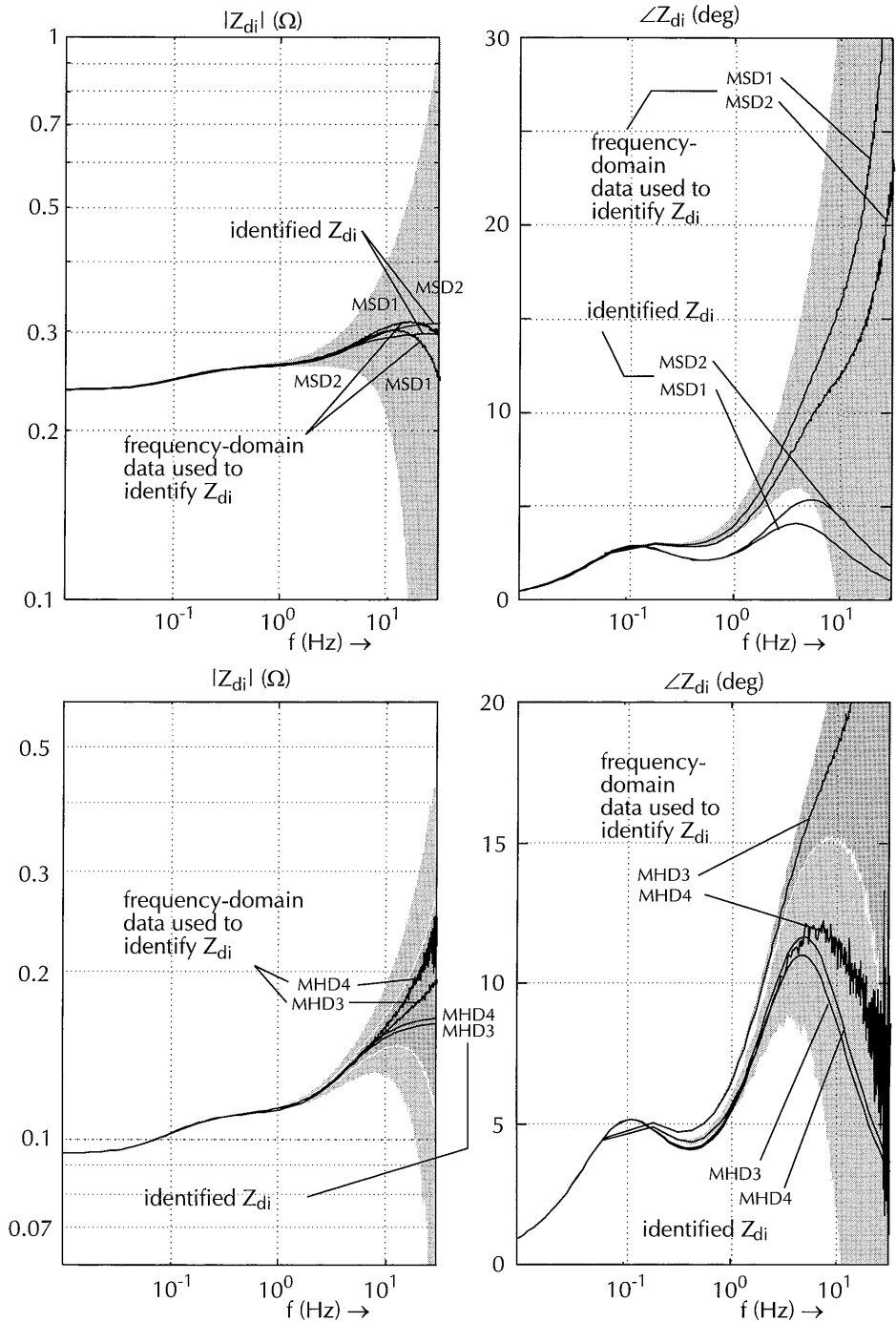
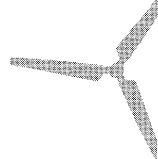


Figure 7.26
Variations in the identified $Z_{di}(s)$, responsible for the simulation differences in figure 7.25.
a) Siemens machine
b) Heemaf machine

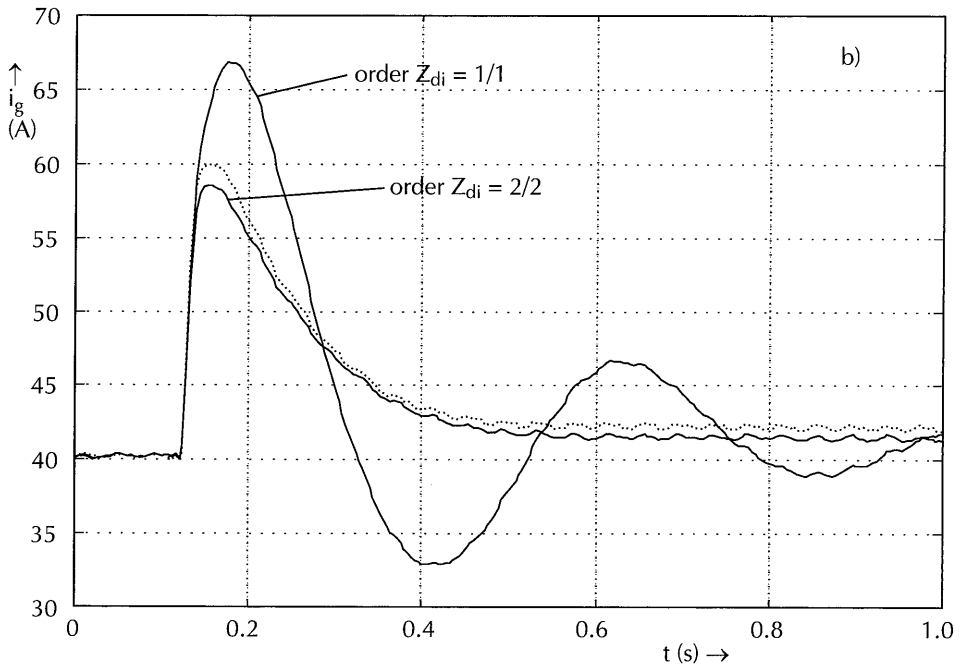
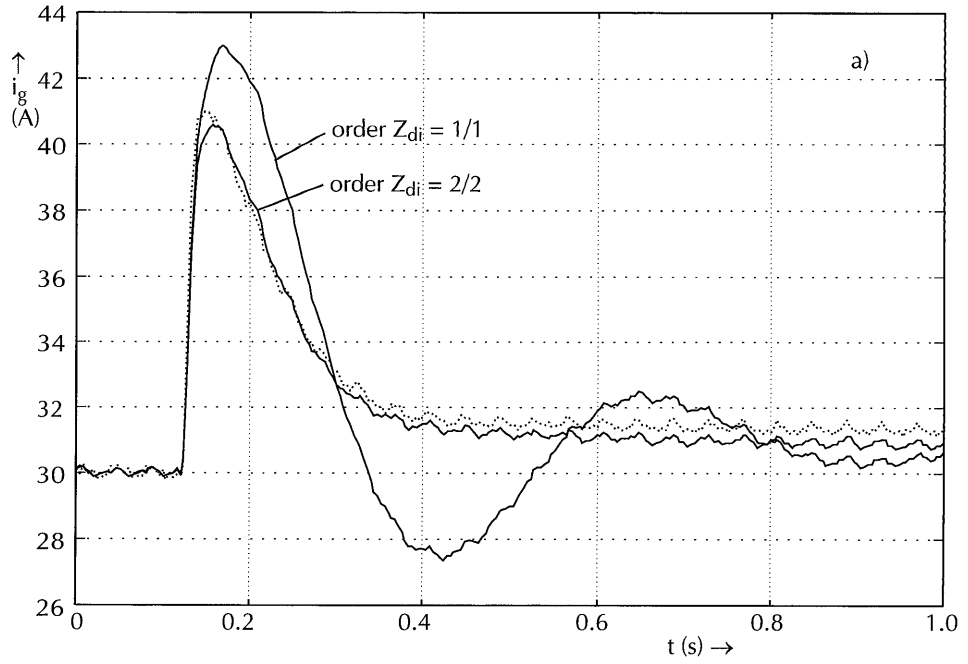
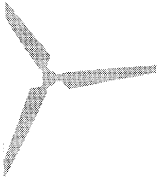


Figure 7.27
Variations in the simulated rectifier DC-current i_g as a result of using different model orders in the identification of individual transfer functions; simulations based on:
a) Siemens measurement RS12-g
b) Heemaf measurement RH10-g

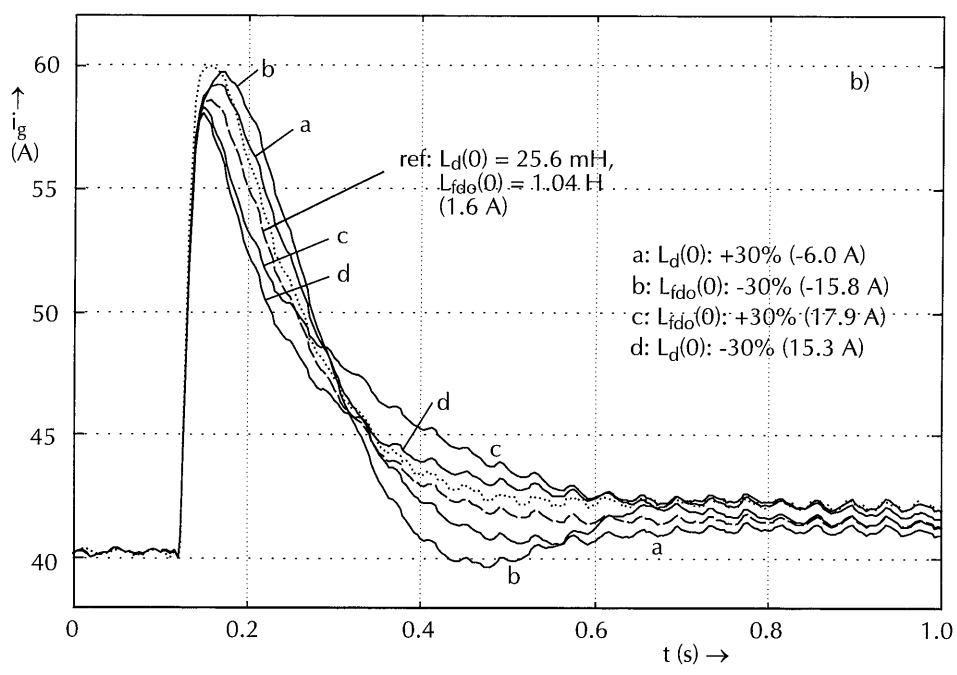
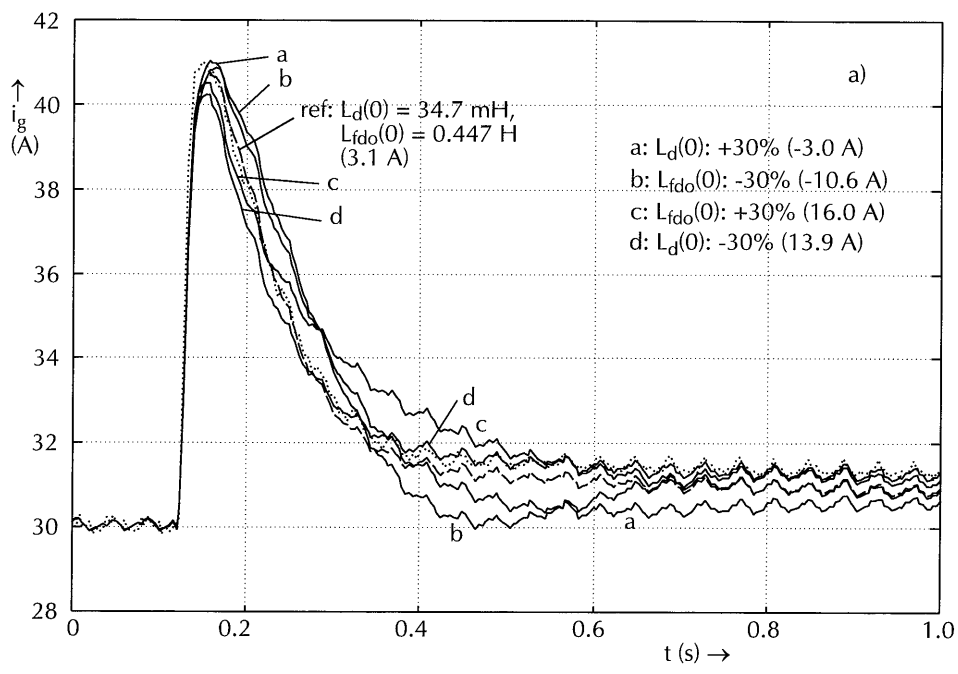
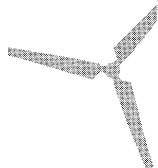


Figure 7.28
Variations in the simulated rectifier DC-current i_g , as a result of fixing $L_d(0)$ and $L_{fdo}(0)$ at different values than originally estimated; simulations based on:
a) Siemens measurement RS12-g
b) Heemaf measurement RH10-g

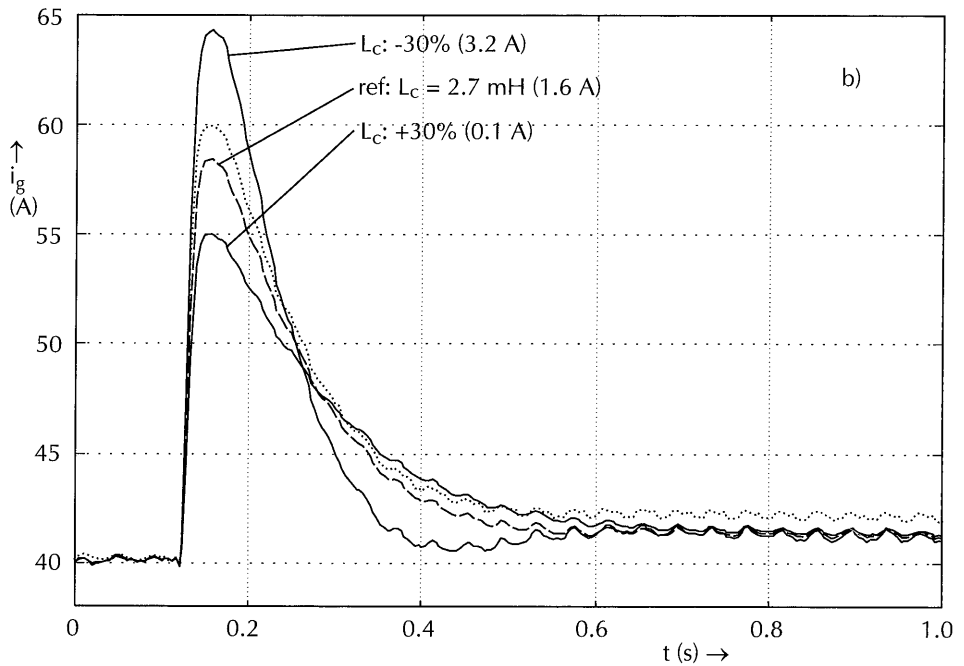
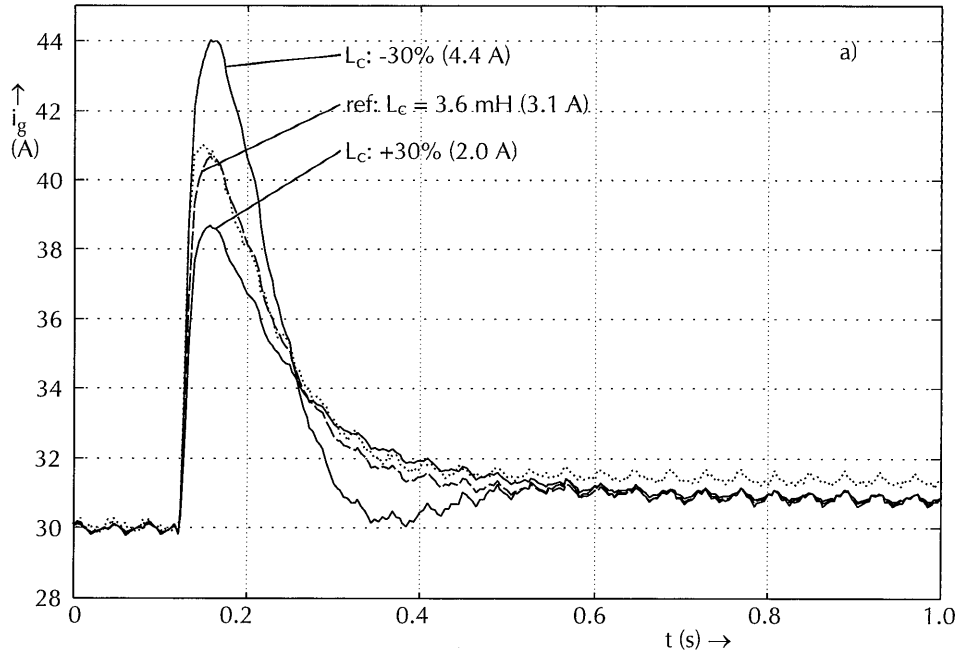
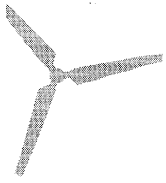


Figure 7.29
Variations in the simulated rectifier DC-current i_g as a result of using different values of L_c in the simulation:
a) Siemens (measurement RS12-g)
b) Heemaf (measurement RH10-g)

Stellingen

behorend bij het proefschrift

Synchronous machine
identification
by a simple
step-response test

van

Jan Vleeshouwers

Eindhoven, 8 juni 1998

1

De verschillen in taal en cultuur tussen de vakgebieden van de elektromechanika en van de regeltechniek zijn zo groot, dat ze over het hoofd worden gezien.

2

Identificatietechnieken worden slechts zelden op elektrische machines toegepast vanwege de ongefundeerde opvatting dat dat veel tijd zou kosten.

3

Omdat er toch ook argumenten tégen windenergie moesten zijn, vond men de term 'horizonvervuiling' uit.

4

Eenvoud is geen laagvlakte, maar het dal na een berg.

5

Vooruitgang is niet gelegen in het toepassen van techniek, maar in het kunnen afzien van gebruik ervan.

6

De slechte zichtbaarheid van voetgangers en fietsers is te wijten aan de overdadige verlichting van andere objecten op straat.

7

Bij schemering moeten automobilisten hun ogen gebruiken, niet hun koplampen.

8

Files lossen zichzelf op.

9

Voor supportersrellen moet een gedoogzone worden ingericht. De uitzendrechten daarvan gaan naar de KNVB, en we horen en zien er niets meer van.

10

Stellingen bij Nederlandse proefschriften getuigen van spitsvondigheid, maar niet van overtuiging.

11

Een goede stelling verdraait de waarheid.

Operators

<i>Description</i>	<i>Unit</i>
\angle angle of	[deg]
* complex conjugation	
- (bar over symbol) mean	
arg min the function argument which minimises	
cov covariance (function of two arguments)	
d differentiation	
Im imaginary part (function of a complex variable)	
min minimum of	
Re real part (function of a complex variable)	
T transpose	

Quantities

...		
$\underline{\theta}$	general vector of parameters	
	$\underline{\theta}_{\min}$ parameters which minimise loss function (section 2.4)	
μ	angle of overlap (commutation angle)	[rad]
	μ_c calculated angle of overlap (section 7.6)	
	μ_m measured angle of overlap (section 7.6)	
...		
P	normalised Park-transformation matrix (defined in eq. (3.1))	[1]
q	(referring to) synchronous-machine quadrature axis	
Q	<i>with respect to MSR-test</i> : quadrature-axis measurement	
...		
	ΔR_f change in R_f (appendix 3)	
...		
S	<i>in figures</i> : switch	
t	time	[s]
...		
T	<i>in figures</i> : thyristor	

Errata

June 13th, 1998

Title page:

College van Promoties

→

College voor Promoties

Contents, 2nd page:

The title of appendix A4 is: Figures of chapter 7

Page 50 and 51 should have a page number.

List of symbols (pages 119 – 122)

Several lines have an incorrect font size and indentation.

The correct lay-out of these lines is given overleaf.

Appendix A1

Page 126, after equation (A1.1a):

spectrum $|X_n(\omega)|^2 = T\eta$ →

spectrum $|X_s(\omega)|^2$

page 126, below equation (A1.4):

<ea1_x2> →

$\sin^2\left(\frac{1}{2}\omega T\right) = 1$